THE GLOBAL CLIMATE SYSTEM REVIEW

CLIMATE SYSTEM MONITORING

June 1991 - November 1993

WORLD METEOROLOGICAL ORGANIZATION
WORLD CLIMATE DATA AND MONITORING PROGRAMME

UNITED NATIONS ENVIRONMENT PROGRAMME

Front cover: Hurricane Andrew, August 23, 1992 (NOAA)

WMO - No. 819

ISBN 92-63-10819-6

FOREWORD

The fifth edition of the Global Climate System Review is based on climate system events of the 1991 to 1993 period. The Review continues the biennial series tradition that started with a review of the 1982-1984 period. The continuity with previous issues is maintained by updating analyses of traditional climate system monitoring (CSM) parameters and phenomena such as the El Niño/Southern Oscillation. At the same time, this issue attempts to broaden the perspective for its audience with expanded information on the oceans and timely review essays on pertinent climatological topics.

As in previous reviews, this publication intends to make readers aware of the evolution and inherent variability of the global climate system, attempting to set short-term climatic fluctuations in a historical context. It serves as a reference document on current climate issues and fulfils an educational role as well. The Review also serves to demonstrate to WMO Members the value of the climate data and products provided by their countries and regional centres. The preparation phase of the Review provides an opportunity for CSM experts from around the world to exchange information on the global climate system, thereby contributing to a greater understanding of the system. The Review is an informative and reflective document on the global climate system that complements the WMO Climate System Monitoring Monthly Bulletins and the annual WMO Statements on the Status of the Global Climate that have been produced since 1984 and 1994 respectively.

The Review is produced under the auspices of the Climate System Monitoring Project of the World Climate Data and Monitoring Programme (WCDMP) that was initiated in 1984 following a recommendation of the Ninth Congress of the World Meteorological Organization (WMO). The co-sponsorship of the CSM project by the Global Environmental Monitoring System (GEMS) of the United Nations Environment Programme (UNEP) and the contribution of Canada's Atmospheric Environment Service to the editorial preparation of the Review are gratefully acknowledged.

Special appreciation is extended to Mr David Phillips, Senior Climatologist with the Atmospheric Environment Service of Environment Canada, for his excellent work as editor of this publication.

Prof. G.O.P. Obasi,
Secretary-General WMO

This Global Climate System Review is the fifth in a series of reviews, primarily designed to provide meteorological and hydrological services and other national and international organizations with information about the state of the global climate system although it is hoped that it will be of interest to a wider audience. In particular, there is a review of significant climate events and a description of large-scale anomalies of regional and global consequence. Also featured in this edition is background information on the Mount Pinatubo eruption, the story of El Niño/Southern Oscillation (ENSO), WMO's Global Precipitation Climatology Centre in Germany, reference periods and climate normals, and the North Atlantic Oscillation. An addition to the Review that first appeared in the fourth edition is a concluding chapter featuring climate subjects of topical interest including the International Decade for Natural Disaster Reduction, the Global Climate Observing System, metadata, and international and national climate responsibilities following the Earth Summit Conference in Rio de Janeiro (1992). The Review covers in detail the period from June 1991 to November 1993, inclusive. Brief mention is made of some significant events which occurred in December 1993 and January-February 1994.

The Review contains summaries of large scale anomalies and variables, important for interpreting more detailed analyses at subregional, national and local levels. Also included are global analyses of temperature and precipitation anomalies, and details on the persistence of hot/cold and wet/dry episodes. Events causing much mortality, suffering, environmental degradation and economic loss - such as floods, drought and major storms - are well documented, as are changes in the concentrations of ozone and trace gases implicated in the enhanced greenhouse gas effect.

With every issue of the Review, attempts are made to encompass the full breadth and scope of the global climate domain -atmosphere, oceans and hydrosphere, biosphere, and cryosphere. To show the full extent of the total climate system, short illustrative chapters on biological systems and processes, on fluctuations in water levels and on the cryosphere are presented. Wherever possible, recent events are placed in a historical context through the use of long data time series. The significance of climate anomalies is defined by the departures of various components of the climate system from their "normal" values and not necessarily by their impacts. The Review borrows heavily on published analyses of regional and global anomalies carried out by several national meteorological centres. Many of these centres publish this information in monthly bulletins, much of which is in WMO's Climate System Monitoring (CSM) Bulletin published monthly by the World Climate Data and Monitoring Programme.

▲ Cumulus and towering cumulus over Appalachian Mountains in North Carolina

INTRODUCTION AND HIGHLIGHTS

CHAPTER 1

1.1

HIGHLIGHTS

The review period from June 1991 to November 1993 witnessed a number of remarkable extremes and anomalous climate events. Floods and droughts occurred across every continent, sometimes in the same localities during the same year. In the USA, in a period of 12 months, hurricanes, floods and blizzards inflicted more than US$ 50 billion in property damages and losses to the American economy. While droughts came to an end in the western USA and the Mediterranean Rim, they continued to ravage northeastern Brazil and reached a record degree of severity in southern Africa. Drenching rains generated the largest floods in 40 years over central and eastern China, inflicting hardship on 100 million people. Heavy July 1993 rains led to catastrophic flooding in Nepal and the country's worst natural disaster. A record number of tropical storms plagued the Philippines in 1993. On a more optimistic note, several ozone-depleting trace gases showed a reduction in their growth rate. Climate highlights for the period included:

- *A warm phase El Niño persisted during the entire review period.*
- *Slight surface temperature cooling over many regions was probably related to the eruption of Mount Pinatubo. The year 1992 was the coolest since 1985, but still the eighth warmest since 1951.*
- *The eruption of Mount Pinatubo had the greatest impact on global climate since Krakatoa in 1883.*
- *The American Midwest Great Flood (1993) surpassed all floods in recent USA history.*
- *The Indian monsoon in 1993 was the most favourable for agriculture since 1989. Only one depression formed over the Bay of Bengal during the season - the lowest number to occur in 54 years.*
- *Powerful hurricanes devastated parts of Florida and Hawaii in 1992.*
- *The worst bush fires in 200 years ravaged eastern Australia at the close of 1993.*
- *Northern hemispheric snow cover in the autumn of 1993 was the largest in extent since 1976 and the third largest in 22 years. No trends were revealed in Arctic and Antarctic sea-ice cover.*
- *Water levels were above average in the middle and lower Great Lakes system, the Great Slave Lake in northwestern Canada, the Great Salt Lake in Utah and the Caspian Sea.*
- *Growth rates for trace gases decreased in the review period, especially for CO_2, methane and CFCs, the latter probably as a result of implementation of provisions of the Montreal protocol and its amendments.*
- *During 1992 and 1993, the Antarctic ozone hole and the mid-latitude, winter-spring, northern hemisphere ozone layer were both measured at record low values, but there is some reason for optimism following the predictions of the latest Ozone Assessment.*

2.1 EL NIÑO/SOUTHERN OSCILLATION (ENSO) CYCLE - AN UNUSUALLY LONG LIVED EPISODE

The El Niño/Southern Oscillation (ENSO) cycle is the dominant global climate fluctuation with time scales of a few months to a few years. ENSO is associated with a remarkably coherent pattern of ocean and atmospheric anomalies, whose appearance and evolution are intimately tied to the annual El Niño cycle off the west coast of South America (Figure 2.1). The ENSO cycle is a consequence of the large climatological difference in sea surface temperature (SST) between the huge pool of warm water in the western equatorial Pacific and the cool upwelling water in the eastern equatorial Pacific.

The ENSO cycle owes its existence to coupled ocean-atmosphere interactions. The eastward expansion and westward contraction of the western Pacific warm pool during the ENSO cycle results in an alternation of positive and negative SST anomalies in the eastern and central equatorial Pacific. The effect of these SST anomalies on the atmosphere is strongly amplified by the associated shifts in the large-scale rainfall regime of the western Pacific, which migrates eastward and westward with the warm water. The resulting changes in the low-level atmospheric circulation lead in turn to changes in the ocean current systems and thermal structure of the low-latitude Pacific, which produce further changes in SST, thus completing an interactive feedback loop.

The relative contribution of the ENSO cycle to interannual climate variability is largest over the tropical Pacific/Indian Oceans and adjacent land areas, where high amplitude swings of the cycle lead to massive dislocations of the regional rainfall regimes as well as severe disruptions of the marine ecosystems along the west coast of the Americas. The related atmospheric circulation anomalies extend around the tropical belt and, in some cases, deep into the extratropical zones, where they are associated with unusual wintertime

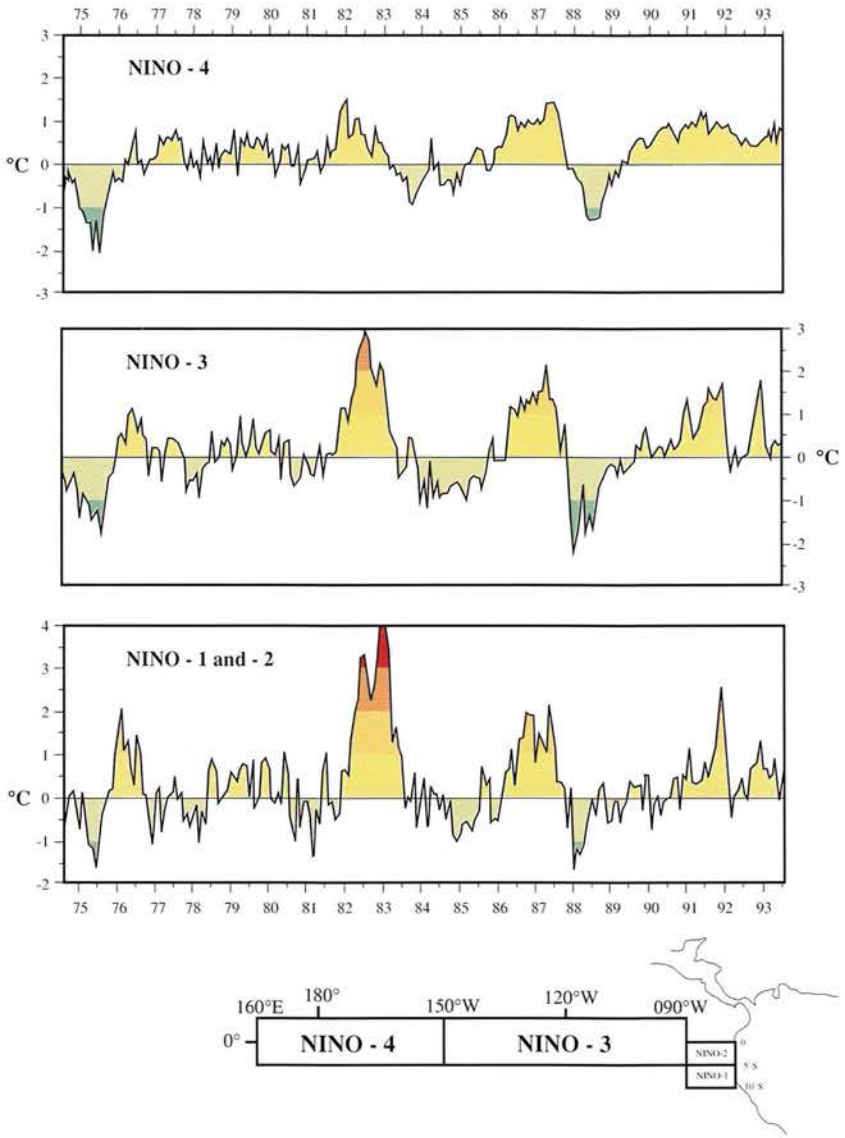

▲ *Figure 2.1* – Equatorial Pacific sea surface temperature (SST) anomalies (°C) for the areas indicated in the figure. NINO 1+2 is the average over the NINO 1 and NINO 2 areas. The NINO 3 area is often used as an index of SST anomalies associated with the ENSO cycle (from NOAA/NWS/NMC/CAC, Washington, DC).

conditions over regions as far apart as the USA and New Zealand.

A warm phase or "El Niño phase" of the ENSO cycle usually recurs at intervals of two to six years and typically evolves over a period of roughly one year. Most El Niño phase warmings have broadly similar characteristics, but each event also has a personality of its own (Figure 2.1). The global consequences of a particular warm episode depend on its strength and the way it evolves in relation to the time of year.

Overall, the 1991-1992 ENSO pattern was not drastically different from the typical event. What distinguished this warm episode was the fact that it was embedded in an extended period of warm conditions that spanned the entire period 1990-1993. Following the pronounced cold phase of the ENSO cycle (1988-89), above-normal SSTs reappeared in the central equatorial Pacific in early 1990 (Figure 2.2). At the same time, negative sea-level atmospheric pressure (SLP) anomalies developed over the eastern tropical Pacific while positive anomalies emerged over Indonesia and the western tropical Pacific. This east-west seesaw pattern in SLP anomalies, which is typical of the ENSO cycle, is tracked by the Southern Oscillation Index (SOI). The SOI becomes negative during an ENSO cycle warm phase. Weaker than normal low-level equatorial easterly winds develop in association with the weakening of the east-west pressure gradient across the equatorial Pacific.

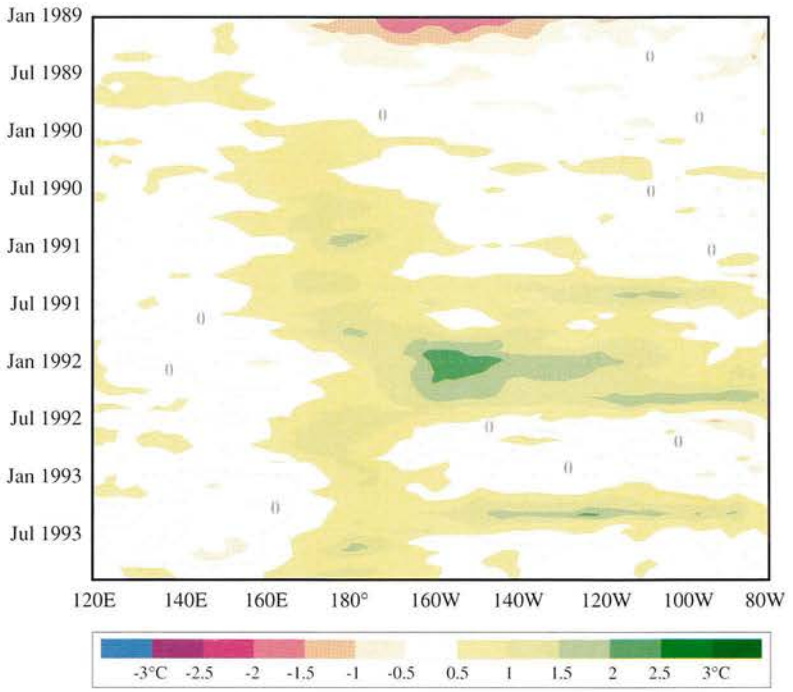

◀ *Figure 2.2* – SST anomalies (°C) in the equatorial belt (5°N-5°S) between 80°W (near the South American coast) and 120°E (Sulawesi). Note that anomalies were predominately positive in the central and eastern equatorial Pacific between 1990 and 1993, with the most pronounced peak occurring between late 1991 and early 1992 (from NOAA/NWS/NMC/CAC, Washington, DC).

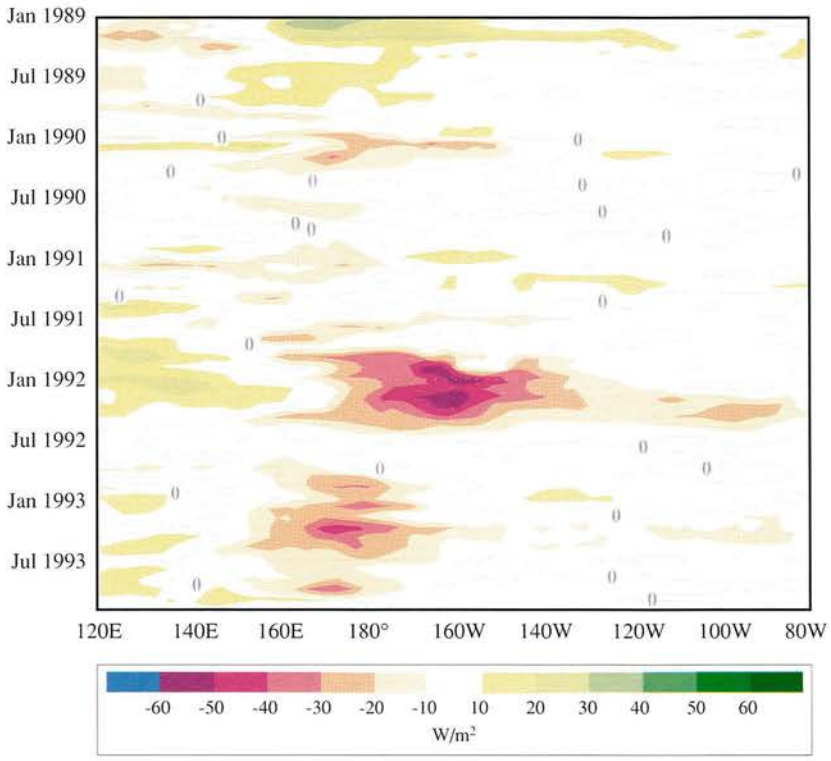

◀ *Figure 2.3* – Outgoing longwave radiation (OLR) anomalies in the equatorial belt (5°N-5°S) between 80°W (near the South American coast) and 120°E (Sulawesi). OLR serves as a good index of rainfall in the tropics, i.e., low values of OLR indicate numerous high cloud tops and heavy precipitation. Note the correspondence between positive sea surface temperature anomalies in the central Pacific (Figure 2.2) and enhanced precipitation associated with negative OLR anomalies (from NOAA/NWS/NMC/CAC, Washington, DC).

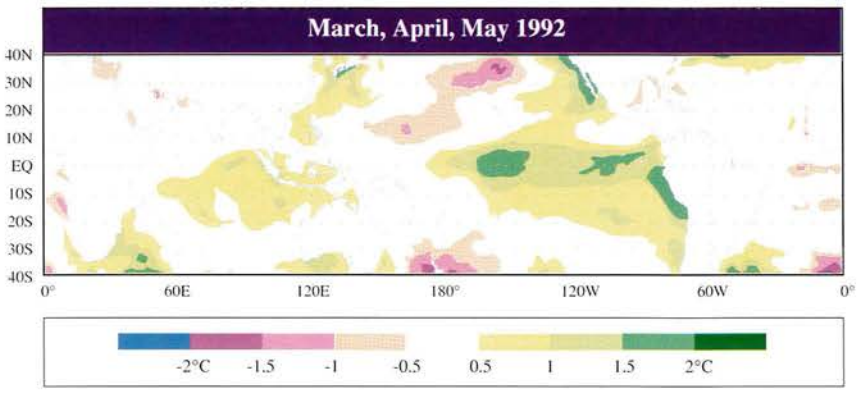

◀ *Figure 2.4* – SST anomalies (°C) during March, April and May, 1992, at the peak of the 1991-1992 warm episode. The pattern of above-normal SSTs in the equatorial eastern and central Pacific, with eastward and poleward extensions of below-normal SSTs from the western Pacific into middle latitudes is typical of the mature phase of a warm episode. The above-normal SSTs in the Indian Ocean are also a typical feature of the tropical SST anomaly field (from NOAA/NWS/NMC/CAC, Washington, DC).

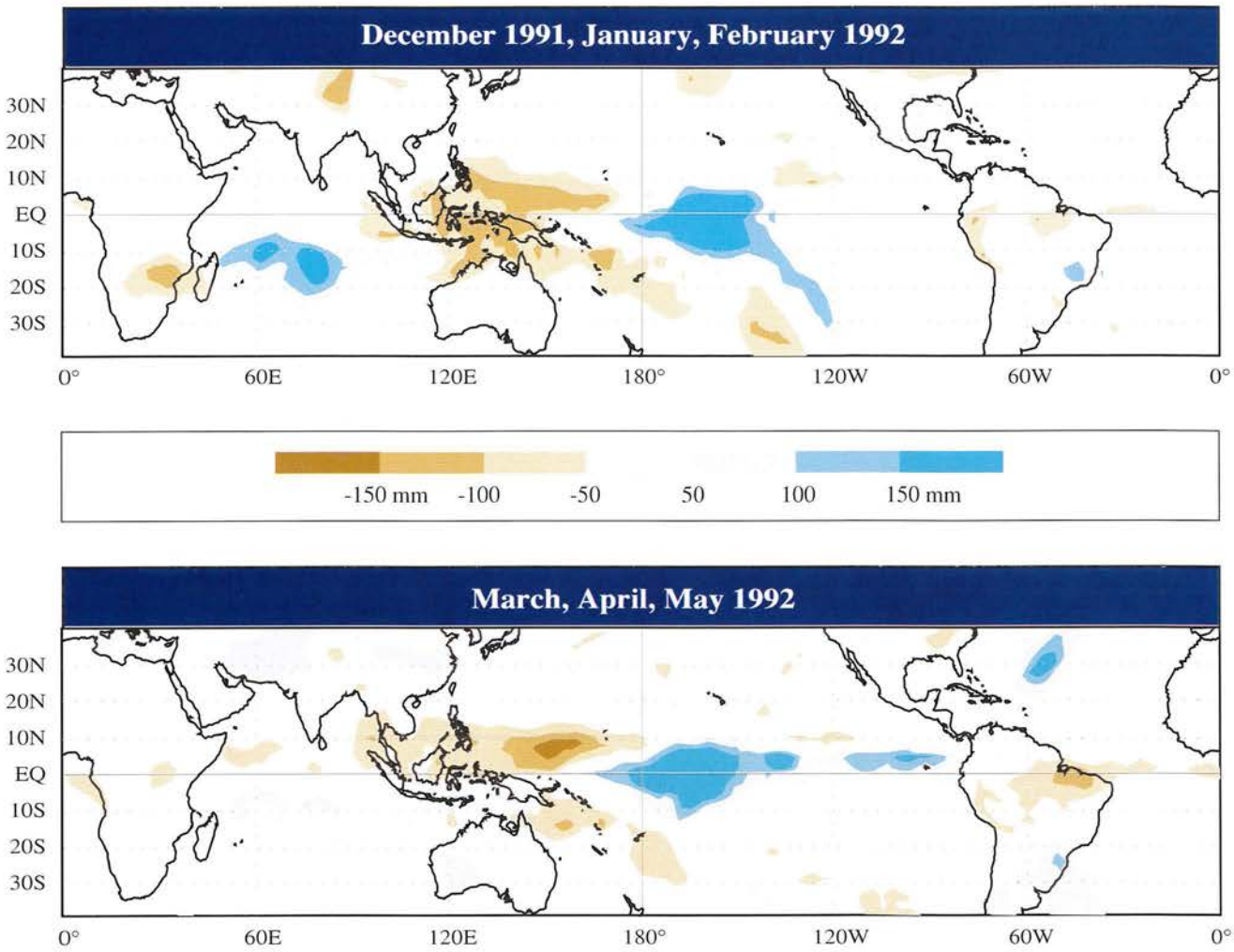

▲ *Figure 2.5* – Seasonal precipitation anomalies (mm per month) for (a) December 1991-February 1992 and (b) March-May 1992 (from the WCRP Global Precipitation Climatology Project (GPCP), Deutscher Wetterdienst, Germany).

Although weak warm episode conditions appeared in early 1990, there was no significant further development until mid-1991. By late 1991, conditions typical of the mature phase of a warm or El Niño episode had developed fully (Figures 2.3 and 2.4). Global atmospheric circulation anomalies during the period December 1991 through April 1992 were typical of the warm phase of the ENSO cycle. An anticyclonic anomaly couplet straddled the equator over the region of enhanced precipitation in the central Pacific. This was associated with enhanced equatorial easterlies and subtropical westerlies. The enhanced westerlies are associated with eastward extensions of the North Pacific and South Pacific jet streams. Poleward of the tropical anticyclone anomalies are anomalous cyclonic circulations in both hemispheres. The North Pacific cyclonic anomaly is part of the Pacific-North American (PNA) teleconnection, which is a prominent feature during the mature phase of an ENSO warm episode.

Precipitation anomalies (Figure 2.5) were also typical of the warm phase of the ENSO cycle. Severe drought plagued northeastern Brazil, southern Africa, the Philippines, northern Australia and islands in the western Pacific, where fresh water had to be imported in some cases. In contrast, unusually heavy rainfall occurred over the central equatorial Pacific and, by March 1992, this anomalous convection extended along the equator from the central Pacific to the South American coast. Excessive precipitation was also observed over southeastern Brazil and in a band from northern Mexico/southern California eastward across the western Gulf of Mexico coastal region of the USA. This included heavy rains and flooding in eastern Texas throughout much of the period and in southern California during January.

El Niño conditions developed along the coast of Peru in late 1991 and SST anomalies were reported to be locally greater than 4°C. As the equatorial cold tongue was temporarily re-established during late May to mid-July, SST and precipitation anomalies decreased rapidly in the eastern equatorial Pacific. SST anomalies then showed little change from mid-July through December 1992, since weak warm episode conditions, similar to those observed from 1990 to mid-1991, characterized oceanic and atmospheric anomaly fields.

The evolution of the oceanic subsurface thermal field along the equator from mid-1991 to mid-1992 was in many respects similar to that observed during the previous warm phase of the cycle (1986-1987). Between August 1991 and October 1991, the depth of the thermocline,

as tracked by the 20°C isotherm (see Figures 10.4 and 10.5) increased in the central and eastern equatorial Pacific and decreased in the western portion of the basin. This resulted in positive mixed layer temperature anomalies in the central equatorial Pacific. There was a steady eastward propagation of the subsurface temperature anomaly pattern from October 1991 through March 1992. Thus, as the thermocline continued to deepen in the eastern equatorial Pacific, a shoaling of the thermocline also spread eastward from the western into the central Pacific. By May 1992, the thermocline was anomalously shallow throughout much of the equatorial Pacific, so that temperature anomalies near 100-m depth were negative from the western Pacific eastward to near 110°W.

Subsurface conditions changed little along the equator from May through September 1992, but the thermocline again deepened in the central and eastern equatorial Pacific between October and December, while subsurface temperature anomalies increased. Thus, at the end of 1992 the subsurface thermal field again strongly resembled that observed during the mature phases of the 1986-1987 and 1991-1992 warm episodes.

By the end of 1992 the SOI was near minus one (Figure 2.6) and the atmospheric anomaly fields had again developed warm episode characteristics. The equatorial easterlies were weaker than normal throughout the Pacific and enhanced convection had redeveloped along the equator near the dateline. Warm episode conditions continued until mid-1993. Temperature and precipitation anomaly patterns corresponded to those generally observed during the mature phase of a warm episode, but were somewhat weaker than those during the previous year. Weak El Niño conditions were observed at this time along the Peruvian Coast. Positive SST anomalies persisted in the central equatorial Pacific during the latter half of 1993.

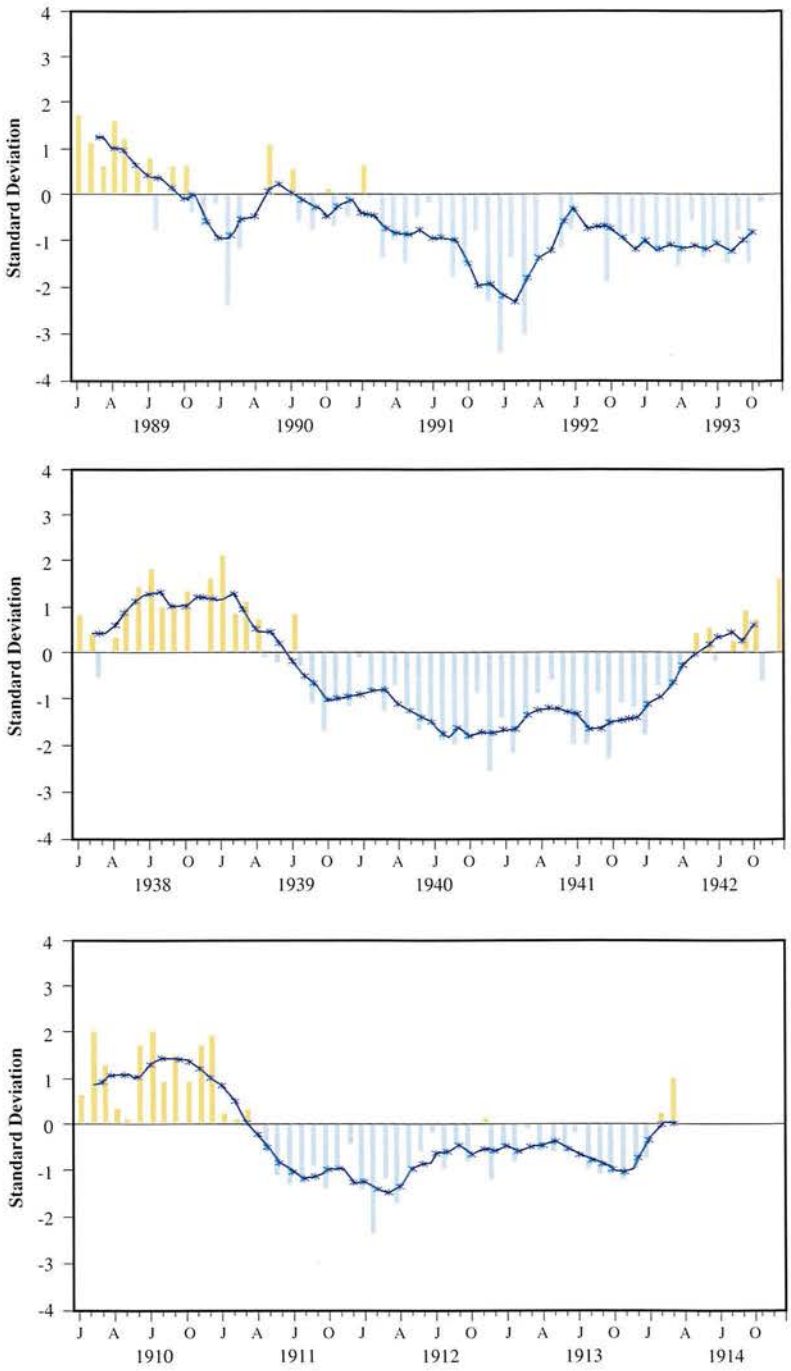

▲ *Figure 2.6* – The Southern Oscillation Index (SOI) during the three longest periods of low SOI (above-normal SSTs) in the twentieth century historical record. The SOI is the difference between the sea-level pressure anomalies at Tahiti and Darwin (Tahiti-Darwin), standardized with respect to the mean annual standard deviation. Monthly and five-month running mean values are indicated by the bars and the curve line respectively (from NOAA/NWS/NMC/CAC, Washington, DC).

2.2

PERSISTENT WARM PHASE OR WEAK WARM EPISODE?

Although extremely atypical, an extended period of warm phase anomalies such as that observed during 1990-1993 is not unprecedented. Similar periods were also evident during 1911-1913 and 1939-1942 (Figure 2.6), but due to insufficient data, these periods cannot be accurately compared with 1990-1993. Several hypotheses have been suggested to explain the abnormal nature of the most recent warm period. For example, there is evidence that low-frequency variability on the multi-decadal time scale has resulted in an increase in the mean or "base state" SST of the tropical Pacific on which the ENSO cycle anomalies are

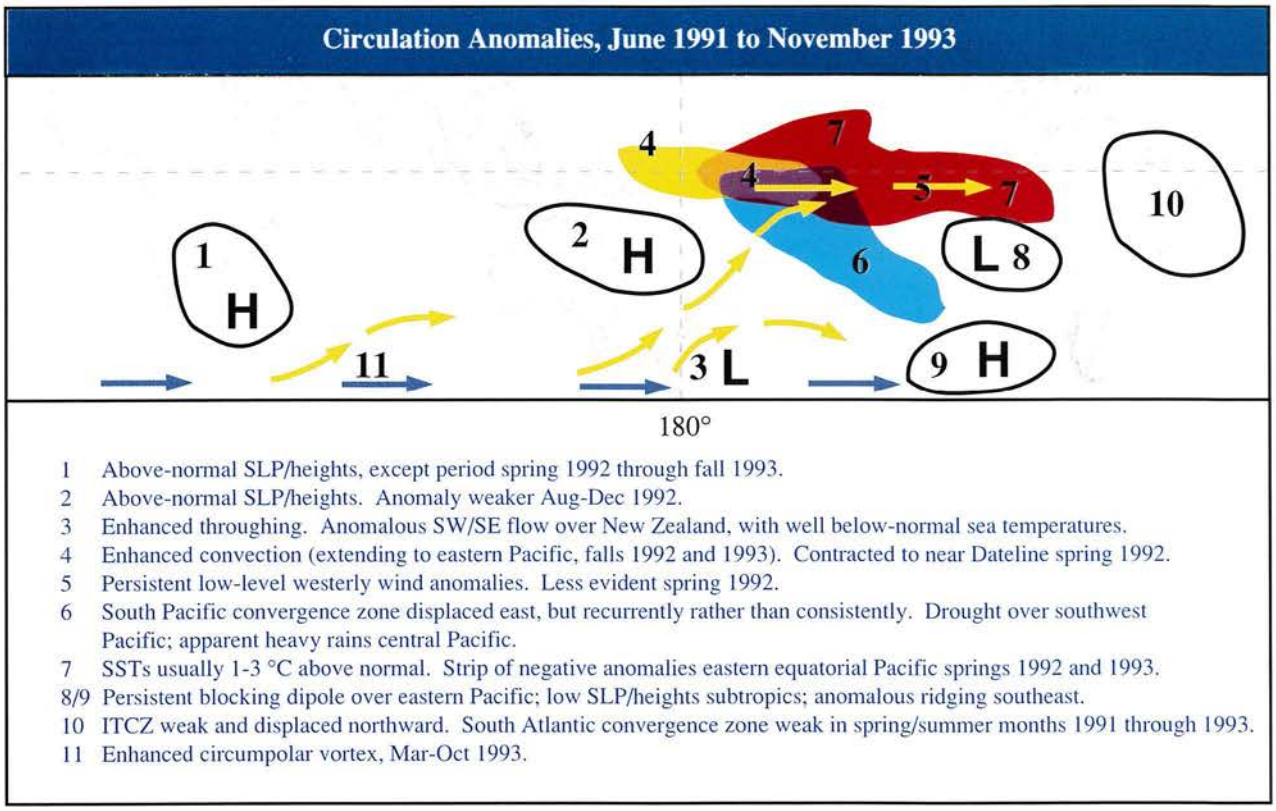

1 Above-normal SLP/heights, except period spring 1992 through fall 1993.
2 Above-normal SLP/heights. Anomaly weaker Aug-Dec 1992.
3 Enhanced throughing. Anomalous SW/SE flow over New Zealand, with well below-normal sea temperatures.
4 Enhanced convection (extending to eastern Pacific, falls 1992 and 1993). Contracted to near Dateline spring 1992.
5 Persistent low-level westerly wind anomalies. Less evident spring 1992.
6 South Pacific convergence zone displaced east, but recurrently rather than consistently. Drought over southwest Pacific; apparent heavy rains central Pacific.
7 SSTs usually 1-3 °C above normal. Strip of negative anomalies eastern equatorial Pacific springs 1992 and 1993.
8/9 Persistent blocking dipole over eastern Pacific; low SLP/heights subtropics; anomalous ridging southeast.
10 ITCZ weak and displaced northward. South Atlantic convergence zone weak in spring/summer months 1991 through 1993.
11 Enhanced circumpolar vortex, Mar-Oct 1993.

▲ *Figure 2.7* – Southern hemisphere circulation and weather anomalies during the period June 1991-November 1993 (season references area those in the southern hemisphere). Most of these anomalies were associated with the long-running Pacific warm episode (from National Climate Centre, Bureau of Meteorology, Melbourne, Australia).

superimposed. Furthermore, there is also evidence that persistent global anomalies associated with this long time-scale increase in SST are for the most part similar to the seasonal anomalies associated with an ENSO cycle warm episode. If this is true, then the current ENSO cycle anomalies might be represented as departures from the mean SST of the past few years rather than departures from the longer period mean. This might change our perception of the recent event from that of a persistent warm phase to one of a weak warm episode during 1991-1992 superimposed on "recent" background SSTs that are higher than the long-term normals.

2.3 SOUTHERN HEMISPHERE CIRCULATION

Significant and persistent atmospheric circulation anomalies in the southern hemisphere during 1991-1993 were largely dominated by the long-lived warm episode (Figure 2.7). Many of these anomalies (and their related surface climate anomalies) were similar to those observed during past ENSO episodes. The anomalies reached maximum strength in the periods December 1991 through May 1992 and March-July 1993, corresponding to the "mature" phase of ENSO on both occasions. Conversely, in the period around August-December 1992 most anomalies temporarily weakened, corresponding to a general waning

THE STORY OF ENSO

Home of El Niño*

El Niño episodes bring a warm ocean current to the South American coast.

The story of how diverse lines of oceanographic and meteorological research converged to reveal the elegant system of physical and ecological interactions we now know as El Niño and the ENSO cycle is a fascinating tale of scientific progress. The major elements of this climate oscillation were linked together only in the 1960s. By the 1980s meteorologists and oceanographers could monitor a developing El Niño event as it occurred. By the early 1990s climate modellers had demonstrated skill in forecasting the evolution of the cycle.

**Source:* Australia Bureau of Meteorology

UNDERSTANDING ENSO

Until the middle of the twentieth century, little was known about conditions during El Niño years over the vast expanse of the Pacific Ocean west of Peru. Climatologists had no reason to believe that the coastal El Niño warming was anything but a local feature of climate variability. The key event that drastically changed this picture occurred in 1957-1958, which, by good fortune, was a special period of enhanced ocean and atmosphere observations during the International Geophysical Year. The new observations revealed a remarkable and unexpected ocean warming during 1957-1958 that extended westward from the South American coast across much of the equatorial Pacific, more than a quarter of the distance around the globe!

The unexpected 1957-1958 basin-wide warming caught the attention of a distinguished meteorologist from the University of California at Los Angeles (UCLA) named Jacob Bjerknes, who as a young scientist working with his father in Norway had made landmark contributions to our modern understanding of the behaviour of temperate latitude weather systems. From his meticulous study of the 1957-1958 tropical Pacific warming and two subsequent warmings in 1963 and 1965, it became apparent to Professor Bjerknes that alternate warmings and coolings of the sea surface temperatures over the eastern and central equatorial Pacific were a recurrent feature of climate variability and, furthermore, these broad-scale Pacific warmings usually coincided with coastal El Niño events. New observations from meteorological satellites, the first of which was launched in 1960, together with merchant ship observations, showed that the changing patterns of sea surface temperature were accompanied by large shifts in the rainfall regimes of the tropical Pacific and even larger-scale changes in the atmospheric circulation.

Upon further study, it became clear to Professor Bjerknes that the tropical Pacific sea surface temperature variations were intimately linked to a global pattern of climate anomalies that had been discovered almost a half century earlier by a British meteorologist, Sir Gilbert Walker, while he was searching for a method to forecast the year-to-year variations in Indian monsoon rainfall.

The most significant feature of this atmospheric oscillation, which Walker named the Southern Oscillation, is a slow "swaying" or seesaw in atmosphere surface pressure between the Indian Ocean and the central tropical Pacific. The linking of the coastal warmings near Peru with the much larger scale warmings over the equatorial Pacific and the linking of tropical Pacific sea surface temperature variations to Walker's Southern Oscillation meant that the coastal warmings were simply one regional aspect of a much larger climate oscillation involving both atmosphere and ocean. This global pattern of variability is now called the El Niño/Southern Oscillation (ENSO) cycle. With this new understanding of the global scope of the ENSO cycle, the term El Niño, first applied to the annual warm current off the Peru coast and later to the occasional strong warmings in that area, is now often used, in a global sense, to denote the warm phase of the ENSO cycle. The term La Niña ("little girl") is sometimes used to denote the cold phase.

ORIGIN OF EL NIÑO

The cold Peru Current sweeps northward along the South American coast from southern Chile toward the equator. At first attributed to the equatorward flow of colder water from the south, oceanographers later discovered that the low sea surface temperatures along the Peru coast are primarily due to the "upwelling" of cold water from below the surface. However, near the end of each year, a seasonal warming takes place as a southward flowing coastal current, counter to the main Peru Current, develops. Centuries ago, the local fishermen named this the "Corriente del Niño" or in English the "Christ Child Current" because it appeared around the Christmas season.

The local residents also observed that this annual ocean warming differed from year to year; every few years it was unusually intense. With time, the term El Niño became more closely associated with these occasional intense warmings than with the more typical annual warmings.

of ENSO conditions in the Pacific. Detailed circulation anomalies for South America and Australia are highlighted in Figures 2.8 and 2.9 respectively.

2.4

CIRCULATION INDICES

The atmospheric circulation exhibits substantial low-frequency variability. These low-frequency fluctuations often strongly influence the temperature and precipitation patterns observed during a given month or season and are also accompanied by major shifts in the location and intensity of the jet stream and significantly influence

Figure 2.8 – Significant weather and circulation anomalies over South America during the period June 1991-November 1993 (from CPTEC/Instituto Nacional de Pesquisas Espaciais, Brazil).

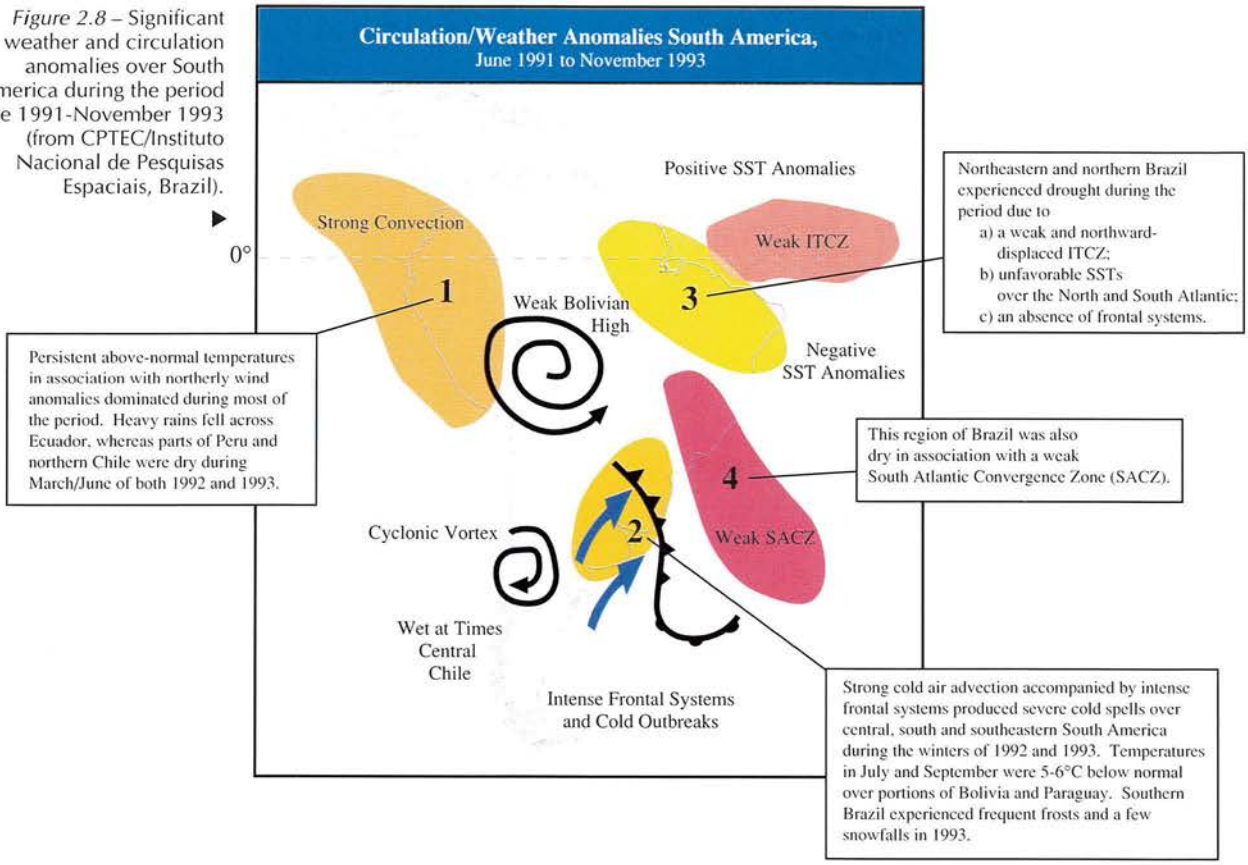

Figure 2.9 – Significant circulation and weather anomalies over Australia during the period June 1991-November 1993 (from National Climate Centre, Bureau of Meteorology, Melbourne, Australia and the National Institute of Water and Atmospheric Research, Ltd., Wellington, New Zealand).

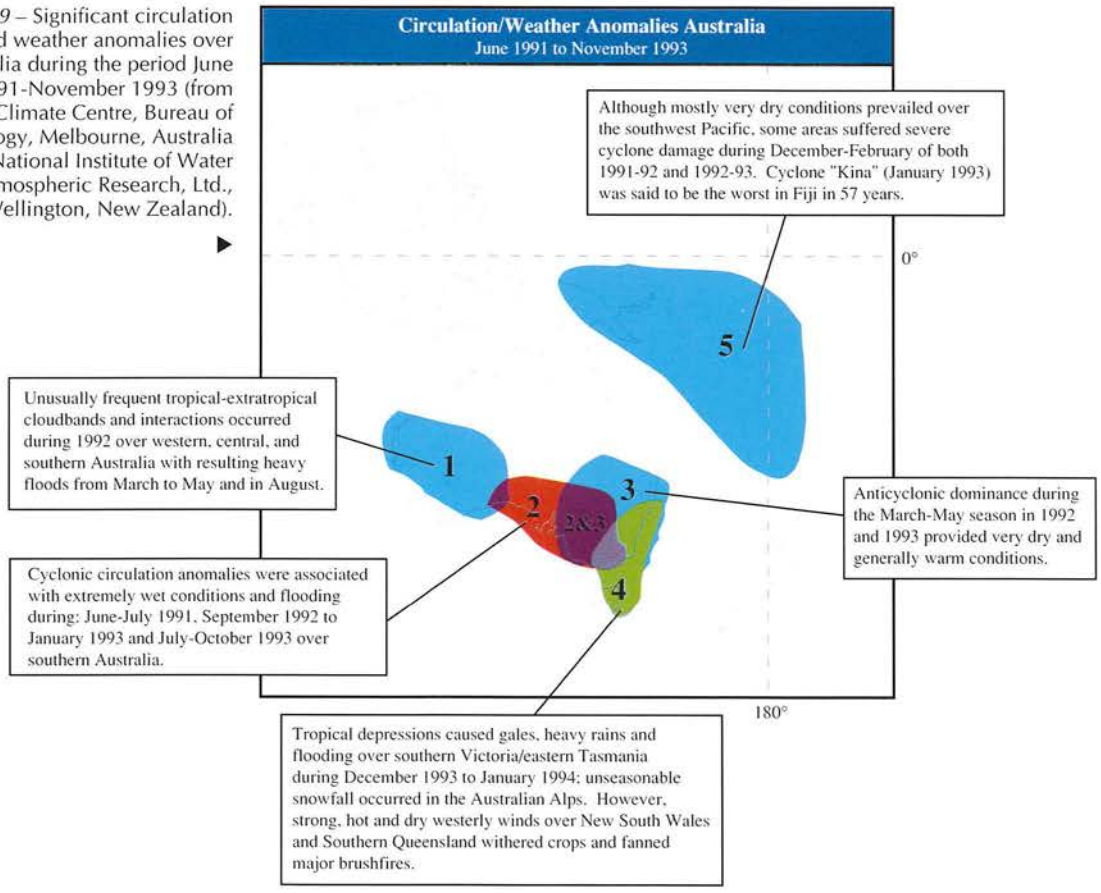

storm frequency, intensity and position. Recurrent patterns of low-frequency variability are often referred to as "teleconnections". The primary teleconnection patterns are centred over the North Pacific, North America and North Atlantic/European sectors.

Pacific/North American Pattern - PNA

The positive phase of the Pacific/North American pattern

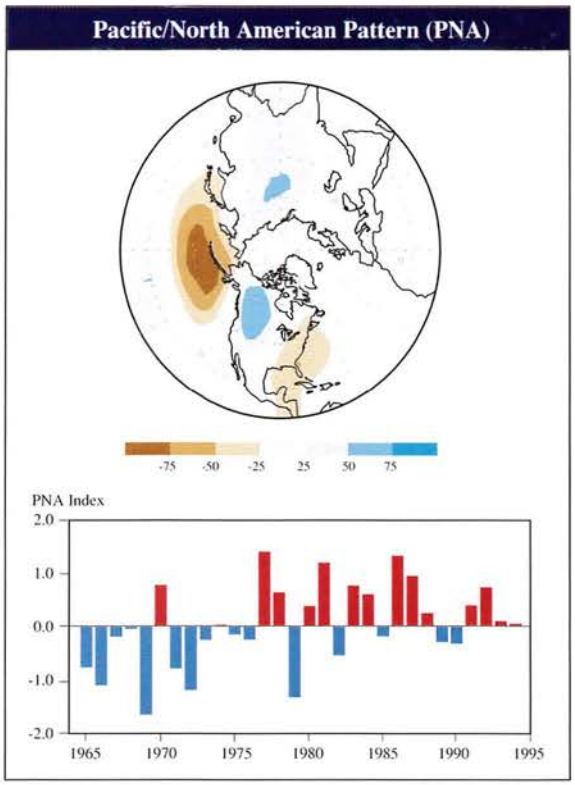

▲ *Figure 2.10.1 – top:* shown is the typical positive index Pacific-North American (PNA) pattern during the December-February season with isolines relating to the 700 hPa pressure-level height anomalies; *bottom:* standardized time series of the seasonal PNA pattern. The pattern and time series are determined by performing an orthogonally rotated principal component analysis (RPCA) of northern hemisphere monthly mean 700 hPa Heights for the December-February (DJF) period between 1964 and 1994. Year on the x-axis denotes the end of the winter season. This analysis is identical to that performed by Barnston and Livezey (1987), except that these patterns were computed for the entire DJF season, instead of for each month independently (from NOAA/NWS/NMC/CAC, Washington, DC).

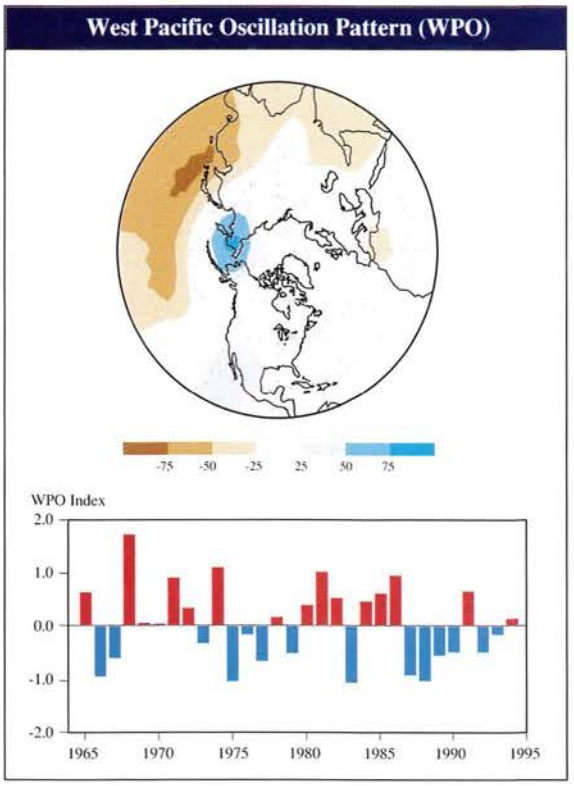

▲ *Figure 2.10.2* - same as Figure 2.10.1, except for the West Pacific Oscillation (WPO) (from NOAA/NWS/NMC/CAC, Washington, DC).

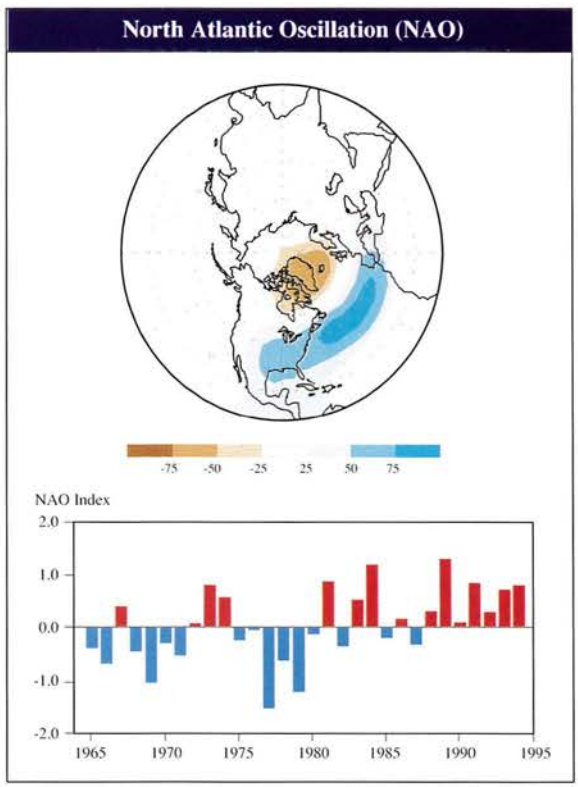

▲ *Figure 2.10.3* - same as Figure 2.10.1, except for the North Atlantic Oscillation (NAO) (from NOAA/NWS/NMC/CAC, Washington, DC).

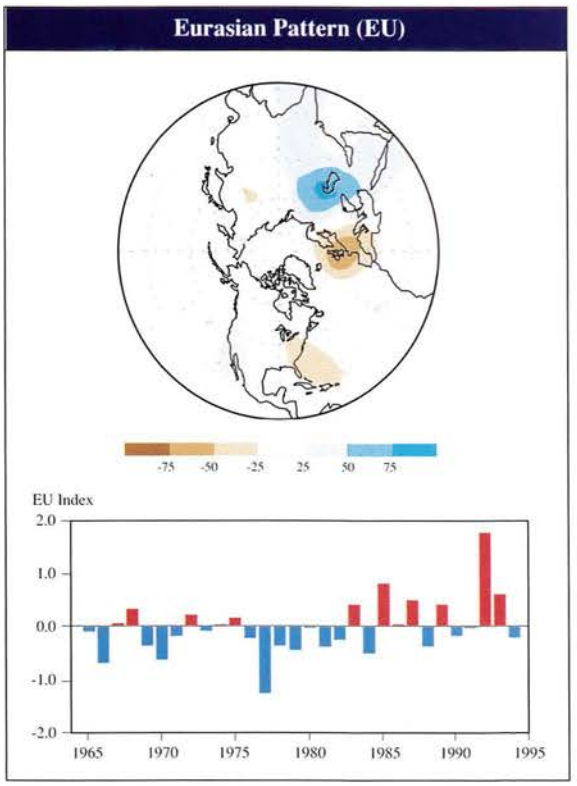

▲ *Figure 2.10.4* - same as Figure 2.10.1, except for the Eurasian (EU) pattern (from NOAA/NWS/NMC/CAC, Washington, DC).

(Figure 2.10.1) reflects above-normal pressure-level heights in the atmosphere over the subtropical eastern North Pacific and over western North America and below-normal pressure-level heights over the Gulf of Alaska and the southeastern USA. The negative phase of the PNA has pressure anomalies of opposite sign in these regions.
Positive phases of the PNA pattern tend to occur during periods of the El Niño phase of the ENSO cycle over the tropical Pacific, while negative phases of the pattern are sometimes observed during La Niña episodes. In association with the long-lived warm episode, the PNA index was above-normal during the winters of 1991-92 and 1992-93. However, large positive and negative phases of the pattern occur regularly and the development and decay of these patterns is driven largely by internal atmospheric dynamics, rather than by a direct response to external atmospheric forcing.

West Pacific Oscillation - WPO

The West Pacific Oscillation (Figure 2.10.2) is associated with large north-south variations in the entrance region of the western Pacific jet stream. The positive phase of the WPO is associated with above-normal pressure-level heights over the Bering Sea and eastern Siberia and with below-normal pressure-level heights east of Japan. This pattern reflects a weakening of the Pacific jet stream at high latitudes of the western North Pacific and a strengthening of the jet stream over the lower extratropics of the western North Pacific.
The negative phase of the WPO reflects wind and pressure-level height anomalies of the opposite sign in these regions. The WPO was slightly negative during both 1991/92 and 1992/93. As with the PNA pattern, the WPO exhibits considerable annual variability and much of this variability occurs independently of conditions in the tropical Pacific associated with the ENSO cycle.

Figure 2.11 – Standardized anomalies of the northern hemispheric zonal index computed over the band from 35-65°N for the winter season (November-March). Anomalies are computed from the 1970-71 to 1989-90 base period. Year on the x-axis denotes the end of the winter season (from Deutscher Wetterdienst, Seewetteramt, Hamburg Germany). ▶

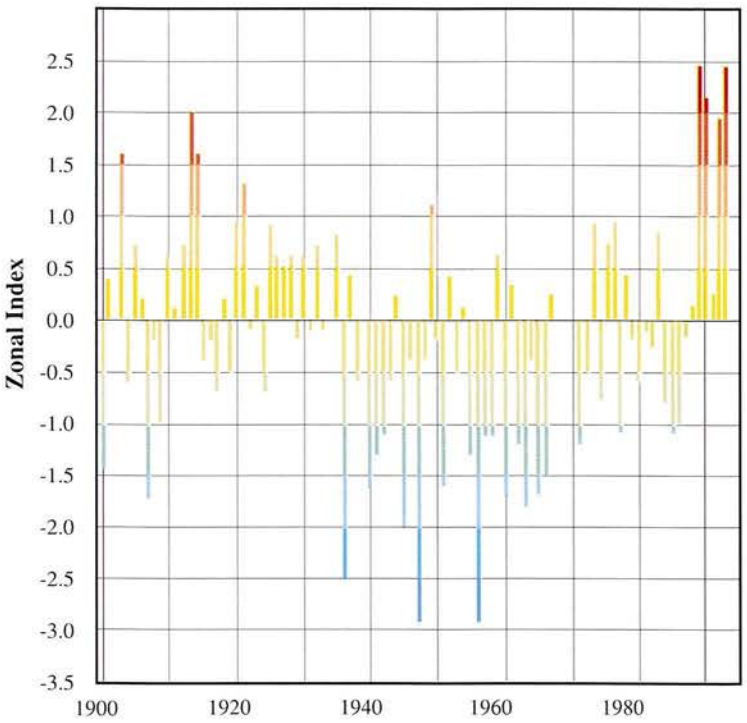

North Atlantic Oscillation - NAO

The North Atlantic Oscillation (Figure 2.10.3) is a prominent teleconnection pattern in all seasons. Pronounced positive and negative phases of this pattern are particularly noteworthy, since they are associated with anomalous weather from eastern North America to central Europe, when the winter air temperature seesaw occurs between Greenland and northern Europe and there are dramatic variations in the distribution and intensity of cyclone activity over the North Atlantic. After the winter of 1987/88, seven consecutive winters have recorded positive NAO patterns. This extreme persistence of the positive NAO is unprecedented in the past 30 years. The positive NAO is generally accompanied by an abnormally intense low pressure-level-height centre over Iceland and by above-normal pressure-level heights throughout the middle latitudes of the North Atlantic. The positive NAO is also associated with enhanced westerlies across the North Atlantic in middle and high latitudes, below-normal temperatures in the Greenland-Labrador area and in the Middle East and above-normal temperatures in the eastern USA and Europe (Walker and Bliss 1932, Wallace and Gutzler 1981). The negative phase of the NAO reflects circulation, temperature and precipitation anomalies of the opposite sign.

Eurasian Teleconnection Pattern - EU

The Eurasian teleconnection pattern (Figure 2.10.4) reflects a wave-like pattern of circulation anomalies that extends across western Europe and much of central Russia. Positive phases of this pattern are associated with above-normal pressure-level heights throughout Europe and below-normal pressure-level heights over the Caspian Sea sector. Persistent positive phases of the EU pattern often reflect major blocking anticyclones that become centred over Europe. During these periods, severe cold-air outbreaks are observed over eastern Europe and western Russia and, in severe cases (1991/92), these cold outbreaks can extend southward to the eastern Mediterranean Sea and the Middle East. In contrast, negative phases of the EU are often accompanied by abnormally warm conditions over much of eastern Europe and western Russia and often by above-normal precipitation throughout southern Europe and the Mediterranean Sea.

Zonal Index

A zonal index (Figure 2.11), computed as the difference in

Figure 2.12 – Number of North Atlantic low pressure systems (950 hPa and lower, counted once per lifetime) determined from four to eight weather maps per day for the winter season (November-March 1956 to 1994) (from R. Franke, Deutscher Wetterdienst, Seewetteramt, Hamburg Germany). ▶

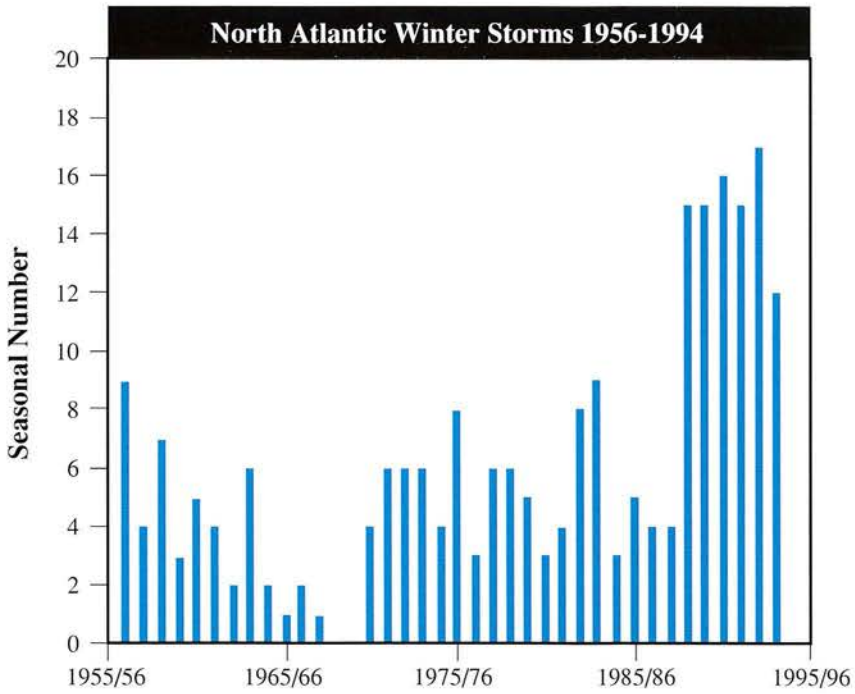

THE NORTH ATLANTIC OSCILLATION *

The North Atlantic Oscillation (NAO) is the alternation of atmospheric mass between the subtropical and subpolar regions of the North Atlantic Ocean. It was named and first described by Sir Gilbert Walker in a series of papers in the 1920s and 1930s on weather correlations. NAO is characterized by variations on monthly and seasonal time-scales in the regional sea-level pressure gradient, the mid-latitude westerlies, sea surface temperatures and the climate of adjacent land areas. As with ENSO, the NAO can be defined in terms of pressure variability at key centres of action. One centre is over the Azores, under a subtropical high pressure cell, and the other is over Iceland where relatively low sea-level pressure predominates in all seasons. The NAO occurs throughout the year but its role in the circulation and climate variability outside of winter is not as well understood.

The positive mode of the NAO is where the subtropical high is anomalously strong while the Icelandic low is simultaneously very deep. The Atlantic westerlies are then abnormally strong and warm surface ocean water and mild air masses advect northeastward across the Atlantic toward Europe and the Atlantic Arctic. Western Greenland and Labrador are unusually cold and large amounts of sea ice may be transported southward from Davis Strait. In the negative mode of the NAO, the two pressure centres are both anomalously weak. The Icelandic low is displaced to the southwest near Newfoundland while atmospheric blocking patterns occur in the flow aloft and polar anticyclones push southward over the eastern Atlantic and Europe. The winters of this mode are comparatively mild in Greenland but they are unusually harsh in northern and western Europe and are often long remembered by the populace. Some examples are the winters of 1941-42, 1962-63 and 1968-69. It has been argued that the negative mode of the NAO is a good analogue to the atmospheric circulation that prevailed during both the European Little Ice Age, from about 1450-1850, and the last ice age glacial maximum. Temperature and precipitation variations associated with the NAO also extend to the eastern USA and the countries of the Mediterranean basin.

The NAO and ENSO are disparate in the sense that circulation and climate variations in the northern hemisphere associated with each take place in different regions (Rogers, 1984). The approximately three-to-seven year quasi-periodicity of ENSO is not a prominent characteristic of the NAO. The winter index of the NAO has a near-biennial high-frequency variability on the interannual time-scales (see Figure 2.13, light line) but it also exhibits multiple-decade trends in which it generally tends to have the same sign persistently over longer periods of time (bold line in Figure 2.13). The index was generally positive in the milder period from 1905 to 1940 but was negative in the 1960s and in the late 1970s, as well as during the late nineteenth century. Our understanding of the role of the Atlantic in global climate variability is rapidly improving through the efforts of ongoing and proposed international research programmes.

** Adapted from a contribution by Jeffrey C. Rogers, Department of Geography, The Ohio State University*

zonally averaged sea-level pressure between 35 and 65°N, shows that for the November-March season, the strength of the north-south pressure gradient over the past five years has been unprecedented. This index has exceeded two standard deviations in three of the past five winters. This is also consistent with the large increase in observed intense extratropical cyclones (central pressure less than 950 hPa) in the North Atlantic (Figure 2.12) since the winter of 1988/89.

2.5

NORTHERN HEMISPHERE WINTER BLOCKING

Atmospheric blocking is associated with large weather anomalies that persist on time-scales of one week to one season (Korovkina, 1989). A blocking episode is defined as the occurrence of at least seven consecutive days during which large positive 500 hPa geopotential height deviations from the corresponding latitudinal mean persist at a given point (Gruza and Korovkina 1991a, b). Blocking indices characterize seasonal total duration (TD) and intensity (TI).

Time series of seasonal blocking indices were averaged for three sectors of the latitudinal zone 40-70°N: Atlantic-Europe (AE) (40°W-30°E); Eurasia (EA) (40-100°E); and Pacific Ocean-North America (PA) (180°-110°W) (Figure 2.14). These are regions

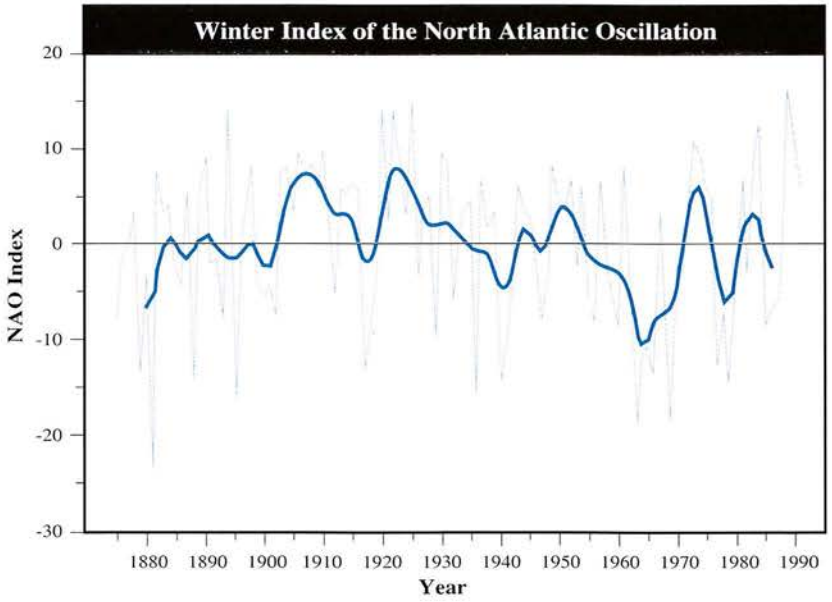

▲ *Figure 2.13* – Time series of the winter index of the North Atlantic Oscillation (NAO) (light line), obtained by subtracting the mean pressure departure in Iceland from that over the Azores. Year on the x-axis denotes the end of the winter season. The binomially filtered index values (bold line) represent low frequency variations in the NAO.

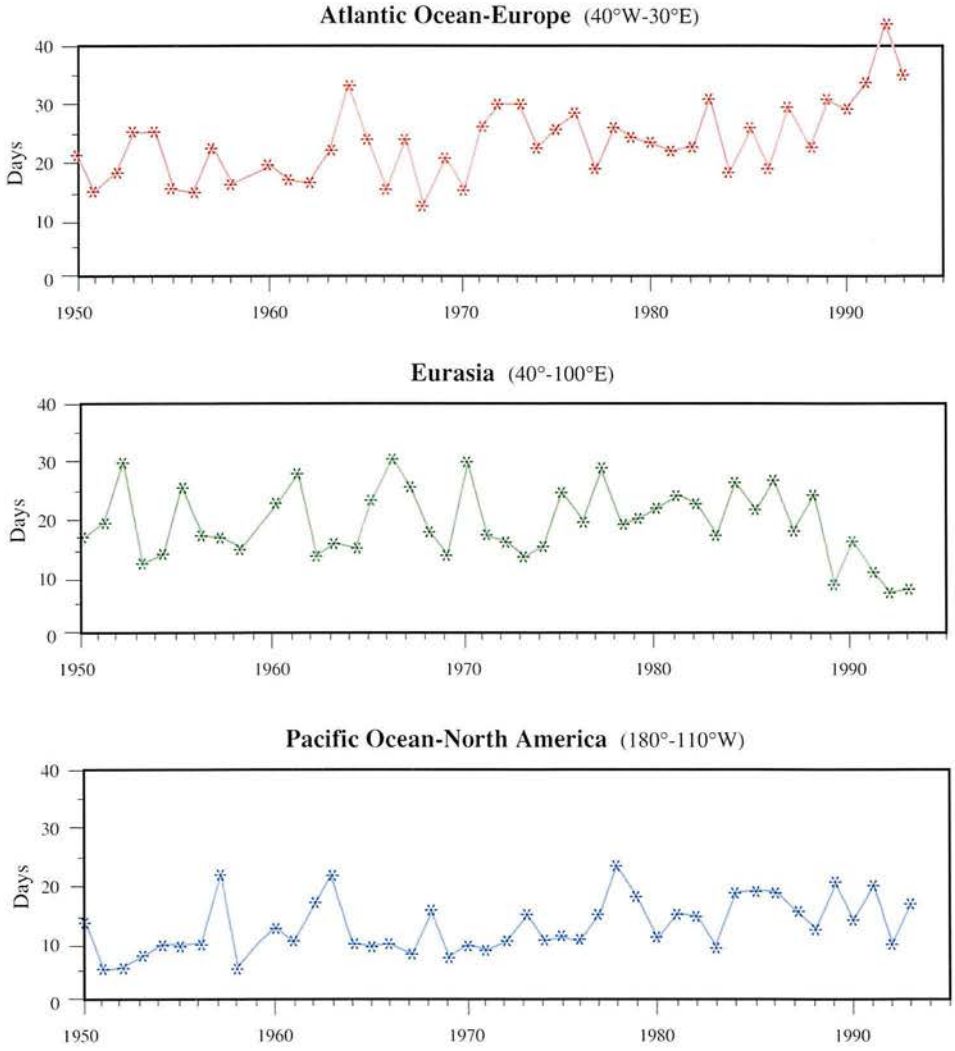

◀ *Figure 2.14* – Time series of regionally averaged winter season (mid-November to mid-March) total blocking duration in the 40-70°N latitudinal band for Atlantic Ocean-Europe (40°W-30°E); for Eurasia (40-100°E); and for Pacific Ocean-North America (180°-110°W).
A blocking episode at a point of a 5x10 grid is defined as a large positive 500 hPa geopotential height deviation (greater than one standard deviation) from the latitudinal mean lasting for seven or more days (from Institute for Global Climate and Ecology, Moscow).

where blocking duration maxima were concentrated during the 1949-1993 period. These time series suggest the tendency for increased blocking in recent years in the sector AE in winter, with a simultaneous decrease in blocking observed over the EA region. This is suggestive of a westward shift in blocking activity throughout Europe and Asia. During the winter of 1991-92, record-high blocking activity was observed (maximum values of the regional blocking indices TD reached 44 days) over AE sector.

The blocking indices presented in Figure 2.15 characterize duration (TD in days) and intensity (TI in decameters) at 60°N latitude as a function of longitude for winters 1991-92 and 1992-93. A period of non-interrupted blocking was observed during the entire 1991-92 winter over the AE sector. This blocking situation was associated with a warmer and drier than normal winter in the latitudinal zone 50-70°N of the AE sector (positive seasonal temperature anomalies reached 5-6°C in eastern Europe), while colder and wetter than normal conditions were observed south and northward of the block. Blocking during spring, summer and fall of 1992 (not shown) was near the 30-year mean. During the winter of 1992-93, blocking duration and intensity was again above normal over the AE sector, although not as persistent or strong as during the previous winter.

Figure 2.15 – Northern hemisphere blocking indices for the 1991/92 and 1992/93 winter seasons: duration in days (TD) and total intensity in decameters (TI) at 60°N latitude as a function of longitude. Blocking is defined as a positive 500 hPa geopotential height deviation from the latitudinal mean value for seven or more days. TD values are shown by a downward dashed line; TI, by an upward solid line across every 10° of longitude. The 30-year mean (1951-1980) is shown by a solid curve (from Institute for Global Climate and Ecology, Moscow).

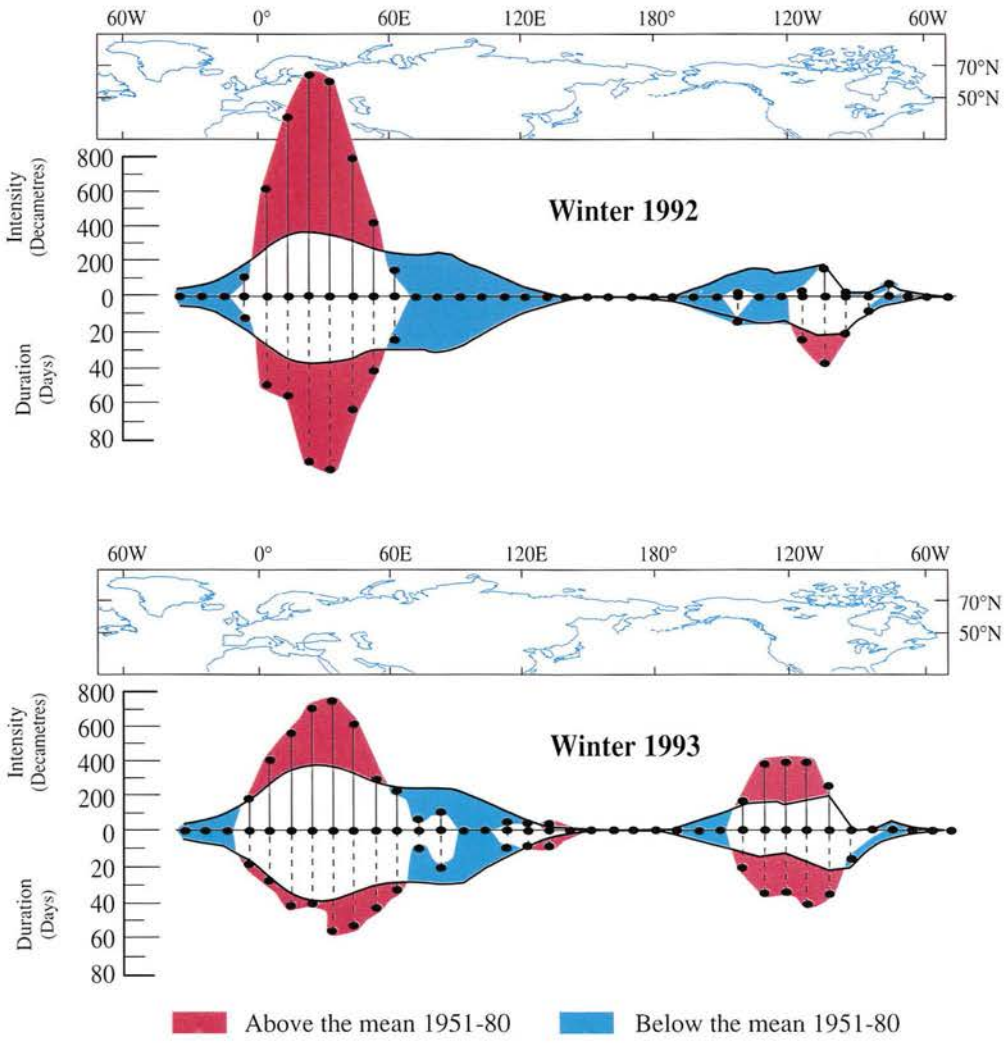

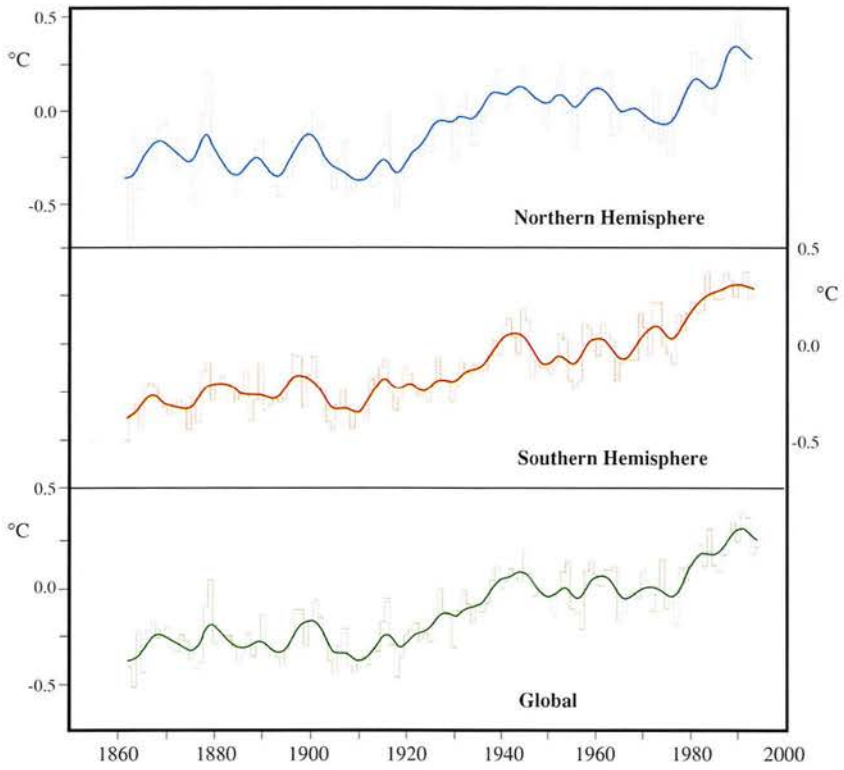

Figure 3.1 – Average annual temperature anomalies for the land and marine regions of both hemispheres and their average, i.e., the global series. Anomalies are computed departures from the 1951-80 mean values. The smooth lines depict variations on decadal and longer time-scales (from IPCC, Hadley Centre, UK Meteorological Office and Climatic Research Unit, University of East Anglia).

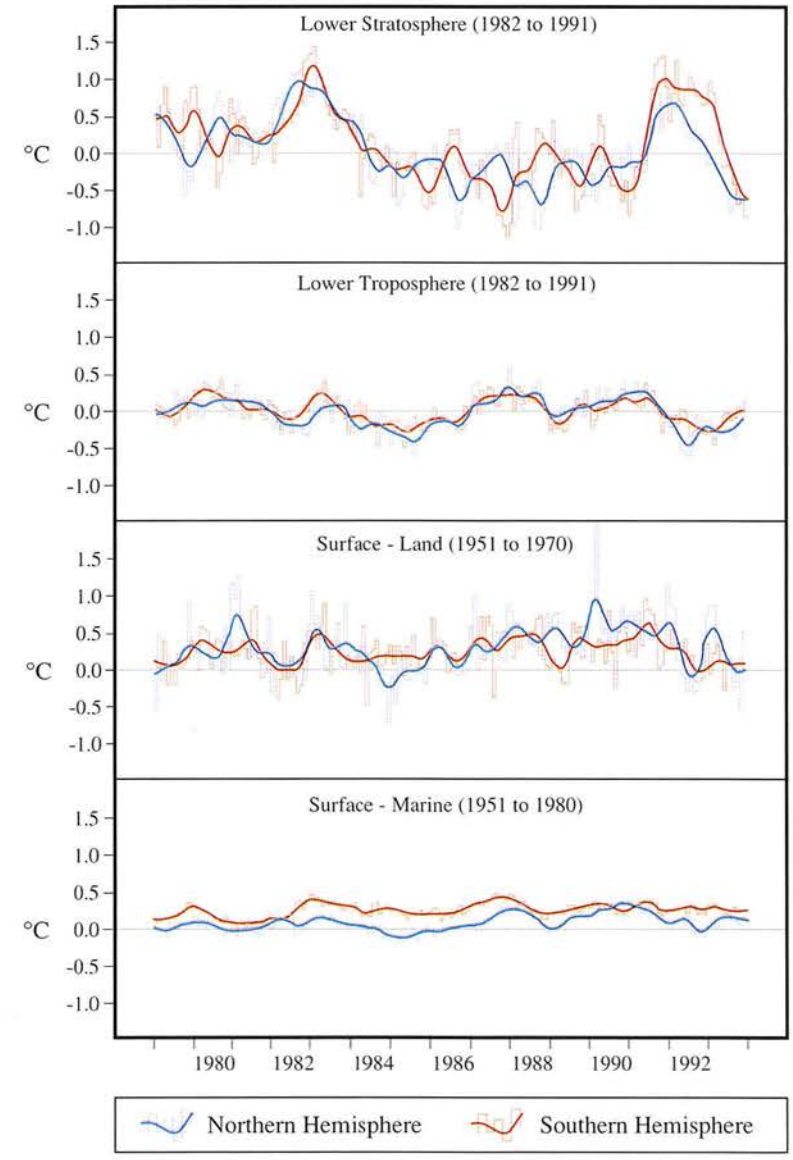

Figure 3.2 – Monthly temperature anomalies for the northern and southern hemispheres for four different domains: lower stratosphere (MSU Channel 4, Spencer and Christy, 1993, revised), lower troposphere (MSU Channel 2R, Spencer and Christy, 1992, revised), land surface (Jones and Briffa, 1992) and ocean surface (Folland and Parker, 1991). Anomalies are computed departures from the mean values over the periods shown in parentheses.

TEMPERATURE – SURFACE COOLING AND VOLCANIC ACTIVITY

CHAPTER 3

3.1 GLOBAL AND HEMISPHERIC TEMPERATURE TRENDS

Since the last review period (December 1988 - May 1991), surface temperatures averaged globally have cooled slightly, although the average values for 1992 and 1993 are still at the mean level experienced during the 1980s. Figure 3.1 shows the time series of hemispheric and global temperature departures from the mean for the period 1951-1980 back to the mid-nineteenth century. Global average values for 1991, 1992 and 1993 are 0.35, 0.17 and 0.21°C above those for the 1951-80 reference period. Values for the northern hemisphere for 1991, 1992 and 1993 are 0.35, 0.13 and 0.18°C above and for the southern hemisphere, 0.35, 0.21 and 0.24°C, above. The value for 1991 makes it the warmest of the entire record period except for 1990 (0.39°C). The subsequent drop in global temperature, while it may have been due to intrinsic climatic variability, is probably related to the volcanic dust and debris injected into the stratosphere by the explosive eruption of Mount Pinatubo in the Philippines in June 1991. Global and northern hemisphere temperatures were slightly higher in 1993 than in 1992, the coldest year since 1985, but the eighth warmest year since 1951.

Looking at the last 15 years in more detail, various temperature

June, July and August 1991

Average Temperature Anomaly 0.42°C

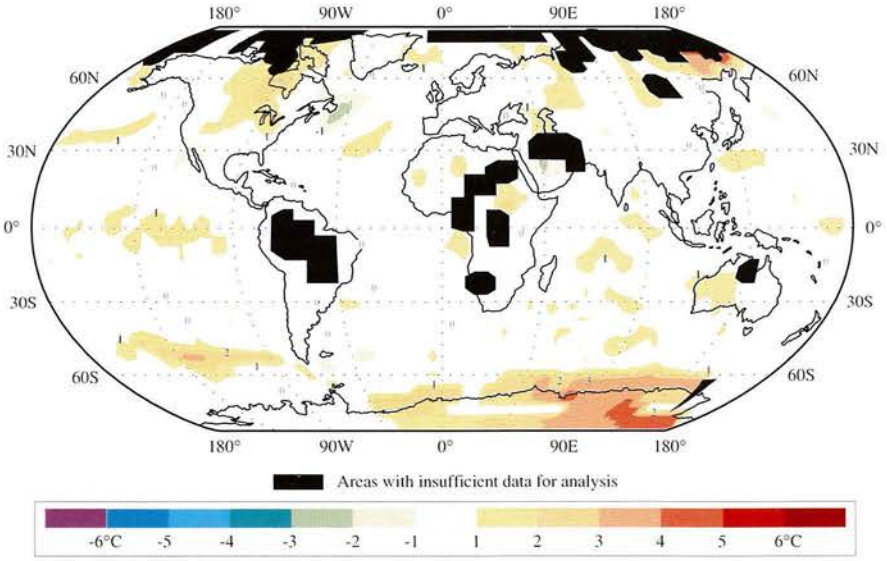

Figure 3.3.1

December1991, January and February 1992

Average Temperature Anomaly 0.34°C

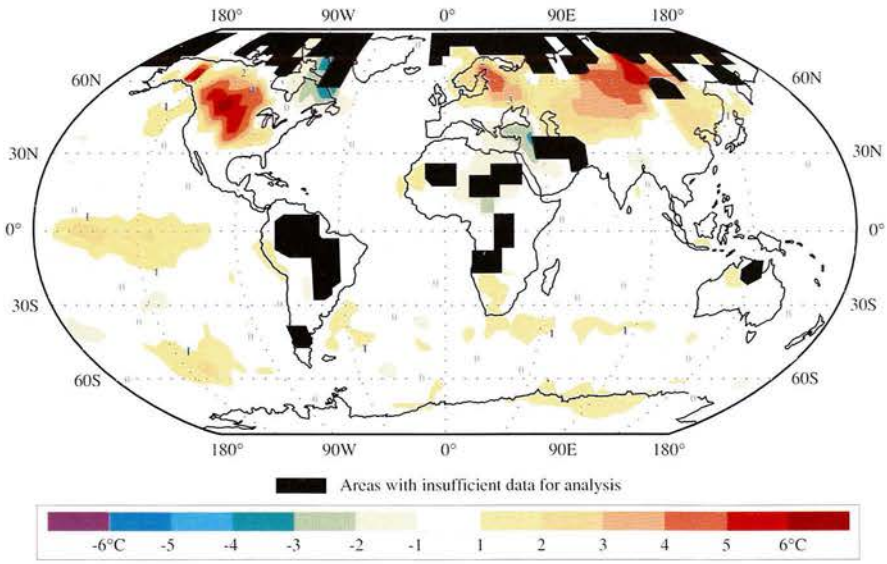

Figure 3.3.2

June, July and August 1992

Average Temperature Anomaly 0.11°C

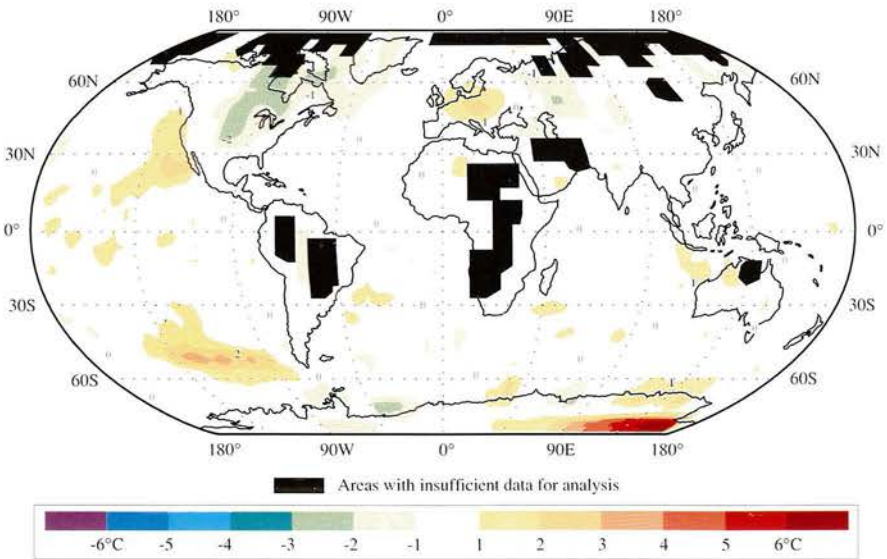

Figure 3.3.3

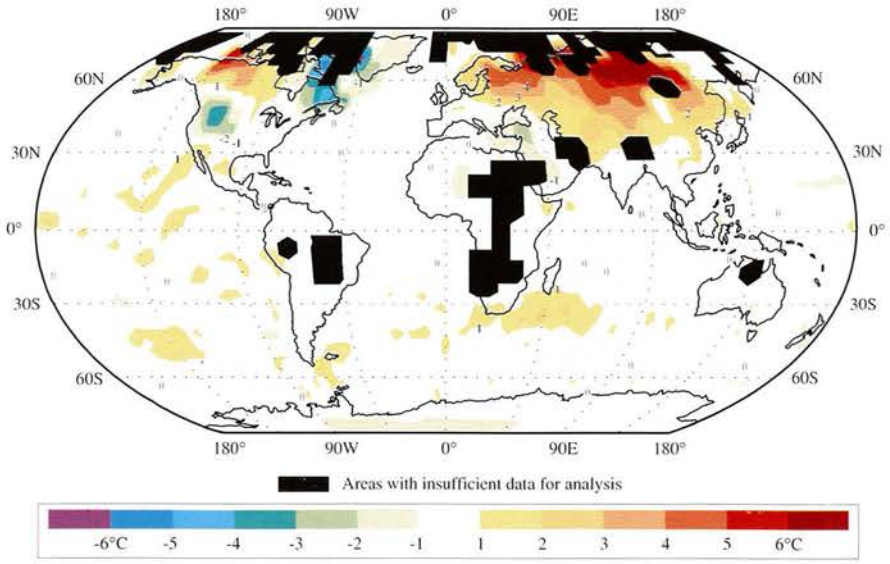

Figure 3.3.4

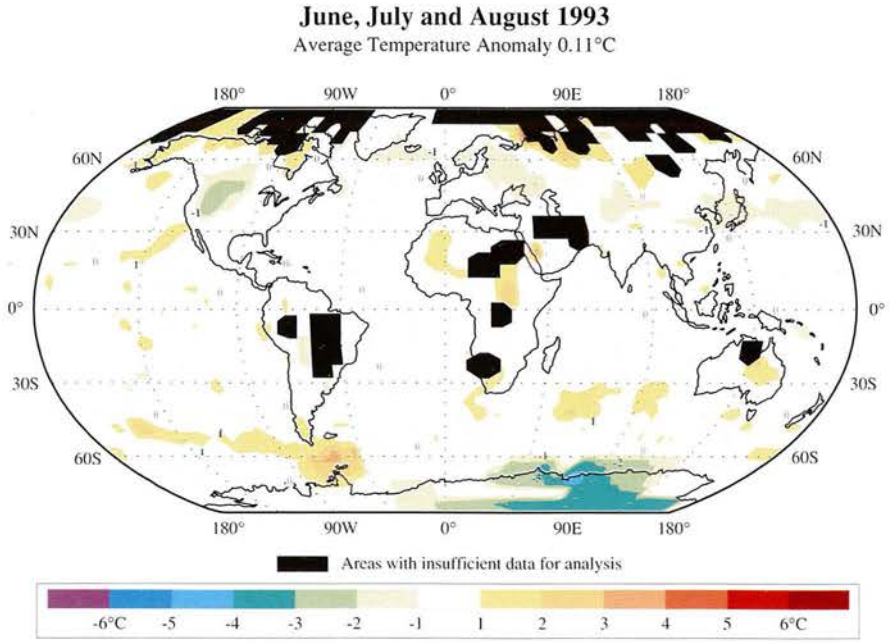

Figure 3.3.5

◀ ▲ *Figure 3.3.1 to Figure 3.3.5* – Seasonal temperature anomalies for selected seasons during the review period June-August 1991 to September-November 1993. Anomalies are computed departures from mean values for the reference period 1951-80. Areas with missing land data are shaded black (from a combined surface temperature analysis produced at the Climatic Research Unit, University of East Anglia (land) and the Hadley Centre, UK Meteorological Office (ocean). Over all oceanic areas, except the Arctic Ocean, any gaps have been infilled with analyses from satellite data produced at the NOAA/NWS/NMC/CAC, Washington, DC).

series (Figure 3.2) for both hemispheres, shows a number of intriguing features. Temperatures in the lower stratosphere warmed by about 1°C following both the Mount Pinatubo and the El Chichòn (Mexico in April 1982) eruptions, but by the end of 1993 had cooled to values near to the lowest ever recorded. The lower troposphere cooled by about 0.5°C more rapidly over the northern compared to the southern hemisphere. At the surface, cooling dominated but principally only over terrestrial areas in the northern hemisphere. Cooling was smaller in magnitude over oceanic areas and over the terrestrial southern hemisphere. The cooling over land in the north occurred principally between April and November with little change during winter months (December to March).

3.2 SEASONAL TEMPERATURE ANOMALIES

The main feature of the review period has been the cooler temperatures experienced over many regions as a result of the effects of the volcanic eruption. Selected seasonal temperature anomalies from June-August 1991 to June-August 1993 are shown in Figures 3.3.1-3.3.5. Overall, the coolest seasons were June to August (JJA) and September to November (SON) during both 1992 and 1993, with mean global temperatures near to their 1951-80 values. Terrestrial areas were relatively cooler than marine regions, which in most seasons show the cycle of temperature anomaly patterns

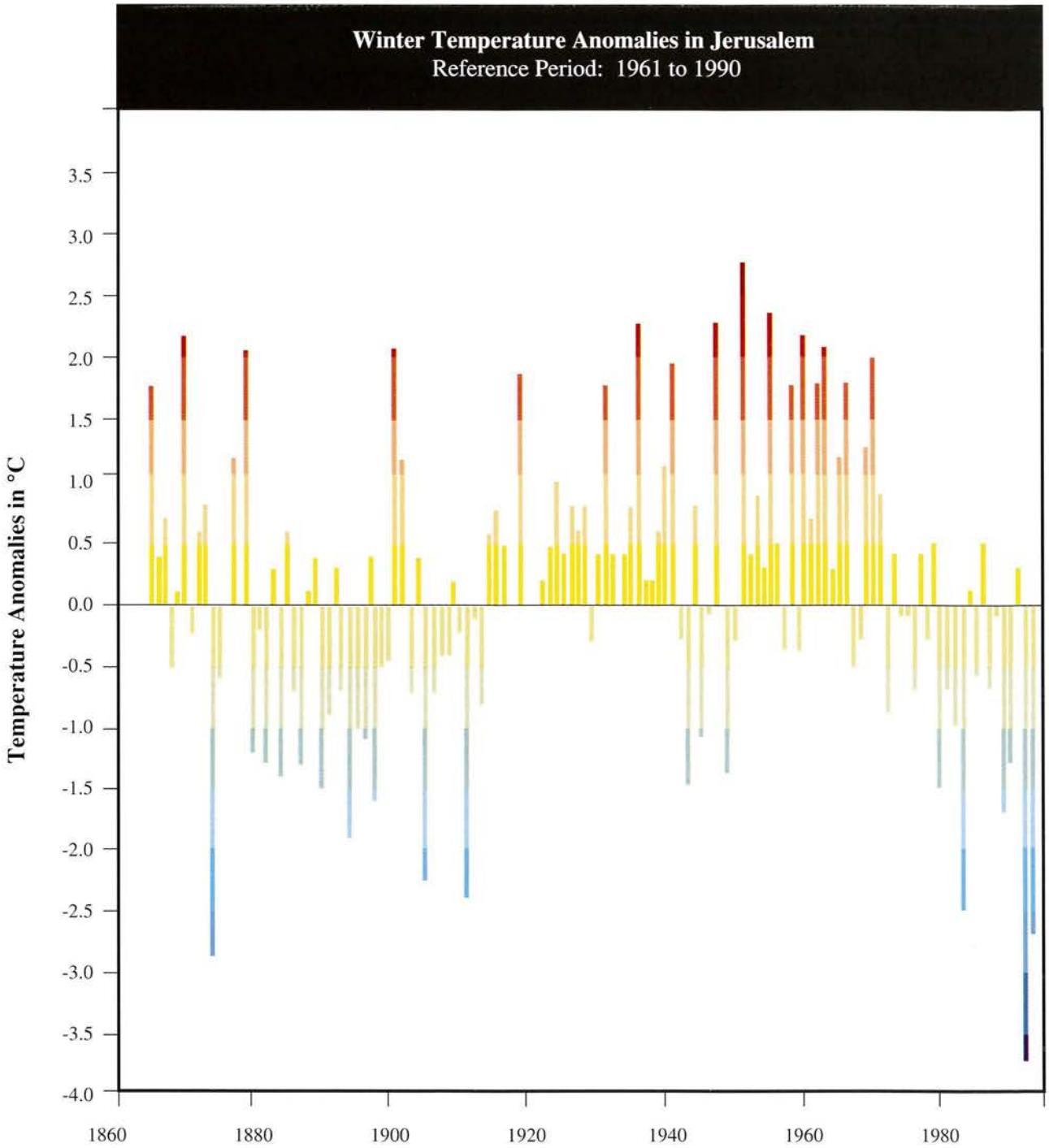

▲ *Figure 3.4* – Winter mean temperature anomaly time series for Jerusalem from December to March 1865 to 1993. Anomalies are computed departures from the 1961-1990 mean values (from Deutscher Wetterdienst, Seewetteramt, Hamburg, Germany).

expected during a warm ENSO event.

During the 1992 and 1993 JJA seasons, temperatures were cooler than normal over large parts of North America (eastern during 1992, western during 1993), Eurasia (Siberia during 1992 and northern and eastern Europe during 1993) and China. In the 1993 summer, the average temperature was 2°C below normal in central China from the Yellow River to the south side of the mid-lower Yangtze River basin. Record low temperatures, some 4°C below normal, occurred during the last week of July. North America and Eurasia continued to experience cool conditions during the SON season (eastern and central North America in both years, most of Europe and central Siberia in 1992 and all of Europe and western Siberia in 1993). Over the tropical continents during these seasons (JJA and SON) temperature anomalies were smaller in magnitude, but most significant departures were negative ones.

Temperatures during the other two seasons - December, January and February (DJF) and March, April and May (MAM) - were relatively warmer, particularly DJF. Positive temperature anomalies in both seasons were experienced over large parts of northern Eurasia and northwestern North America. However, unlike some recent winters, significant negative anomalies were evident during the northern winters in mid-latitude regions, in southern North America and north Africa and the Middle East.

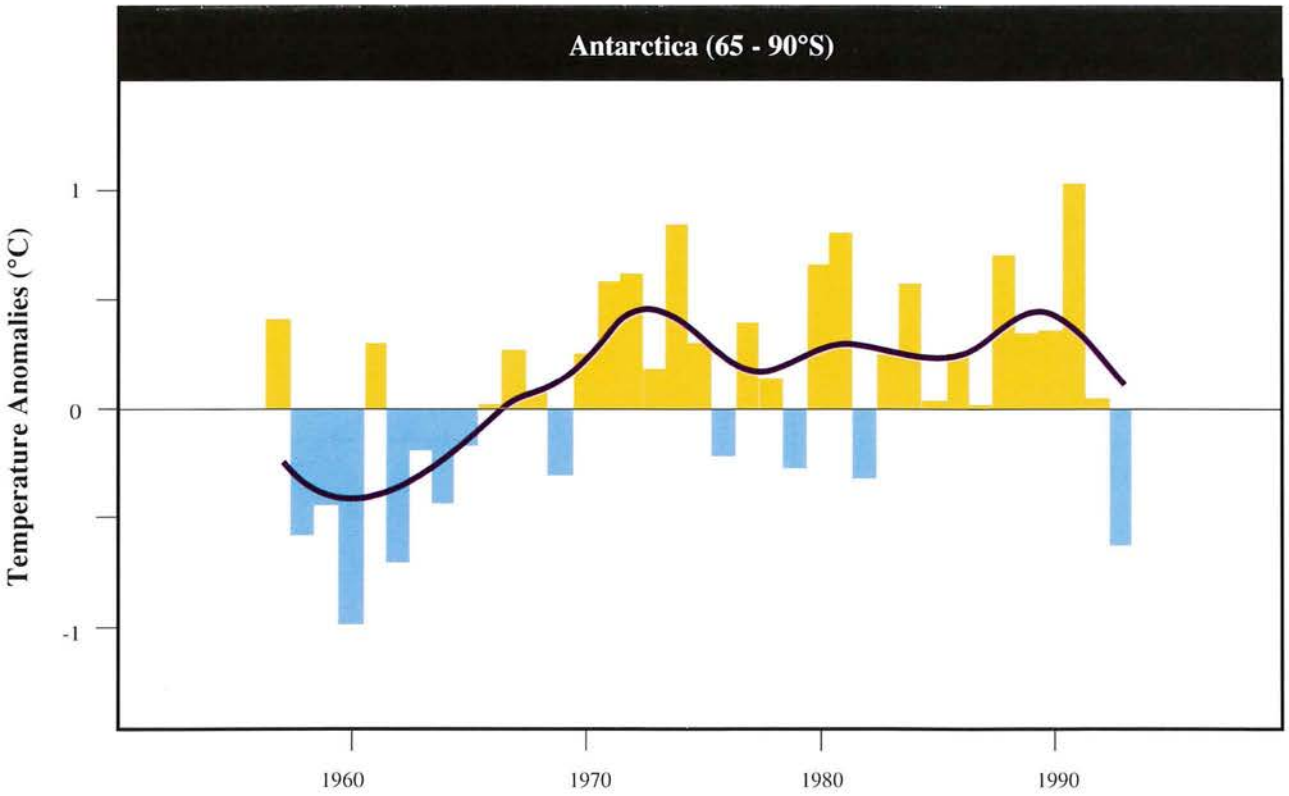

▲ *Figure 3.5* – Antarctic (65-90°S) annual temperature anomalies from 1957 to 1993.

3.3

TEMPERATURE EXTREMES 1991 TO 1993

The coldness of both winters in the Middle East was remarkable with rarely seen snowfall in many areas of north Africa and the eastern Mediterranean. Regions of Turkey were up to 7°C colder than normal with heavy snowfall and avalanches leading to many deaths. Blizzard conditions closed numerous roads and isolated villages and towns. Large cities such as Damascus, Beirut, Jerusalem and Amman were repeatedly paralysed by snow. The winter of 1991-92 was more anomalous, both in temperature and snowfall terms than that of 1992-93. Although not as harsh, this winter was still severe compared to most winters of the last 40 years. December to March 1991/2 was the coldest on record in Turkey (from 1930) and at Jerusalem (Figure 3.4) (from 1865).

Most land regions of the tropics and the southern hemisphere experienced conditions typical of a moderate warm ENSO event. Throughout most of the review period, New Zealand and the southwest Pacific were colder than normal with the cold conditions extending to Australia from time to time. In fact, New Zealand had its coldest year in 1992 (-0.94° with respect to 1951-80) since 1930. Argentina and southern Brazil experienced a number of cold outbreaks during the JJA and SON seasons, principally during 1992. Southern Africa began the study period warm (clearly related to prolonged drought in the region) but cooled to near-normal temperatures by the end of 1993.

3.4

ANTARCTICA – COOLING FOLLOWING RECORD WARM YEAR

The largest change in temperatures over any continent occurred over Antarctica between 1991 and 1993. Figure 3.5 shows that temperatures had been relatively stable during the 1970s and 1980s over the continent, having risen during the 1960s by 1°C above those experienced around 1960. Since the mid-1960s, temperatures have oscillated within a range of 0-1°C above the 1957-75 reference period. The warmest year of the entire record was 1991 at 1°C above the mean. Since the end of that year, temperatures across the continent have tumbled at most stations to the 1993 level, 0.6°C below the reference period, the third coldest temperature since comparative records began during the International Geophysical Year in 1957. This value had been lower on only two occasions (1960 and marginally in 1962). Thus, in three years, we have witnessed almost the entire range of observed temperatures across the continent. In 1993, the entire continent experienced cooler temperatures, although the drop has been least over the Antarctica Peninsula. Here, conditions were still clearly warmer than the 1957-62 period. Elsewhere, they have fallen back to their lowest observed values during that time.

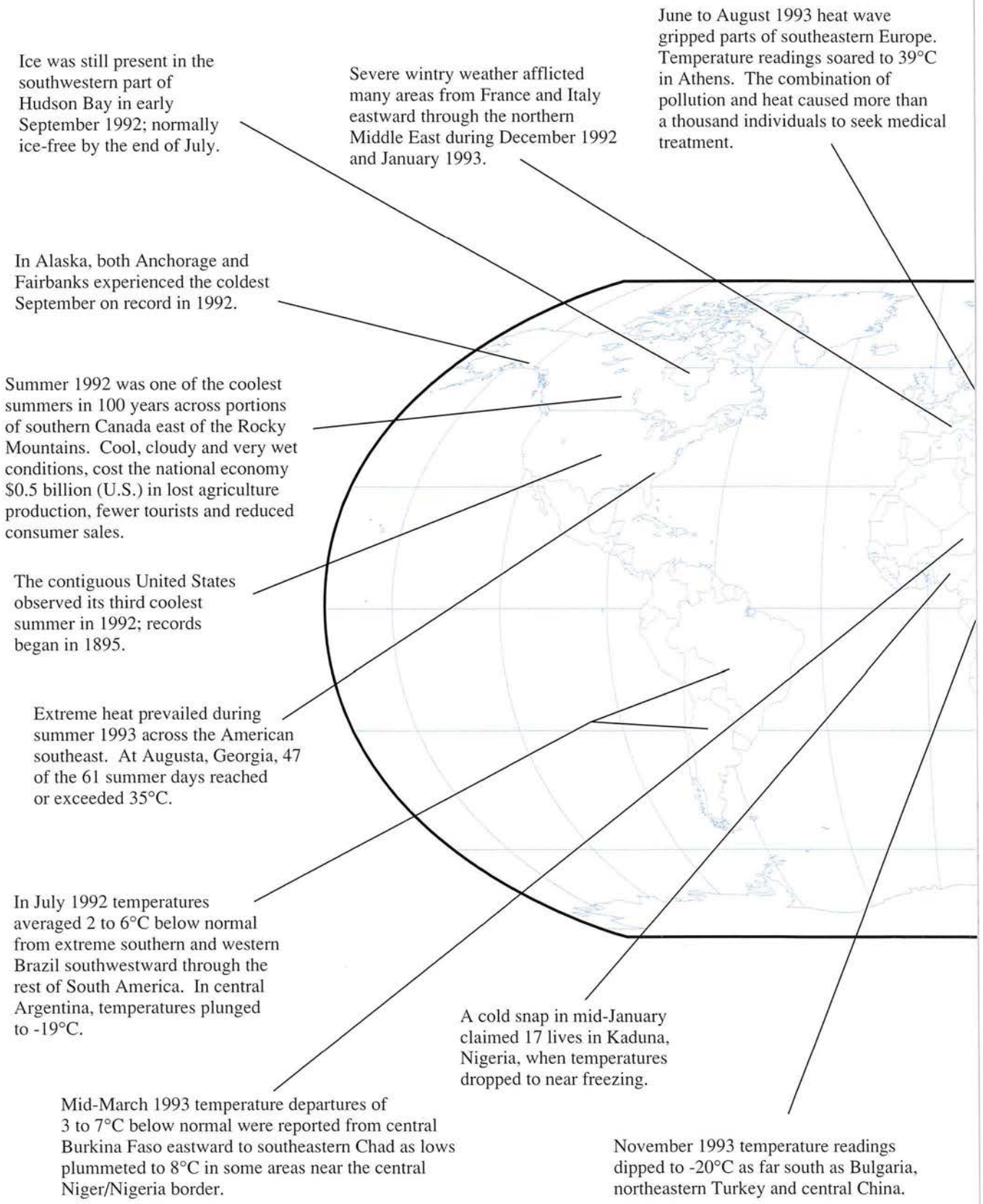

▲ *Figure 3.6* – Global temperature highlights for the review period, 1991-1993.

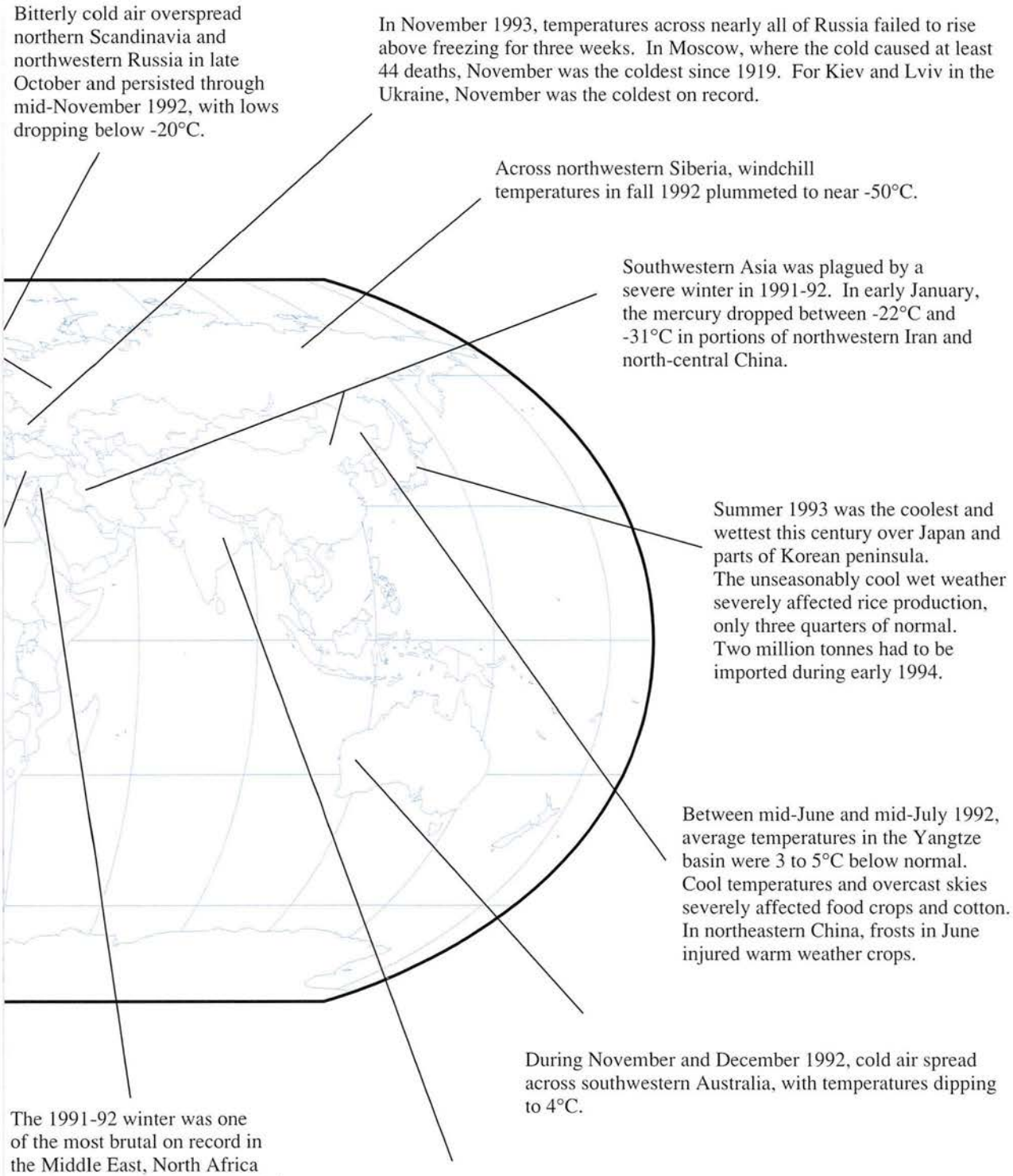

Bitterly cold air overspread northern Scandinavia and northwestern Russia in late October and persisted through mid-November 1992, with lows dropping below -20°C.

In November 1993, temperatures across nearly all of Russia failed to rise above freezing for three weeks. In Moscow, where the cold caused at least 44 deaths, November was the coldest since 1919. For Kiev and Lviv in the Ukraine, November was the coldest on record.

Across northwestern Siberia, windchill temperatures in fall 1992 plummeted to near -50°C.

Southwestern Asia was plagued by a severe winter in 1991-92. In early January, the mercury dropped between -22°C and -31°C in portions of northwestern Iran and north-central China.

Summer 1993 was the coolest and wettest this century over Japan and parts of Korean peninsula. The unseasonably cool wet weather severely affected rice production, only three quarters of normal. Two million tonnes had to be imported during early 1994.

Between mid-June and mid-July 1992, average temperatures in the Yangtze basin were 3 to 5°C below normal. Cool temperatures and overcast skies severely affected food crops and cotton. In northeastern China, frosts in June injured warm weather crops.

During November and December 1992, cold air spread across southwestern Australia, with temperatures dipping to 4°C.

The 1991-92 winter was one of the most brutal on record in the Middle East, North Africa and in extreme southwestern Asia. The upper-air flow forced both frigid Siberian air and moist subtropical air into the region, generating exceptionally cold, wet weather. In Israel, the winter was the worst in more than 100 years.

During January and February 1992, only 3 people were reported to have died from the effects of heat in India compared to the 275 who died from cold weather in Bihar.

MOUNT PINATUBO - THE JUNE 1991 ERUPTIONS

Mount Pinatubo (15°N, 121°E) was active for several days during mid-June 1991, with a cataclysmic eruption on June 15. Satellite instruments determined that the ensuing volcanic dust cloud initially reached heights of at least 35 km, well above the typical local tropopause at that time of year of about 17 km. Prevailing east-northeast winds of the middle and lower stratosphere transported the dust cloud in a general westerly trajectory. The cloud circled the earth in 22 days and, for the first months, was generally confined to a tropical belt of 20°S to 30°N latitude (Bluth et al., 1992). Later, as illustrated in Figure 3.7, the cloud dispersed into mid- and polar latitudes of the southern hemisphere (during the last quarter of 1991) and northern hemisphere (during the first quarter of 1992) (Trepte et al., 1993).

Figure 3.7 – Aerosol optical depth at 0.55 micrometres wavelength as a function of latitude and year (January 1991 to December 1992) as compiled from satellite, aircraft and ground-based measurements by Sate et al. (1993). Contour intervals are 0.01 optical depth units; colour change occurs at 0.1 units (from Dutton, private communication, 1994).

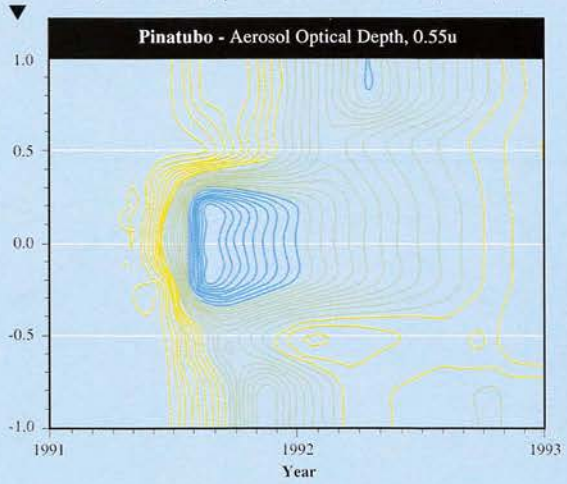

Stratospheric particles injected by the eruption only gradually settled out from the atmosphere. Volcanic particles, greater than 1 micron diameter, initially injected into the stratosphere settled out within a few months to a year. Small (less than one micron) sulphate particles, however, had a much longer lifetime. The sulphur dioxide (SO_2) cloud from Mount Pinatubo was rapidly converted into aqueous sulphuric acid - water vapour aerosols (droplets) and these, in turn, converted to ammonium sulphate aerosols over time (Sheridan et al., 1992). By the end of 1993, stratospheric aerosol concentrations were approaching background levels, but could still be detected by sensitive techniques (Figure 3.8).

The amount of material injected by Mount Pinatubo was greater than any eruption since Katmai, Alaska in 1912. The Katmai cloud did not spread much beyond the northern hemisphere mid-latitudes, however, due to its subpolar location. Most likely, Mount Pinatubo had a greater climatic impact than Katmai because of its tropical latitude, large SO_2 emissions and the pole-to-pole spread of its aerosols. Its impact probably approached that of Krakatoa in 1883, but was certainly less than Tambora in 1815.

The Mount Pinatubo eruption significantly increased the aerosol optical depth around the world. Visually, this was evident from unusually colourful skies during sunrise and sunset. It produced a measurable climate forcing of decreased solar radiation at the ground. Direct solar radiation decreased by 25-30% at several remote sites and monthly mean, clear-sky, total solar irradiance at Mauna Loa Observatory, Hawaii, decreased by 2.7% for the first ten months after the eruption (Dutton and Christy, 1992).

Figure 3.8 – The "apparent" transmission, or transmission ratio (Ellis and Pueschel, 1971), is derived from broadband (0.3 to 2.8 micrometre wavelengths) direct solar irradiance measurements at Mauna Loa Observatory in Hawaii. Data are for clear-sky mornings between solar elevations of 11.3 and 30.0°. The plotted points are monthly averages and the plotted curve results from a statistical smoother. The decrease in 1982 following the El Chichòn eruption is greater than that following Mount Pinatubo because the Mauna Loa Observatory was directly downwind in the path of the El Chichòn stratospheric dust plume (from Dutton, private communication, 1994).

Determining the impact of explosive volcanic eruptions on surface climate from observation data is not an easy matter. Numerical models indicate that such volcanoes should generate a global surface cooling of up to a few tenths of a degree Celsius on time-scales of months to a couple of years (Hansen et al., 1992). Perturbations of this kind are, however, close to the range of natural climatic variability on interannual time-scales, making identification difficult. The signal in the past from other eruptions has, for example, been obscured by the effects of ENSO (Jones and Kelly, 1988). Further difficulties in identification relate to the scarcity of eruptions over the instrumental climate period (about one eruption per decade), implying a small statistical sample and the paucity of surface climate data during the late nineteenth and early twentieth centuries. The final problem is that prior to the lidar measurements, which began in the 1950s, it is impossible to be certain which volcanic events had the greatest

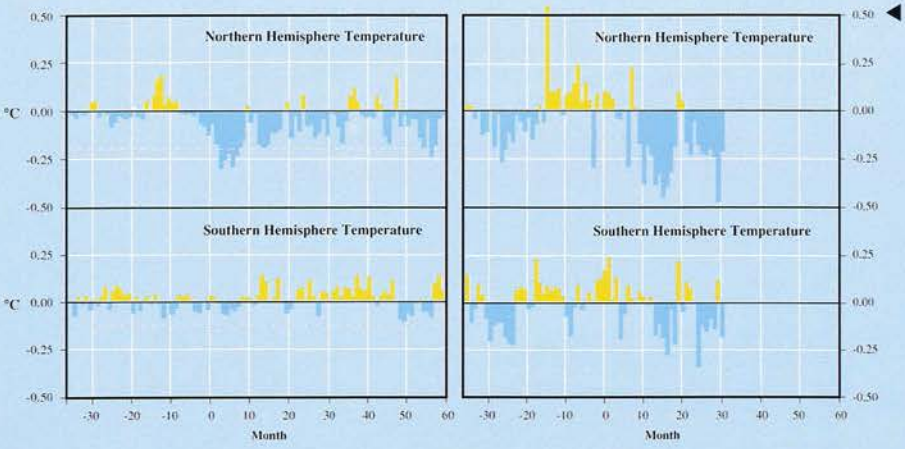

◀ *Figure 3.9 – Left:* Composite temperature profiles for the sample of five northern hemisphere eruptions. Month zero is the month of the eruptions and, for each of the five eruptions, the monthly surface temperature anomalies following the eruption are computed as departures from the relevant monthly mean for the three years prior to the event. The composite response is the average of the five events. Significance levels (the dashed line) are estimated using a Monte Carlo technique based on the generation of random eruption dates. *Right:* Hemispheric response following Pinatubo (month zero is June 1991). The last point plotted is December 1993 (month 30). It is not possible to estimate significance for one event (from IPCC, Hadley Centre, UK Meteorological Office and Climatic Research Unit, University of East Anglia).

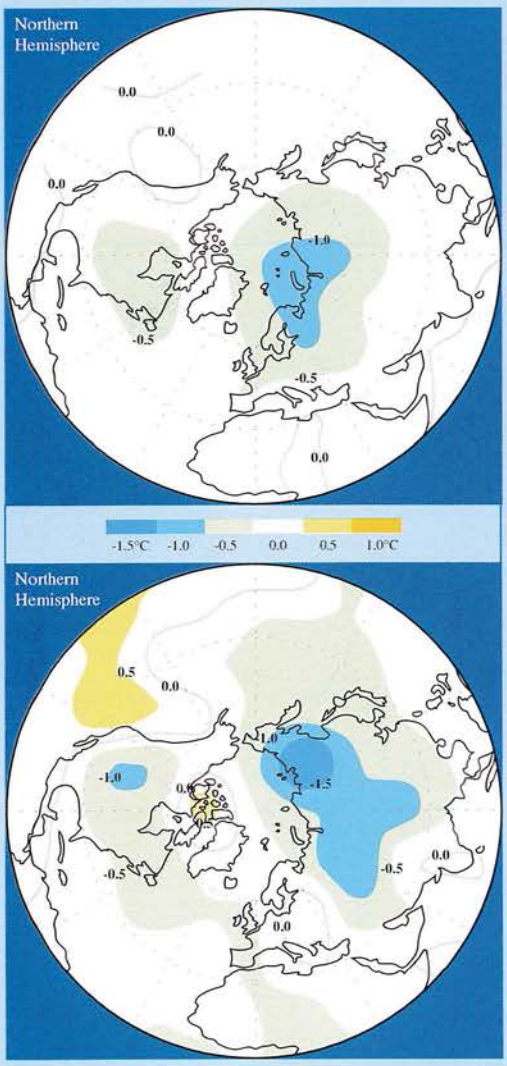

◀ *Figure 3.10 – Top:* Average temperature anomalies for months 1-6 following each of the five historic eruptions. For each of the five eruptions, anomalies for the six-month period following the eruptions are calculated as departures from the mean of the corresponding period during the three years prior to the eruption. *Bottom:* Average temperature anomalies for months 13-18 (July-December 1992) following the eruption of Pinatubo. Anomalies are calculated departures from the mean of the three periods July-December 1988, 1989 and 1990 (from IPCC, Hadley Centre, UK Meteorological Office and Climatic Research Unit, University of East Anglia).

impact on radiative fluxes.

Despite these problems, it is highly likely that the marked cooling in the northern hemisphere records (see Figure. 3.2) during 1992 and 1993 is a result of the Mount Pinatubo eruption in June 1991. The cooling reached its maximum during the second half of 1992 with renewed cooling in 1993 following a warm 1992-93 winter. The relative warmth of the boreal winters after the eruption provides some observational evidence for winter warming following eruptions (proposed by Robock and Mao, 1992; Graf et al., 1993), though this has been common after about 1980 even in years with no influence of eruptions. The effects of the earlier eruption of El Chichòn in April 1982 are not readily distinguished because of the occurrence of a large warm ENSO event at the same time.

How does the timing and spatial response of Mount Pinatubo at the surface compare with earlier eruptions? The likely response is identified through a superposed epoch analysis (see Sear et al., 1987, for details of the method - land and marine temperature data from Jones and Briffa, 1992) of the five major northern hemisphere eruptions of the twentieth century: 1902 (Peleé and Soufrière, Caribbean), 1907 (Ksudach, Kamchatka), 1912 (Katmai, Alaska), 1956 (Bezumianni, Kamchatka) and 1982 (El Chichòn, Mexico). Figure 3.9 shows the composite temporal response of the five eruptions compared to that of Mount Pinatubo. The response of the eruptions (both the composite and Pinatubo) is clearly greatest in the northern hemisphere. Responses are smaller and less significant in the southern hemisphere. The maximum Pinatubo cooling response of 0.3-0.4°C was experienced during the second half of 1992 (months 13-18 following the eruption). The composite response showed a maximum cooling of 0.2-0.3°C occurring during the first year. The delay in the Pinatubo response may be related to the timing of the eruption and phase of the ENSO phenomenon at the time. With respect to the five historic eruptions, the response of the Caribbean eruptions of 1902 was most similar in character and timing to Mount Pinatubo.

Figure 3.10 compares the spatial temperature response for the composite with that of Mount Pinatubo for the time of maximum cooling. From Figure 3.7, this is months 13-18 for Pinatubo and months 1-6 for the composite. For the composite (months 1-6) there is strong and significant cooling over land with little or no cooling over the ocean. The greatest cooling occurs over eastern North America and northern Eurasia. For Pinatubo (months 13-18), negative temperature departures affect most of the northern land masses. The spatial response of Pinatubo shows many of the same features of the composite.

RECENT RISE OF NIGHT-TIME TEMPERATURES

The mean temperature of the earth has increased over the past century by about 0.5°C. New information about how this warming has occurred indicates that a substantially greater warming is occurring during the night compared to the day. Data have been analyzed for over 50% (10%) of the northern (southern) hemisphere land mass, accounting for 37% of the global land mass. Based on the period 1951 to 1990, over the areas studied, indications are that the daily mean minimum temperature is rising at a rate three times faster than the daily mean maximum temperature (0.084°C/10 yr versus 0.028°C/10 yr). As a result, the average daily temperature range (the difference between the maximum and minimum temperature) has decreased at a rate approximately equal to the increase of mean temperature (Figure 3.11).

Figure 3.11 – Time series of anomalies of annual mean daily minimum temperature for 37% of the global land mass. The smooth curve is a nine-point binomial filter with "padded" ends.

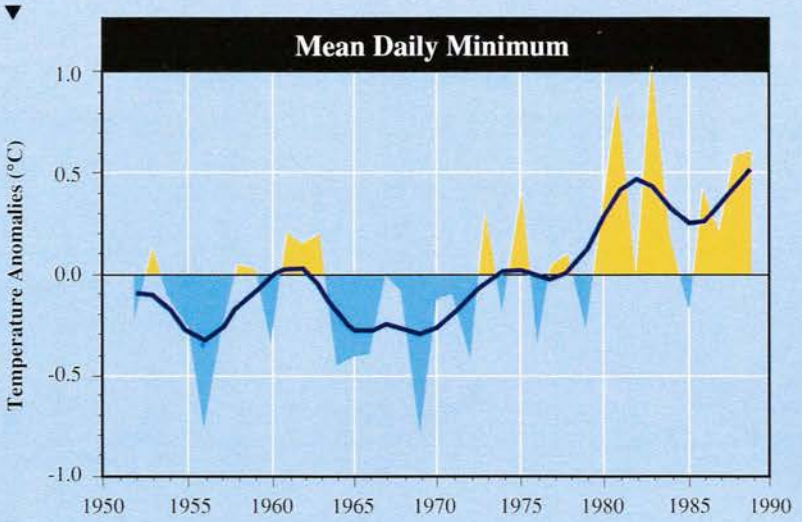

The effect is thought to be due to a combination of greenhouse gas-induced warming, increased cloud cover and anthropogenic sulphates emitted from burning fossil fuels.

** Adapted from the contribution by Thomas R. Karl, National Climatic Data Center, Asheville, NC*

The high spatial and temporal variability of precipitation makes it difficult to compile meaningful statistics, e.g. averages, intensities, frequencies, extremes, etc. for large areas. A dense observing network is needed to obtain an adequate sample of precipitation measurements in order to minimize the effects of extreme variability. Precipitation averages for global, hemispheric, or even regional or national areas, could be dominated by very high or very low precipitation amounts from

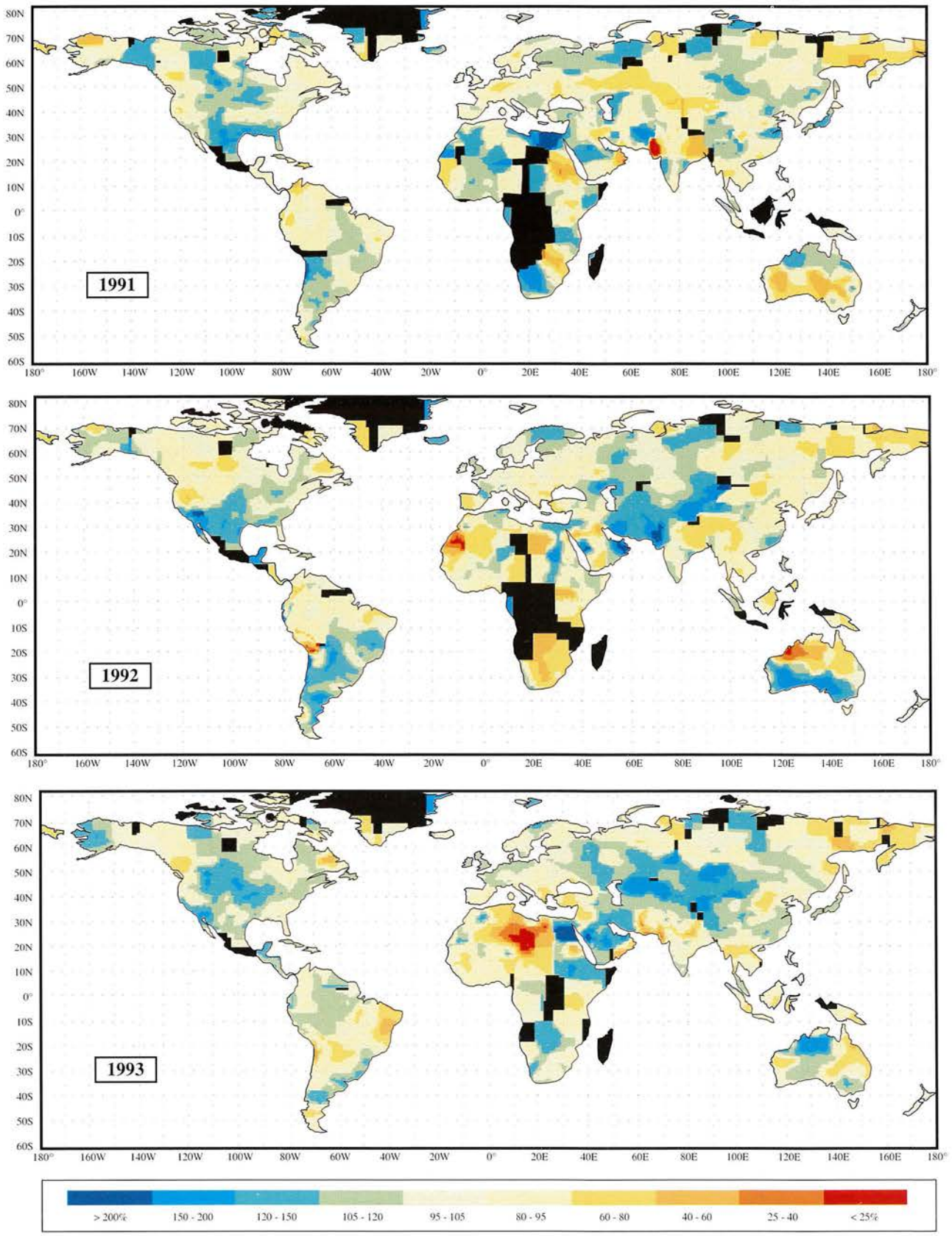

▲ *Figure 4.1* – Percentage departure (relative to the 1961-90 normal) of annual precipitation (January to December) for 1991, 1992 and 1993 (from Deutscher Wetterdienst, Seewetteramt, Hamburg, Germany).

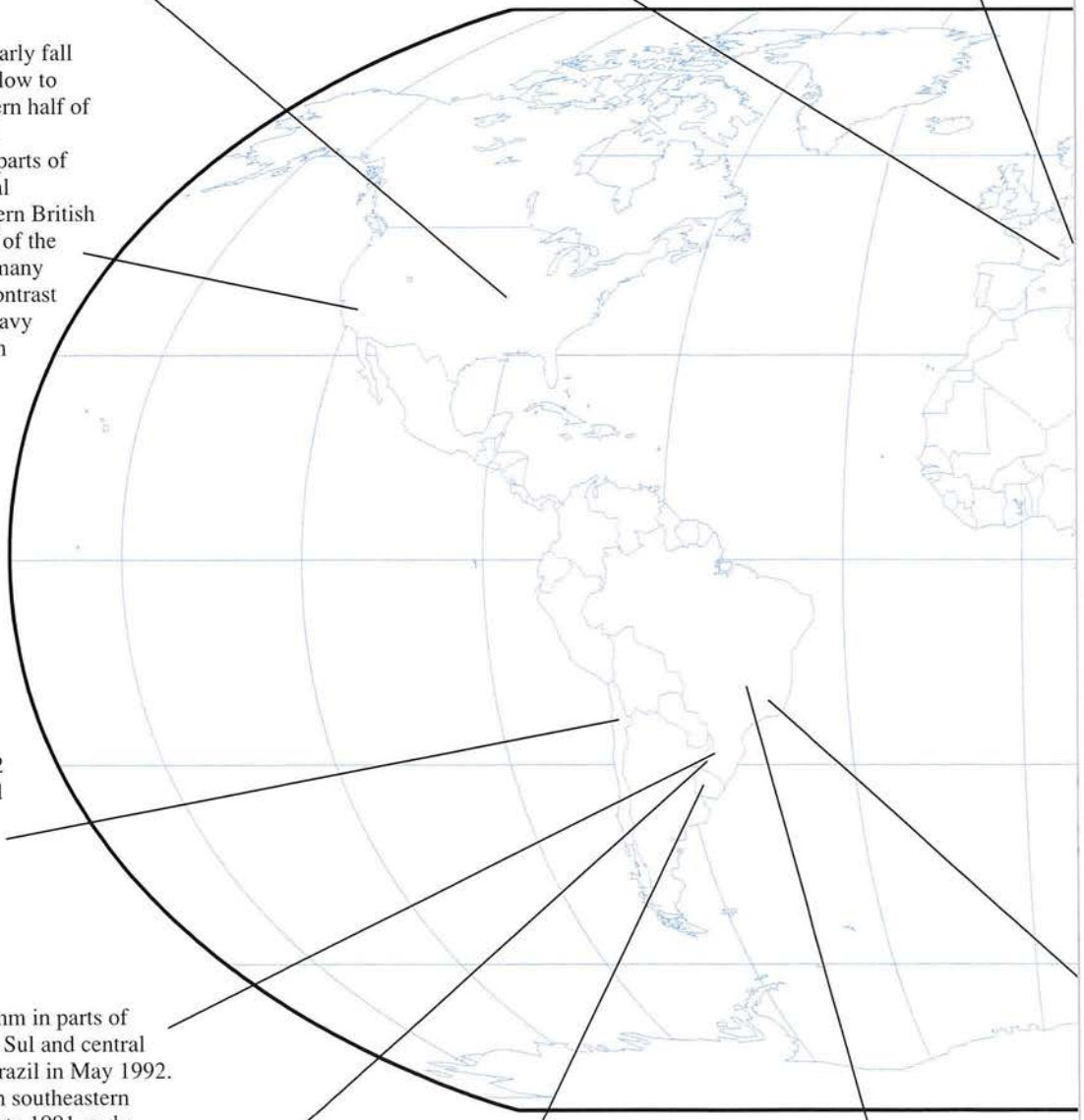

In the upper Mississippi Valley from April through May 1993, more than 400 mm of rain fell, making these three months the wettest such period since records began in 1895.

Weekly rainfall totals of 50 to 200 mm soaked southern and central France, northern Spain and northern Italy in late September and early October 1992 (Figure 4.2.2). Isolated locations received as much as 350 mm. These totals represent more than three times the normal for the period.

In November 1992, storms delivered as much as 200 mm of precipitation in one week to parts of Switzerland.

The late summer and early fall 1993 wet season was slow to begin across the northern half of California, central and northwestern Oregon, parts of central and west-central Washington and southern British Columbia. Under half of the normal rainfall fell at many locations, in marked contrast to the exceptionally heavy precipitation that fell in the Pacific Northwest in 1992.

During early May 1992 rare heavy rains caused flash flooding in the desert regions of northern Chile.

Rainfall exceeded 400 mm in parts of northern Rio Grande do Sul and central Catarina provinces of Brazil in May 1992. The wetness observed in southeastern South America during late 1991-early 1992 corresponded with expected anomaly patterns during low-index (warm) ENSO episodes.

Six-week moisture surpluses around the end of 1992 approached 300 mm in northern Uruguay and adjacent parts of Brazil, Bolivia and Argentina - 6 to 13 times the normal amount for the period.

At the end of 1993, rainfall totals exceeded 500 mm across western Uruguay and adjacent sections of southern Brazil and Argentina - over twice the normal rainfall (Figure 4.2.3).

Southern Brazil experienced very cold temperatures during the winter of 1993. At the end of July, frost and snow occurred on several days. Figure 4.2.1 is a satellite photograph featuring a snowfall event during the passage of a frontal system and an extratropical cyclone on July 29-31, 1993 (from INMET and CPTEC/Instituto Nacional de Pesquisas Espaciais, Brazil).

▲ *Figure 4.2* – Selected precipitation highlights around the world during the review period.

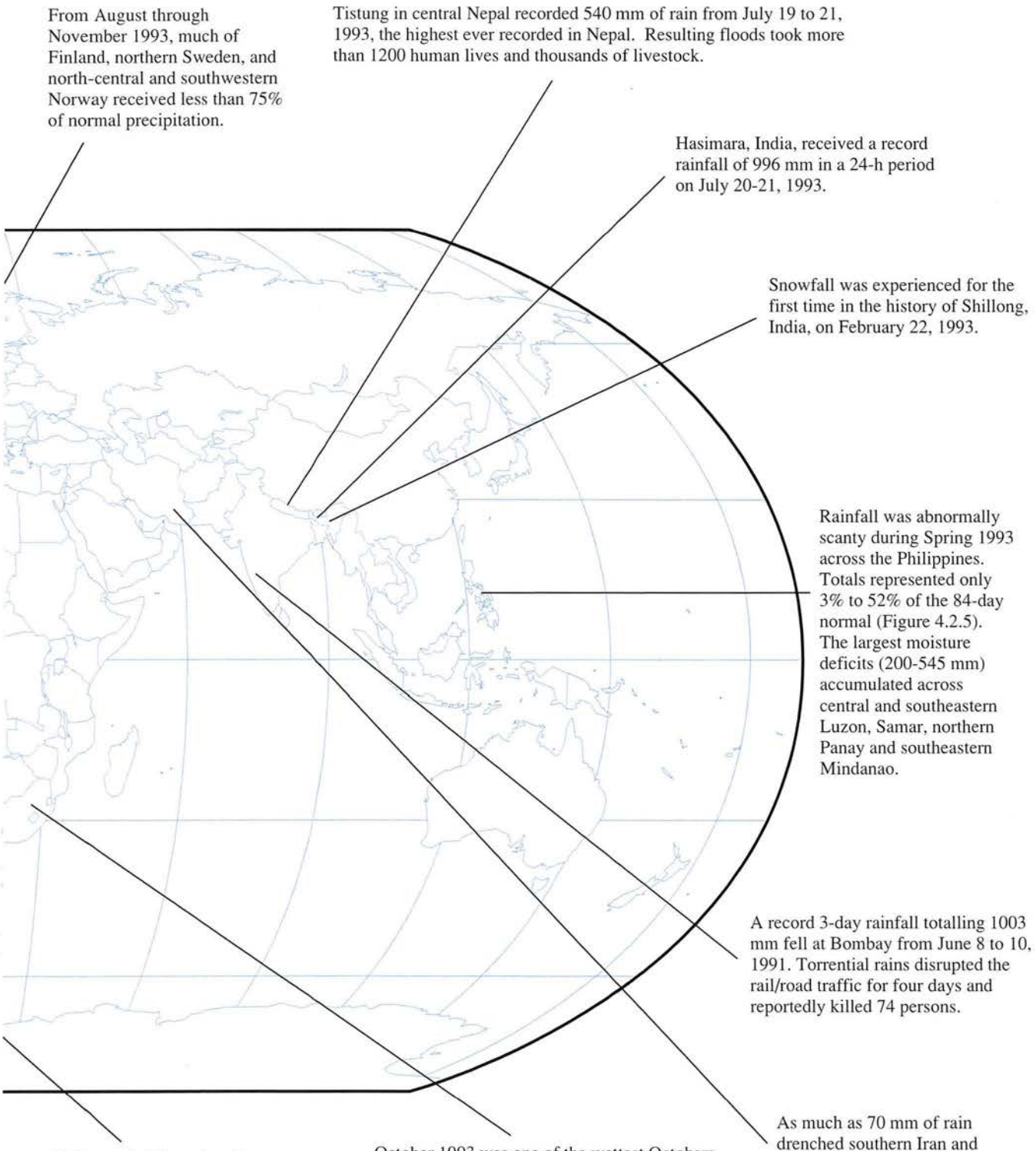

From August through November 1993, much of Finland, northern Sweden, and north-central and southwestern Norway received less than 75% of normal precipitation.

Tistung in central Nepal recorded 540 mm of rain from July 19 to 21, 1993, the highest ever recorded in Nepal. Resulting floods took more than 1200 human lives and thousands of livestock.

Hasimara, India, received a record rainfall of 996 mm in a 24-h period on July 20-21, 1993.

Snowfall was experienced for the first time in the history of Shillong, India, on February 22, 1993.

Rainfall was abnormally scanty during Spring 1993 across the Philippines. Totals represented only 3% to 52% of the 84-day normal (Figure 4.2.5). The largest moisture deficits (200-545 mm) accumulated across central and southeastern Luzon, Samar, northern Panay and southeastern Mindanao.

A record 3-day rainfall totalling 1003 mm fell at Bombay from June 8 to 10, 1991. Torrential rains disrupted the rail/road traffic for four days and reportedly killed 74 persons.

As much as 70 mm of rain drenched southern Iran and western Pakistan as unusually wet weather persisted in January 1993.

Copious rainfall produced flash flooding and mud slides in the western and northern suburbs of Rio de Janeiro in early January 1992.

October 1993 was one of the wettest Octobers on record across South Africa (Figure 4.2.4). In Pretoria it was the wettest October since 1929. The heavy rains have helped to recharge soil moisture following two drier-than-normal seasons, but caused local flooding and delayed fieldwork.

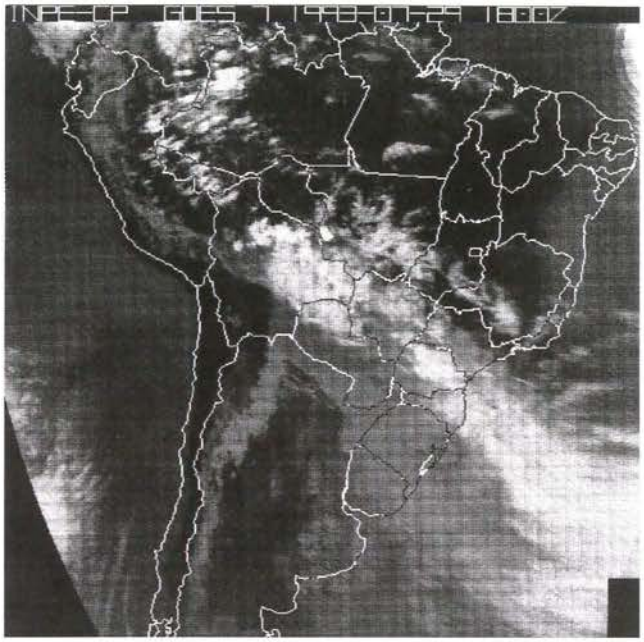

▲ *Figure 4.2.1* – Satellite photograph of a frontal system associated with an extratropical cyclone, July 29, 1993 (from INMET and CPTEC/Instituto Nacional de Pesquisas Espaciais, Brazil).

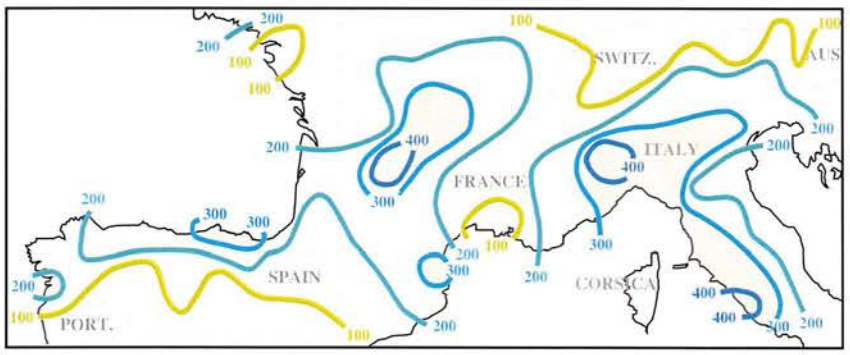

▲ *Figure 4.2.2* – Percent of normal precipitation for south-central and southwestern Europe from September 20 to October 10, 1992 (from NOAA/NWS/NMC/CAC, Washington, DC).

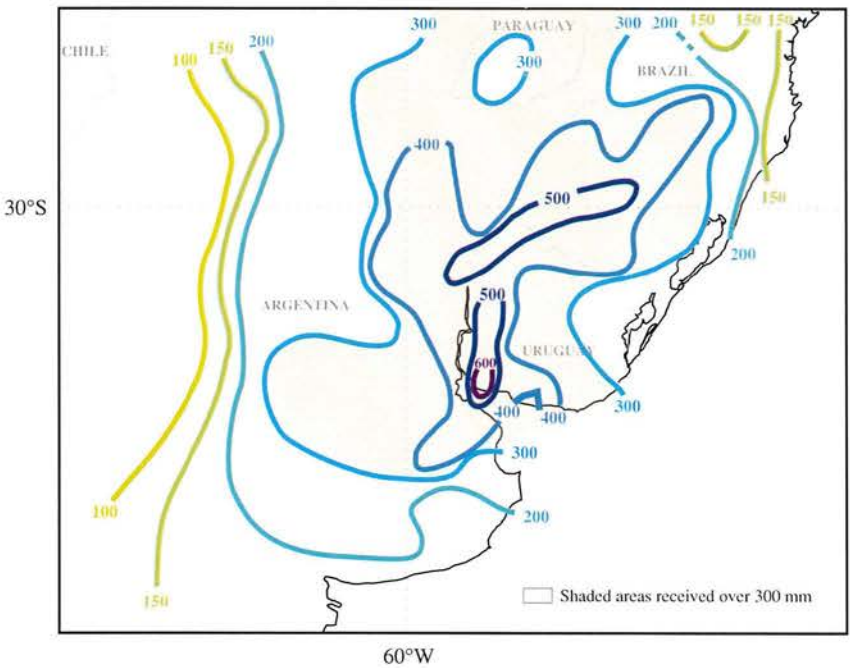

▲ *Figure 4.2.3* – Percent of normal precipitation for east-central South America from October 12 to December 5, 1993 (from NOAA/NWS/NMC/CAC, Washington, DC).

a small cluster of stations.

For many years, studies of large-scale changes in precipitation have been hindered by the lack of a database that is geographically and temporally extensive. For example, precipitation was being measured globally at more than 40,000 meteorological stations and 140,000 precipitation-only stations in 1990. However, only about 5% of the data are in digital form and thus available for near-real time monitoring and climate research. Further, more than 70% of the earth's surface are oceans and this area is not represented in any global analysis.

Precipitation measurements suffer from instrumentation inhomogeneities and biases. Seldom are the data corrected to account for such gauge-induced biases as systematic errors caused by wind, wetting on the interior walls of the gauge and evaporation from the gauge. Snowfall measurements have a host of additional biases to be considered.

The only way to get climatological information on a global scale without too much delay is to use the data transmitted via the WMO World Weather Watch Global Telecommunication System (GTS). But over many parts of the continents, the station density resulting from GTS reports is insufficient. The strong need of accurate knowledge of the precipitation distribution is reflected in the decision of the WMO to establish the Global Precipitation Climatology Centre.

4.1 PRECIPITATION PATTERNS 1991, 1992 AND 1993

The maps of the annual precipitation distribution, plotted in per cent of the long-time averages (Figure 4.1) for the years 1991, 1992 and 1993 reflect its high spatial variability. Beyond that, one becomes immediately aware of the huge areas where sufficient data are not available.

Despite the difficulties of analyzing precipitation data, several persistent anomalies during the

review period from 1991 to 1993 could be identified, for example, drought in northeast Brazil and scanty precipitation in northeast Asia.

In 1991, drier than normal conditions stretched from the UK, over central and eastern Europe to Central Asia. Large areas of below-normal rainfall also existed in western and south-central Australia, northern India, Bangladesh, in the Sudan, southeast Africa, most of Central America, northern South America and along the west coast of North America from California to British Columbia. Abundant precipitation occurred in states ringing the Gulf of Mexico in the USA, western South Africa, northern Egypt, northern Australia and central Chile.

Significant precipitation anomalies during 1992 were related to the prolonged ENSO event. The devastating drought over southeast Africa was the worst in more than 100 years. Precipitation was generally less than normal in the monsoon regions of India and Australia. Other dry areas included the western Sahel, eastern Russia, and south and central Europe. December 1991 to May 1992 was an extremely wet period for the southwest of the USA. A resurgence of ENSO late in the year brought much-needed rain to the American west coast. A vast belt of copious rain stretched from Oman over Iran, Pakistan to Sinkiang and in southeastern South America over Uruguay, neighbouring parts of Argentina and southern Brazil.

On the whole, 1993 was the wettest of the three years. The USA Midwest and the eastern Canadian Prairies had record summer rainfalls that led to catastrophic floods. Other wet areas in 1993 were northwest Australia and a broad belt from Egypt to central Asia. Significantly dry areas were found in north-central Africa and again around the Mediterranean Sea, in some parts of South America from northern Chile northeastward, in northeastern Australia and on the northern coasts of the Arabian Sea. The northeast region of Brazil was afflicted by extremely dry weather for the third year in a row.

4.2

SIGNIFICANT PRECIPITATION EXTREMES AND EVENTS 1991-93

Figure 4.2 illustrates a selection of precipitation highlights around the world during the review period.

4.3

PRECIPITATION REMAINS NEAR NORMAL OVER FORMER USSR

Distribution of annual and seasonal total precipitation over the former territory of the USSR was very similar to normal patterns in both 1992 and 1993. However, in the northeast, annual precipitation amounted to only 80% of normal, continuing a long run of dry years, and south of Kazakhstan and Central Asia it was more than 120% of normal. In 1993, similar wet conditions were observed in the southern Urals. For most of the territory as a whole, negative monthly precipitation anomalies were observed only once during these two years (in November 1993, 78% of normal). Annual total precipitation was near normal across basins of three large rivers: Ob, Yenisei and Lena (Figure 4.3). Over the past four years, the Lena River basin has experienced drier than normal conditions.

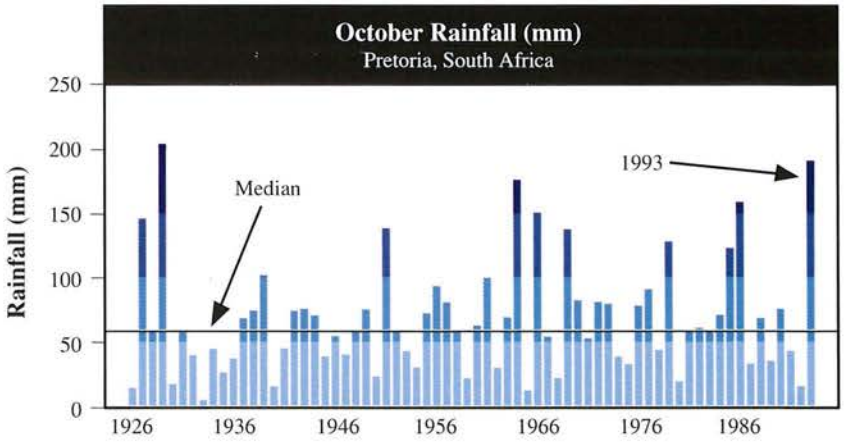

▲ *Figure 4.2.4* – October rainfall series for Pretoria, South Africa, 1926-1993 (from U.S. Weekly Weather and Crop Bulletin, October 26, 1993).

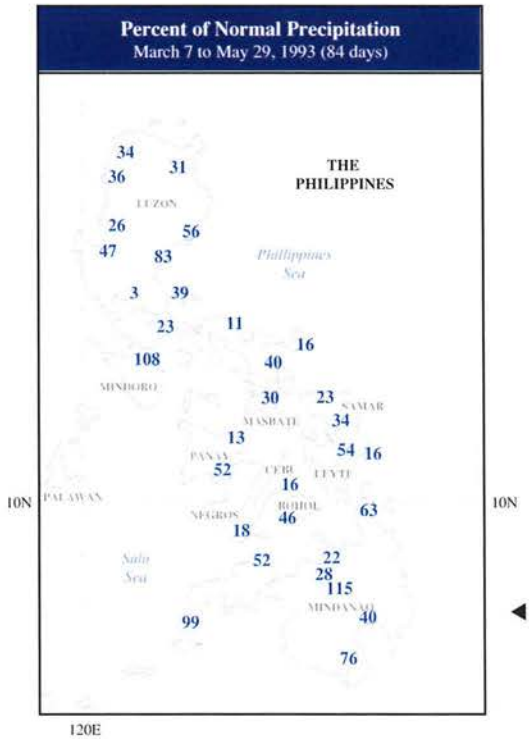

◀ *Figure 4.2.5* – Percent of normal precipitation for the Philippines from March 7 to May 29, 1993 (from NOAA/NWS/NMC/CAC, Washington, DC).

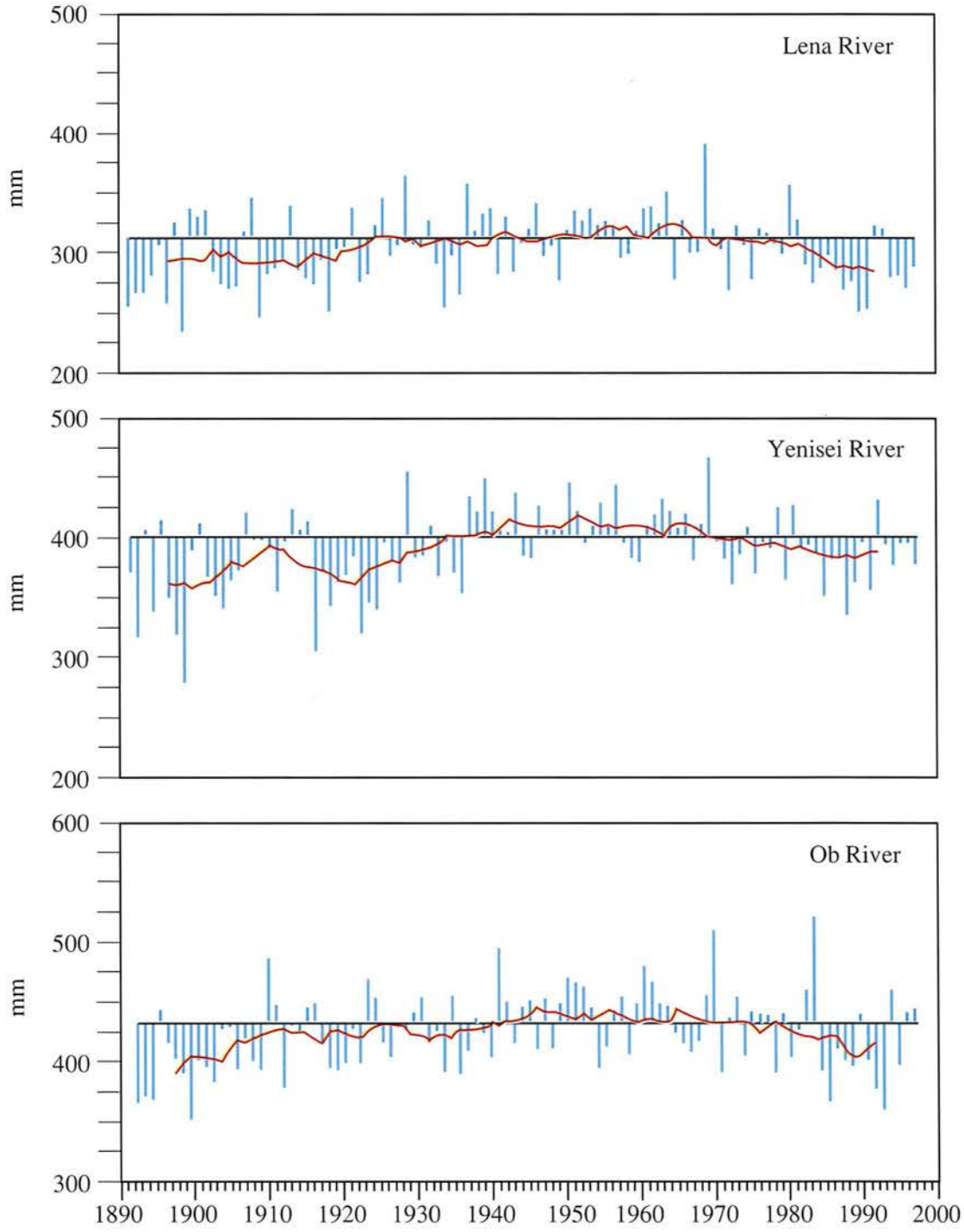

▲ *Figure 4.3* – Annual precipitation totals (December-November, 11-year running means and normal (1951-1980) over three major river basins in the Asian part of the former territory of the USSR (from Institute for Global Climate and Ecology, Moscow).

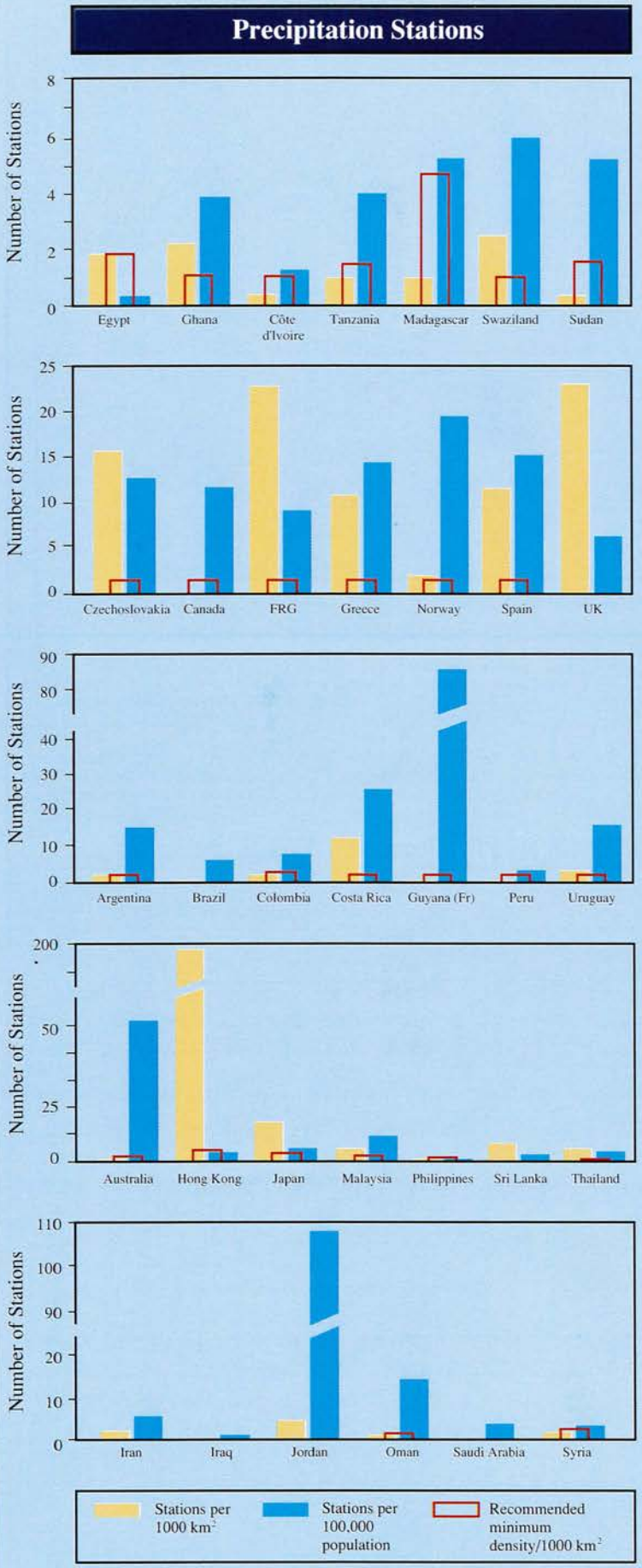

▲ *Figure 4.4* – Precipitation network densities for selected countries (from World Meteorological Organization WMO No. 801. Assessing a precious resource...water. 1994).

Global Precipitation Climatology Centre*

WMO initiated the Global Precipitation Climatology Centre (GPCC) in order to provide global monthly and annual precipitation analyses. GPCC is operated by the Deutscher Wetterdienst in Offenbach, Germany. Since 1989, the Centre has designed and operated a data processing system with the following functions: (a) collect and archive monthly precipitation data world-wide, (b) quality control these data, (c) calculate areal mean totals on the basis of the conventional measurements over land, (d) merge these analyses with precipitation estimates from other observational techniques, e.g. satellite images, or from model simulations in order to obtain global precipitation data sets and (e) determine the error range of the analysis results. Up to now, preliminary results have been produced for the years 1987 and 1988 and are available in printed maps and as digital data on floppy diskettes.

The accuracy and usefulness of the products strongly depend on the availability of observed data. Monthly precipitation observations are regularly exchanged world-wide for about 4,500 stations, based on international conventions, in synoptic and CLIMAT messages via the WMO World Weather Watch Global Telecommunication System (GTS). Over many parts of the world, the station density from GTS reports is insufficient to permit reliable calculations of areal monthly precipitation (Figure 4.4).

The required station-density lies between at least two and eight stations on an area of 10,000 km² depending on orographic and climatic conditions. Up to now, 100 countries are contributing data to the GPCC archive. However, large data gaps still exist. The cooperation of all Member countries is essential to update and enhance the global precipitation archives at the GPCC.

** Adapted from a contribution by Bruno Rudolf, Global Precipitation Climatology Centre, Deutscher Wetterdienst, Offenbach/Main.*

Reference Periods/Climatic Normals*

Throughout this Review and, in many other publications, time series graphs and spatial maps are generally shown as departures, anomalies or percentages from the average value for a specific reference period. This is generally done to highlight the principal features. Sometimes the averages relating to these reference periods are referred to as "normals", but this terminology gives a false impression that there are normal modes in the climate system, which, given the intrinsic variability, is clearly not the case. Ideally, we would like to use a common period for all figures but this is not generally possible for a number of reasons.

First, the time series of many new, important climatic parameters, particularly those based on satellite information or derived products, are invariably short records. Anomalies, perforce must be based on periods encompassing the 1980s. Reference periods are, therefore, to a large extent determined by data availability. Second, the various meteorological and climatological centres use different reference periods, with the periods used changing as time progresses. For example, the standard WMO reference periods are 1901-1930, 1931-1960, 1961-1990.

It is important to realize, therefore, that the character of well-known time series analyses and even some spatial anomaly maps may change with a change in reference period. This is illustrated with two examples. Figure 4.5 shows the Sahel rainfall series. This series is constructed by averaging all raingauge data for the region as standardized anomalies. Standardization is achieved by dividing the anomaly value by the standard deviation of the seasonal rainfall with both the first and second moments of the station rainfall distribution (the mean and standard deviation) being calculated over the same period. Standardization is common practice with precipitation as it not only takes the average precipitation at a site into account but also, to some extent, the variability. The figure shows the Sahel rainfall series calculated with two reference periods, 1931-60 and 1961-90. Standardization with precipitation and simple anomalies for other variables, such as temperature, has the added advantage of allowing, to a large extent, for the changing station availability through time when developing a time series. The character of the Sahel rainfall series has been changed by the new reference period. The change here is not just a substantial level change due to the use of different standardized anomalies, but also due to some slight changes in the interannual variations, though, decadal variability (smoothed line) is little altered.

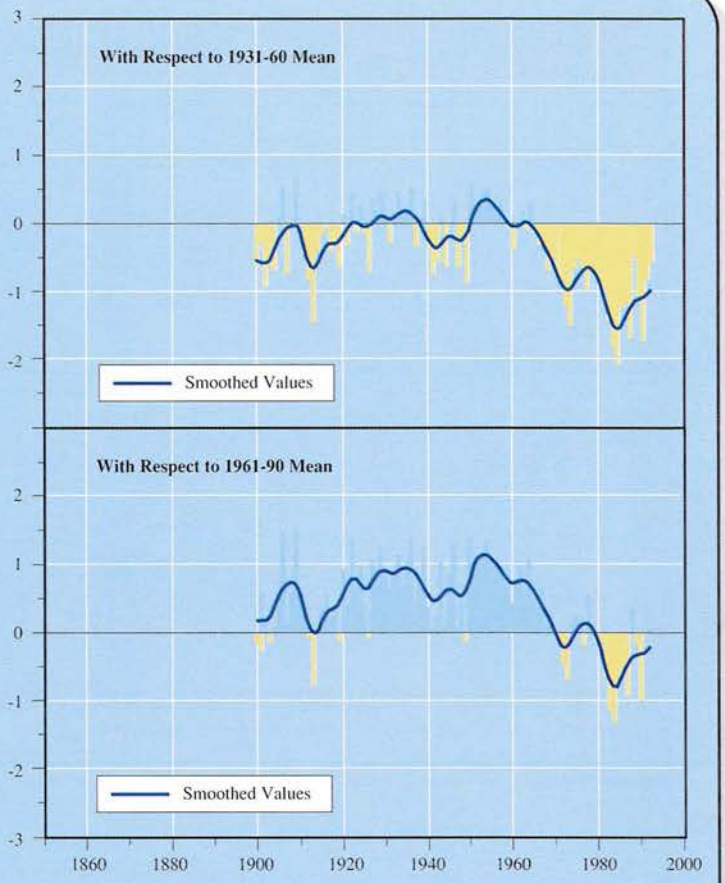

▲ *Figure 4.5* – Regional annual precipitation anomalies for the African Sahel for 1900-1992 standardized using the mean rainfall from 1931-60 and 1961-90 (from Mike Hulme, Climatic Research Unit, University of East Anglia, Norwich, UK).

Figure 4.6 shows the ratio of precipitation normals, for the world's land areas between 1931-60 and 1961-90. Although the world is drier in the later period, the spatial pattern of this change is not the same everywhere. Some regions show less precipitation, a smaller number more precipitation. Notable wetter areas include the northern part of eastern Asia, Australia, western parts of the Americas and some of the Middle East. Dry periods (precipitation less than 80% of normal) occurred recently in the Sahel and southwestern Africa. Time series for regions where these changes are greatest will be offset depending on the period used. Similarly, seasonal and monthly maps would show different spatial patterns depending on the relative changes between the two periods.

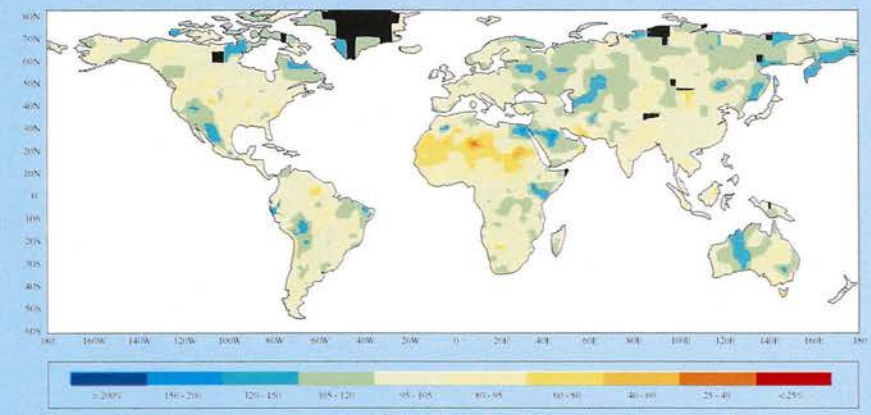

▲ *Figure 4.6* – Ratio of the normal 1961-90/1931-60 of the annual amount of precipitation for the world's land areas in percent (from Deutscher Wetterdienst, Seewetteramt, Hamburg, Germany).

In conclusion, therefore, whilst the use of anomalies aids interpretation, the effects of the choice of reference period can be appreciable.

** Adapted from a contribution by Philip Jones, Climatic Research Unit, University of East Anglia, Norwich, UK.*

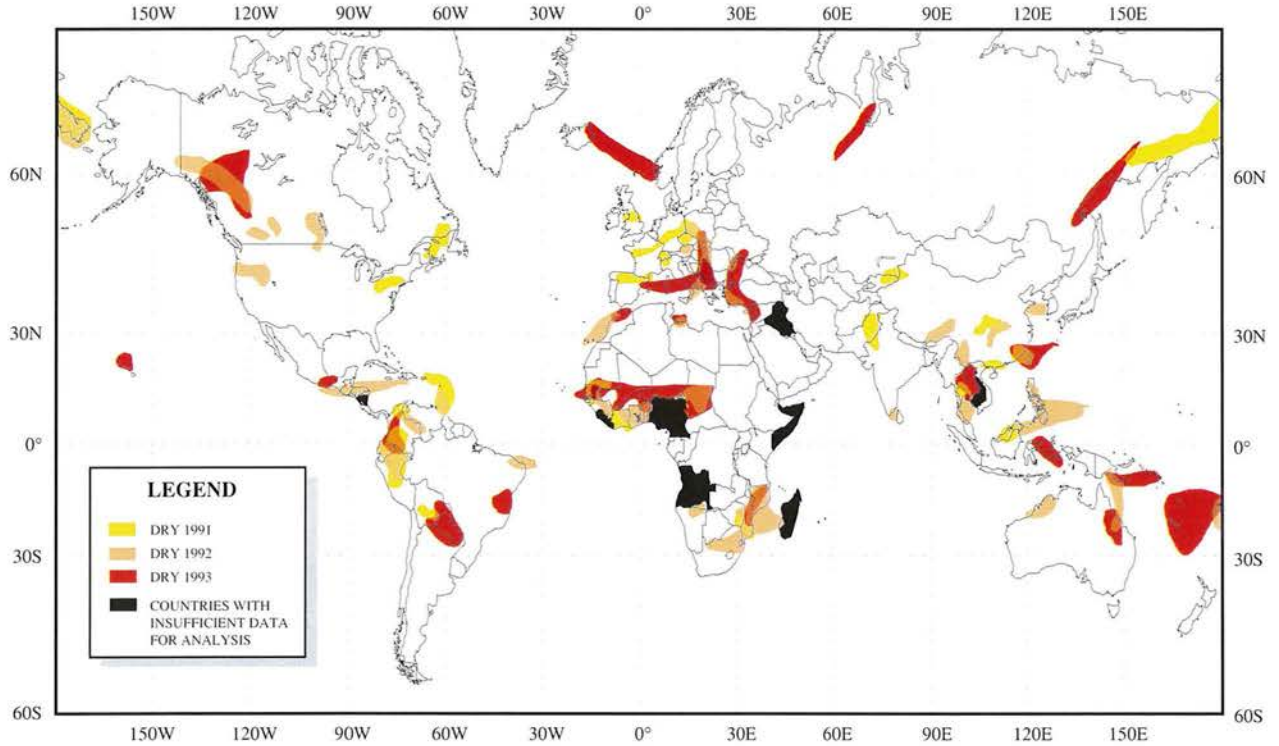

▲ *Figure 5.1* – Areas where precipitation anomalies were estimated to be within the driest 10% of climatological occurrences, January to December 1991, 1992 and 1993 (from NOAA/NWS/NMC/CAC, Washington, DC).

Droughts have occurred over many parts of the globe in varying degrees of severity and duration throughout human history. Many nations have experienced considerable distress arising out of drought occurrences - mass starvation, famines, cessation of economic activity, particularly within the developing world where economies are inextricably and intrinsically tied to agriculture. During the review period, June 1991 to November 1993, droughts occurred in every region of the world (Figure 5.1). Much talked about were the ravages of the 1991-92 drought that crippled southern Africa, in particular, and also northeastern Brazil, Australia and the Mediterranean Rim. In the Sahel, the drier than normal trend that commenced in the mid-1960s continued in the 1991 season. Elsewhere, California suffered persistent drought. Dryness also afflicted the cornbelt and mid-Atlantic states in 1991 and the American southeast in 1993. Many countries in Asia had droughts, e.g. Russia and Pakistan in 1991, Malaysia, Indonesia, Pakistan and India in 1992 and northern China from 1991 to 1993.

Droughts are not necessarily freak events. They are rooted in the global ocean-atmospheric circulation variations, some of which occur dramatically at the time of El Niño/Southern Oscillation (ENSO) episodes. The warm phase of ENSO has been shown to be associated with droughts in many parts of the globe, notably, India, southern Africa, Australia and northeastern Brazil. The actual physical, causal mechanisms are not fully understood at present. The review period showed an unprecedented persistence of the warm phase of ENSO. It is also important to note that in other areas that are prone to droughts, e.g. the Sahel in Africa or Europe, droughts are not well correlated with ENSO events. Disasters caused by droughts are also strongly affected by such diverse factors as agricultural practices, changes in population density and the country's ability to provide alternative supplies of food, water and employment.

5.1 RECORD DROUGHT IN SOUTHERN AFRICA

Extensive droughts have afflicted southern Africa in recent times, e.g. 1946-47, 1965-66, 1972-73, 1982-83 and 1986-87 culminating in the most severe drought in 1991-92. These times were also major ENSO years. The precipitation regime (1901 to 1993) in Zimbabwe is generally in phase with that of the southern Africa subregion (Figure 5.2). Droughts in southern Africa do not always coincide with those in eastern Africa, where there were severe droughts in 1933/34, 1938/39, 1949/50, 1973/74 and 1983/84.

The 1991/92 drought had a most crippling effect over much of southern Africa (Figure 5.3), with many countries from central Zambia through central Malawi and Mozambique southwards having seasonal deficits of up to 80% of normal rain. Large sections of Orange Free State, the Transvaal, Mozambique, Zimbabwe, Botswana and Zambia received scanty rainfall (20 to 75% of normal) during the rainy season from October 1991 through April 1992 (Figure 5.4). The extreme dryness was exacerbated by abnormally high temperatures. Temperatures above 40°C seared the region for days. Readings reached 47°C along the South Africa-Zimbabwe border. Together, South Africa and the Southern Africa Development Community (SADC)

countries, which include Angola, Botswana, Lesotho, Malawi, Mozambique, Namibia, Swaziland, Tanzania, Zambia and Zimbabwe, experienced the worst drought of the century. There were unprecedented crop failures. Roughly five times more food had to be brought into southern Africa than that delivered to the Horn of Africa during the famine of 1984-85. The southern subcontinent, usually a food exporter, had to import 11.6 million tons of food worth over US$ 4 billion and an additional US$ 200 million of non-food items such as medicines. Regional grain production fell some 60% short of expected levels. There was a virtual collapse of industries since both water shortage and hydropower failures were frequent.

Although previous droughts in southern Africa were severe, this one impacted most negatively on the food security situation. The drought struck during the crucial growing period for corn. Further, it came following a decade of largely deficient rainfall and slow recovery from a series of droughts. Back-to-back "rainy" seasons with inadequate rainfalls exacerbated conditions. The food stocks that could have been in reserve had been depleted, owing largely to exports. Furthermore, the land use pattern may not be in harmony with the climate. High population densities and poor water resource management tax the carrying capacity of the environment and may well have contributed to the near catastrophic impact of the drought. Even though 1992-93 and 1993-94 could be considered to be largely post-drought periods in the subregion, the recovery was rather slow. Too often, even good wet spells do not adequately recharge the ground water sources. As a result, even short dry spells cause a much stressed environment leading to poor harvests.

Over eastern Africa, poor rains had been affecting many countries as early as June 1991. The main rain-producing system, the monsoon trough or the Intertropical Convergence Zone (ITCZ), was quite inactive. This led to deficient rains in large areas of Kenya, Uganda and the

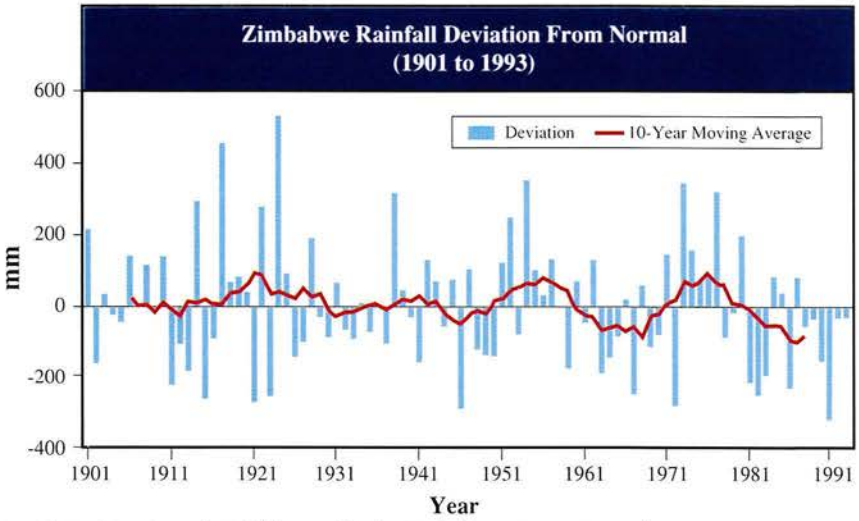

▲ *Figure 5.2* – Annual rainfall anomalies for Zimbabwe, 1901-1993 and 10-year running mean.

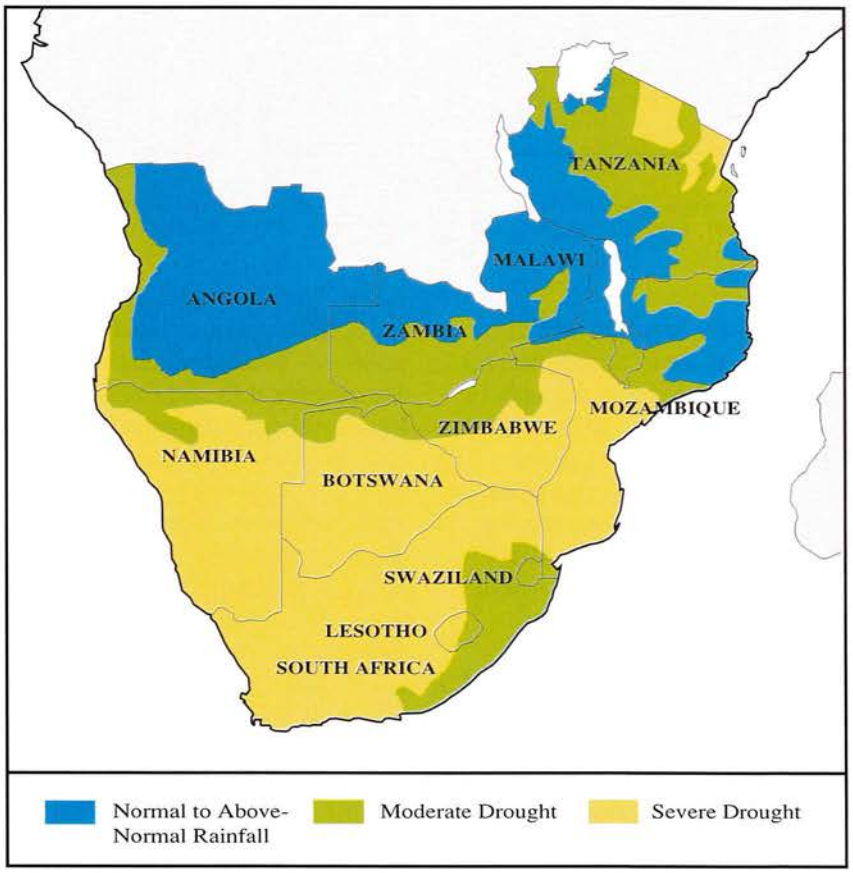

▲ *Figure 5.3* – Extent of the 1991-1992 drought across southern Africa (from Zinyowera and Unganai, 1993).

Sudan to the extent that by September, several areas in these countries had well below 75% of their normal seasonal rains. Towards the end of the year, most of Kenya, Tanzania and southwestern Ethiopia recorded 50% of the long-term average. In 1992, the onset of the summer monsoon over equatorial east and north Africa was delayed and subsequently, the season had poorly distributed, insufficient rains.

Over western and central Africa, there was an alternation of wet and dry conditions from 1991 to 1993. However, the trend of below-normal precipitation over the last 30 years (Figure 5.6) largely continued unabated. The 1991 rainy season started early across much of west-central Africa, except for the extreme west where cool, wet conditions persisted in May. Much of the region experienced a significantly drier-than-normal June and early July, but mid-July and August rains, particularly in the extreme west, brought some relief.

Across the western Sahel, rainfall totals in February to April 1991 were among the lowest 10% of the 1951-80 normal period. During early September, when the Intertropical Convergence Zone (ITCZ) typically withdraws southward and rainfall totals normally decrease across the northern and central Sahel, generous rains, between 50-150 mm fell on northern Senegal and southern Mauritania, easing dryness and aiding late-planted crops.

As of late July 1993, exceptionally dry conditions dominated large sections of sub-Saharan Africa (especially across the western half of the region) while the ITCZ remained considerably south of its climatologically typical location. The

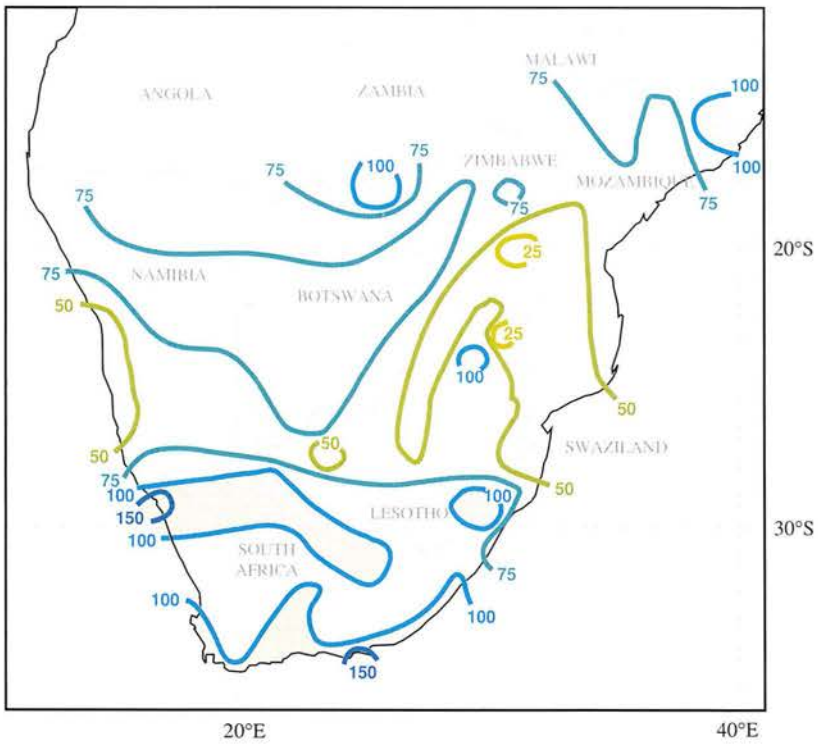

Figure 5.4 – Percent of normal precipitation in southern Africa from October 1, 1991 to April 30, 1992 (from NOAA/NWS/NMC/CAC, Washington, DC).

CONSECUTIVE DRY YEARS IN SOUTHERN AFRICA

The normal total precipitation for summer rainfall areas in South Africa is 664 mm. After 1963, the country has recorded 16 seasons below normal and 14 above normal. Since the 1982-83 season, seven seasons have been below normal and four have been above normal. Of these last 11 years, two rainy seasons recorded less than 75% of normal rainfall, which is an indication of the severity of the drought. In 1982-83, an average total of only 408 mm was measured and in 1992-93, the average total was 484 mm. Although 1991-92 has been called the worst drought this century, for the stations used in the analysis, the average total was 510 mm, or about 77% of normal.

Taken together, the 1991-92 and the 1992-93 seasons were close to having only 75% of normal rainfall. These are the only occasions in the last 70 years that two consecutive summer rainy seasons have had such seriously inadequate rainfall. Fortunately, the geographical and temporal distribution of rainfall varies seasonally and, in 1992-93, adequate rain fell on the main summer cropping areas to save the region from experiencing two disastrous crop failures. Figure 5.5 shows those areas which suffered two consecutive severe droughts. The greatest impacts of these two very dry seasons were the low levels of surface water stored in dams on which most industrial and urban areas depend and low ground water reserves for boreholes, which support most irrigation and many rural communities. In addition, the sugar industry in Natal and Zululand, on the normally wet east coast, was seriously damaged and many sugar mills have closed.

Farming and rural communities with accumulated capital losses and mounting debt cannot hope to recover as quickly as the grazing grasses did following good rains in October and November 1993.

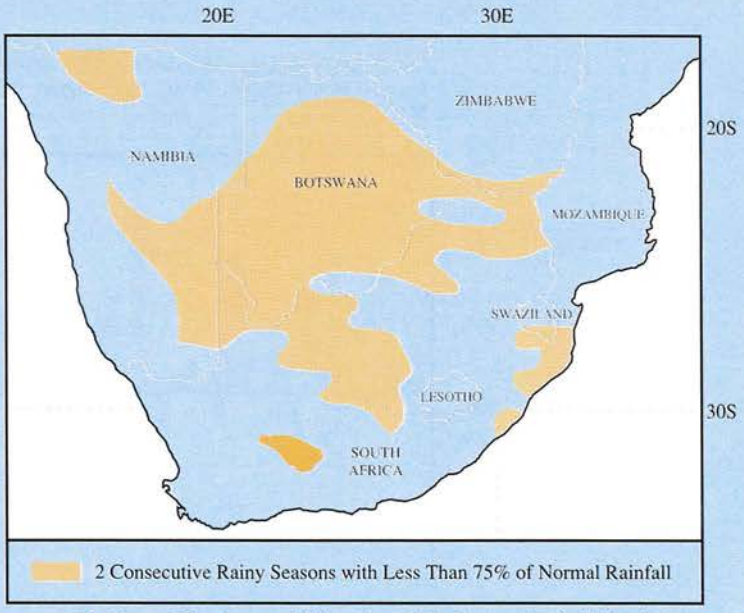

▲ *Figure 5.5* – Areas with less than 75% of normal rainfall for the two consecutive seasons 1991-92 and 1992-93 (from *Drought Network News*, A Newsletter of the International Drought Information Center, University of Nebraska).

** Adapted from an article on Drought Monitoring and Advisory Services in South Africa. Drought Network News. A Newsletter of the International Drought Information Center, 1994.*

dryness was most acute across northern Senegal, southwestern Mauritania, southwestern Mali, southeastern Guinea, south-central and central Niger, and central and southwestern Chad, where approximately half of normal rainfall or less was reported. By the end of September, accumulated totals were close to normal in northern Senegal and southwestern Mauritania. Farther south, moisture levels were from 45 to 85% of normal and, in eastern sections of the Central African Republic and Ethiopia, seasonal rainfall amounts were 60 to 85%.

5.2 DROUGHTS IN SOUTH AMERICA

Rainfall across northeastern Brazil demonstrates high interannual variability that reacts closely with large-scale circulation and sea-surface temperature anomalies associated with the ENSO, particularly warm phase episodes of ENSO. The dynamic mechanism which causes dryness in the northeast is large-scale subsidence when the Walker cell is displaced eastward. A wave-train pattern from the North Pacific Ocean through North America and the Caribbean region is also responsible for subsidence over the northeast. Normally, the northeast region has its rainy season from February to May, when the ITCZ is displaced to the south. Other systems -cyclonic vortices at upper levels of the troposphere, the approach of frontal systems and disturbances from the east -also bring precipitation. With large-scale subsidence, the ITCZ becomes very weak or is not displaced to the south and even the presence of an upper-level vortex does not produce convection in the region. Large-scale subsidence associated with the upper-level anticyclonic circulation, called the Bolivian High, also affected central Brazil.

Figure 5.7 shows the percentage departure from normal of precipitation in northeastern Brazil for February to May in 1992 and in 1993. By 1993, the drought was extreme, leading to much suffering. Conditions were much worse than the droughts of 1942, 1951, 1953, 1970 and 1983 because there had not been any significant recharge of soil moisture in the preceding two years. According to reports, millions of people were pushed to the brink of starvation. Lands sowed with cotton, sugar and other crops were raked by winds and baked by high temperatures.

Towards the end of 1991, dry spells were affecting west central Argentina and southeastern Brazil. After a fairly normal 1992 season across most of South America (apart from northeastern Brazil), parts of Paraguay, southeast Bolivia, Brazil and Argentina experienced excessive dryness in 1993. In general, July to September precipitation totals varied from as low as 25 to 60% of normal.

5.3 DROUGHTS IN NORTH AMERICA

California and the Pacific Northwest of North America normally receive much of their annual precipitation during the winter months. Precipitation is strongly dependent on the prevailing wind direction and on the location and intensity of the storm track. Above-normal precipitation is often associated with southwesterly flow and active cyclone activity, whereas below-normal precipitation corresponds with northwesterly flow and below-normal cyclone activity. For the winters of 1983-84 to 1991-92, the region received significantly below-normal

Figure 5.6 – Precipitation index for the western sub-Saharan Sahel (June-September) 1921-1993 (from NOAA/NWS/NMC/CAC, Washington, DC).

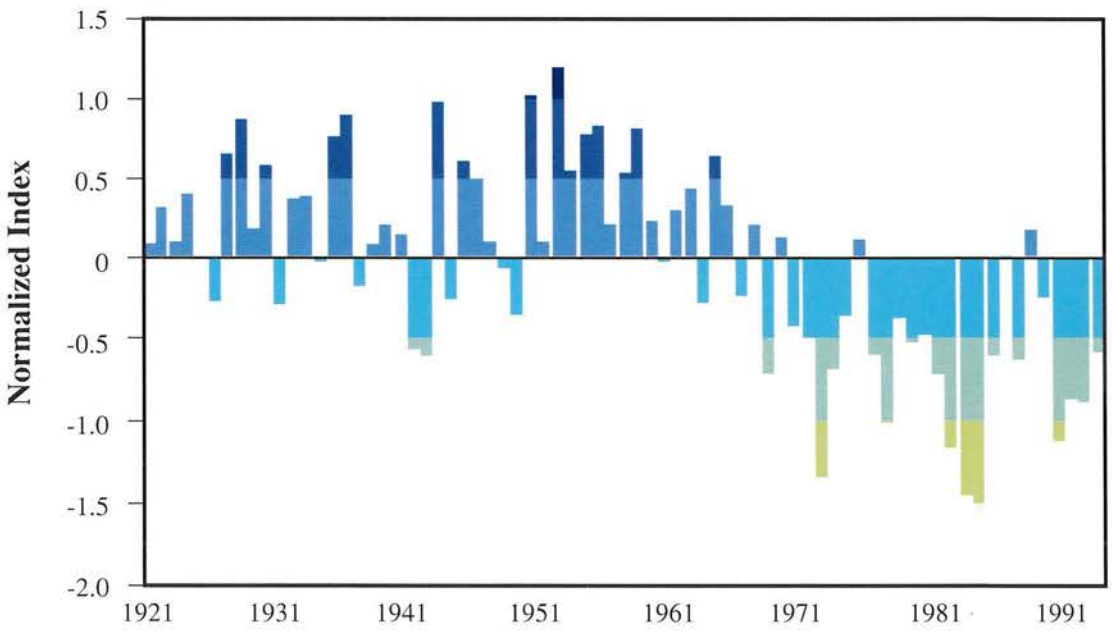

precipitation. These conditions resulted in severe long-term drought that dominated California's hydrology since the winter of 1986-87 (Figure 5.8).

During the winter of 1992-93, significantly above-normal precipitation finally fell throughout California, thus temporarily alleviating the long-term drought conditions. Precipitation totals were the largest recorded since 1968 and the second largest observed in the past 40 years. By the end of the season, overall reservoir storage increased to 85% of capacity. From December to mid-January, the circulation was dominated by a persistent blocking anticyclone over the eastern North Pacific. Storms east of the block generally amplified while moving southeastward from the Aleutians into California. These conditions, along with above-normal moisture transport into California from the tropics in the anomalous southwesterly flow, contributed to the extremely high precipitation totals. Winter deficiencies reappeared in California during late 1993. The dryness helped generate and spread uncontrollable wild fires across the western states, particularly in California.

As the six-year drought was ending in the western USA and extensive floods and inundating rains were plaguing the Midwest, abnormally hot weather and well below-normal rainfall brought drought conditions through much of the southern and eastern USA. The dryness was due to the North Atlantic High (or Bermuda High), a ridge of high pressure in the upper atmosphere that expanded over the eastern USA. A persistent cold trough in the upper atmosphere ahead of the warm ridge brought record cold temperatures to several states in the Pacific Northwest and northern Rockies along with record wet conditions. The summer dryness was especially severe in the southeastern USA. South Carolina experienced the driest summer this century (Figure 5.9) and Florida, North Carolina and Virginia had their second driest summer on record. Some parts of Texas recorded the first precipitation-free July in 30 years. The moisture deficit was persistent during all three summer months in this region, resulting in considerable crop loss and poor pasture, especially in South Carolina. Farther north, less than half of normal rainfall was measured on Long Island in greater New York City and southern New Jersey during June and July.

Figure 5.7 – Percent departure of precipitation in northeastern Brazil during February to May in 1992 and in 1993 (from V.B. Rao, K. Hada and D. Herdies, personal communication, INPE, São Paulo, Brazil).

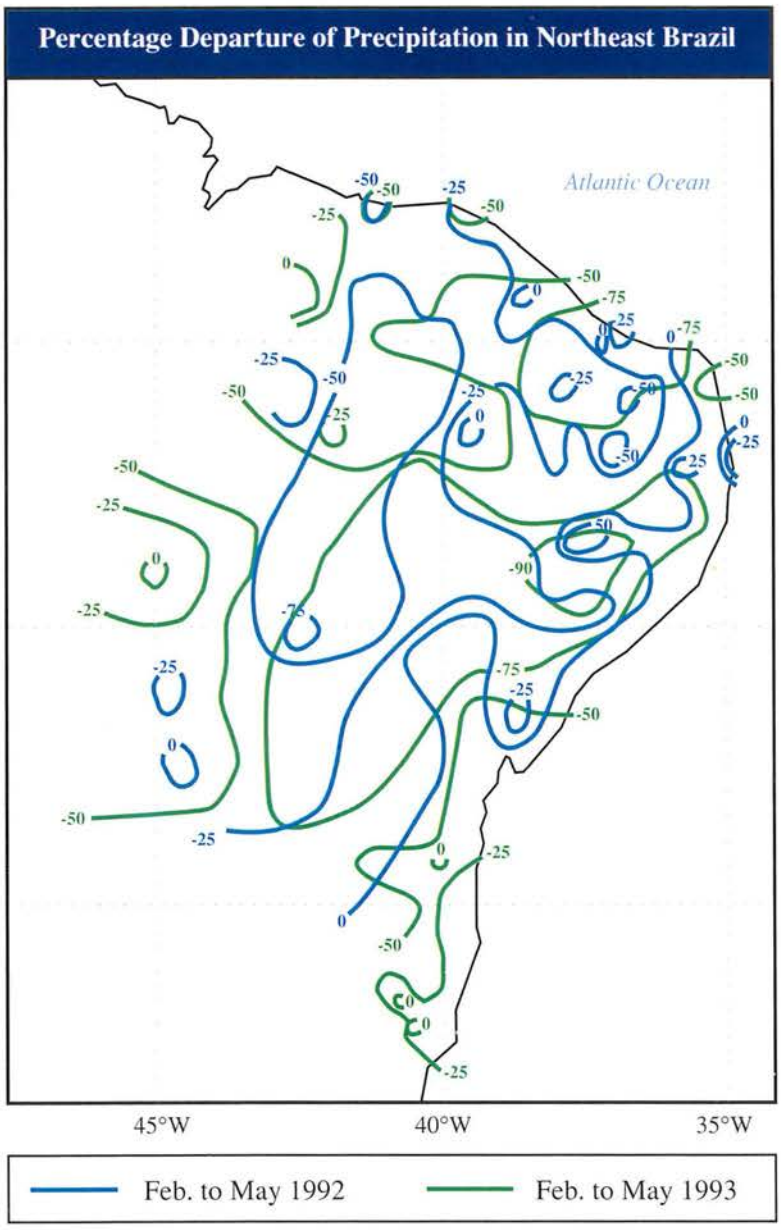

5.4 DROUGHTS IN AUSTRALIA AND NEW ZEALAND

Northern and eastern Australia experienced rather patchy precipitation, resulting in moisture deficits during the review period. Over northeastern New South Wales and central, southern and eastern Queensland, rainfall deficiencies from early 1991 to the end of 1993 were the worst on record (Figure 5.10). Both the 1991-92 and 1992-93 wet seasons failed. Rainfall deficits for the period 1990 to 1994 in Toowoomba compared with historical droughts are shown in Figure 5.11.

The 1991-92 wet season failed

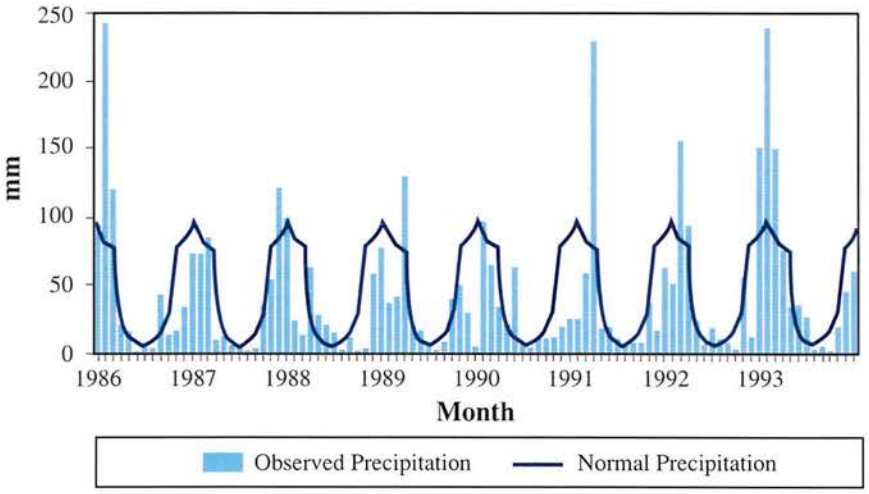

▲ *Figure 5.8* – Monthly mean precipitation totals (mm) in California (January 1986 to December 1993). Solid curve shows the mean annual cycle (1961-1990) of precipitation (from NOAA, National Climatic Data Center, Asheville, NC).

over northwestern Australia, where some areas received record low amounts of rainfall. The 1992-93 wet season also commenced late (second half of January) and finished early, but did produce very heavy rains over inland northern Australia for six weeks. During the review period, parts of southern Australia also experienced drought for periods up to about a year, for instance, northern and eastern Tasmania and parts of southern South Australia and adjacent southwestern Victoria (autumn through late spring 1993) and southwestern Australia (spring 1992 through winter 1993).

The extremely dry conditions over northeastern Australia extended over the southwest Pacific, with eastern Papua New Guinea, Vanuatu, New Caledonia, Fiji and Tonga often receiving only a fraction of normal rainfall for many months on end.

New Zealand also experienced long dry spells from 1991 to 1993. Persistent southerly-component flow meant that certain areas were shielded from rain-bearing winds for extended periods. However, periodic shifts in the flow (between southwest and southeast) caused the areas affected by dry weather to vary. In the South Island, conditions were very dry on the West Coast and nearby hydro lakes districts in the autumn-early winter period of both 1991 and 1992. In 1991, the hydro lakes dropped to their lowest levels since the 1950s. Similarly, severe drought affected the Gisborne-Hawke's Bay region (east coast of North Island), throughout the period May to late October 1991, until broken by heavy rain.

Rainfall in 1992 was well below normal in much of South Island. Fiordland (west coast), normally very wet, along with Otago and the MacKenzie Basin area to the east, were particularly affected. In 1993, the northern regions of the North Island were exceptionally dry; for example, the Bay of Plenty area, with only about 50% of normal, had their driest year on record, while Auckland and Rotorua had their driest year since 1919.

Figure 5.9 – Southeast USA precipitation, June to August 1895-1993. The straight horizontal line is the long-term mean. The bold smooth curve is a nine-point binomial filter that filters out the year-to-year fluctuations and shows the longer term variations (from the National Climatic Data Center, Asheville, NC.).

▼

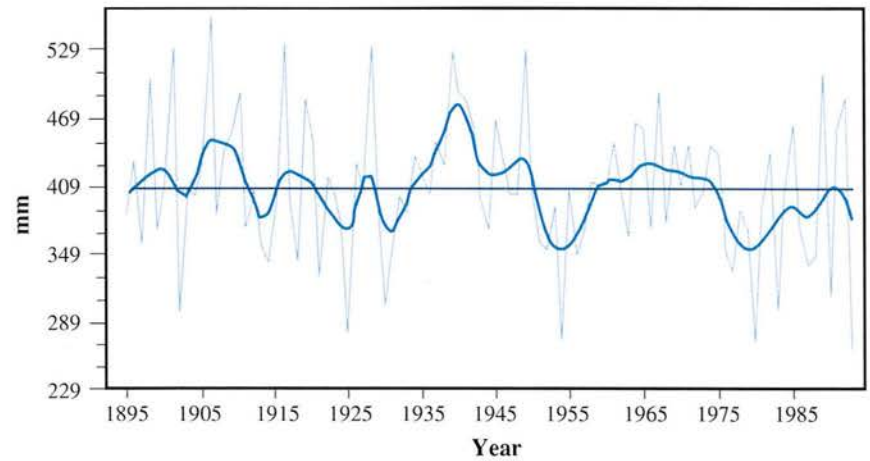

5.5 DROUGHTS IN EUROPE

Blocking high pressure during summer 1992 kept western Europe hot and dry. The dry spell in the early summer was in some regions one of the worst of the last decade devastating crops and causing several wild fires, especially in eastern Denmark, central Poland and northern and western Germany. In some areas, there was no rain at all in June, a rare happening. Denmark received only 10% of its normal summer rainfall. Less than 25 mm of rain fell on southeastern France, parts of central and northwestern Italy, central and western Hungary, northern Serbia, western and southern Romania, western Russia and southern and eastern Poland.

Temperatures averaging 3-6°C above normal made August 1992 the hottest ever in central and eastern Europe. In Austria, a reading of 36°C was reportedly the highest ever recorded for the month. Romania had its hottest summer in 28 years. Agriculture across Europe was adversely affected. In eastern Germany, drought cut the grain yields by 25% from 1991 totals. Norwegian wheat production was expected to drop 40% from 1991 and, in Finland, production dropped some 48% from a year ago. In Hungary, the beginnings of the

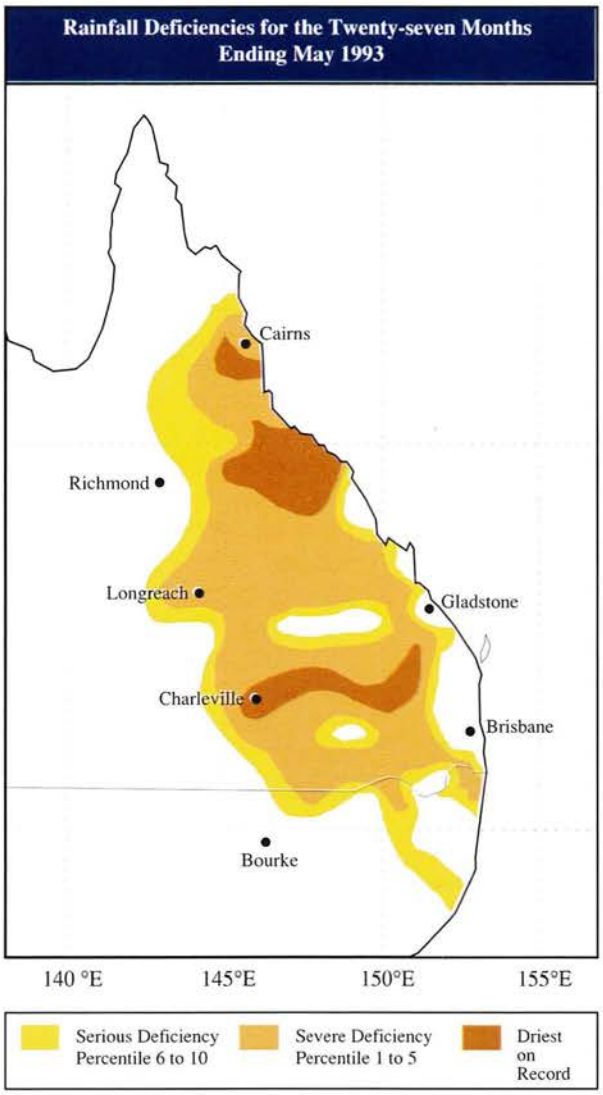

◀ *Figure 5.10 –* Rainfall deficiencies for the twenty-seven months ending May 1993 in northeastern Australia (from National Climate Centre, Bureau of Meteorology, Melbourne, Australia).

drought could be traced to early in January and February when the country received less than half of its normal precipitation. April was very dry, May had spotty showers and June was wetter than normal. By the middle of July, drought had gripped the country. August was the driest in the last 120 years, with only 13% of the normal precipitation and extremely high temperatures.

Repeatedly since the 1980s, winter precipitation in southern Europe has been deficient. The Mediterranean Rim suffered from record-lasting droughts which seriously affected agriculture, lowered or dried up ponds and lakes and forced water rationing. The increased frequencies and intensities of droughts are related to a recent trend towards higher upper atmospheric pressure-level heights and higher surface pressures in the Mediterranean basin in winter.

Severely dry weather spread across much of southern Europe and northwestern Africa from November 1991 to March 1992, following four to five consecutive years with below-normal rainfall. Central Spain and Portugal, and northern Morocco received only 6 to 25% of normal

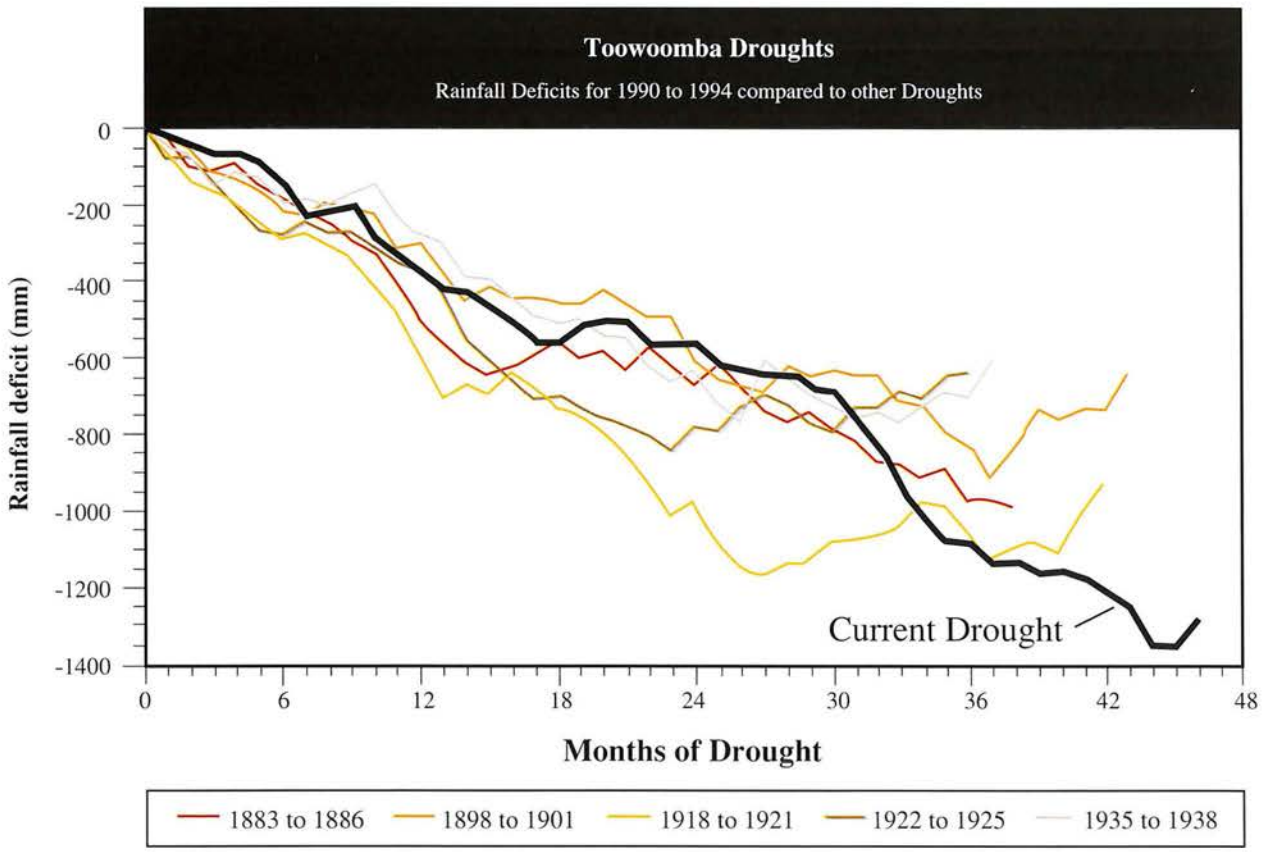

Figure 5.11 – Cumulative rainfall deficits in Toowoomba (inland southeast Queensland) during the 1990 to 1994 drought compared with other historical droughts (from Queensland Regional Office, Bureau of Meteorology, Australia). ▼

precipitation from late November 1991 (Figure 5.12). Portugal's dry spell was one of the nation's worst ever. Reservoirs were half empty and the fodder crop production was very poor. In the following winter season, an extensive area from the Atlantic coast of Portugal and southern France eastward to the Balkans received less than half of normal precipitation. Some districts in southern Spain and France, northern Italy as well as Slovenia had less than 10% of normal precipitation from December 1992 to March 1993.

The prolonged dry spell affected the 1992-93 winter wheat crop of Morocco and forced restrictions on irrigation and reductions in hydro-electric output. Except for some brief rains in early March, the abnormally dry weather persisted around the Mediterranean Rim until widespread rains dampened much of Europe in mid-April. The relief, however, was short-lived, as abnormally hot and dry conditions slowly redeveloped in May and covered most of southern Europe through the summer. By the middle of September, powerful storms ended the dry spell across most of the region.

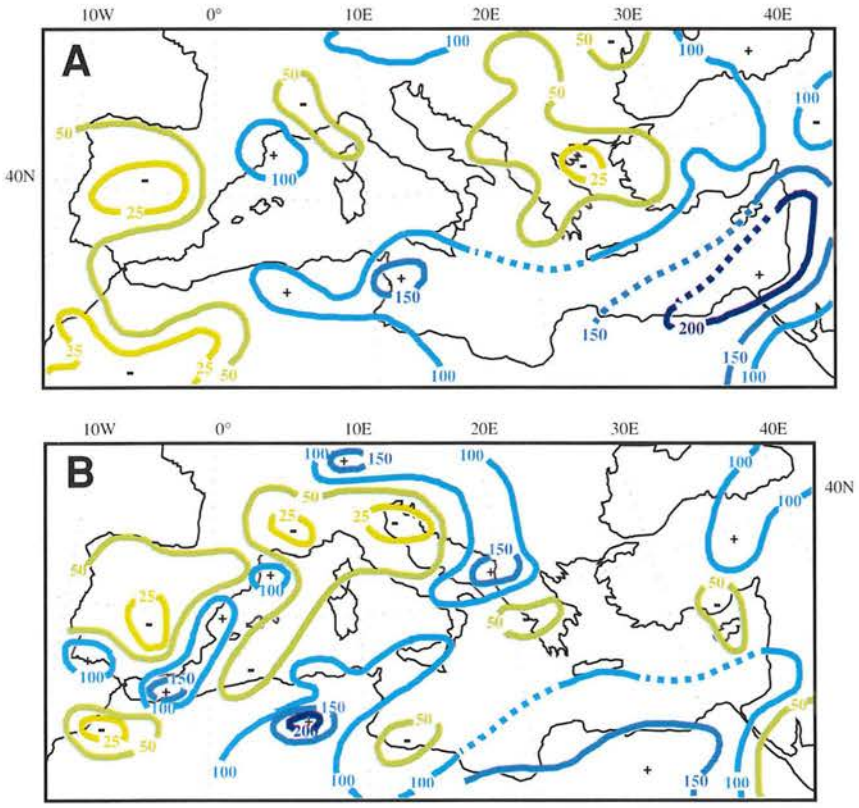

▲ *Figure 5.12* – Precipitation, in percent of normal, in the Mediterranean region from November to March (A) 1991-92 and (B) 1992-93.

5.6

DROUGHTS IN ASIA

Most of Asia had intermittent precipitation through 1991, characterized by dry and wet spells. Notable deficits in precipitation occurred across central Pakistan and the far north of India. This dryness continued until mid-July 1992 when heavy rains broke the drought. Meanwhile, Sri Lanka and southeastern India were experiencing drought as were parts of China, Southeast Asia and northern Philippines. Whereas several tropical cyclones brought heavy rainfall to southeastern coastal China, the interior provinces in the southeast recorded less than half of normal rainfall during the last half of 1992. Crops were severely stressed throughout the region. In Sri Lanka, the drought during the first half of 1992 was the worst since 1983. By the end of March, much of Sri Lanka had only received under 10 mm of rain compared with normal totals by that time of the year of 150 to 370 mm. The government requested humanitarian aid to combat the effects of the drought.

Although 1993 witnessed copious rainfalls over most of Asia, Taiwan and the southern Ryukyu Islands experienced unrelenting dryness, especially between mid-June and mid-October when many stations reported less than one quarter of their normal rainfall. As a result, water rationing was enforced while the worst drought in 40 years ravaged Taiwan. Dry weather that began over portions of northwestern Thailand in June 1993 seriously affected the nation's corn crop.

In a normal year, north China has an annual rainfall of between 500 and 700 mm of which 60% falls within the monsoon summer season of July and August. However, there is large interannual variability. Since 1980, summer precipitation has declined by about 20% compared to the normal rainfall. This trend to drought in mid-summer has coincided with a southward shift of the West Pacific High (WPH) pressure system. Hence the northern monsoon rainy belts are found farther south, leaving the vast region of north China in a dry zone. While north China has experienced precipitation between 20 and 30% below the normal rain during the period 1980-1993, the Yangtze basin had floods (Figure 5.13). The alternating pattern of drought-flood has occurred in eight of the last 14 years -1980, 1982, 1983, 1984, 1987, 1989, 1991 and 1993, which is unusual in an historical record dating back to A.D. 950. Through the work of Xu, it has been found that the droughts in north China correlate positively with those in the Sahel. A possible cause of this southwardly displacement of the high summer monsoon system may be related to decreasing global solar radiation and clear skies in China since the late 1970s, mainly due to the increased discharge of SO_2 from the rapidly increasing industrialization of China.

The higher incidence of recent droughts that occurred in north China has had disastrous effects on

the economy. Water consumption since 1949 has increased more than ten times. Underground water has been extracted, resulting in an accelerated decline of underground water levels in most areas of north China. Today, the water supply is deficient even in a normal year, let alone in years with persistent droughts.

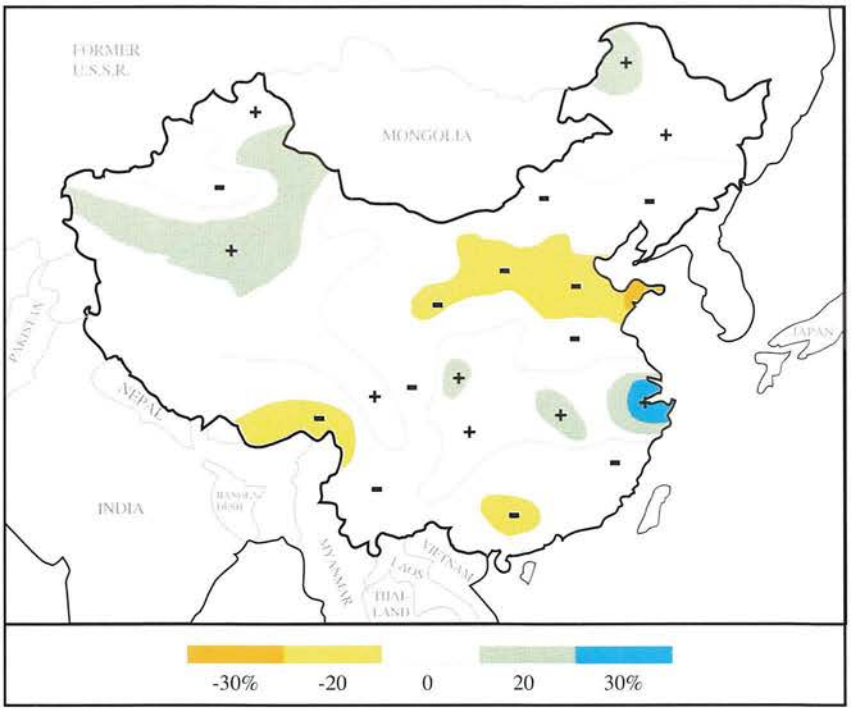

Figure 5.13 – Precipitation anomalies, expressed as percentages above and below normal for high summer in China during 14 recent years (1980-1993) (from Jiangsu Meteorological Institute, Nanjing, China).

Floods are one of the most widespread and destructive of natural disasters. Floods are recurring in many parts of the world, causing loss of life, destruction of property and natural environment, as well as economic disruption. However, two major flooding events stand out as being particularly noteworthy, one in the midwestern USA and the other in western Europe, both occurring in the second half of 1993.

Flooding is caused by a variety of factors, not all of which are meteorological. Topography and the hydrological capacity of the subsoil are critical factors. Deforestation and covering the earth with impermeable substances such as asphalt are two human activities that can contribute to the increased frequency and intensity of flooding. Meteorological factors include major tropical and extratropical storms, rapid snow melt, ice jams on rivers, wind-driven surges, prolonged wet spells and severe thunderstorms. Floods also occur during long periods of continuous, heavy rains during monsoons.

So-called flash floods, caused by very short-term localized and intense thunderstorm activity, are very common and sometimes extremely destructive. Examples of this type of flooding abound during the review period. The catastrophic floods at Vaison-la-Romaine in the southeast of France on September 21-22, 1992 were particularly devastating causing numerous deaths. In the southern hemisphere there were record rainfall totals of over 500 mm in southeastern New South Wales in June 1991. In South America, rains of up to 300 mm in two hours caused a dam to burst in northern Argentina, killing dozens of people in January 1992.

Typically, major floods occur when too much water accumulates in too short a time. This is precisely what happened in western Europe and the Mississippi watershed in 1993. In both cases, the prolonged period of wet weather was caused by persistent atmospheric circulation patterns that produced a flow of moisture-laden air masses over the region from the southwest and west.

During the review period, several major floods around the world, shown in Figure 6.1, resulted from tropical cyclones, hurricanes and typhoons and intense thunderstorms.

Flooding from monsoons and tropical cyclones is covered principally in Chapters 7 and 8.

6.1 FLOODING IN ASIA

In the spring-summer period of 1991, a series of low-pressure systems travelling along a stalled polar front triggered heavy rain over central China. Most of the rain fell in three surges - May, mid-June and early July. Flooding along the Yangtze and Huaihe rivers became catastrophic when 100 to 530 mm of rain fell from 30 June to 6 July.

Total spring-summer rainfall in some regions of the Yangtze/Huaihe river basins reached 1000 mm with a maximum centre at 31.2°N, 115.7°E, receiving up to 1613 mm. Figure 6.2 shows the distribution of total rainfall and anomalies in the Yangtze/Huaihe river basins during an especially wet period, 18 May to 13 July 1991. The flooding afflicted

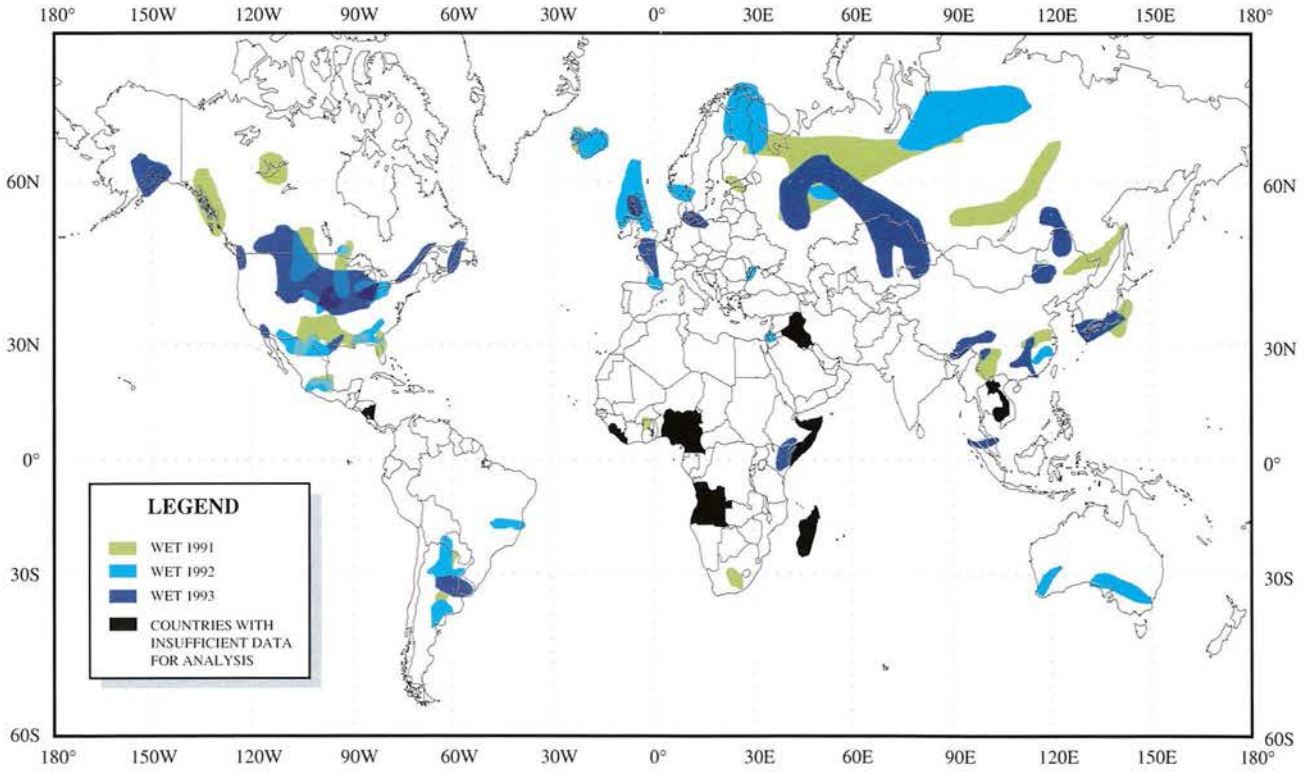

▲ *Figure 6.1* – Areas where precipitation anomalies were estimated to be within the wettest 10% of climatological occurrences, January to December, 1991, 1992 and 1993.

nearly one hundred million people and inundated more than 13 million hectares of farmland. It was the largest flood in nearly 40 years in central-eastern China, resulting in severe economic losses of up to US$ 9 billion. The water devastated crops, houses, roads, bridges and rail lines, with the most severe damage in the eastern provinces of Jiangsu and Anhui. By late July, the death toll had reached nearly 1,800. In Anhui Province, the flooding was said to be the worst since 1949. More than 6.5 million homes were destroyed or damaged and 10 million people had to be evacuated. Damage from heavy rains elsewhere in China only added to the summer carnage. By late August, at least 2,295 people had died and nearly 50,000 had been injured in torrential rain and flooding in 20 Chinese provinces.

From early March through late April 1993, two to twelve times the normal rainfall amount fell across central portions of the Middle East. Much of southern Syria, eastern Jordan, Saudi Arabia and western Iran were affected. The Karun and Dez rivers of Iran spilled over causing considerable damage.

During February, March and early April 1993, moderate to heavy precipitation soaked much of eastern China, Taiwan, the Ryukyus, South Korea and western Japan. From the Yangtze River valley southward, a torrential cloudburst dumped huge amounts of rain (up to 850 mm) on saturated soils, generating widespread flooding. Fujian province experienced the worst flooding in almost half a century. From mid-June to mid-July, heavy rains (up to 780 mm) continued to drench large sections of Japan, Taiwan and southeastern China, causing severe flooding in the Chinese provinces of Jiangxi, Guizhou and Zhejiang. In Japan, over 2,000 mm inundated parts of Kyushu during the period as tropical cyclones affected the islands, generating localized flooding and taking several lives. Farther south, a steady progression of tropical cyclones brought strong winds and torrential rains to the Philippines, Viet Nam and southeastern China beginning in late July. In September, heavy rains from two typhoons

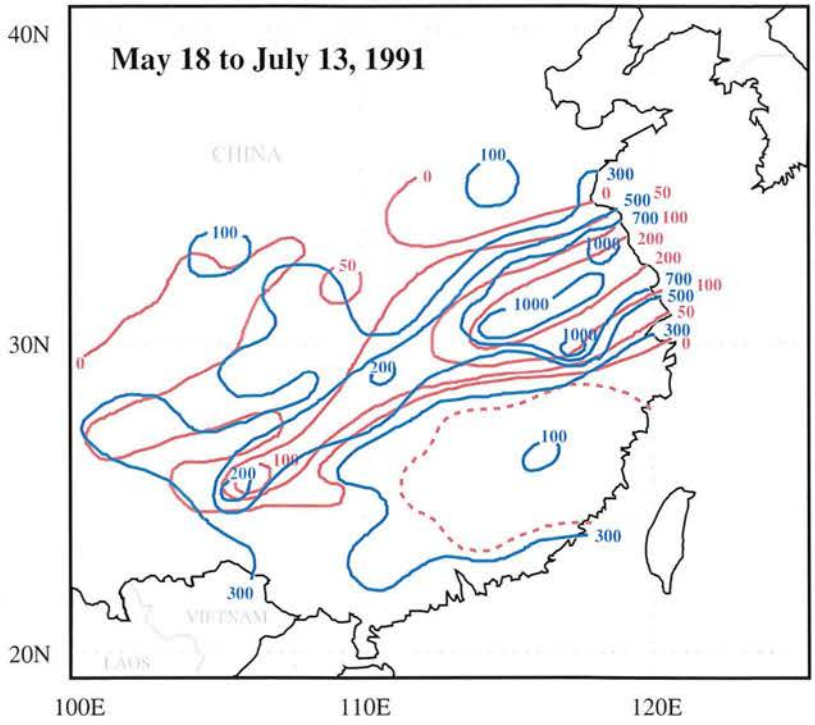

▲ *Figure 6.2* – Total precipitation amounts and precipitation anomalies (in percent of normal) in the Changjiang and Huaihe river basins from 18 May to 13 July 1991 (from Jiangsu Meteorological Institute, Nanjing, China).

drenched Hong Kong and southern China (Figure 6.3). Almost 500 mm of rain inundated Hong Kong and 15-day totals of 200 mm or more extended well into adjacent southern China. The Shenzhen River, which marks the Sino-Hong Kong border, overflowed its banks, forcing the closure of the main road connecting Hong Kong and southern China.

Of major significance, the Philippines were affected by 32

▼ *Figure 6.3* – Total precipitation from two typhoons, 12-26 September 1993 in Hong Kong and southern China (from NOAA/NWS/NMC/CACWashington, DC).

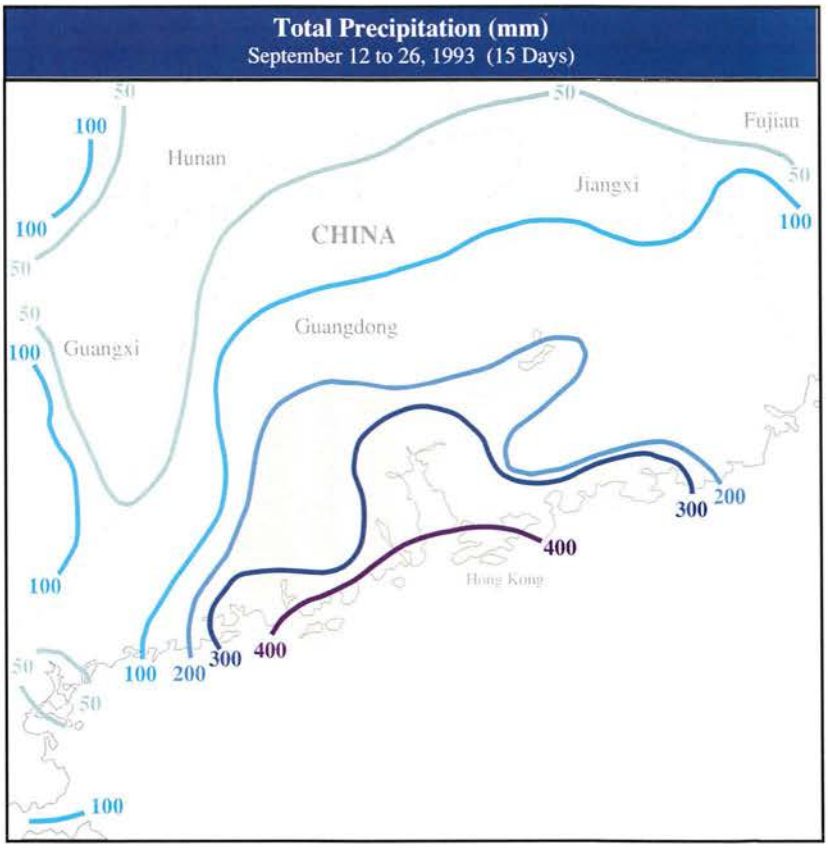

tropical systems during 1993 (the most on record for a single year), with as much as nine times the normal precipitation deluging parts of southern Luzon during the last 45 days of the year.

6.2 MAJOR FLOODS IN AUSTRALIA, NEW ZEALAND AND THE SOUTH PACIFIC ISLANDS

The period June/July 1991 was particularly warm and wet in southeastern New South Wales, Australia, with a combination of cut-off lows and tropical-extratropical cloudbands producing torrential rains in southeastern New South Wales (over 500 mm in the June event) and over eastern Victoria. Severe drought in the Gisborne-Hawke's Bay area between May-late October was broken by very heavy rains in late October-early November 1991. Major flooding occurred during both seasons.

Although the 1991-92 wet season generally failed over northern Australia, parts of eastern New South Wales and Queensland received torrential downpours in December and again in February (e.g. 200 mm in 9 hours in southeast Queensland), generating some of the century's worst flooding. Severe flooding occurred in Northland, Hawke's Bay and Wairarapa between July 21 and 23, 1992, with numerous land slips and road closures throughout the area.

Autumn 1992 was particularly wet over the southwestern half of the continent, with record rainfall amounts and some flooding over inland southwestern Australia. This rain was mostly associated with tropical-extratropical cloudbands, which were especially well developed in autumn and most of winter 1992. One surge across the Northwest Cape area of Western Australia in June generated 80 to 170 mm of rain (June normal 20 to 30 mm), with subsequent flooding. Another event triggered heavy rains in southeastern Australia late in August, culminating in devastating flash floods in the Adelaide Hills.

The five-month period September 1992-January 1993 featured consistently cool, wet conditions over southeastern Australia with frequent flooding. Record wet conditions drenched extensive areas of the southern half of South Australia, southwestern New South Wales and northern Victoria, particularly in the October-January period. Heavy downpours and thunderstorms, many of them producing flash flooding, were a feature of this period, especially the last three months.

Despite a generally late start and early finish to the 1992/93 wet season in Australia, very heavy rains did produce flooding. As a result of Tropical Cyclone Niña, some 500 mm of rain drenched Cape York Peninsula in the second half of December. The period from late January to the end of February was exceptionally wet over northern Australia, as slow moving monsoonal depressions unloaded up to 200 mm per week over much of the tropics (Figure 6.4). The systems also drenched parts of the Sunda Islands of Indonesia, where flooding claimed

▼ *Figure 6.4* – Total precipitation from 17 January to 6 February 1993 across northern Australia and southwestern Indonesia (from NOAA/NWS/NMC/CACWashington, DC).

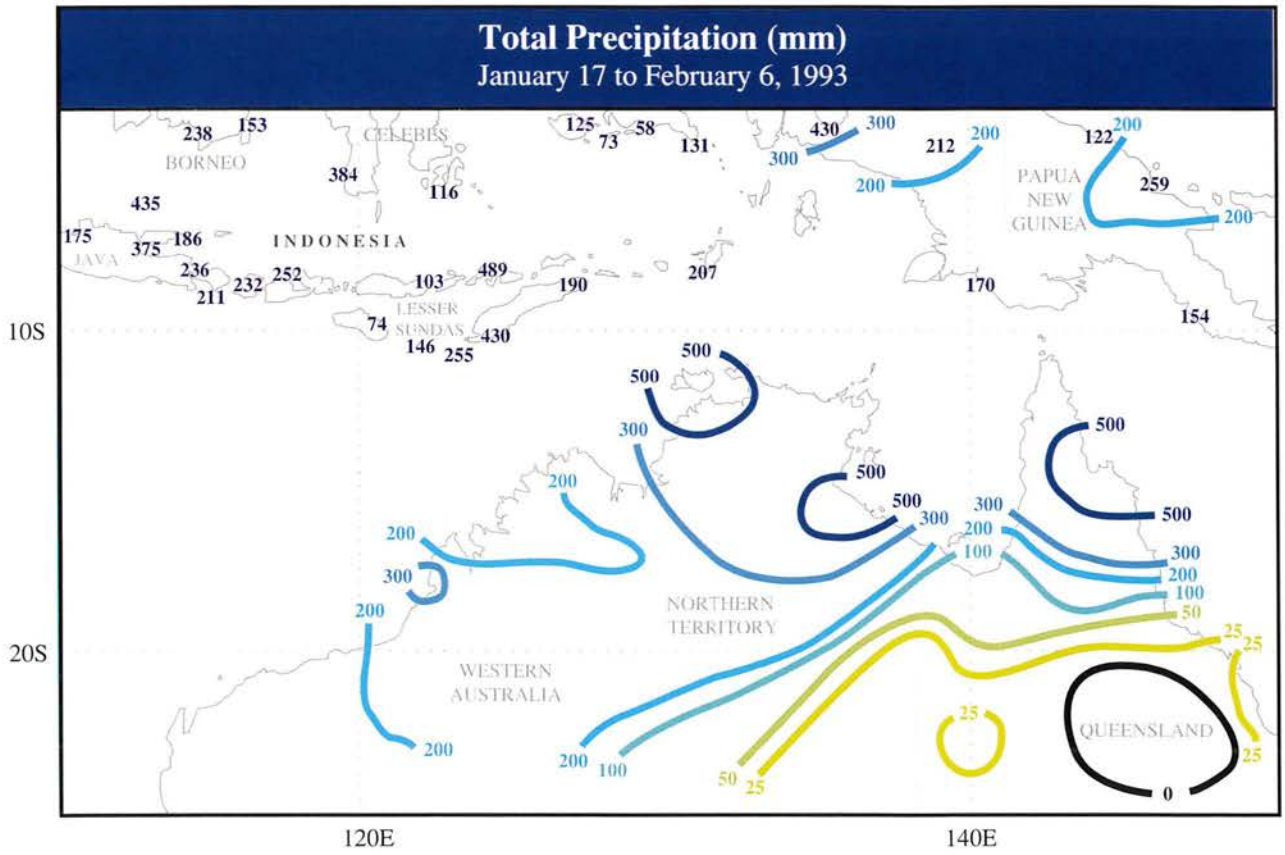

▲ An optimistic Benalla resident tries to make a telephone call from a flooded telephone booth during the October 1993 floods (from Shepparton News)

thousands of lives, left 250,000 homeless and destroyed over 500 km² of rice fields.

Very heavy rains in southeastern Australia in September and early October 1993 triggered frequent and sometimes major flooding on rivers in New South Wales and northeastern Victoria. Torrential rains (150-250 mm within 24 hours) overnight on October 3-4, over the already saturated highland catchments of southern New South Wales and northeastern Victoria, triggered devastating flooding on rivers draining the area with the degradation of much valuable agricultural land and infrastructure. In New Zealand, high rainfall in catchment areas on December 22-23, 1993 caused rivers to overflow in Kaikoura and Otago. Resultant flooding was most severe in Kaikoura.

Conditions were very wet in the area around the Dateline (e.g. the Gilbert Islands area) and over the island groups to the east, including the Marquesas and French Polynesia, and over the Cook and Society Island groups. The Kiribati group, which includes Canton and Fanning Islands,as well as the Gilberts, had extremely variable conditions - record rains in some months (including 1,650 mm in March 1992 at Fanning), interspersed with long spells (up to nine months) of typically arid conditions. Tropical cyclones Esau and Fran caused extremely heavy rains in Vanuatu and New Caledonia in March 1992. A tropical cyclone at Nadi (Fiji) set a record - 788 mm in February 1993 -

▼ *Figure 6.5* – Total precipitation across central Europe from 8 September to 4 October 1993 and daily cumulative precipitation totals for four locations (from NOAA/NWS/NMC/CACWashington, DC).

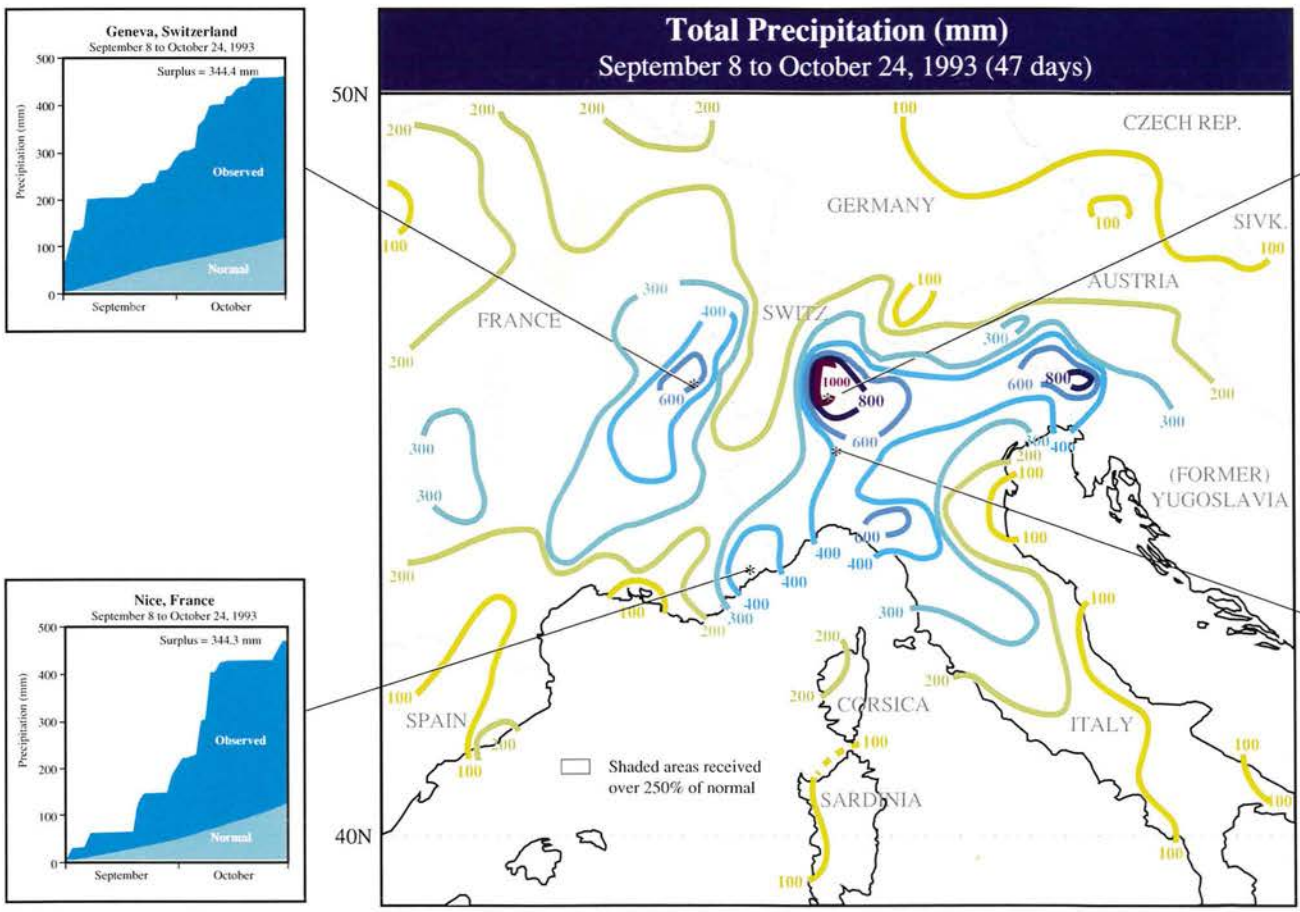

with severe flooding late in the month, while in March 1993, Apia (Western Samoa) had a record 890 mm, most of which fell in a 5-day period.

6.3

FLOODING IN AFRICA

November/December 1992 featured exceptionally wet conditions in Zimbabwe (where severe flooding occurred), eastern Botswana, northern South Africa and southern Mozambique. Although the 1992-93 wet season got off to a late start, torrential rains affected Zimbabwe, northern Mozambique, most of Malawi, Tanzania and Kenya during February and April 1993, generating local flooding in some cases.

Wet season (May to September) rainfalls in 1993 were near to above normal (120%) in parts of southern Senegal, central Burkina Faso, central Mali, central Niger, southern Cameroon, and central and northwestern Kenya. In early August, flooding along the Blue Nile in Sudan forced sharp cuts in the nation's hydro-electric power production. In late September, heavy rains flooded farmlands and left over 10,000 people homeless in northern Ghana. Several hectares of farmland were completely submerged for a short time. Heavy rains soaked large sections of southern Africa in late September/early October 1993, followed by further heavy rains in December. Some areas received up to 250% of the normal quota between late September and December.

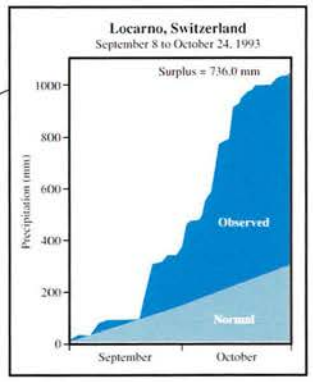

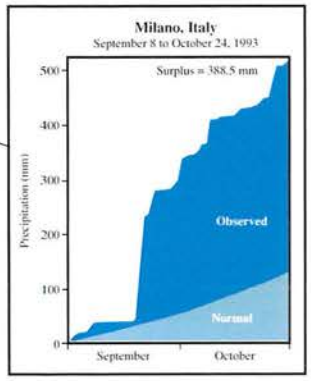

6.4

MAJOR FLOODS IN SOUTH AMERICA

The 1991/92 wet season was very wet over much of east/central South America. The wetness corresponded with low-index warm phase ENSO episodes. Although flooding was not generally a serious problem, some significant floods and mud slides affected northern Argentina in late 1991 and flash floods in January 1992, associated with local torrential rains, affected parts of Rio de Janeiro and northern Argentina. In the latter event, rains up to 300 mm in two hours caused a dam to burst, killing dozens of people. May was also exceptionally wet, with rainfall exceeding 400 mm in parts of northern Rio Grande do Sul and central Santa Catarina provinces of Brazil. River flooding was a chronic problem along the Pilcomayo, Paraguay and Parana rivers in northern Argentina when abundant rains persisted well into July.

Heavy rains deluged Argentina and Bolivia in December 1992; in the latter country, a resulting land slide claimed hundreds of lives. The autumn/early winter period in both 1992 and 1993 featured heavy rains in Ecuador and rains with local flash flooding in those very dry parts of Peru and the northern desert region of Chile where normally the only time rain falls is during El Niño events. Extremely heavy rains deluged south-central Chile, Uruguay, northeastern Argentina and southeastern Paraguay during April/May 1993; up to 400 mm fell in three weeks.

6.5

MAJOR FLOODS IN EUROPE

Torrential rains inundated parts of Europe during July 1991, drenching areas from southern Germany southeastward to the Black Sea. Over 200 mm of rain deluged the area around Salzburg, Austria, taking at least five lives and closing dozens of roads. The swollen Danube River was closed to shipping between Linz and Vienna. The flooding was the worst in Austria in 30 years. In addition, heavy rains in northeastern Romania caused a dam to burst, washing away entire villages and claiming over a hundred lives. In the western Ukraine, 11 people were reported killed or missing after five villages were flooded.

A persistent upper-level trough brought frequent storms to the western Mediterranean region in September and October 1992. In southern France, torrents of rain, 200 to 450 mm in 12 hours, fell on September 21-22, causing one of the country's deadliest floods on record. The flood extended from the Mediterranean coast to the Rhone Valley in Provence. According to witnesses in the Vaucluse region at Vaison-la-Romaine, a wall of water up to 15 m high simply rushed through the town, sweeping away cars and caravans, some of which were occupied. Huge trees pierced the walls of houses and vehicles. Throughout the region, roads and bridges were destroyed. Thirty-two people were drowned and another 50 reported missing. Flooding, a few days later, took several lives in eastern parts of the Pyrenees and on Corsica. The storms lasted only a few hours, but there were extreme intensities (50 mm/30 min and 80 mm/h) in many places - the highest ever observed. Several rivers overflowed their banks and entire villages were isolated.

Heavy rains across parts of western Europe during September and October 1993 forced the Rhone, Saone and Durance rivers out of their banks at some locations. The effects of the wet spell reached south of Rome, where mud slides caused power outages and runoff fouled

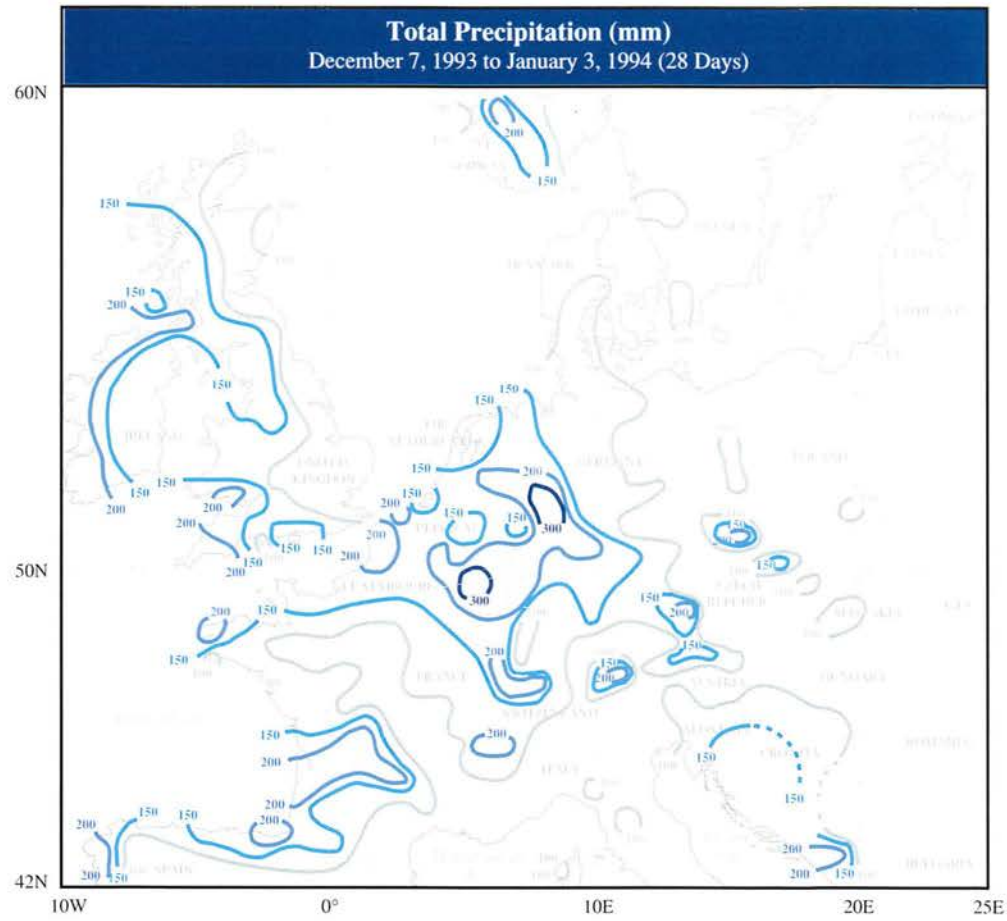

Figure 6.6 – Total precipitation in Europe from 7 December 1993 to 3 January 1994 (from NOAA/NWS/NMC/CAC Washington, DC).

drinking water. In Madrid, 192 mm of precipitation fell, the highest amount registered since the meteorological observing programme began in 1854, exceeding the previous October maximum of 171 mm (1960).

Flooding occurred along the shores of the Lago Maggiore and the Lago di Como after lake-level rises of up to 5 m. In Rome, heavy flooding occurred on the Tiber River. Wide areas of Venice, including the famous Piazza di San Marco were also flooded; so was the Camargue where 10% of the French rice crop was lost.

Mid-November rains caused flooding in Greece that forced evacuations. Abundant precipitation continued until mid-December. At the end of the year, localized flooding claimed two lives, closed highways and disrupted electrical power in southern Israel. Eilat received 43 mm from December 20 to 23, some 130% of its normal annual rainfall.

Large sections of southeastern France, western Spain, central Portugal, Corsica and northern Morocco recorded from two to three

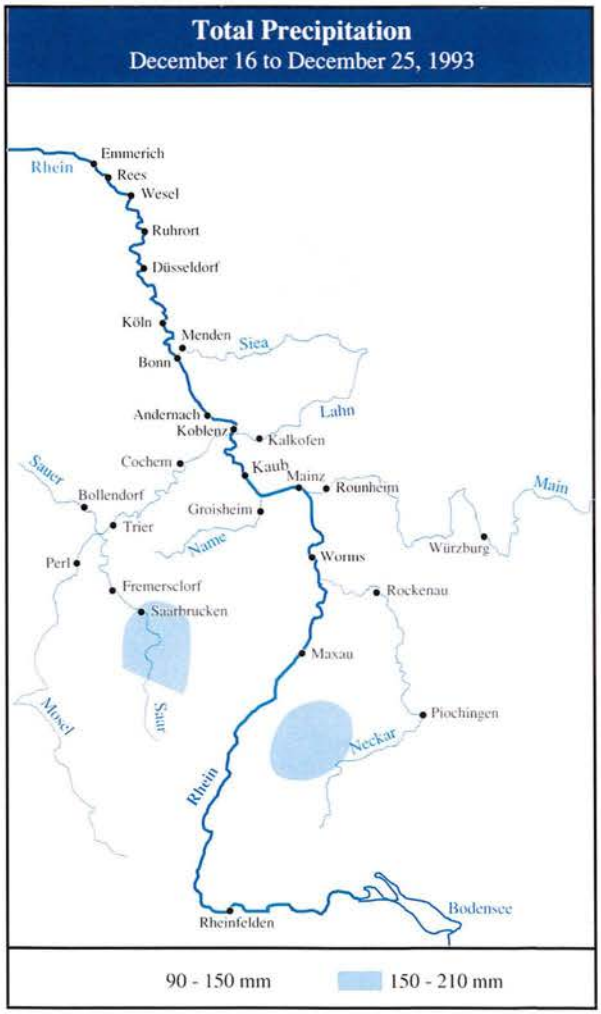

Figure 6.7 – Total precipitation in the Rhine River basin from 16-25 December 1993. Map of the Rhine area with positions of the most important water level gauges (from Jahresbericht 1993, Bundesanstalt für Gewässerkunde, Koblenz, 1994).

times the usual precipitation during September 22 to November 6, 1993. Through much of south-central France, across the Alps into Switzerland, northern Italy, Austria and Slovenia, rainfall totals were between two and four times the normal (Figure 6.5). Southern England, where rain fell from September 19 through October 13, endured one of its wettest Octobers on record.

A series of intense storms in December 1993 invaded Europe causing severe flooding to much of central western Europe (Figure 6.6). Winds gusted to 145 km/h and rainfalls exceeded 250 mm. Some of the worst flooding in sixty years occurred across much of Germany, Belgium, eastern France and the southeastern Netherlands. Severe flooding at the confluence of the Mosel and Rhine rivers left one quarter of Koblenz under water (Figure 6.7). The floods claimed several lives, forced thousands to flee their homes just before Christmas and swamped roads and rail lines. The flood caused more than US$ 580 million in damages in Germany alone.

6.6

MAJOR FLOODS IN NORTH AMERICA - "THE GREAT FLOOD OF 1993"

Soaking rains in late June and most of July 1991 plagued central Mexico, resulting in extensive flooding. Near-normal conditions returned during August.

In Canada, more than 130 mm of rain drenched the lower mainland of British Columbia during the final week of August 1991, causing severe flooding in the Howe Sound area, north of Vancouver. Washouts and flooding occurred along many points of the Squamish Highway between Vancouver and Whistler. Hundreds of people were forced to flee their homes. Rail lines near Alta Lake were washed out. Flood damage was estimated to be about US$ 4 million.

At the end of the year, torrential downpours deluged much of central Texas around mid-December and combined with above-normal totals during the rest of the month to generate some of the century's worst flooding along the Guadalupe, Trinity, Brazos and Colorado Rivers. Weekly totals of 200-415 mm fell from Austin southward to San Antonio. Precipitation across Texas during December 1991 was greater than during any previous December since records began in 1895. Rains continued through March 1992 as an almost unrelenting spate of storms thrashed Texas and eastern Oklahoma. The vigorous flow of moisture from the tropical Pacific was associated with the El Niño/Southern Oscillation, which remained in a warm phase in the spring. State average December-February precipitation totals of 460 mm tripled the normal amount, making this by far the wettest Texas winter on record. Flooding killed more than 15 people and caused over US$ 75 million damage.

In the USA, national flooding totals in 1992 were below average in both deaths and damage - 55 deaths and about US$ 800 million. A 200 to 300 mm deluge in Puerto Rico triggered the nation's deadliest flood of the year, on January 5-6, 1992. Nearly the entire island suffered flash flooding and 23 people died. On February 9-13, flooding in southern

▼ Aerial view of wide area flooding along Mississipi River south of St. Louis, MO

Figure 6.8.1 – Midwest floods of June-July 1993. Series of small maps and diagrams illustrating hydrometeorologic features of the Midwest USA (NOAA, Office of Hydrology and Climate Analysis Center, Washington, DC; and Jack Williams, 1994).
▼

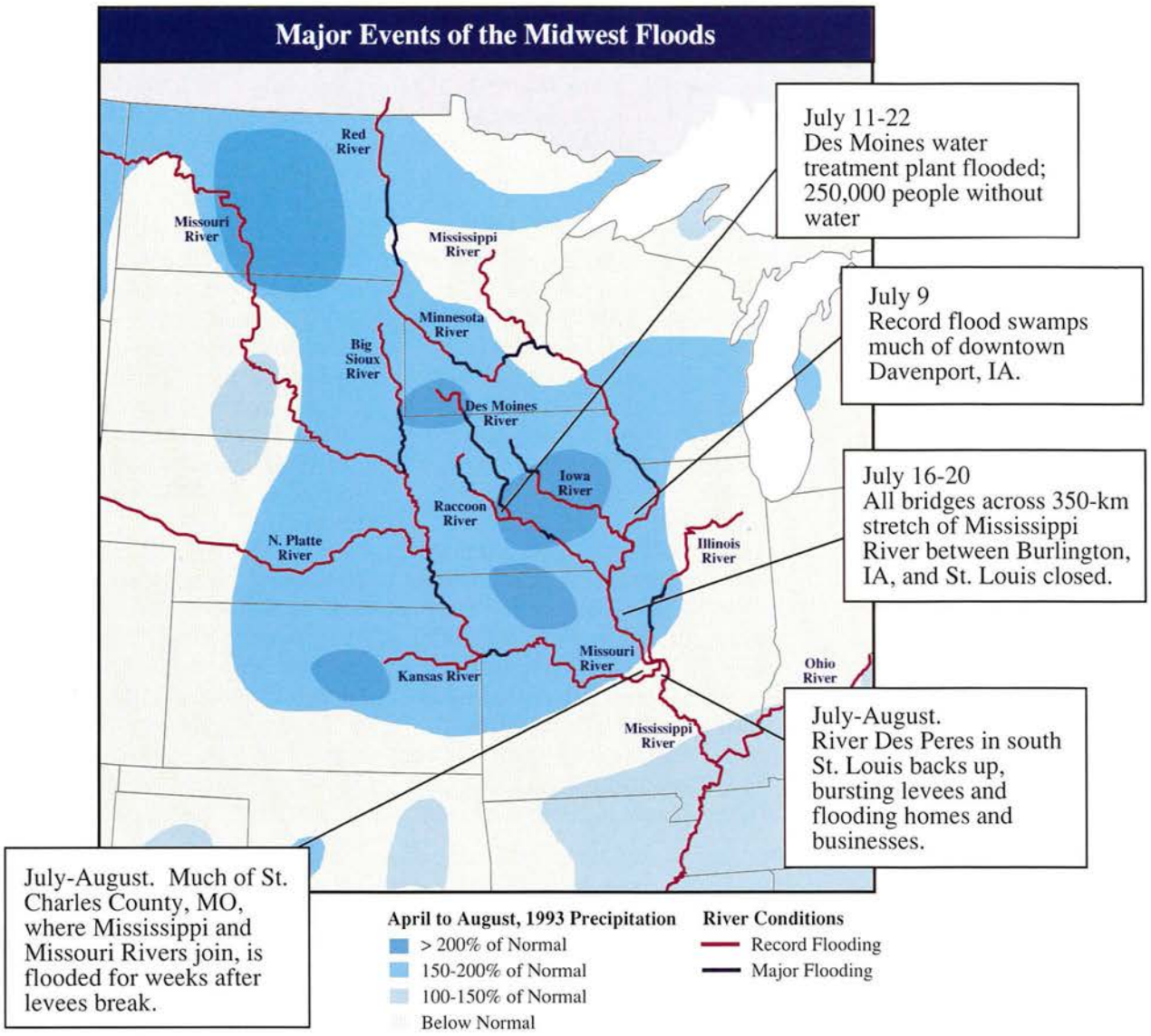

California caused eight fatalities and US$ 88 million damage.The Midwest flood was the dominant weather story across North America in 1993. Before the great flood, serious flooding in January occurred in Arizona and southern California. Flash floods and mud slides claimed several lives and caused considerable property and crop damage as Arizona's Gila River swelled to over 50 times its normal flow at the head of the Safford Valley.

The Great Flood of 1993 surpassed all floods in the USA during modern times in terms of precipitation amounts, record river stages, areal extent of flooding, persons displaced, crop and property damage, and flood duration (Figures 6.8.1-6.8.6).

▼ Flooded riverside park along the Mississipi, near St. Louis, October 1993.

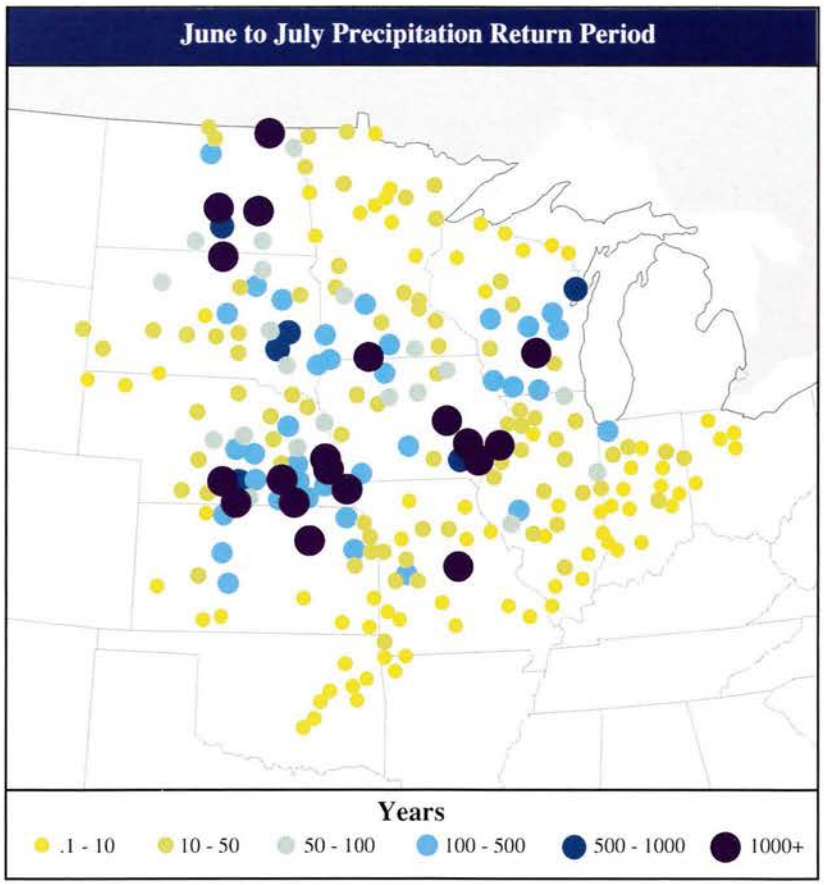

◀ *Figure 6.8.2* – 1993 June to July precipitation return period (years)

Figure 6.8.3 – Histograms showing river levels for select locations along the Mississippi River (top and bottom) and Missouri River (middle) during the Midwest floods.
▼

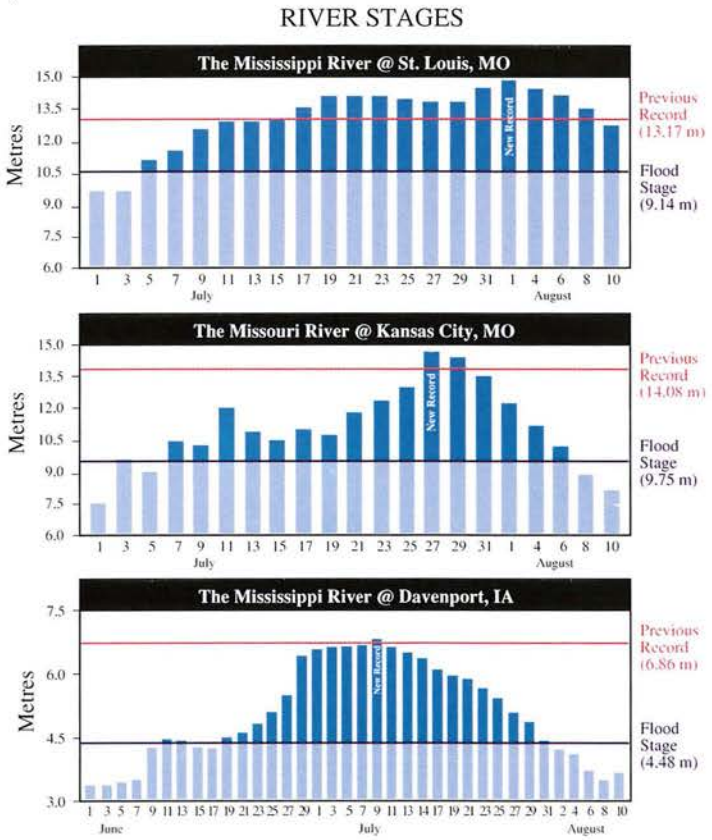

▼ *Figure 6.8.4* – Precipitation totals (mm) during June-August 1993.

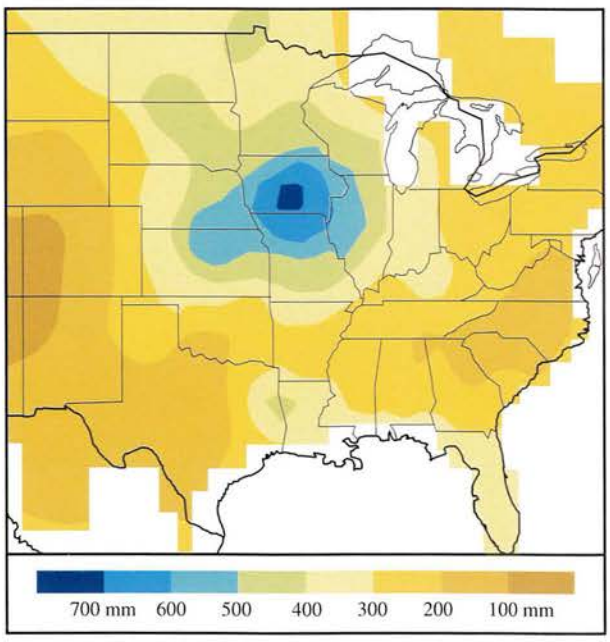

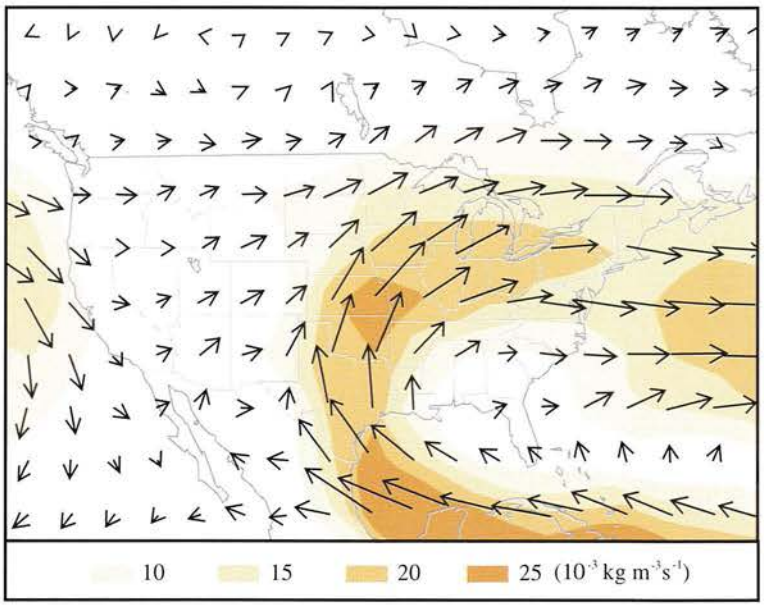

◀ *Figure 6.8.5* – Mean vertically integrated moisture transport (shaded, units are 10-3 kg m-3s-1) and 850-mb vector wind (m s-1) during June-July 1993 (from NOAA/NWS/NMC/CACWashington, DC).

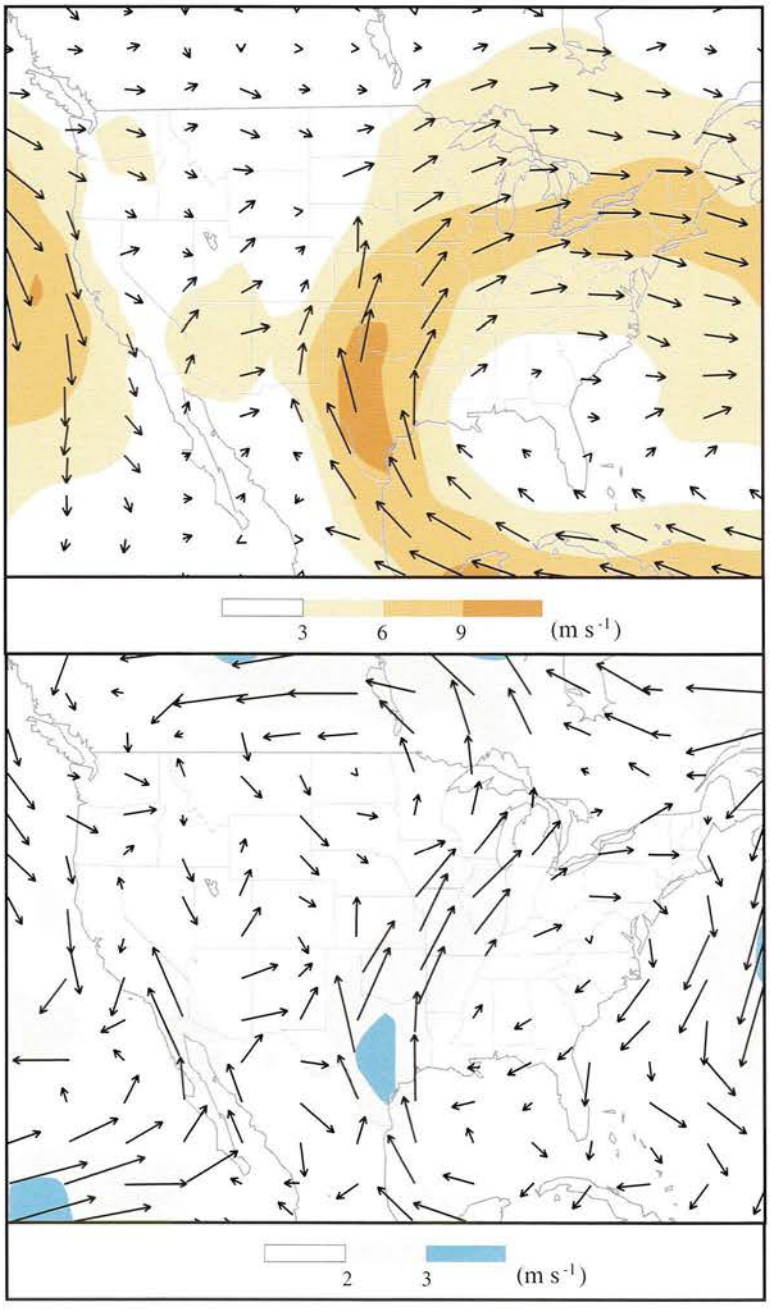

◀ *Figure 6.8.6* – Mean (top) and anomalous (bottom) 850-mb vector wind for June-July 1993. Anomalies are departures from the 1979-1988 base period. Contour intervals for isotachs are 3 m s-1 (top) and I ms-1 (bottom) (from NOAA/NWS/NMC/CAC, Washington, DC).

JULY 1991 FLOODING IN NORTHWESTERN TURKEY*

Severe weather in the form of exceptionally heavy showers and thunderstorms struck the coastal and inland areas of northwest Turkey in early July 1991 and led to widespread flooding that caused several deaths and a swath of material damage stretching from Istanbul to Samsun between July 6 and 8, 1991. The total rainfall recorded on July 6-7, 1991 exceeded 100 mm at Ataturk Airport. Warm moist air, coupled with upper atmospheric lows and cold pools, gave rise to very heavy rainfall, especially on north-facing mountain slopes. On July 7-8, 1991 heavy showers and thunderstorms drenched northwestern Anatolia with over 100 mm of rain at a few locations. Figure 6.9 shows combined rainfall totals for July 6-7 and July 7-8, 1991 on the south shore of the Black Sea. A large area, roughly from Bolu and Safranbolu to the Black Sea coast recorded over 50 mm during these two days; this comprised 70 to 90% of the month's rainfall. The region was badly flooded and there were at least 15 drownings. Apart from the loss of life, property losses were extensive, with hundreds of homes and work places flooded, several bridges demolished, roads swept away and hydro lines toppled. Agricultural land lay under several metres of water for a time, roads became impassable and many villages were isolated. Trees, carried by flood waters down from the forests on the slopes high above Goynuk, wreaked havoc in the town itself, knocking down electricity poles and bringing traffic to a standstill.

**Adapted from an article by E. Kirvar (1993).*

▼ *Figure 6.9* – Total rainfall in the Istanbul region for 6-8 July 1991.

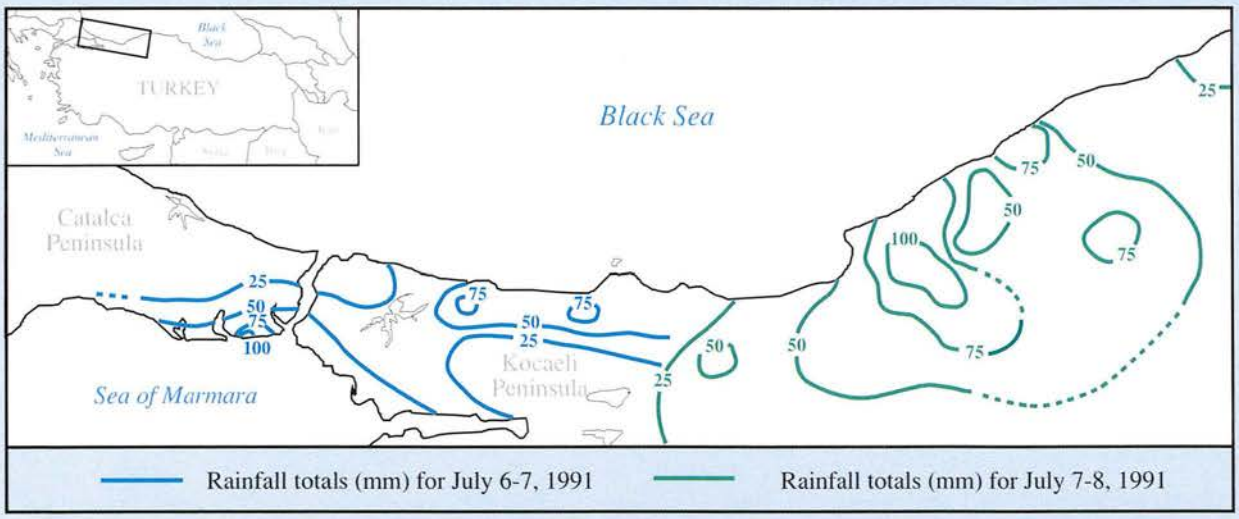

Record and near-record precipitation during the spring of 1993, on soil saturated from previous seasonal precipitation, resulted in flooding along many of the major river systems in the Midwest, including the Mississippi and Missouri and their tributaries. In the upper Mississippi Valley, from April through June, an average of 410 mm fell making these three months the wettest such period since records began in 1895. The normal for that period is 280 mm.

Prior to these excessive rains, however, the region was made ripe for flooding by above-normal precipitation that was persistently observed through most of the region beginning in July 1992, generating waterlogged ground and high streamflows and reservoir levels. There had been an excessive winter snow pack in the Rocky Mountains, saturated soil conditions in the Midwest and critical runoff conditions. As a result, long-term moisture surpluses occurred across a large portion of the east-central Great Plains and the middle Mississippi Valley. For some locations, rainfall totals amounted to an extra year's worth of rain over fourteen months.

At the beginning of summer 1993, the mean position of the unusually strong jet stream was dipped southward over the northern portion of the Mississippi basin, oriented SW-NE between a persistent low-pressure trough to the northwest and an unusually strong Bermuda High over the southeastern USA. Clockwise winds around this high-pressure area pumped humid, Gulf of Mexico air northward along the Mississippi Valley. The high pressure also helped block the eastward movement of thunderstorm clusters from the Midwest. The unusually large contrast between low pressure and the high pressure helped create stronger south-to-north winds, which brought in moisture-laden air causing the record-breaking rains. The boundary between the cool air and warm air stayed locked in place over the upper Mississippi Valley. Warm, humid air flowed over the

cool, dry air, which helped create thunderstorms. Another contributing factor was the influence of the sea-surface temperature anomaly in the tropical Pacific associated with the El Niño/Southern Oscillation (ENSO) phenomenon.

The combination of these circumstances resulted in the worst flooding in more than a century in the northern Mississippi basin. Record flooding occurred at nearly 500 forecast points in a nine-state region and surpassed old record flood stages by nearly 2 m in some cases. The duration of the flood was as overwhelming as its areal extent; for example, on September 1, 1993, some towns had experienced 153 consecutive days of flooding. The flooded region finally began drying out in early August when the upper-air pattern changed, bringing unseasonably cool and dry weather to the Midwest.

The severity of this event may be examined in a probabilistic manner. Precipitation probabilities were statistically calculated for given periods during the event. Expected return periods for an event of this magnitude were then calculated from these probabilities. Figure 6.8.2 shows the recurrence interval (or return periods) for a number of sites throughout the midwestern USA for June and July 1993. Although some caution must be used when interpreting these statistics literally, the presence of such extremely long return periods (most in the 500-1000+ year range) dramatically indicates the extraordinary nature of this event.

The duration and magnitude of the flood, as well as its antecedent conditions, strongly support the premise that this event was a significant climate variation. It is quite possible that one or more climate-driving forces (e.g. El Niño/Southern Oscillation) significantly contributed to this climate variation.

The monsoon, though mainly a south Asian phenomenon, has been found to occur, on a lesser scale, in other parts of the world in west Africa, Australia and some parts of North America. In the Indian Subcontinent, it is a major rain-bearing system for India, Pakistan, Bangladesh, Sri Lanka and other countries and has a great impact on the lives of millions of people. The economy of these countries is dependent, to a large extent, on the timely arrival and subsequent distribution of rains during the monsoon.

India, being essentially an agricultural country, depends for its food production on the southwest summer monsoon rainfall that occurs from June to September every year. About three quarters of the annual rainfall of the country is received in these four months. Besides bringing copious rains and relief to the farmers and replenishing the water resources, comparatively cool monsoon winds bring welcome respite from the heat, since they herald the end of the hot season in cooling surface temperatures by about 10°C.

The Asian summer monsoon, though a regional phenomenon, does have teleconnections with other climatic features elsewhere and thus is an important component of the global climate system. As an example, the monsoon has been found to be highly correlated with, among other phenomena, the El Niño/Southern Oscillation, variations of pressure over South America, temperature over the northern hemisphere and the extent of Eurasian snow cover. It also exhibits a large interannual and intra-seasonal variability, particularly over the Indian Subcontinent. Much of the rainfall over India and Pakistan during the monsoon season is generated by the westward passage of depressions and low pressure systems forming in the Bay of Bengal. Their number varies considerably from season to season. Furthermore, some of the seasons are punctuated by long breaks whereas others have practically no breaks. All this results in droughts in some years and floods in others. The annual rainfall departure over India in the monsoon months (June through September) from 1875 to 1993 is shown in Figure 7.1.

7.1 INDIAN SUBCONTINENT MONSOON

In 1991, the southwest monsoon reached Southeast Asia by 24 May and progressed to southern parts of Myanmar by 30 May. Later, covering Sri Lanka, it set in over the southernmost part of the Indian peninsula, i.e., Kerala State by June 2; the normal date is June 1. It advanced northward covering peninsular, northeast and central India, Bangladesh, the rest of Myanmar and other major parts of the region by June 15. Then it appeared to stop and did not advance for the next three weeks, probably

▼ *Figure 7.1* – Rainfall anomalies in India during the southwest monsoon (June to September) 1875-1993 (from India Meteorological Department, New Delhi).

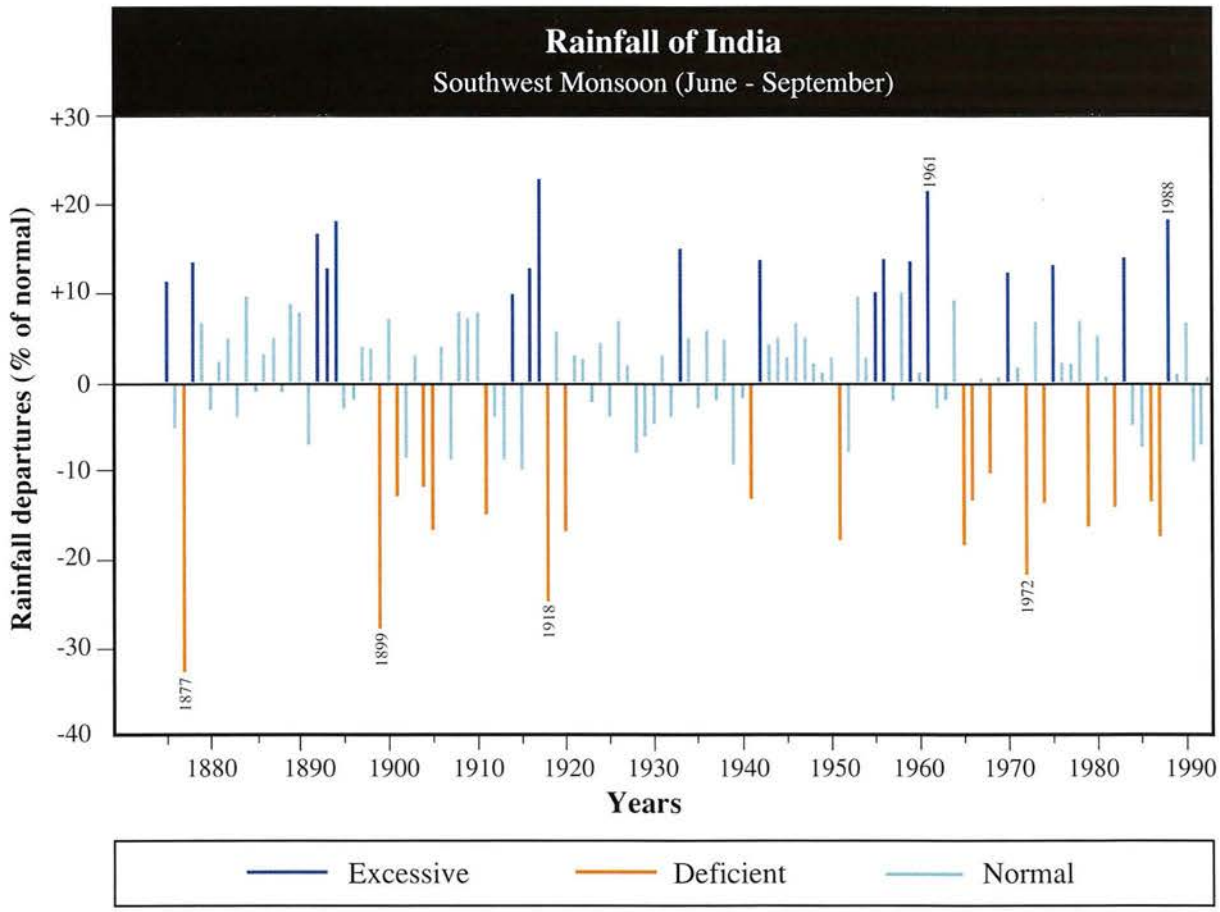

due to a blocking situation in the upper troposphere over the Caspian Sea. Such a prolonged hiatus in the advance of the monsoon had not been observed in four decades. However, it started to advance again on 11 July and by 19 July it covered all of India and parts of Pakistan. The isochrones of advance of the southwest monsoon in 1991 are shown in Figure 7.2.

The 1991 summer monsoon rain over India was 91% of the seasonal normal. Out of a total of 35 subdivisions, 26 received normal rainfall (up to +19%), only one excess rainfall (+20% or more) while eight received deficient rainfall (-20% to -59%). The normal to excess precipitation belt comprised peninsular India and the eastern and central parts of the country. Deficient rainfall areas were mostly in northwestern India, Saurashtra and Kutch. No meteorological subdivision received scanty rainfall (-60% or less). The monsoon season's departures for excess and deficit ranges by subdivisions, are shown in Figure 7.3. Area-wise, about 75% of the Indian land mass received normal or excess rainfall. During the summer monsoon a total of four cyclonic storms formed in the Bay of Bengal - one each in June, July, August and September. No depression formed in the Arabian Sea. The southwest monsoon started withdrawing from northwest India on September 18 and, by September 30, it had departed most of the country. The isochrones of withdrawal are shown in Figure 7.4.

During the 1991 monsoon season, nearly 23.5 million people were affected and property and crops worth Rs 2900 million were damaged. Official reports indicated that 673 human lives were lost as a result of heavy rains and floods.

The Asian summer monsoon in 1992 reached the south Andaman Sea and southern parts of Myanmar on May 20, around the normal date. After crossing Sri Lanka, it set in over Kerala on June 5, i.e., about four days later than normal. It advanced slowly northward covering remaining parts of Myanmar by June 13, Bangladesh by June 18, parts of peninsular, eastern and central India by June 20,

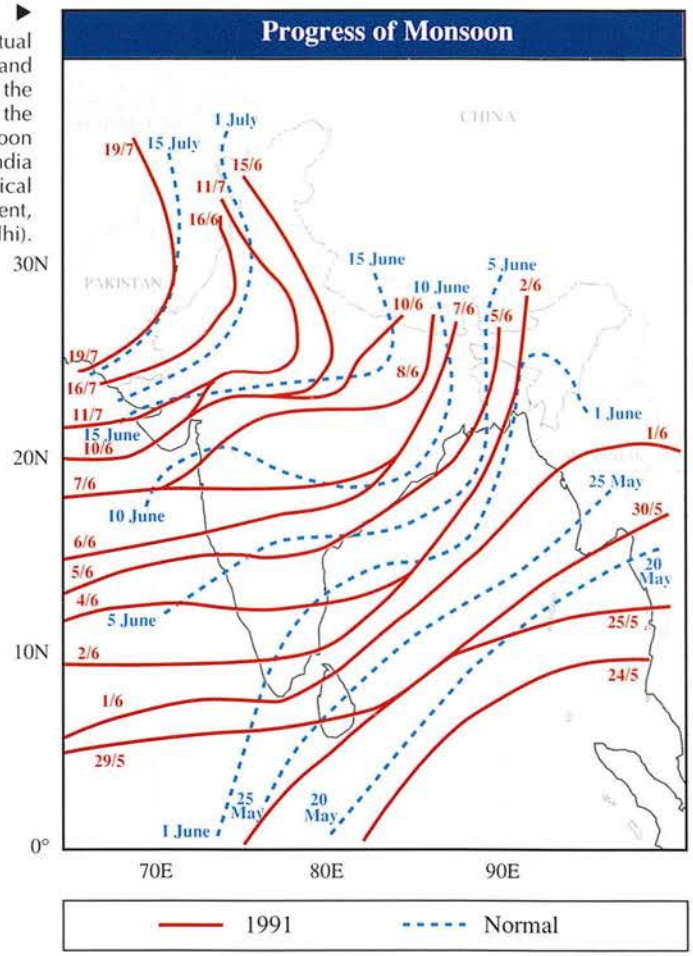

Figure 7.2 – Actual dates in 1991 and normal dates of the onset of the southwest monsoon over India (from India Meteorological Department, New Delhi).

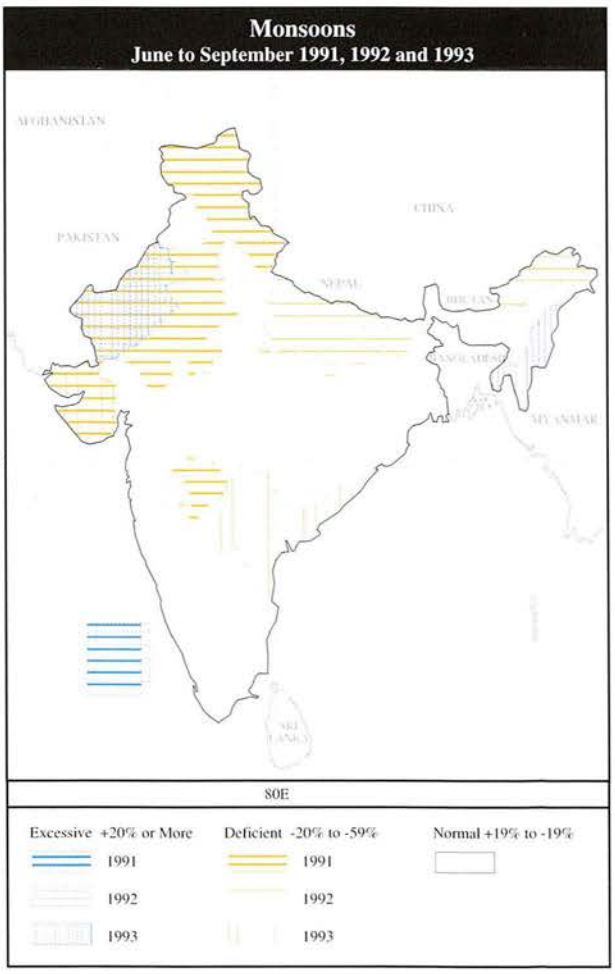

Figure 7.3 – Distribution of June-to-September rainfall totals in India during the 1991, 1992 and 1993 monsoon (from India Meteorological Department, New Delhi).

and Pakistan by July 14, which are normal dates.

For the most part, the 1992 monsoon was sluggish until the middle of July and continued without break thereafter up to the first week of September. The southwest monsoon rainfall from June to September 1992 over India was 93% of the long-period average. Out of 35 meteorological subdivisions, the seasonal rainfall was excessive in two, normal in 30 and deficient in three. No subdivisions reported scanty rainfall. The seasonal rainfall departures for excess and deficit categories are shown in Figure 7.3 by subdivision.

There was one cyclonic storm (June 8-12) over the Arabian Sea and two deep depressions over the Bay of Bengal during the 1992 monsoon season. The cyclonic storm moved in a westerly direction without causing any significant weather over India. There were no depressions in August and September, although, on average, four or five are formed. Although the early part of the monsoon season was abnormally dry, heavy late-season showers dropped widespread, abundant rains on much of central, northwestern and southwestern India, on much of Pakistan and over the southwest quarter of Sri Lanka. The southwest monsoon withdrew from west Rajasthan on September 17 and from India by October 19.

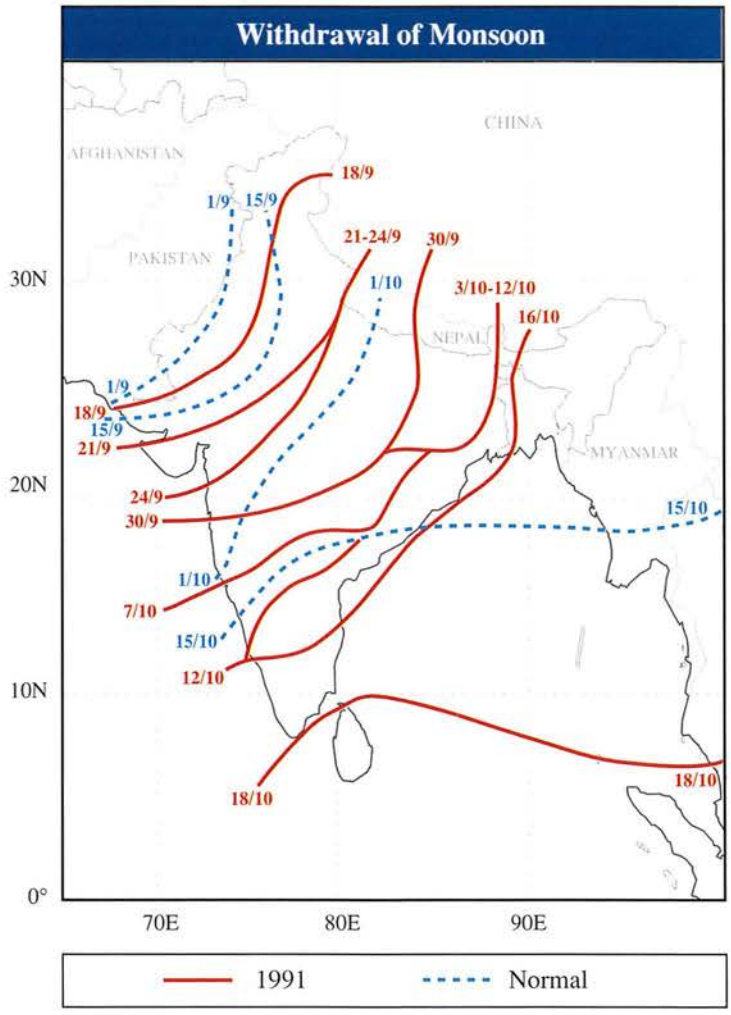

▲ *Figure 7.4* – Actual dates in 1991 and normal dates of withdrawal of the southwest monsoon over India (from India Meteorological Department, New Delhi).

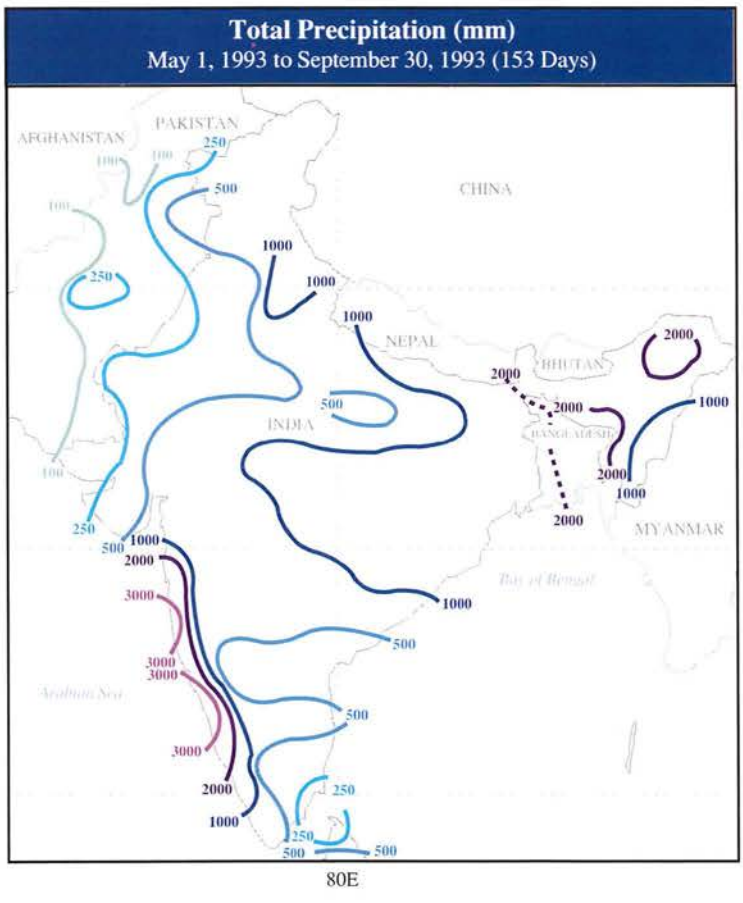

Figure 7.5 – Total precipitation from May 1 to September 30, 1993 in southwest Asia (from NOAA/NWS/NMC/CAC, Washington, DC).

No tropical depressions emerged in the Bay of Bengal during the 1992 monsoon season while eight systems recurved northeastwards. Only one tropical storm formed in the south Indian ocean in the last week of September 1992. It moved in a southwesterly direction and dissipated over the Indian Ocean.

Torrential rains, mainly in the first week of September melted mountain snows in parts of northern India and Pakistan, producing land slides and catastrophic flooding. On September 9, Islamabad reportedly

measured 172 mm of rain in less than 20 hours. Flooding killed at least 1,184 people. The heavy rains and floods reportedly caused more than 2.8 million houses to collapse and left more than 4 million people homeless. Satellite imagery showed rivers in Punjab province swelling to some 20 miles wide during the flood.

With torrential downpours also hitting the northern Himalayas, massive flooding affected northern India, especially the state of Kashmir. Northern India reported 980 deaths. Flooding also affected Afghanistan in early September. According to reports, the death toll topped 4,000 in Pakistan and India, several million more were displaced, and agricultural and property losses were extensive. All told, this was the worst flooding in Pakistan since the country was founded in 1947.

The 1993 southwest monsoon was described as the most favourable for India's summer agricultural production since 1989. Its onset was characterized by a timely arrival and practically continuous progress over Southeast Asia. The monsoon reached the south Andaman Sea on May 17. After covering Thailand, Sri Lanka, southeastern Bay of Bengal and a major part of Myanmar, it set in over Kerala on May 28, three days earlier than usual. Its further advance over peninsular India by June 12 was almost normal. Covering the remaining parts of Myanmar, Bangladesh, Bhutan, Nepal and the remaining parts of the country, the monsoon reached eastern parts of Pakistan by July 5, 1993 - about 10 days earlier than the normal date.

The monsoon rainfall in 1993 in India was normal with most of the subdivisions receiving well distributed rain, both in space and time. It was the sixth successive normal monsoon year. Out of the 35 meteorological subdivisions in the country, monsoon rains were excessive in two, normal in 29 and deficient in four subdivisions. Again, no meteorological subdivision received scanty rainfall.
The 1993 seasonal departures for excessive and deficient rainfall are given in Figure 7.3 by subdivision.

June and July rainfall was generally normal or above normal. Until this year, floods had never before been reported from Punjab and Haryana in the first fortnight of July. Another rather extraordinary feature of 1993 was that only one monsoon depression (June 17 to 19) formed in the Bay of Bengal, compared with the more usual five or six. This was an unprecedented feature of the 1993 monsoon season that had not occurred since 1940.

Heavy rains and floods caused considerable damage across the northern and eastern tiers of the Indian Subcontinent during June and July 1993. According to reports, besides considerable damage to crops and property, it was estimated that 270 persons lost their lives in India and another 66 in Bangladesh.

During July 19-21, 1993, central and eastern Nepal experienced unprecedented heavy precipitation. The 24-hour rainfall recorded at Tistung in Central Nepal was 540 mm, the highest ever recorded in Nepal. This precipitation event resulted in a catastrophic flood that took more than 12,000 lives and thousands of livestock. Thirty-six villages were buried by land slides or submerged by rising rivers, resulting in the worst national disaster in Nepal's history. Katmandu was inaccessible by road for more than 11 days. Elsewhere, the heaviest rains in five years generated severe flash flooding in Dhaka, Bangladesh. Figure 7.5 shows the total precipitation for the May to September period.

The monsoon activity in 1993 was slightly weaker than normal over Indo-China and the Philippines in June whereas it was active throughout July across the Asian continent. The rainfall was heavy over Southeast Asia in July and moderate in August and September. Japan received large rainfall totals throughout the period of June to September 1993, with several areas receiving record rainfall. Rainfall activity over southern and northern regions of the Lao People's Democratic Republic was below normal while it was nearly normal over its central region. Heavy damage to property and human losses due to heavy rains and floods were reported from the eastern provinces of China and Bangladesh.

Figure 7.6 shows the per cent of districts in India with normal or above rainfall and deficient or scanty

▼ *Figure 7.6* – Percent of districts in India with excessive, normal, sufficient and scanty rainfall at the end of the monsoon season (June to September) from 1984 to 1993 (from India Meteorological Department, New Delhi).

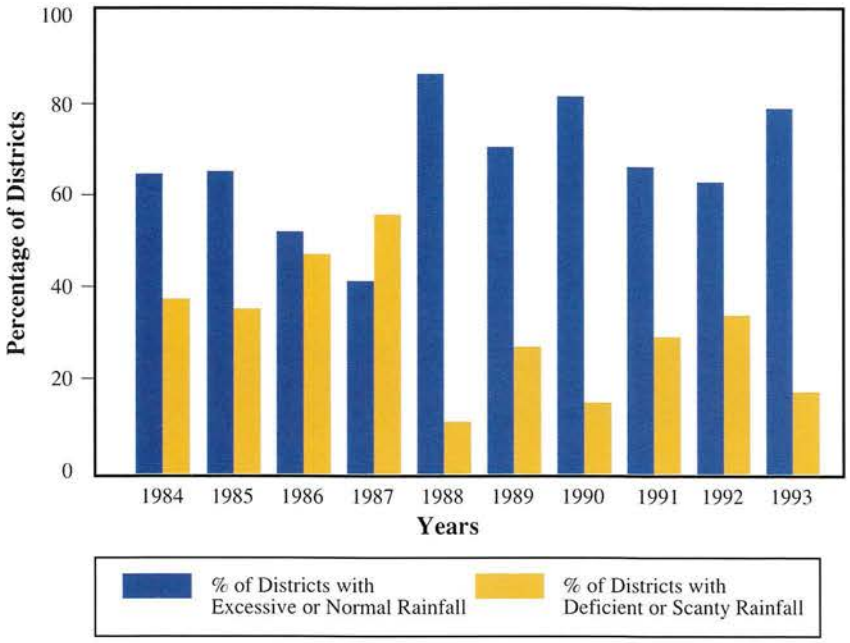

Excessive	+20% or more
Normal	+19% to -19%
Deficient	-20% to -59%
Scanty	-60% to -99%

rainfall during the monsoon season over the last 10 years.

7.2 THE AUSTRALIAN "WETS" OF 1991-92 AND 1992-93

The 1991-92 northern Australian "wet" was basically a failure, with well below-normal rains and record low amounts in far northwestern Western Australia. In early April 1992, Tropical Cyclone Neville brought some relief to northern parts of Arnhem Land, slightly alleviating what had been one of the poorest "wets" on record.

By contrast, despite a late start, the 1992-93 "wet" was bountiful, with record amounts of rain in February over a large area of inland Northern Territory and adjacent northeastern Western Australia. An extremely moist six-week spell between late January and the end of February, featuring slow-moving monsoon depressions, led to the 1992-93 season as a whole being among the wettest ever over the northern half of the Northern Territory and far northern Queensland, with record amounts in the northern Cape York Peninsula (see Figure 6.4).

Northeastern Australia suffered two consecutive failures of the "wet", resulting in very serious drought. In both 1992 and 1993 the "wet" came to an abrupt end at the end of the calendar summer.

Consequently, the following autumnal seasons had well below average rains in the tropics, where rains can normally be expected to linger well into March.

7.3 HEAVY WINTER MONSOON IN MALAYSIA

The annual onslaught of the northeast monsoon (northern winter monsoon) in Malaysia was rather late in 1993. The first heavy rain occurred on December 10, 1993, about three weeks later than normal. Rainfall after the onset was very intense, however, with widespread rain occurring over the whole of peninsular Malaysia and part of Kalimantan almost every day until the end of December (Figure 7.7).

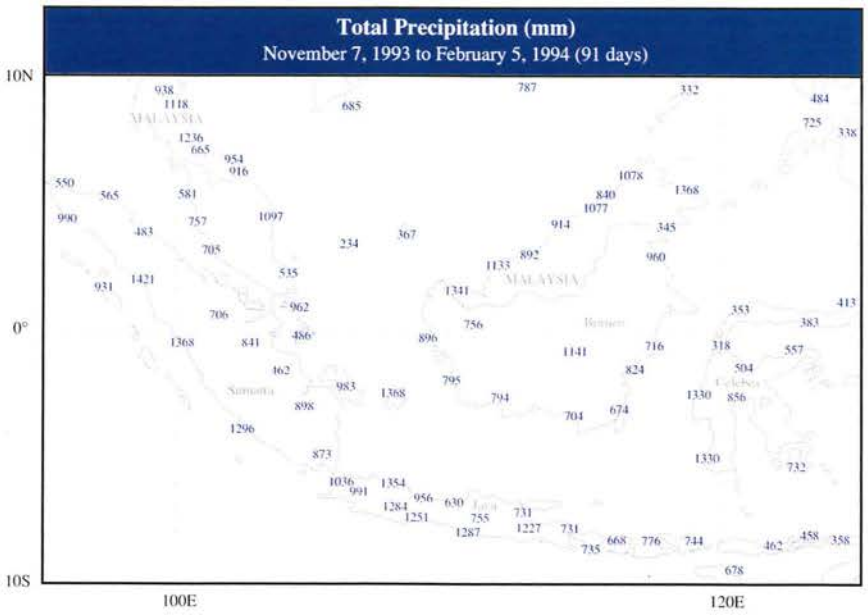

▲ *Figure 7.7* – Total precipitation from November 7, 1993 to February 5, 1994 for Indonesia and nearby areas (from NOAA/NWS/NMC/CAC, Washington, DC).

The most severe spell of rain occurred during December 16 to 23, covering almost the whole span of the east-coast states of peninsular Malaysia. At the height of the flood, as many as 13,284 people had to be evacuated to relief centres. Some 30 people were drowned and flood waters rose as high as 1.3 m in Kota Bharu, the capital of Kelantan, and the east-coast state facing the South China Sea. The east-west highway linking the east coast of peninsular Malaysia to the west was closed by land slides caused by the heavy rain. During December, most stations in Malaysia recorded a total monthly rainfall 60% above normal, a few recorded 100% above normal.

Below-normal rainfall was recorded in most places in January 1994, but the monsoon became active again in February, with above-normal rainfall in many areas. This active monsoon occurred five years after the severe monsoon in 1988, when there was also an ENSO event.

7.4 SUMMER MONSOON RAINS IN EASTERN CHINA

The summer monsoon in eastern China is directly influenced by the seasonal displacement northward from spring to mid-summer of the West Pacific High (WPH) (at the 500 hPa level). The main monsoon rainy belt is located along the northwestern side of the WPH. During the 1980s, its summer position changed significantly to a more southerly position compared with the long-term climatology. Consequently, northern China has suffered from a deficiency of rain during the high summers of the 1980s, whereas central China (Yangtze and Huaihe basins) was waterlogged several times.

In 1991, the plum rains came to the mid-lower Yangtze-Huaihe river basin on May 18, nearly a month earlier than normal. The rainy season ended on July 13, lasting for 56 days. Total rainfall was as much as 2 1/2 times that of normal. More than 100 million people were affected by catastrophic flooding and more than 13 million hectares of farmland were waterlogged. It was the largest flood in forty years in central-eastern China resulting in economic losses totalling US$ 10 billion. The direct cause of this severe flood was a persistent WPH at 500 hPa supplying warm moist air from the Bay of Bengal. Again in late July-August, the WPH moved abnormally southward. Torrential rains returned to the mid-lower Yangtze-Huaihe basins,

▼ *Figure 7.8* – Areal distribution of summer (June to August) rainfall anomalies in China in 1991 (from Jiangsu Meteorological Institute, Nanjing, China).

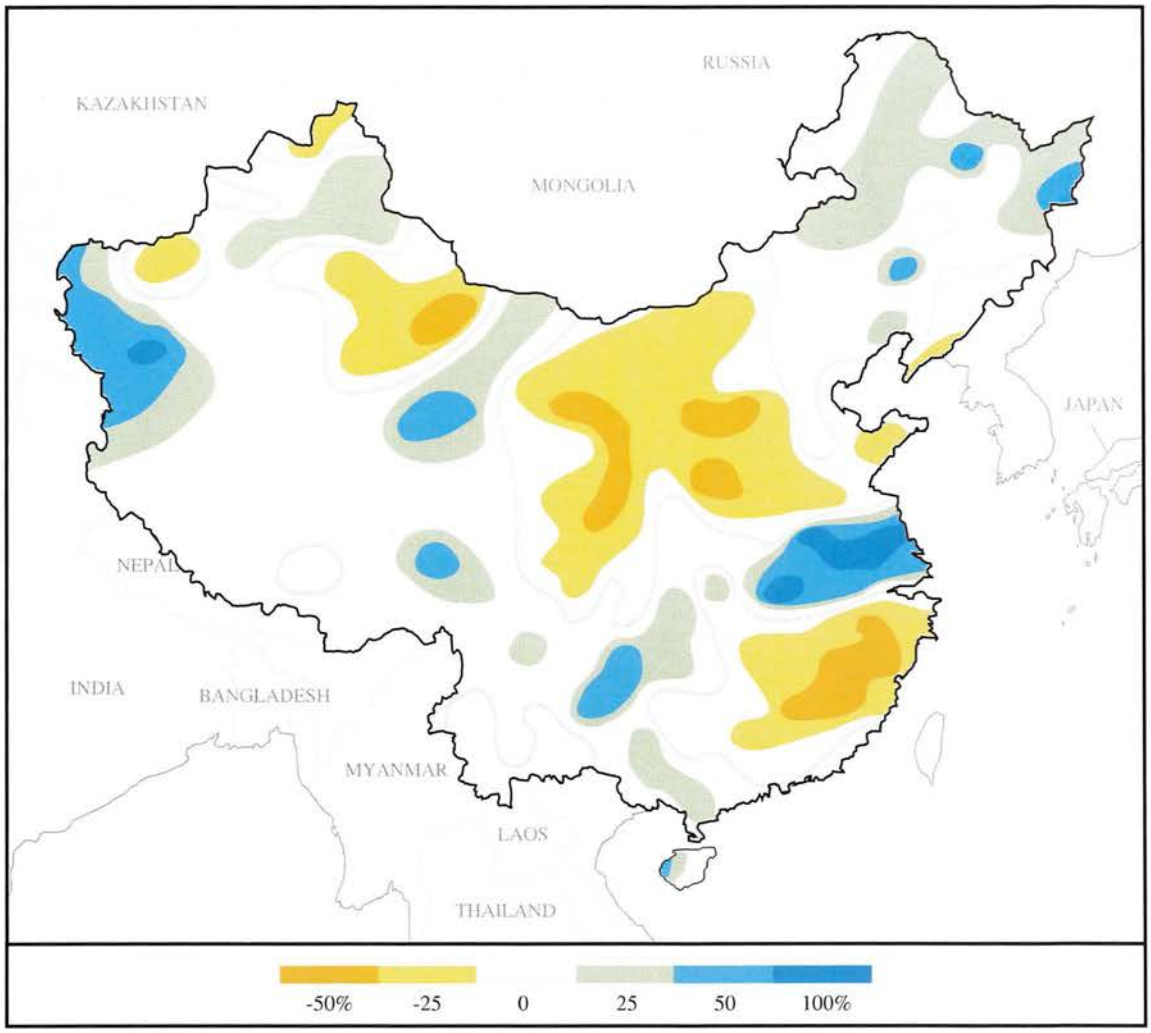

whereas most regions of north China and south of the Yangtze River suffered summer drought (Figure 7.8).

Abnormally cold air from the north invaded China during the early summer of 1992. The average temperature of the Yangtze basin between mid-June and mid-July was about 3 to 5°C below normal. The WPH was weaker than normal and its position more southward and eastward. Consequently, southwest moist air from the Bay of Bengal was abnormally weak in this early summer with the monsoon rainy belt located more southeasterly than normal. In marked contrast to 1992, drought prevailed over eastern China from the Yangtze basin to northeast China. Greater rainfall appeared in the mid-south part of Zheniang and northern Fujian provinces. Severe flooding in northern Fujian was the worst in 50 years.

Throughout the summer of 1993, the WPH was positioned more southward than normal. The plum rains occurred in the mid-lower Yangtze basin in late June, although it was later than normal by about 10 days. The rains continued intermittently until the end of August. Flooding was reported in the provinces of Human, Jiangsi, Zhejiang and southern Jiangsu. Farmland, of about 1.33 million hectares, was waterlogged and more than 100 persons were killed. In eastern China, the summer monsoon rains were late. The rainy belt moved more southwardly than normal, whereas drought prevailed over most regions of north China (Figure 7.9).

The year 1993 was also characterized as a "no high summer" year. Abnormal cooling prevailed in most regions of China during July and August, which is very rare. The average temperature ranged from 2°C below normal in central China around the Yellow River to 4°C below normal on the south side of the mid-lower Yangtze Basin.

It is interesting to note the coincidence between the prolonged ENSO and the only persistent climate feature in China for the three summers being the drought in north China. The summer monsoon rains south of 35°N (especially the plum rains) were very different during the review period.

▼ *Figure 7.9* – Areal distribution of summer (June to August) rainfall anomalies in China in 1993 (from Jiangsu Meteorological Institute, Nanjing, China).

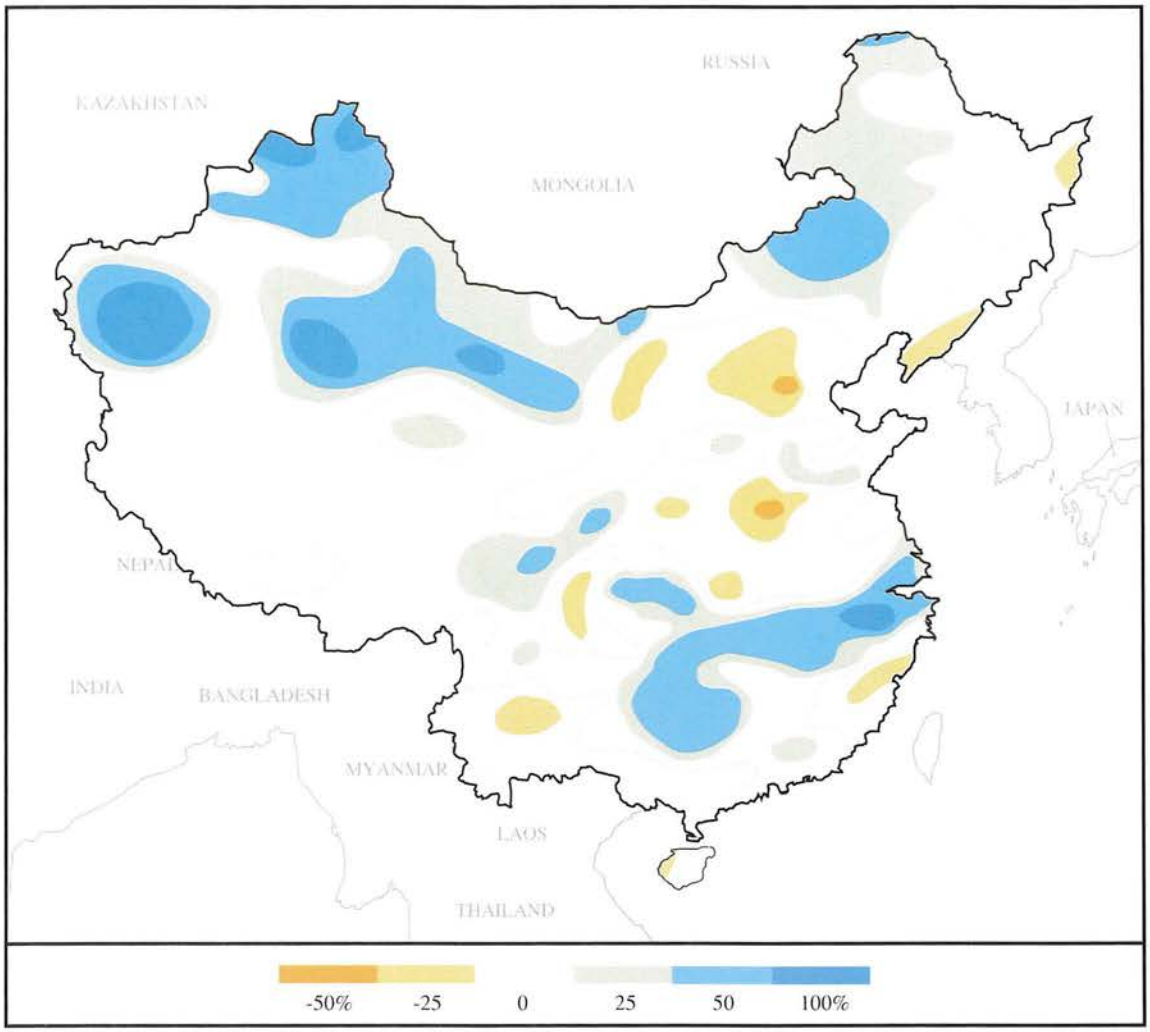

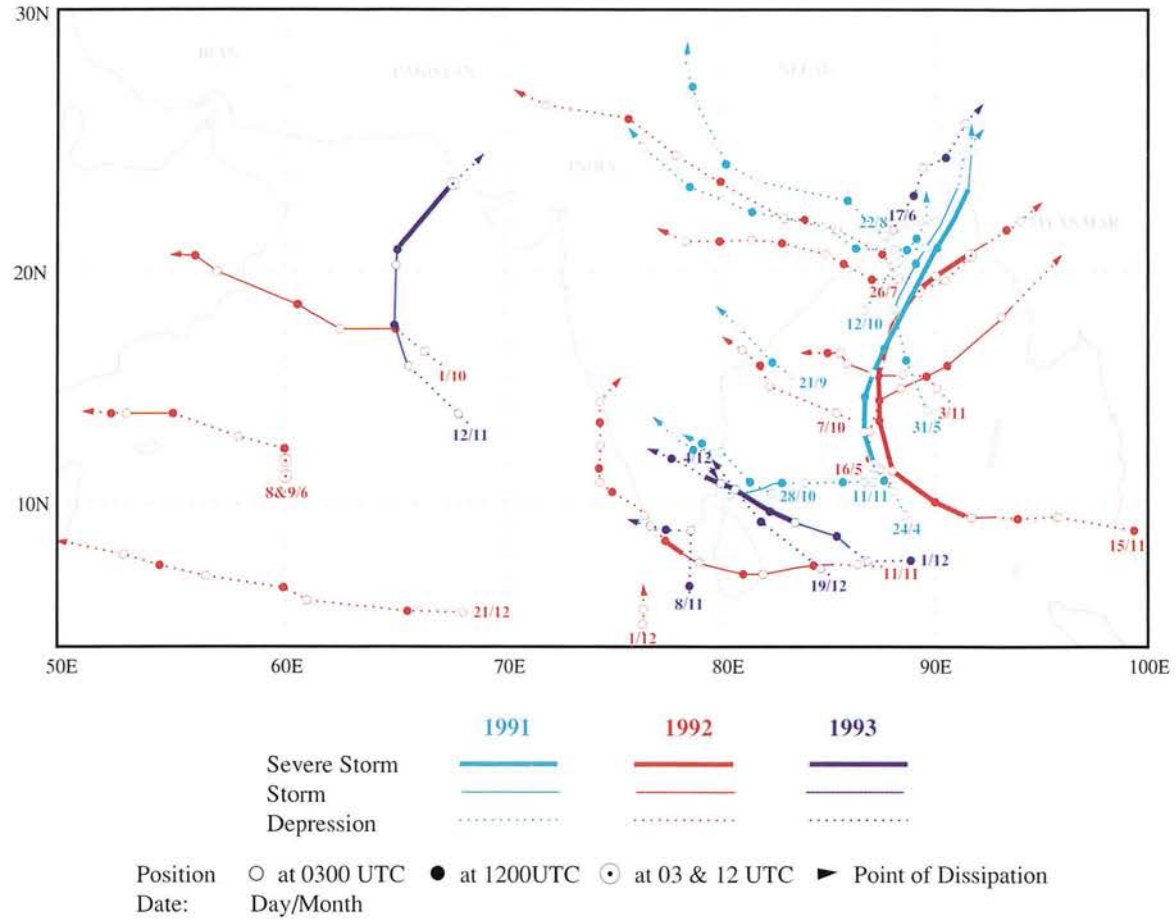

▲ *Figure 8.1* – Tracks of tropical cyclones and depressions in the northern Indian Ocean during 1991, 1992 and 1993 (from India Meteorological Department, New Delhi).

STORMY TIMES – TROPICAL CYCLONES, TYPHOONS, HURRICANES, TORNADOES

CHAPTER 8

Storms have affected virtually everyone on the planet. They are violent explosions of the great energy available in the climate system, fuelled by solar power, oceanic and atmospheric moisture, temperature and moisture gradients and atmospheric circulation patterns. Each year about 80 large-scale, severe storms - tropical cyclones, hurricanes and typhoons - occur throughout the world. The average annual damage has been estimated at about US$ 1500 million and the average annual death toll over the past 30 years or so is about 15,000. The great storms, both tropical and extratropical, get most of the attention and their impact is felt dramatically, but the everyday storms, associated more with convective and frontal activity play a major part in the lives of the inhabitants of this planet.

Storm impacts are usually to the detriment of society. The cost in terms of loss of life and property can be staggeringly high and depends upon density of population, time of year and other factors. We must also keep in mind, however, that there have been many cases of storms that have resulted in benefits, e.g. delivering rainfall in a period of long-term drought, filling reservoirs and lakes, recharging ground water supplies and providing winter snow cover for sensitive crops.

The period of mid-1991 to the end of 1993 had more than its share of powerful storms. A record number of tropical storms plagued an area from the western Pacific Ocean into the South China Sea, inflicting particularly heavy damage on the Philippines. Two powerful hurricanes struck the USA - *Andrew* in Florida and *Iniki* in Hawaii.

8.1 CYCLONES AND DEPRESSIONS IN THE BAY OF BENGAL AND THE ARABIAN SEA

The Bay of Bengal and the Arabian Sea were not dramatically affected by large-scale storms during the review period. Certainly, none even approached the destructive force and devastating impact of the Bangladesh storm of April 24-30, 1991, which was one of the worst natural disasters on record ever. The casualties were staggering - 125,000 drowned and 10 million left homeless. Following that storm several tornadoes and continued very heavy rainfall severely hampered relief efforts and caused more damage in the region. In late May 1991, tornadoes and river flooding claimed an additional 200 lives. Conditions slowly improved after that.

Between 14 to 16 November 1991, Tropical Storm 4B, a remnant of Pacific Tropical Storm *Thelma*, pounded southern India (see photograph) for two days before diminishing in northern Tamil Nadu. The storm winds gusted to 100 km/h and torrential rains locally reached 580 mm along the southeastern coast. Homes collapsed and more than 50,000 individuals were evacuated after several rivers

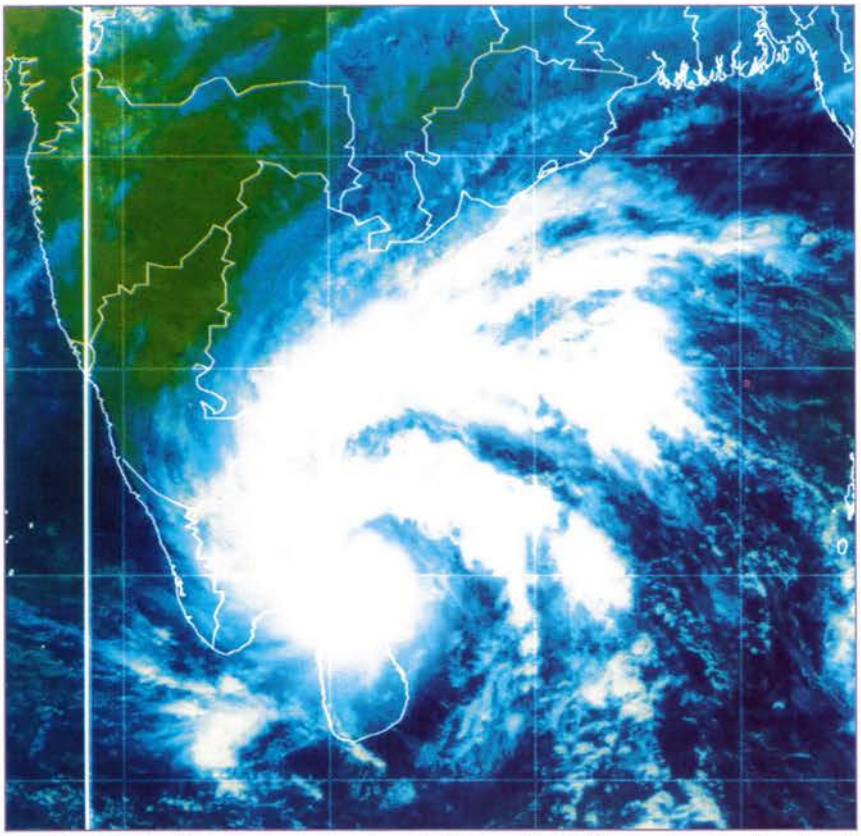

▲ INSAT-1D cloud imagery on November 14, 1991 at 0600 UTC showing cloud bands and spiral associated with Karaikal Cyclone (from India Meteorological Department).

overflowed and sea water inundated the coastline, resulting in extensive property and crop damage, but there was little loss of life.

Storm 4B was particularly noteworthy because the rains exacerbated the effects of three weeks of abnormally heavy rain through much of southern India and Sri Lanka. Rainfalls of 350 mm in north-central Sri Lanka and as much as 632 mm occurred on extreme southern Andhra Pradesh. The heavy rains in extreme southern India and Sri Lanka correlate well with the global anomaly patterns expected during an El Niño episode, which generally coincides with above-normal October-to-December rainfall totals across southern sections of Kerala and Tamil Nadu and throughout Sri Lanka.

In mid-November 1992 hundreds of people were drowned and thousands left homeless in Sri Lanka and southern India as a result of flooding caused by the heavy rains from Cyclone 10B. Maximum sustained winds reached speeds of 120 km/h. Rainfall totals of 100 to 250 mm soaked some locations, with daily amounts reaching 150 mm. Storm surges of 1.0- to 1.5-m height inundated about 70 km of coastal zone up to 300 m inland in Tamil Nadu at the time of landfall. This storm brought in its wake extensive damage to life and property in coastal districts of Tamil Nadu and Kerala and in Sri Lanka. According to reports, about 175 persons lost

CYCLONE WARNINGS IN INDIA

The Regional Specialized Meteorological Centre (Tropical Cyclones) in New Delhi issues frequent cyclone advisories to all concerned, including neighbouring countries, regarding the progress and movement of tropical cyclones.

These cyclones are tracked and monitored with the help of INSAT cloud imagery, cyclone detection radars and other conventional land and ship observations.

In India, cyclone warnings are disseminated to the general public, central and state governments and other user organizations through telex, telephones, telegrams etc.

Timely warnings issued to the officials and general public greatly help in minimizing the loss of lives and property in the highly vulnerable coastal areas of Andhra Pradesh and Tamil Nadu. The Disaster Warning System, which has been in operation in the coastal areas of the above states since 1987, is used extensively and has proven to be very dependable and effective in quick dissemination of cyclone warnings.

▼ The Masilamani temple in Tamil Nadu was severely damaged by cyclone on December 4-5, 1993 (from India Meteorological Department).

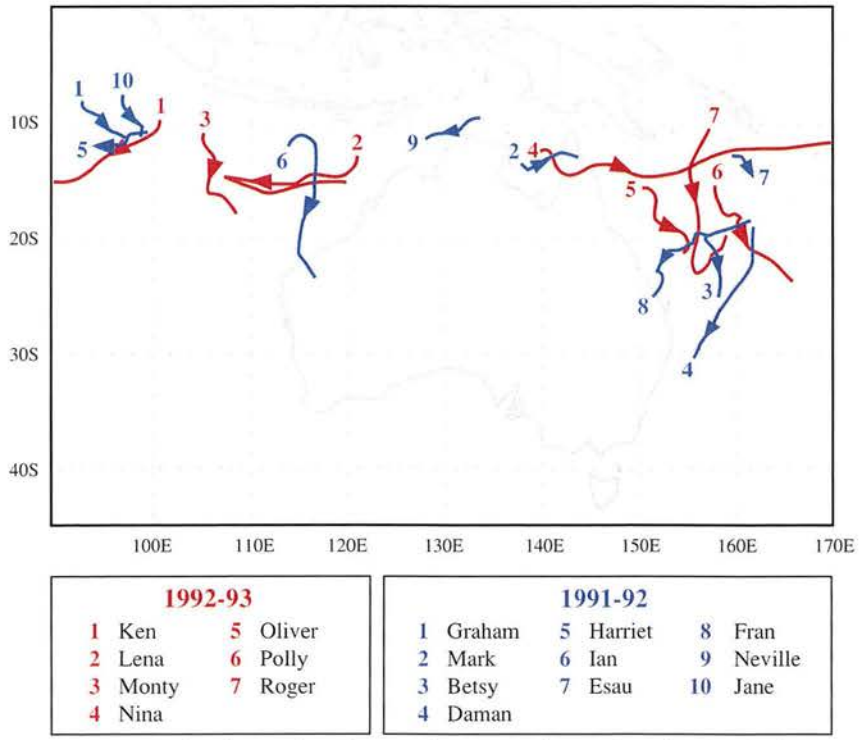

▲ *Figure 8.2* – Tracks of tropical cyclones in the vicinity of Australia and Indonesia during the 1991-92 and 1992-93 hurricane seasons (from National Climate Centre, Bureau of Meteorology, Melbourne, Australia).

their lives and heavy damage to property occurred due to flash floods and land slides.

The year 1993 was a year of exceptionally low cyclonic activity over the north Indian Ocean. There were only five cyclonic disturbances (two cyclones and three depressions) over this region compared with a normal of about 12 such disturbances. Such relative tranquility has been a rare event during the past 100 years and has surpassed the previous minimum of seven cyclonic disturbances of 1984.

The most damaging cyclone of the year developed into a hurricane-force storm on the evening of 3 December off the north coast of Tamil Nadu near Karaikal (see photograph). The storm caused strong winds and generally widespread, heavy rainfall over Tamil Nadu and Andhra Pradesh. About 111 people lost their lives owing to high winds, heavy rains and floods. A peak storm surge of 3 to 4 m occurred over the coastal stretch of 50 to 60 km north of the cyclone's track. Rail and road traffic in the region was disrupted. The cyclone severely damaged the Masilamani temple in Tamil Nadu (see Photograph).

Figure 8.1 shows the tracks of tropical cyclones and hurricanes from June 1991 to December 1993. Only one of these storms reached hurricane intensity.

8.2

TROPICAL CYCLONES AROUND AUSTRALIA AND THE SOUTH PACIFIC

Figure 8.2 shows the tracks of cyclones for the 1991-92 and 1992-93 cyclone seasons. Tropical storm activity was light with only two significant events occurring during the period of the review. Only 8 storms directly affected Australia out of a total of 17 that passed through the region.

February 1992 saw two tropical cyclones, Daman and 18P, generate large amounts of rain across previously parched sections of southeastern Queensland and extreme northeastern New South Wales for the second successive week. Rainfall totals of 100-250 mm drenched the region with torrential downpours producing daily totals of up to 225 mm. The sudden cloudbursts, following months of abnormally dry weather, generated some of the region's worst flooding this century. In March, Cyclone *Fran* hit the Queensland coast causing flooding and damaging sugar cane crops.

In late 1992, Tropical Storm *Nina* spread gusty winds and very heavy rainfall across the Cape York Peninsula. Between 250 and 400 mm

Figure 8.3 – Tracks of tropical cyclones for the western North Pacific Ocean for 1993 (from NOAA, National Climatic Data Center, Asheville, NC).

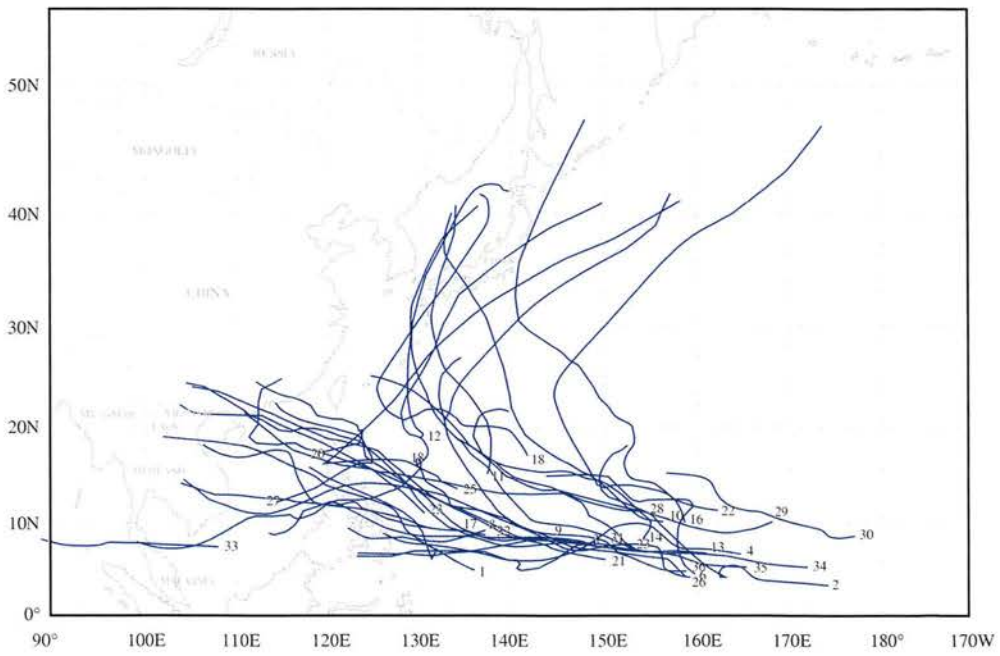

of rain fell on northern and central parts of the peninsula, where daily totals approached 150 mm. On 3 January 1993 Cyclone *Nina* struck Tuvalu Island with winds up to 140 km/h. High seas flooded whole villages. *Nina* also left thousands homeless on the Solomon Islands. A day earlier, Cyclone *Nina* struck Fiji with devastating gusts to 225 km/h. Floods from the storm caused 21 deaths and were reportedly the island's worst since the beginning of the century. Another cyclone on March 30 destroyed 75 to 80% of the buildings on three of Vanuatu's islands.

8.3

WESTERN PACIFIC TYPHOONS - RECORD NUMBER OF STORMS HIT THE PHILIPPINES IN 1993

A record number of 32 tropical storms hit the Philippines in 1993 and most of the rest of the region was also hit hard by tropical storm activity throughout the period of the review. Figure 8.3 shows the high number of tropical cyclone tracks over the Philippines and southern Japan in 1993.

Typhoon *Yunya*, a small but powerful system in June 1991, brought daily rainfall totals up to 185 mm to southern Luzon and Samar. In August, Typhoon *Fred* developed from a tropical depression drenching Luzon with up to 535 mm of rain. While crossing the South China Sea the storm generated high waves that sank a barge east of Hong Kong taking at least 18 lives. The eye of the typhoon proceeded eastward through Hainan Strait battering the island province of Hainan and adjacent south-central China with sustained winds of 185 km/h and gusts to 235. The storm pounded Haikou, capital of Hainan, at the northern tip of the island. Nearly 6000 houses collapsed and seven people died.

From August 21-23, Typhoon *Gladys* drifted northward across the northern Ryukyu Islands, skirted the western coast of Japan's Kyushu Island and moved northward into the southern South Korea coast before turning westward and dissipating. Huge amounts of rain (up to 711 mm in Kyongju, located 280 km southeast of Seoul) inundated southeastern South Korea while Pusan and nearby Ulsan measured up to 410 mm on a single day, the largest 24-hour total measured in the 31-year history of the observatory. Over 60 people lost their lives and 6700 houses were flooded, leaving at least 11,000 people homeless. Property damage was estimated at US$ 62 million. Farther east, up to 225 mm of rain associated with the fringes of the typhoon generated land slides near Tokyo, taking at least 10 lives.

In late September, Typhoon *Mireille* lashed Japan's southernmost main island of Kyushu with 195 km/h winds and torrential rain. The storm claimed 50 lives and caused more destruction than any storm since 1971. On 28 October, the western Pacific's most destructive typhoon since November 1990 struck northern Luzon with 200 km/h winds. The resulting flash floods and land slides left more than 60 people dead and destroyed 21,000 houses. The year's most tragic weather event in the Philippines, however, came in the form of a rather innocuous tropical storm named *Thelma*. The storm packed winds of just 80 km/h when it struck the central part of the archipelago on 4-5 November. A high tide and heavy rain, however, magnified the storm's impact as it hit Leyte Island. Eyewitnesses reported that a 3 m wall of water surged through parts of Ormoc, trapping many of the city's 100,000 residents. Over 3,000 bodies were recovered from the city alone, while the national toll stood at 5,000 killed with 1,400 missing and presumed dead.

The 1992 season was also very significant. In early July, Typhoon *Chuck* drenched northern and central Viet Nam while 100-350 mm of rain caused extensive flooding in Jiangxi and Zhejiang provinces in China. Farther east, Tropical Storm *Deanna* brought high winds and moderate to heavy rains to the Ryukyu Islands and southern Japan. Tropical Storm *Fay* soaked Hong Kong with up to 400 mm of rain in

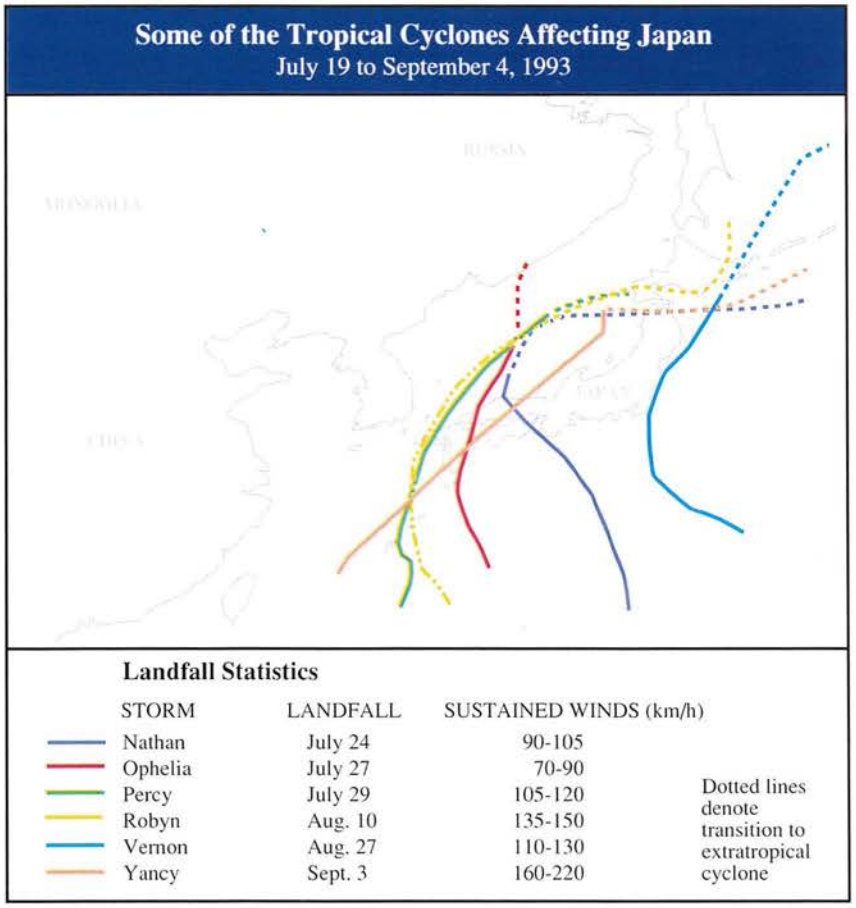

▲ *Figure 8.4* – Tracks of tropical cyclones affecting Japan from July 19 to September 4, 1993 (from U.S. Weekly Weather and Crop Bulletin, September 8, 1993).

late July and Tropical Storm *Gary* spread heavy rains into northern Viet Nam and adjacent parts of south-central China late in the month.

During early August, between 100 mm and 250 mm of rain inundated the southern half of Japan as Typhoon *Janis* made landfall with winds gusting up to 150 km/h. The heavy rains and high winds caused flooding, toppled trees and stranded travellers.

Over the ensuing two months, Tropical Storms *Mark*, *Omar* and *Polly* and Typhoon *Ted* brought strong winds and heavy rains to Taiwan and the Chinese coastline and contributed to the intense cloudbursts that inundated western Luzon. From August 9 to September 26, central and western Luzon received 1000 to 1775 mm of rain, causing severe volcanic mud flows in the vicinity of Mount Pinatubo.

The occurrence of a series of tropical storms complicated dramatically an already drenched situation in central Viet Nam during October 1992. More than a dozen people were killed and much damage occurred as Tropical Storm *Angela* hit during October 21-23. Up until then, from the early part of October, between 150 and 500 mm of above-normal rainfall had drenched much of central Viet Nam. Weekly totals of 200 to 300 mm had been common along the coast during this period. Angela was accompanied by gusty winds and 500-650 mm of rain, generating considerable damage to rice and vegetable crops, cutting communication lines and severing road and rail links. Torrential rains continued as Tropical Storm *Colleen* hit the area one week later. Da Nang ultimately reported an astounding 1,339 mm of rain in October.

The most intense and long-lived storm of 1992 was Typhoon *Gay*, which affected Guam, but had little other impact on the region. *Gay* was judged the most intense tropical cyclone to occur in the western North Pacific since 1979. Maximum sustained winds were estimated at 300 km/h, gusting to 380 km/h - making Gay one of the fiercest

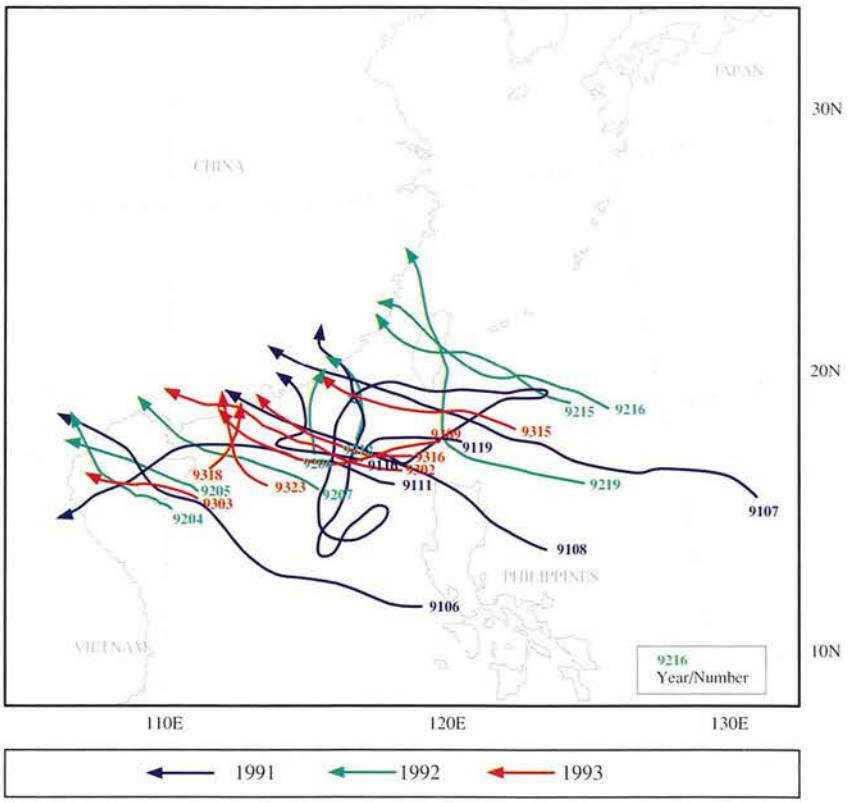

▲ *Figure 8.5* – Tracks of typhoons and tropical storms in the western North Pacific striking China during the 1991, 1992 and 1993 hurricane seasons (from Jiangsu Meteorological Institute, Nanjing, China).

storms of the century.

Between 22 and 27 June 1993 Typhoon *Koryn* brought torrential rains and powerful winds to the northern Philippines and extreme southern China. Winds near the centre of the typhoon dropped somewhat from a peak of 240 km/h (with gusts approaching 280 km/h) as the storm neared the northern Philippine island of Luzon. However *Koryn* produced considerable damage during its 10-hour trek across the island. Winds of up to 190 km/h were measured and peak gusts were estimated at 260 km/h when the system first moved inland across northern Luzon, accompanied by very heavy rainfall. Over 200 mm of rain caused widespread street flooding, numerous land slides and flows of lahar (a mixture of ash and water from Mount Pinatubo) nearly 3 m high at times. At least 7 lives were lost and more than 18,000 individuals were forced from their homes before the typhoon moved northwestward into the South China Sea. Within 24 hours, a slightly weaker *Koryn* was again affecting densely populated areas as strong winds and heavy rains lashed Hong Kong and adjacent sections of southern China. Winds in Hong Kong gusted to 190 km/h while the eye of the storm passed about 170 km south of the territory. More than a hundred persons were injured and at least four lives were lost before *Koryn* moved westward and began to weaken substantially.

The southern parts of Japan and Korea were besieged by 13 tropical storms from July to September 1993. Prior to the onslaught of these storms, the area had already received an abnormally high amount of rainfall during the previous five weeks.

Six typhoons shown in Figure 8.4 (*Nathan, Ophelia, Percy, Robyn, Vernon* and *Yancy*) were among these storms. In late July, Typhoon *Percy* and Tropical Storm *Ophelia* tracked through southwestern Japan generating up to 535 mm of rain in eastern Kyushu in the same week. In addition, heavy rains also fell on northern Honshu and parts of South Korea.

In mid-August, torrential rains from typhoons drenched the area, with as much as 500 mm falling on eastern South Korea and up to 300 mm recorded in Japan. *Robyn* caused heavy loss of life, halted rail and air travel and soaked the island

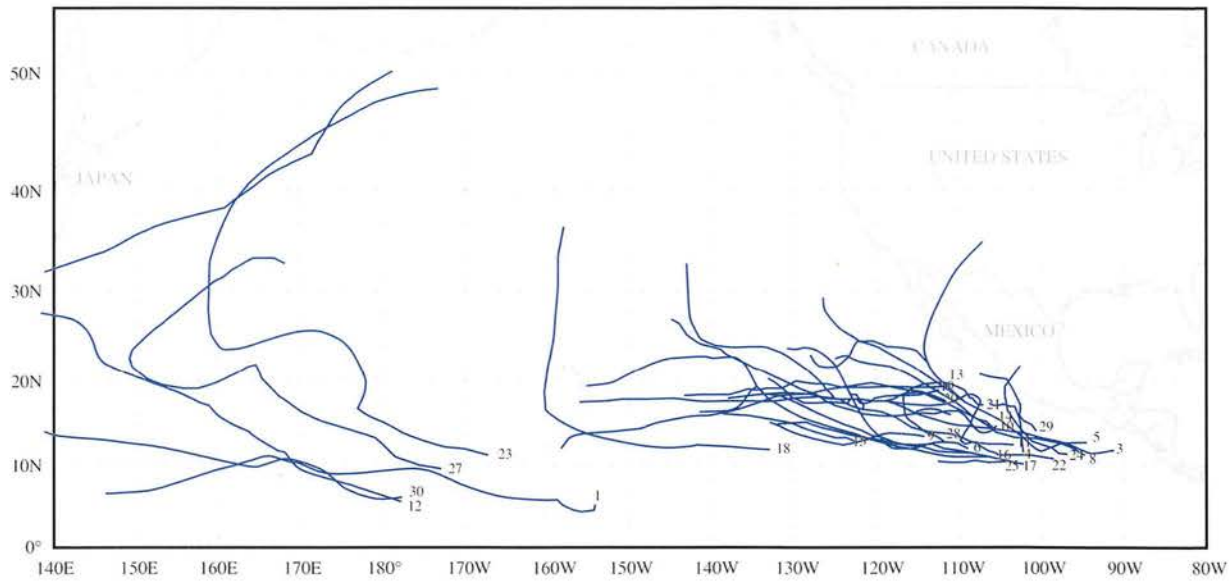

▲ *Figure 8.6* – Tracks of tropical cyclones for the eastern North Pacific Ocean for 1992 (from NOAA, National Climatic Data Center, Asheville, NC).

of Kyushu accumulating 2000 mm of rain from mid-June to mid-August. At the end of August, Typhoon *Vernon* brought torrential rains and high winds to much of Japan. Homes were evacuated, commuters were stranded and transportation was disrupted by winds approaching 108 km/h near Tokyo. Flooding across the Archipelago affected more than 7,800 homes and businesses, caused at least 67 land slides and washed away dikes, bridges, roads and railways at several locations. Rainfall totals reached 160 mm in parts of Korea and 300 mm in Japan. In general almost four times the normal precipitation fell on the region during this time period.

The onslaught continued with Typhoon *Yancy*, the 13th tropical storm, in late August, with winds of 200 km/h and deluging theisland of Kyushu with as much as 255 mm of rain. This raised the precipitation amount to five times the normal over much of the area, with moisture excesses of 400 to 600 mm widespread across the region. Several tropical storms brought rain to Hong Kong. In mid-September, huge waves from Typhoon *Becky*, perhaps the deadliest storm that has hit Hong Kong since 1971, swept more than 70 sailors to their deaths in coastal waters.

From early October to the end of December 1993, a series of tropical cyclones traversed the Philippines and parts of mainland Southeast Asia, bringing periods of intense rainfall, powerful winds, flooding and structural damage to the region. In that period, more than 1000 mm of rain drenched parts of the northeastern Philippines and central Viet Nam. In addition, storms not associated with organized tropical systems dropped over 1000 mm of rain on much of southern Thailand's Isthmus of Kra. In early October, Tropical Storm *Flo* brought heavy rains and gusty winds to northern Luzon, engendering flows of lahar down Mount Pinatubo. *Flo* took 50 lives and damaged 10% of the nation's rice crop. Typhoon *Ira* ploughed through Luzon less than a month later, forcing thousands of individuals from their homes and sending 4 m-deep flows of lahar down Mount Pinatubo. *Kyle* tracked through the central Philippines less than three weeks later, causing relatively minor damage. In late November, *Kyle* made a second landfall as a typhoon on south-central Viet Nam, causing dozens of deaths and the loss of thousands of hectares of crops. In the beginning of December, two destructive typhoons (*Lola* and *Manny*) tore through the central Philippines in quick succession, with the first storm also making a landfall in south-central Viet Nam. The combination of *Lola* and *Manny*, the latter being the 30th tropical cyclone to hit the Philippines in 1993, took at least 300 lives, caused prolonged flooding and disrupted power and communications. Shortly thereafter, *Lola* regained strength in the South China Sea and crossed the southern Viet Nam coast near Cam Ranh Bay. The typhoon claimed dozens of lives and destroyed newly planted winter rice and dwellings. Only two weeks earlier, on 23 November, Typhoon *Kyle* struck the southern Viet Nam coast some 100 km north of *Lola*'s landfall. Typhoon *Manny* maintained a track quite similar to *Lola*'s while crossing the South China Sea, but weakened considerably by the time it reached southern Viet Nam.

The year ended with Typhoon *Nell*, the 32nd tropical cyclone to affect the Philippines during 1993. *Nell* was the fourth cyclone to hit the islands in a month and added to the 1560 mm of rain that inundated southeastern Luzon between 18 November and the end of the year.

The number of typhoons and tropical storms striking China in the period of this review was less than normal, with many of the storm tracks displaced to the south, due to the anomalously southward location of the summer monsoon system of East Asia (Figure 8.5). Such a displacement of the summer monsoon may be caused by the combined influences of a weakened Walker circulation in the tropical west Pacific, of a persistent ENSO event and of volcanic aerosols from the eruption of Mount Pinatubo

in the Philippines.

Six typhoons and tropical storms struck China during 1991, but the landfall sites were more south of normal with five storms centring on Guangdong province, which incurred total economic losses of up to US$ 440 million. Eight typhoons and tropical storms hit China in 1992. Among them, tropical storm numbered "9216" and the Typhoon "9219" resulted in the deaths of more than 100 people.

The tracks of typhoons and tropical storms striking China during 1993 were the most southerly in the past 43 years with the landfall latitude of the most northerly one only reaching 23°N. Six of the seven storms were concentrated in Guangdong province with large losses, the strongest of which was "9309" which also struck Guangxi and Hainan Island.

A freak storm with catastrophic consequences occurred on 5 May 1993 when a cold front with hurricane-force winds set off an enormous four-day sandstorm across Mongolia and northwestern China. The storm took 47 lives in Sansu province, trapped 10,000 railway passengers in Xinjiang province and destroyed 300,000 head of livestock in China's Inner Mongolia.

8.4

CENTRAL AND EASTERN NORTH PACIFIC TROPICAL CYCLONES

Compared to the western North Pacific there was much lighter activity in the eastern and central portions of the Pacific Ocean Basin in 1991. Activity in 1991 was particularly light, since for only the third time in the previous 35 years no eastern Pacific tropical storm or hurricane made landfall. The year 1992 was a different story with 27 tropical storms menacing the eastern Pacific, with 14 attaining hurricane intensity (five more than average). Figure 8.6 shows the cyclone tracks for 1992. There were some significant storms that struck Central America and Mexico and a particularly strong hurricane hit the Hawaiian Islands for the first time in nearly a century. The central North Pacific will remember 1992 as the year of Hurricane *Iniki*.

On September 6, a tropical depression formed over warm Pacific Ocean waters and steadily strengthened into a formidable hurricane as it moved westward, then northwestward, until it was positioned a few hundred miles south of Oahu, Hawaii, early on September 10. During the next 24 hours, *Iniki* strengthened into a Category 4 hurricane (on the Saffir-Simpson scale), about the same strength as hurricane *Andrew*, and took a sharp turn toward the north. *Iniki* reached maximum strength around midday 11 September as it raced across the island of Kauai. The eye of *Iniki* moved onto southwestern Kauai shortly before 3 p.m. (LST) and was northeast of the island by 5 p.m.. Despite *Iniki*'s rapid forward speed, Hawaiian Civil Defense authorities estimated that major damage covered 75% of the island. *Iniki* was the strongest hurricane in at least 90 years to affect Hawaii, which is usually protected from significant tropical cyclones by the cooler waters surrounding the islands. About 10,000 of Kauai's 21,000 homes and most of its 70 hotels were badly damaged as over 8,000 individuals from a population of 52,000 were left homeless. Damage was in the US$ 1 billion range, making *Iniki* the most destructive hurricane ever to strike Hawaii.

In 1993 a near-normal fourteen tropical cyclones, including ten hurricanes, roamed the eastern North Pacific. Eight of these were major hurricanes.

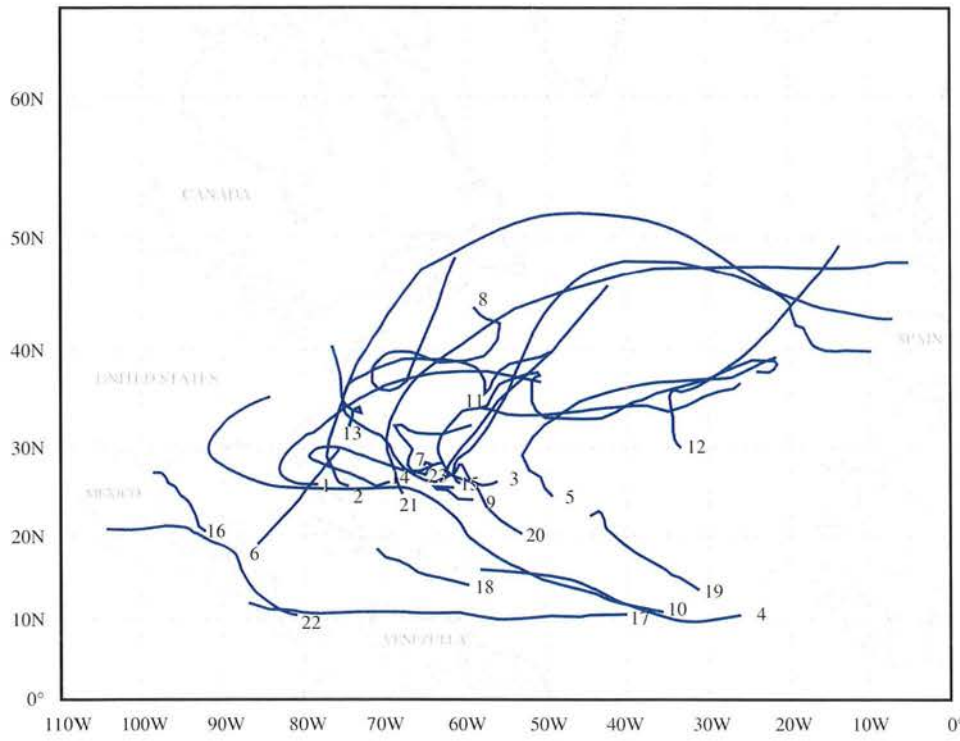

◀ *Figure 8.7* – Tracks of hurricanes and tropical storms in the North Atlantic Ocean during the 1991, 1992 and 1993 hurricane seasons (from NOAA, National Climatic Data Center, Asheville, NC).

In late June of 1993, Tropical Storm *Beatriz* moved northward through central Mexico producing very heavy precipitation. Almost simultaneously, Tropical Storm *Arlene* affected northern Mexico and the southeast part of Texas in the USA, moving in from the Gulf of Mexico.

In early July 1993, Hurricane *Calvin* battered the western Mexico coastline, aggravating five weeks of excessively wet weather raking an extensive stretch of resort beach in Acapulco and Puerto Vallarta. The storm reached winds of 165 km/h with most damage occurring before landfall as it paralleled the coastline. The storm took 37 lives and left 42,000 homeless, while also damaging crops, flooding roads and eliminating running water, electricity and telephone services for 55,000 people.

As much as 140 mm of rain drenched Honduras and Nicaragua when Tropical Storm *Gert* brushed the region on September 16, 1993. The storm claimed 70 lives and left 15,000 homeless. Up to 250 mm of rain soaked the region. Three days later Gert struck east-central Mexico, flooding rivers and lakes in six Mexican states.

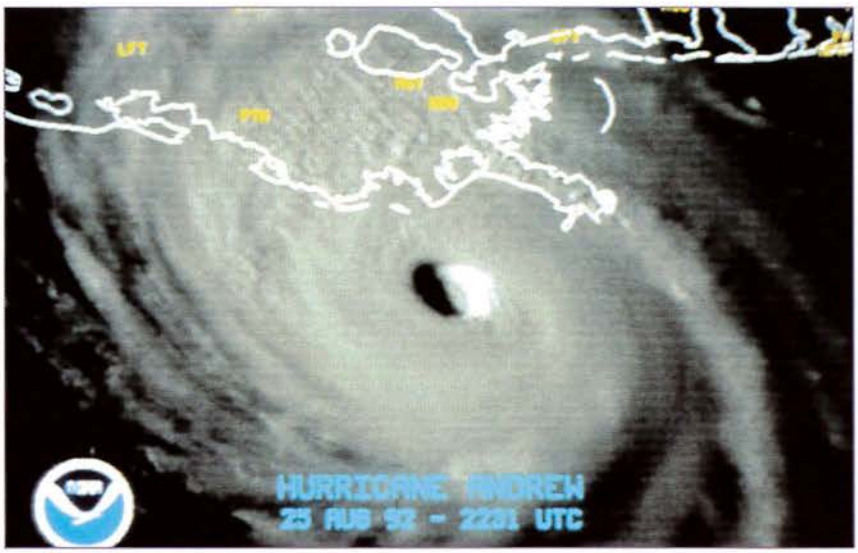

▲ Hurricane Andrew, August 25, 1992.

hurricane then turned to the north and grazed the North Carolina coast. Thunderstorms accompanying the hurricane spawned several tornadoes along the North Carolina coast. *Bob* then raced rapidly up the eastern seaboard with winds up to 220 km/h, bringing torrential rains over 175 mm. By the time the storm moved into Canada, the winds lessened and the storm was downgraded to a tropical storm. Digby, Nova Scotia, reported wind gusts of 130 km/h. Northern New Brunswick received between 60 and 100 mm of rain.

In 1992 there were six tropical storms of which four became hurricanes. For the second year in a row, no system reached hurricane intensity south of 25°N. The most significant storm of the year was Hurricane *Andrew*. *Andrew* started as a tropical storm in late August 1992 in the central Atlantic Ocean and remained a weak system as it drifted northwestward. It began strengthening a few days later and

8.5

HURRICANES AND TROPICAL STORMS IN THE NORTH ATLANTIC

Figure 8.7 depicts tropical cyclone tracks in the North Atlantic for the years 1991, 1992 and 1993. The 1991 hurricane season was characterized by high-latitude tropical cyclone origins and tracks, only one landfall in the USA and no tropical storms or hurricanes in the Gulf of Mexico. This lack of Gulf of Mexico storm activity is a rare event that has occurred only two other times this century, in 1927 and 1962. There were eight tropical storms with four of them hurricanes. The long-term average is ten and six, respectively.

Tropical Storm *Bob* developed from a tropical depression in the middle of August 1991 just northeast of the Bahamas Islands and strengthened to hurricane force as it moved northwestward. The

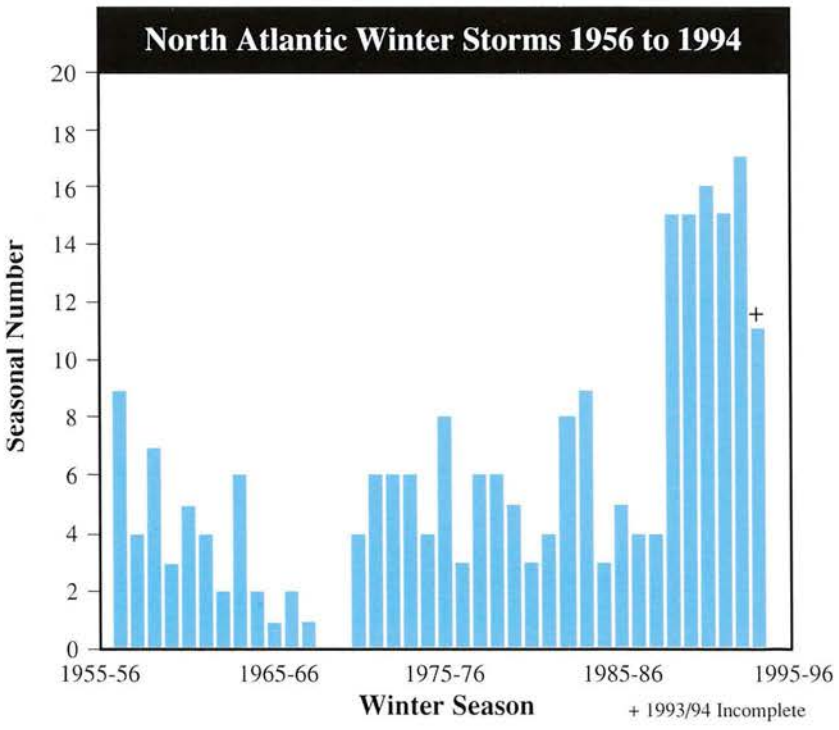

▲ *Figure 8.8* – Number of North Atlantic low-pressure systems (950 hPa and lower, counted once per lifetime) determined from four to eight weather maps per day for the winter season, November-March, 1956 to 1994, (from R. Franke, Deutscher Wetterdienst, Seewetteramt, Hamburg, Germany).

turned westward, becoming a very strong hurricane before tracking quickly through the Bahama Islands and southern Florida, at 24 km/h (the eye of the storm was over southern Florida for less than four hours). *Andrew* crossed the Bahamas at high tide and was accompanied by a phenomenal 7 m storm surge. In Florida, emergency measures were taken and officials ordered one million people to leave their homes before Andrew made landfall around 5 a.m. on August 24, 60 km south of Miami. Later that morning *Andrew*'s eye had moved into the Gulf of Mexico, but not before inflicting approximately US$ 15 to 20 billion damage to Florida. *Andrew* was the costliest storm in USA history. Over one million individuals were left without power, more than one hundred thousand people lost their homes, at least one dozen lives were lost and many of the region's water sources were contaminated, creating a shortage of potable water.

After devastating Florida, the storm crossed the Gulf of Mexico and took aim at south-central Louisiana on August 25 (see photograph). *Andrew* slowed considerably as it moved into the lower Mississippi River Valley allowing the system to dump much more rain on southern Louisiana and Mississippi (up to 250 mm) than it had on southern Florida. The slower forward speed, however, also allowed *Andrew*'s interaction with the land to weaken before it came ashore in southern Louisiana. This, combined with the fact that the eye hit a less populated area, made *Andrew*'s impact on the region considerably less than on southern Florida. Still, damage was at least US$ 500 million. *Andrew* then turned northeastward and quickly weakened but the system and its remnants spawned gusty winds and tornadoes from the lower Mississippi Valley northeastward to north-central Maryland before the low-level circulation finally dissipated.

In 1993, for the third consecutive year, the North Atlantic basin had fewer hurricanes than the 50-year average. There were eight storms and four became hurricanes. With the exception of *Emily*, the hurricanes were short-lived and did not reach major hurricane status. Also, the activity ended earlier (September 21) than in any hurricane season since 1930. Unfortunately, the storms still claimed 280 lives.

8.6

WINTER STORMS OVER EUROPE AND THE NORTH ATLANTIC

Since 1988, a significant increase in intensive storms has occurred over the North Atlantic during the winter season (Figure 8.8). The greater number of severe storms coincides with strengthened temperature and pressure gradient between the subtropics and the polar region. The mean zonal pressure gradient, called the "zonal index", is measured regularly twice each day by the Deutscher Wetterdienst. For this analysis, the winter season spans the period 1 November to 31 March, inclusive, and includes low-pressure centres below 950 hPa. The North Atlantic box spans latitudes 35 and 65°N and longitudes 20°W to 40°E. This area comprises nearly all of Europe. Most of the storms in the winters of 1990-91 and 1991-92 did not hit the European continent. However, there were enormous damages caused by storms in the winter of 1992-93. Insurance companies reported huge losses that even exceeded those of the winter of 1989-90, when the reported losses

DEEP STORM IN THE NORTH ATLANTIC

Intense depressions are no strangers to the North Atlantic, but the storm which passed between Iceland and Scotland on January 10, 1993 was remarkable in that the central pressure fell to the lowest value so far encountered in that region (Figure 8.9). For 15 hours the central pressure remained below 920 hPa and the minimum was reliably estimated to have been between 915 and 912 hPa.

Except in the case of tropical cyclones (and possibly in the vortex of an intense tornado) such a low sea-level pressure has perhaps never been observed before.

Adapted from Royal Meteorological Society's Weather 48(4):98–107.

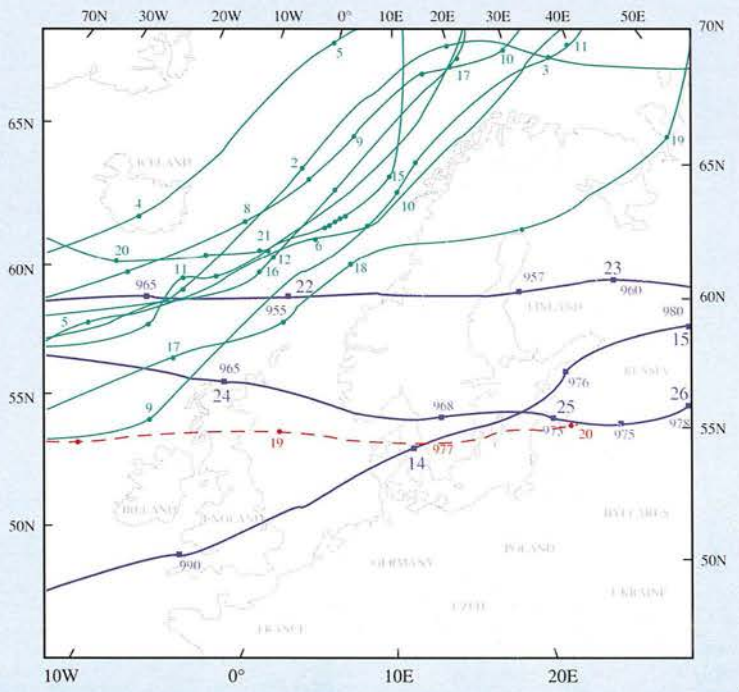

Figure 8.9 – Tracks of the depressions over northwestern Europe in January 1993 (from R. Tiesel, Deutscher Wetterdienst, Seewetteramt, Hamburg, Germany).

were the highest ever recorded. Platforms and vessels were wrecked on the North and Baltic Seas, buildings collapsed and the storms felled many trees.

A 1992 New Year's Day storm brought torrential rain and high wind to parts of the Middle East, forcing roads, schools and businesses to close. In Israel, the storm dumped 172 mm of rain on Tel Aviv, flooding streets, while 45 cm of snow blanketed Jerusalem, blacking out a fourth of the homes by knocking down hydro lines. Snow was reported for the first time in the mountains north of the Red Sea resort of Eilat. Farther east, very heavy snow covered the mountains in the region of Tobuk in extreme northern Saudi Arabia. In Lebanon, snow covered Beirut for the first time in 40 years, damaging the old infrastructure of the country, cutting telephone lines and downing high-tension power cables. The storm paralysed many cities in the region, including Damascus, Syria and Amman, Jordan. Heavy snow also caused avalanches in southeastern Turkey, killing 22 people, However, the snows also helped replenish reservoirs that had become critically low after several years of persistently below-normal rainfall.

Atlantic storms battered the coast of northwestern Europe with nearly non-stop rainfall during November and early December of 1992. One storm lashed the west coast of England with 140 km/h gusts on December 1. This storm spun off the day before from an intense low-pressure centre a few hundred kilometres southwest of Iceland. The weather map on 30 November showed the central pressure down to a phenomenal 936 mb. The closest ship, over 160 km south of the storm, reported sustained winds of nearly 120 km/h.

At the end of 1993 a series of strong storms brought torrential rains and high winds to much of central-western Europe, causing the worst flooding in sixty years across much of Germany, Belgium, eastern France and the southeastern Netherlands. The floods claimed several lives, forced thousands to flee their homes and caused more than US$ 580 million in Germany alone. In addition, wintry weather plagued the UK, hampered travel in Hungary and neighbouring parts of Austria and Slovakia and triggered avalanches in the Pyrenees and the French and Italian Alps.

MORE OR LESS STORMINESS?

The identification of trends in wind speed requires a long and homogeneous time series. But there are no long homogeneous series from land stations owing to changes of observing methods and changes in local environment and exposure.

To ascertain whether storminess really is changing, a systematic examination of the geostrophic wind has been carried out. The geostrophic wind computed from pressure readings from a few stations can be regarded as a proxy of the real wind. In contrast to the wind measurements, pressure readings suffer from no substantial inhomogeneities because the measuring instruments and observing practices have remained unchanged for more than 100 years. From an analysis of geostrophic winds annual frequency distributions of daily wind can be obtained for periods of 100 or more years.

Any trend in the wind statistics will be reflected in the geostrophic wind statistics. This approach has been applied to the German Bight in the southeast part of the North Sea, where three stations (Fanoe, Borkum and Hamburg) have reported air pressure since 1876. The resulting time series of geostrophic wind speed for the period 1876 to 1992 has remained remarkably stationary (Figure 8.10). None of the time series show any indication of a long-term trend.

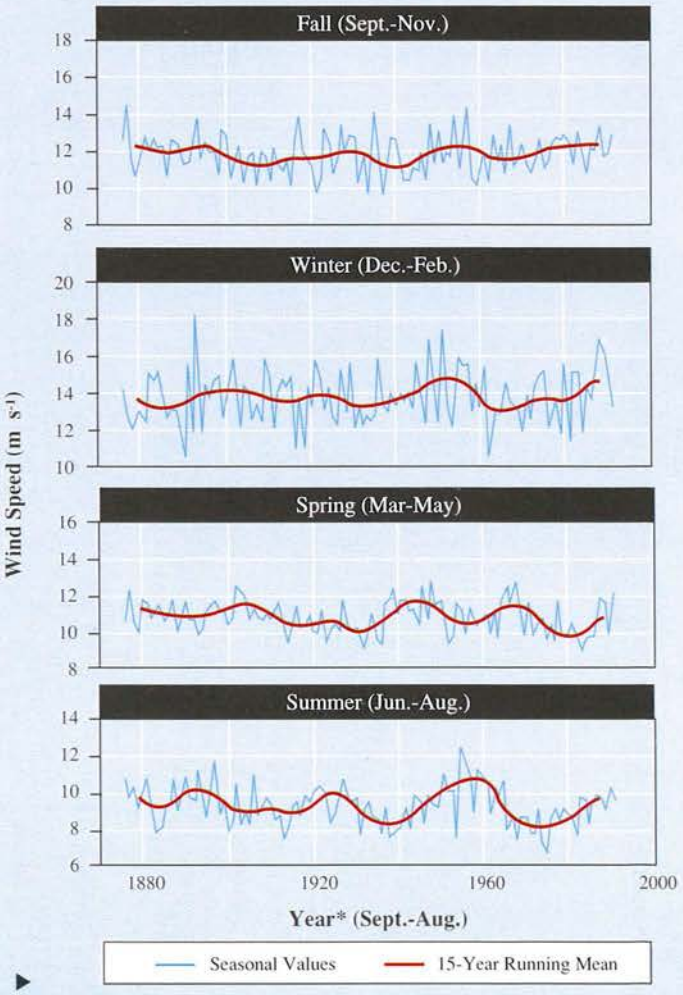

Figure 8.10— Seasonal average geostrophic wind speed, 1876-1992 with 15-year running mean (from Deutscher Wetterdienst, Seewetteramt, Hamburg, Germany).

8.7

NORTH AMERICA'S "STORM OF THE CENTURY"

On March 12-15, 1993 a storm now called "The Storm of the Century" struck the eastern portion of North America. The storm was immense and unleashed tremendous energy which affected the entire eastern section of the USA, from Florida to New England and the Maritime Provinces of Canada. The storm also wreaked havoc on Mexico and Cuba. In western Cuba, 1,500 houses were destroyed and another 37,000 partially destroyed, while 30 per cent of the banana crop was lost. A tornado left 5000 people homeless in Reynosa, Mexico (near the Texas border).

The greatest impact of the storm was from the huge snowfalls in the USA (see photograph). Other destructive forces were the winds approaching hurricane force and the storm surges along the coastlines. Wind gusts exceeding 140 km/h were common. The death toll for the USA (max. over 300 people) is more than three times the combined death toll from Hurricanes Hugo and Andrew. Figure 8.11 depicts the storm track and some highlights. Thousands of people were isolated by record snowfalls, especially in the Georgia, North Carolina and Virginia mountains. The highest snowfall amounts recorded exceeded 140 cm. More than 200 hikers were rescued from the North Carolina and Tennessee mountains. Generally, all interstate highways from Georgia northward were closed.

For the first time, every major airport on the east coast was closed at one time or another by the storm. Snowfall rates of 5 to 8 cm/h were common during the height of the storm. Generally, New York's Catskill Mountains along with most of the central and southern Appalachian mountains received at least 60 cm of snow. Hundreds of roof collapses occurred owing to the weight of the heavy wet snow. Over three million customers were without electrical power at one time due to fallen trees and high winds.

In the wake of the storm, bitterly cold conditions pushed into the region,

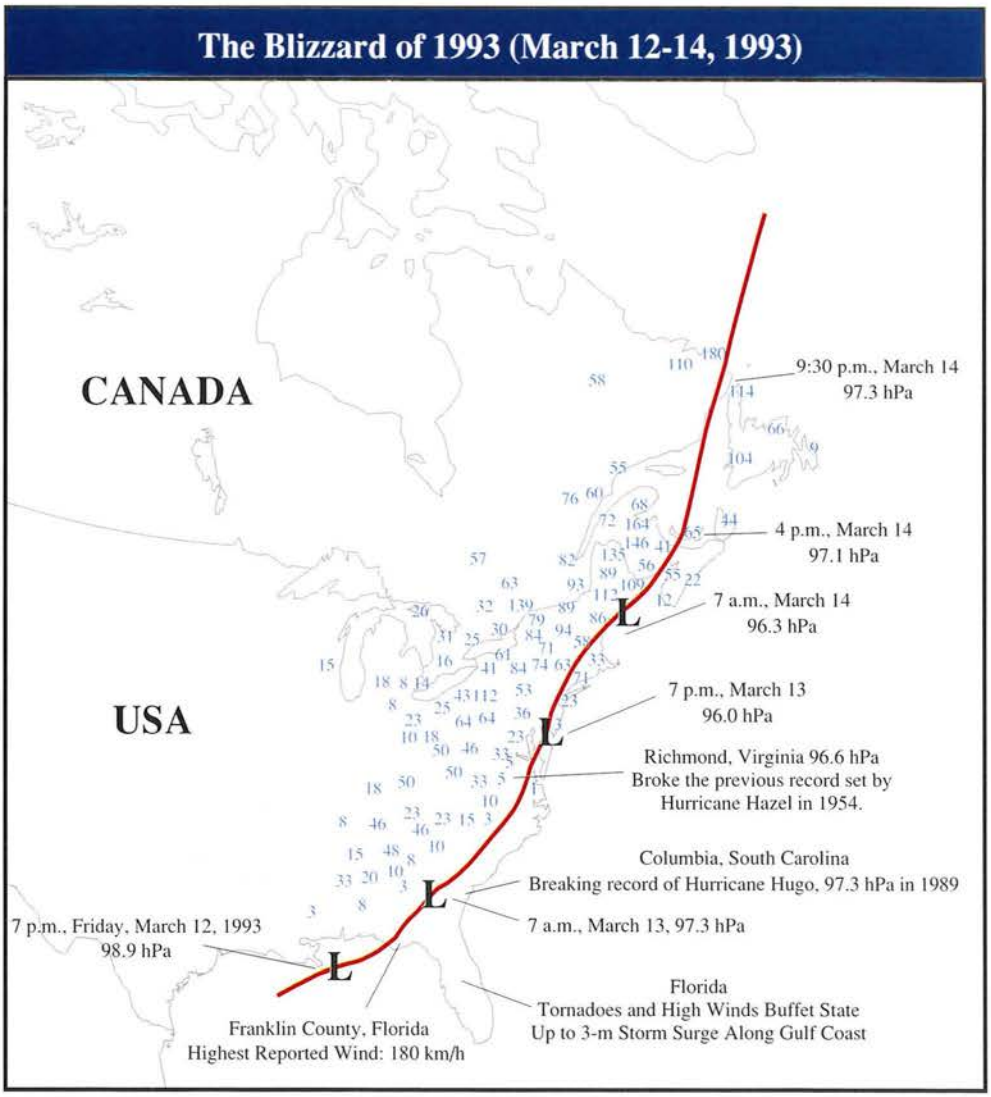

▲ *Figure 8.11* – Track of the "Storm of the Century", March 12-14, 1993 (from NOAA/NWS/NMC/CAC, Washington, DC).

▲ Department store roof in Asheville, NC collapses under heavy snowfall during March 1993 snowstorm.

establishing dozens of new daily record lows, including -14°C at Washington, DC and -13°C at Asheville, NC The cold engendered considerably heavier than normal heating demand from Florida to New England.

At least 18 homes fell into the sea on Long Island owing to the pounding surf. About 200 homes along North Carolina's Outer Banks were damaged. Over 160 people were rescued at sea by the Coast Guard in the Gulf of Mexico and Atlantic. Florida was struck by an estimated 15 tornadoes and 44 deaths were attributed either to the tornadoes or other severe weather. A 4-m storm surge occurred in Taylor County, Florida and up to 15 cm of snow fell in the Panhandle, an extremely rare event.

In Canada, three storm-related deaths were reported in Quebec and one in Ontario. Up to 42 cm of snow fell in New Brunswick and gusts of 200 km/h whipped across Cape Breton Island on March 14. Off Nova Scotia, hurricane-force winds churned up 15 to 20-m seas. A 177-m ship sank in heavy seas 175 km south of Cape Sable Island, Nova Scotia, with all 33 of its crew lost at sea. Twenty-metre waves were reported in the area. Also, a wind gust of 210 km/h occurred at Grand Etang, Nova Scotia.

The USA National Weather Service estimated the volume of water that fell as snow from this storm is comparable to 40 days' flow on the Mississippi River at New Orleans, Louisiana. Overall damage figures exceeded US$ 3 billion making this the fourth costliest storm in American history and by far the most costly extratropical storm.

8.8

TORNADOES

Tornadoes are more prevalent in the USA than any other place on Earth. In approximate terms, about one half of the world's tornadoes occur in the USA and most of the other half occur in about 20 other countries. Perhaps only in parts of Canada, Bangladesh and extreme northeast India do tornadoes reach the violent intensity that they do in the USA. In 1991, tornadoes were reported in Costa Rica, Canada and Trinidad and Tobago, Sweden, Russia, the UK and Belgium.

On April 11, 1993, a series of tornadoes struck five villages in West Bengal, India, killing more than 100 people and injuring 200.

In the USA the years 1991, 1992 and 1993 were very active tornado years. The annual tornado count topped the 1,000 mark in all three years. The year 1992 set a new annual record for tornadoes, with two months, June and November, establishing new monthly records. Figure 8.12, depicts the number of observed tornadoes for each month during 1991-1993 versus the mean for the period. Figure 8.13, shows the combined tornado count by state for

TABLE

Tornado Frequency by Intensity Category in the USA 1991-1993

Category	F-scale	Frequency		
		1991	1992	1993
Weak	0	683	696	718
	1	294	411	318
Strong	2	102	129	81
	3	39	43	28
Violent	4	6	13	6
	5	1	1	1
Totals		1125	1293	1152

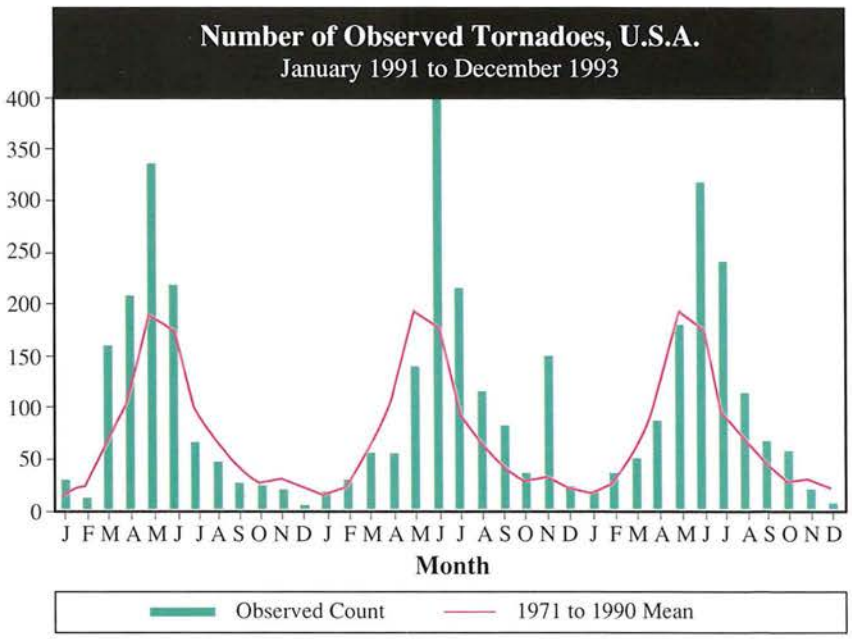

Figure 8.12 – Total number of observed tornadoes occurring in the USA from January 1991 to December 1993 (from NOAA, National Climatic Data Center, Asheville, NC). ▶

the three years in review. The November 1992 total was five times the normal for that month, many associated with an outbreak of strong thunderstorms in the middle of the month across the southern Plains and the deep South. Other record-breaking months were May 1991 and July and October 1993.

By far the most devastating tornado outbreak occurred on 26 April 1992 in Kansas and Oklahoma. At about 5:40 p.m. a violent tornado moved into the southern part of Andover, Kansas, destroying 84 houses and 14 businesses. The tornado reached F5 intensity as it hit a mobile home park, where 13 people were killed; 200 people survived by going to the park's tornado shelter.

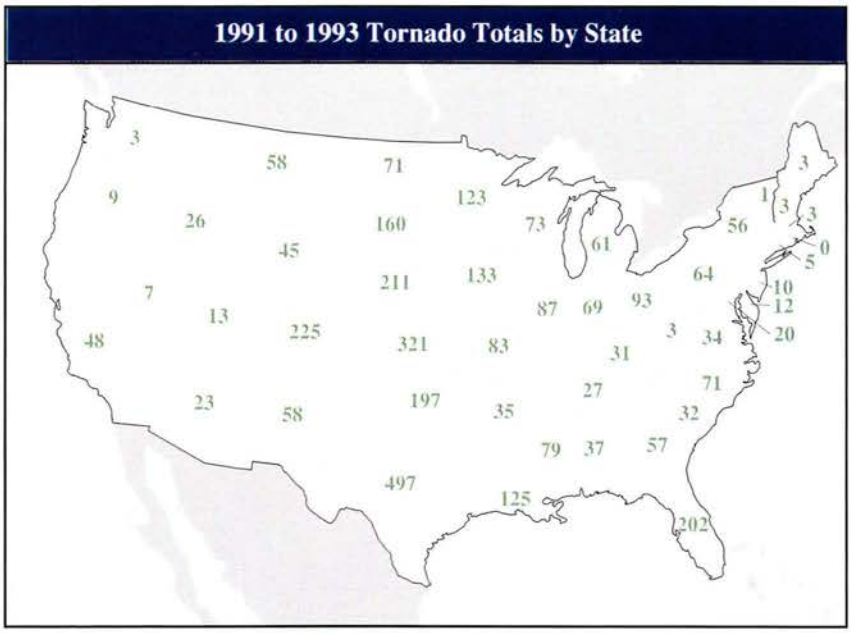

◀ *Figure 8.13* – Combined tornado totals by State for 1991, 1992 and 1993 (composite of annual maps from *Weatherwise*).

9.1

GLOBAL CROP PRODUCTION REVIEW: 1991-93 [1]

Droughts and floods during critical times of the year have a significant impact on crop yields around the world. The timing of the climate anomalies as related to the crop's growing season is of prime importance to productivity. For example, drought or flood episodes occurring prior to the planting season or after the harvest season will have little consequence unless the anomalous conditions persist into the crop season. Climatic extremes not only have a direct impact on yield productivity but also control other factors that affect output. Insect infestation and fungal diseases are often induced by climatic conditions, resulting in a loss of productivity or crop quality.

In 1991, world wheat production fell over 5% from the previous year's, due mostly to dryness in the USA (-28%) and Australia (-34%). In the Newlands of the former Soviet Union, heat and dryness from April to July cut sharply into spring wheat production, down some 25% from 1990 levels. Kazakhstan harvested only half as much grain as the previous year's. South Africa's production was the smallest crop in over 20 years (down 75% from the previous year) owing to lack of rain and, in Indonesia, drought lowered its important rice crop by 2%. These lower crop yields were offset by substantial improvements in production from the previous year in both France and Argentina (+36% and +40%), respectively. Relatively well spaced rains led to good growing conditions this summer for West and East Africa, including the Sahel. World production was up slightly (+2%) from the preceding year. World rice production declined slightly, reflecting drought conditions in Indonesia and intermittent monsoon rains across northern India.

In 1992, more favourable weather boosted world wheat production 3% above the previous year's, while USA production was up 24%. Higher yields returned to the former Soviet Union (up 23%), Australia (up 26%) and Pakistan (up 7%). In contrast, drought struck southern Africa during the crucial growing period, with devastating results: regional grain production fell some 60% short of expected levels. South African farmers harvested their worst crop (3.3 million tons) in 40 years. Drought also slashed grain production in Morocco by over 50% and unfavourable weather in northern and eastern Europe lowered summer crop production by over 25%. Norwegian production was as much as 40% below that of 1991 and, in Finland, production dropped some 48% from that of a year earlier. In Canada, persistent cool weather slowed summer crop development and wet, cool conditions late in the growing season limited yields and quality, especially on the Prairies. World corn production increased 9% over 1991 while the typically stable upward trend in world rice production edged up slightly.

In 1993, excessive wetness was the principal cause of production declines. Whereas China, eastern Europe, Argentina and Australia produced larger wheat crops, the USA, Canada and the European community produced less. Spring wheat production in the northern Plains of the USA fell over 20% due to excessive moisture. Cool, wet weather hampered wheat production in Canada (-6%) and EC-12 (-5%) as well. In Argentina, flooding of four million hectares in early May damaged corn, soybean and sunflower crops. Cold and wet weather dashed hopes for a record harvest in Russia and Kazakhstan, following a summer of near perfect

[1] *Adapted from material submitted by Raymond P. Motha, Joint Agricultural Weather Facility, USA Department of Agriculture/World Agricultural Outlook Board.*

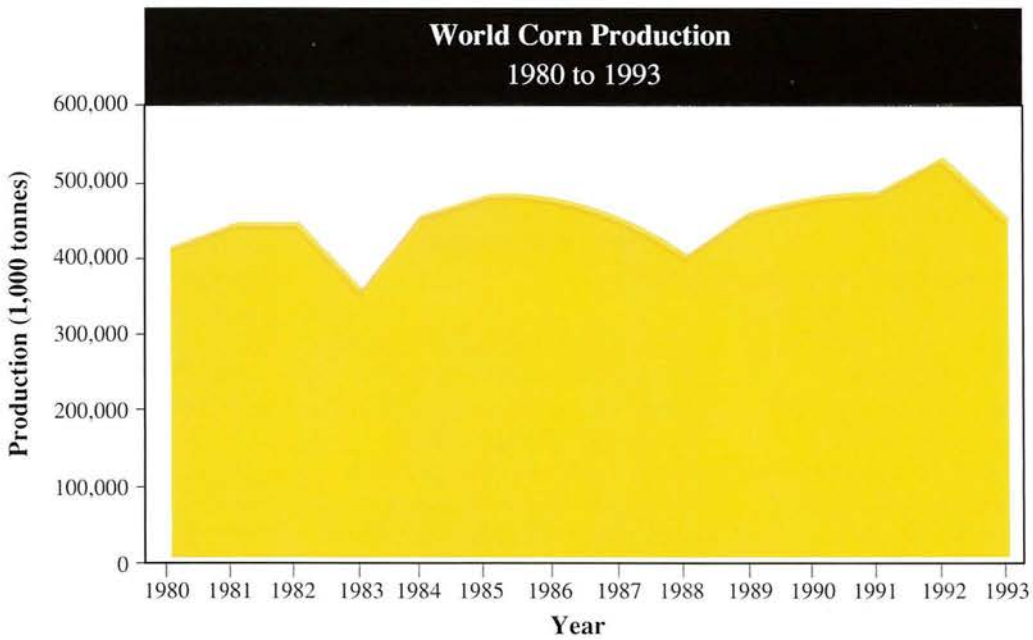

▲ *Figure 9.1* – World corn production 1980-1993 (from material submitted by Raymond P. Motha, Joint Agricultural Weather Facility, USA Department of Agriculture/World Agricultural Outlook Board).

Figure 9.2 – Location of bushfires and forest fire danger index just west of Sydney from January 6 to 8, 1994. The index uses wind speed, relative humidity, temperature and estimated fuel dryness. Values of 50 or higher indicate extreme danger (existing fires cannot be controlled). The weather map for January 8 shows the strong pressure gradient over the southeast of Australia (from National Climate Centre, Bureau of Meteorology, Melbourne, Australia).

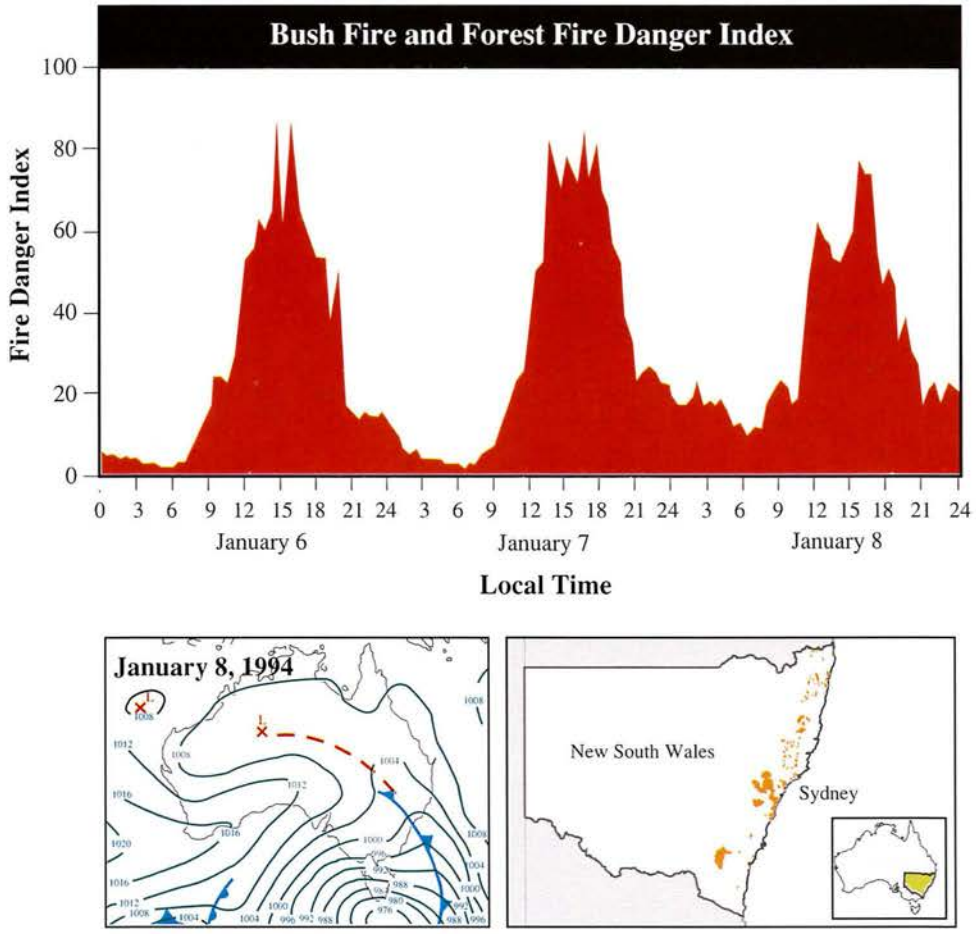

growing weather. In Russia, September rainfall up to four times normal disrupted the harvest and ruined some standing grain. Because of unfavourably cool, wet growing season weather, corn production fell by 30% in the USA and rice declined by 29% in Japan. The scarcity of rain-bearing storms in the Mediterranean Basin from November 1992 through February 1993 dramatically reduced grain production in Morocco and western Algeria. Typhoons in the Philippines cut corn production by 5% from the previous year's. In total, world wheat production showed on a very slight decline, while world rice production dropped 2% from the 1992 output. However, world corn production fell 14% from the preceding year's. From 1980 to 1992, two sharp declines in world corn production were attributed mostly to regional drought conditions. These years were 1983 (-23%) and 1988 (-11%) (see Figure 9.1). The sharp decline in 1993 world corn production illustrated how the opposite extreme of growing season weather, namely too much rain, can also seriously affect crop production.

9.2

DROUGHT DEVASTATION OF CROPS IN SOUTHERN AFRICA [2]

A series of FAO crop and food supply assessment missions to southern Africa in 1992 confirmed that the worst drought in decades has devastated crops in most countries of the region. The rainy season started on time in certain countries but subsequent precipitation was below normal in a number of other countries, seriously affecting crop growth. Nevertheless, as of early January, crop conditions were good in Angola, Malawi, Namibia and Zambia, poor in South Africa, Zimbabwe and central and southern parts of Mozambique and about average elsewhere. However, prolonged drought through January, during the crucial pollination stages, has severely affected crops throughout the subregion except for Angola, causing widespread crop failures in already affected countries and seriously reducing yield potentials in others. Rains in most countries in March came too late to save crops, but did benefit pastures.

FAO's forecasts, at that time, of cereal production by country are

[2] *Adapted from a longer report on Food Outlook issued by the Global Information and Early Warning Service of FAO. The report analyzes the effect of drought on the crops and food supply situation in southern Africa in 1992-93. In the midst of the worst drought this century in southern Africa, FAO completed a series of missions to evaluate food deficits and food aid requirements in the nine drought-affected countries of southern Africa and in Tanzania.*

TABLE 1

SOUTHERN AFRICA:
ESTIMATED CEREAL IMPORTS AND FOOD AID REQUIREMENTS FOR 1992–93, IN THOUSANDS OF TONNAGE

Country		1992 Production: Forecast	Per cent of normal[1]	Total	Import Requirements: Food aid requirements Total	Of Which: Emergency
A.	**THINNESS**					
	Angola	454	143	285	125[2]	116.0
	Botswana	15	24	240	15	3.3
	Lesotho	81	47	297	75	11.2
	Malawi	683	46	876	740[2]	400.0
	Mozambique	226	41	1218	1140[2]	414.0
	Namibia	33	30	125[3]	60	16.5
	Swaziland	53	38	129	60	41.0
	Tanzania	3250	85	500	280	15.0
	Zambia	572	36	970	820	94.0
	Zimbabwe	608	26	1410	660	471.0
	Total Thinness	5975	49	6050	3975	1582
B.	South Africa	3650	30	5500	-	-
C.	Grand Total (A plus B)	9625	40	11550	3975	1582

Source: FAO
1. Average production in the previous five years
2. Includes the needs of refugees, returnees and internally displaced persons
3. New imports

shown in Table 1. These indicated outputs of cereals ranging from 24 to 85% of normal (except for Angola, where production had increased in 1992). Most seriously affected was Mozambique, where drought compounded the effect of years of civil strife, displacement of people and shortages of farming inputs and implements. The almost complete crop failure in many areas of the country had already resulted in significant movements of drought-affected and war-displaced people in search of food and water. More than three million people were exposed to famine. Southern parts of Malawi and Zimbabwe also faced imminent food shortages and emergency feeding programmes were already under way for drought-affected people as well as for about 1.5 million Mozambican refugees in neighbouring countries.

The challenge posed by this emergency was to ensure that the needs of all the affected countries were adequately met, that the existing infrastructure was utilized optimally and that the particular needs of the landlocked countries were not unduly compromised by the competing demands of the coastal transit states.

9.3 AUSTRALIAN EAST-COAST BUSHFIRES

From December 27, 1993 through January 14, 1994 bushfires ravaged one million hectares along 1000 km of tablelands on the coastal fringe of New South Wales, Australia. Closure of the main road and rail link north of Sydney for three days stranded 14,000 people on holidays or returning home from work.

Natural forest and woodland, dominated by eucalypt trees, cover the tablelands. Eucalypts contain high levels of volatile inflammable oils, terpenes and waxes. Low rainfall in the first half of 1993 (linked to ENSO) produced abundant ground litter. High spring rainfall produced a flush of new growth. However, absence of rain in December and strong winds dried the soil and created potential fire danger conditions.

The fires were fanned by strong westerly winds (see photograph on page 88) generated by unseasonably low pressure just south of eastern Australia (more typical of winter than summer). A fire danger index is shown for three of the worst days, January 6-8, along with the weather map for January 8 (Figure 9.2). Peak fire intensity, estimated around 30 MW/m of fire front on some steep slopes, far exceeds the two from spot fires (downstream ignition by firebrands carried by the wind above tree tops). On the worst days, temperatures over 40°C, relative humidities below 15% and average wind speeds of 50 km/h led to spotting several kilometres ahead of the main fire front. The fires were amongst the worst in 200 years for duration and area burnt. Fortunately, despite extremely dangerous conditions, only 200 buildings were destroyed and four lives lost.

9.4 MAJOR FOREST FIRES

Figure 9.3 shows the locations of several major forest and bush fires that occurred during the review period from June 1991 to November 1993.

▼ *Figure 9.3* – Major forest and bush fires during the review period June 1991 to November 1993.

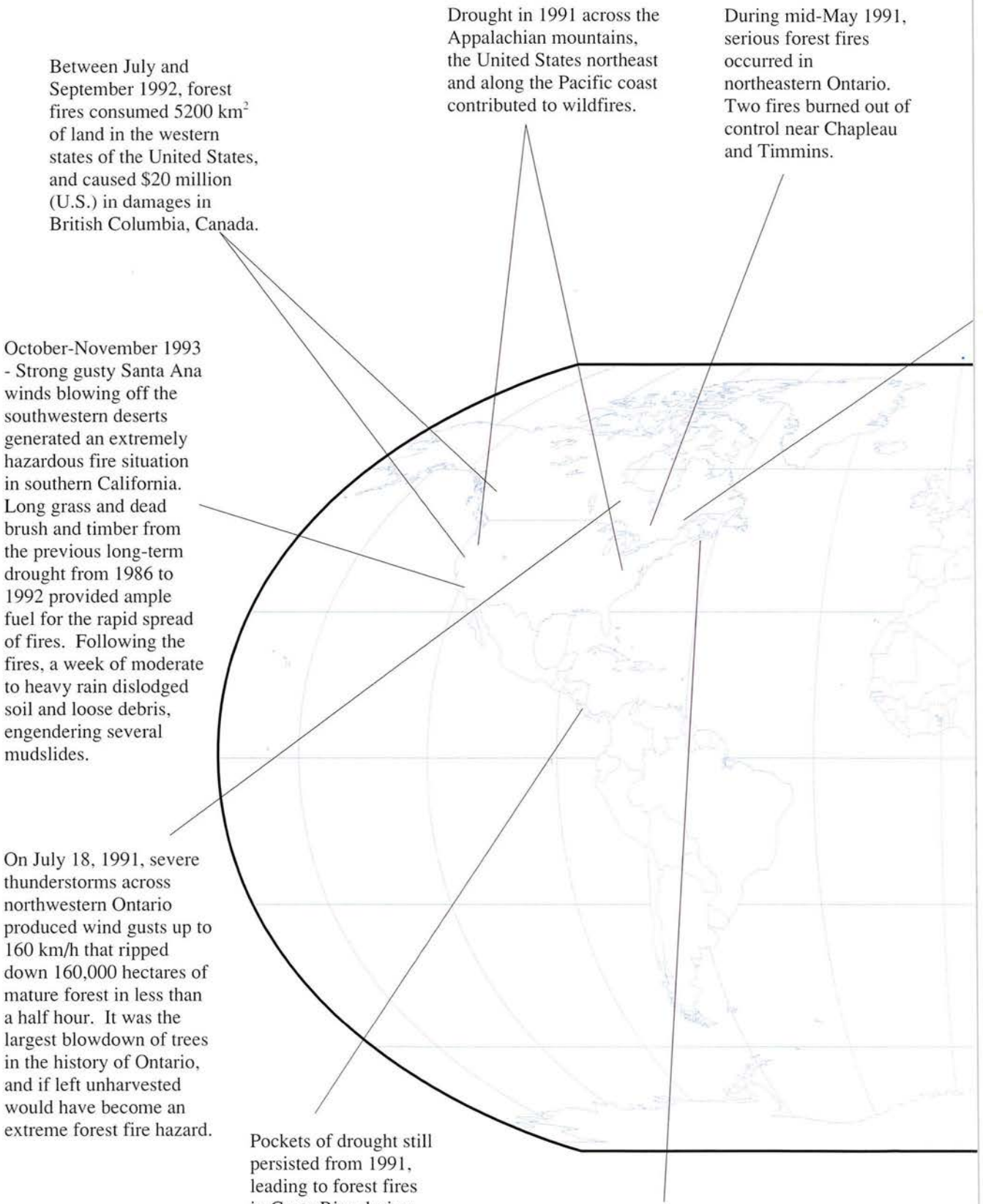

he worst forest fires in
lmost half a century
1089 fires or 120% of
ıe ten-year average)
estroyed 383,000
ectares of Quebec
Canada) forest (almost
00% of the ten-year
verage). The two largest
res covered 1,900 and
00 km^2 along the north
ıore of the St. Lawrence
iver.

In Russia and the Baltics, widespread fires spread a pall of smoke across the region. By August 13, 1992, Russia reported more than 18,000 fires burning two million acres of forests and marshlands.

Very hot weather dominated much of southeastern Asia and the northern Philippines during the spring of 1992. Eastern Mindanao received less than 10% of normal rainfall. To the northwest, excessive dryness contributed to a large wildfire on the island of Negros, and hot weather further exacerbated the island's dryness during April and May.

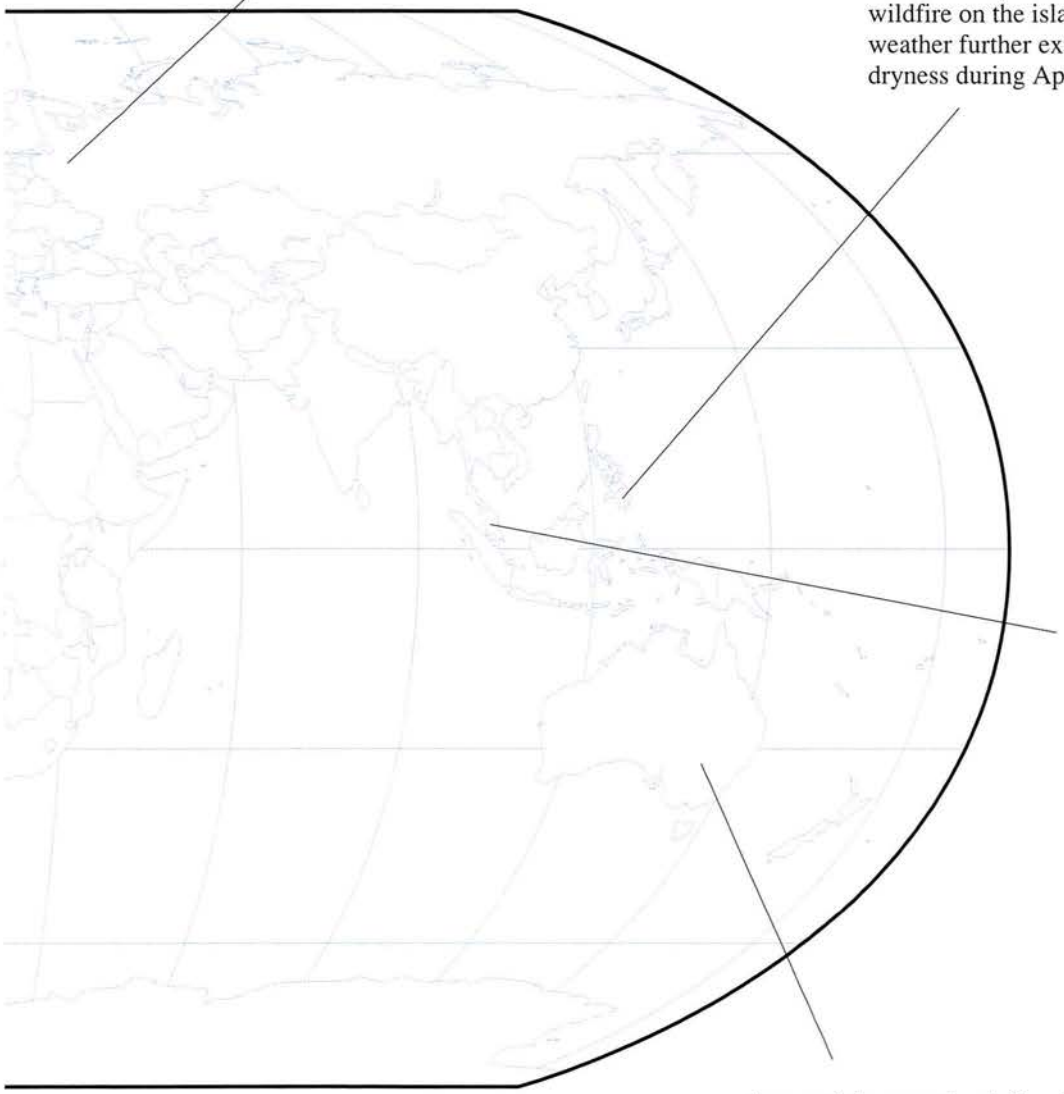

Exceptionally dry conditions in the 1991 spring season over western areas of Indonesia and Malaysia created ripe conditions for extensive wildfires.

Some of the worst bush fires in 200 years ravaged a million hectares of New South Wales in late 1993

An image of bushfires, derived from NOAA-11 Advenced Very High Resolution Radiometer (AVHRR), over the New South Wales coastal region at 18:20 (EDT) on January 8, 1994. Red colour pixels indicate "hot spots" and were determined using the difference between the AVHRR channel 3 and 4 radiances. The background image is from channel 1 data, pseudo-coloured to enhance and distinguish land, sea, clouds and smoke plumes (from Z.-J. Wu and J. LeMarshall, Bureau of Meteorology Research Centre, Melbourne, Australia). ▼

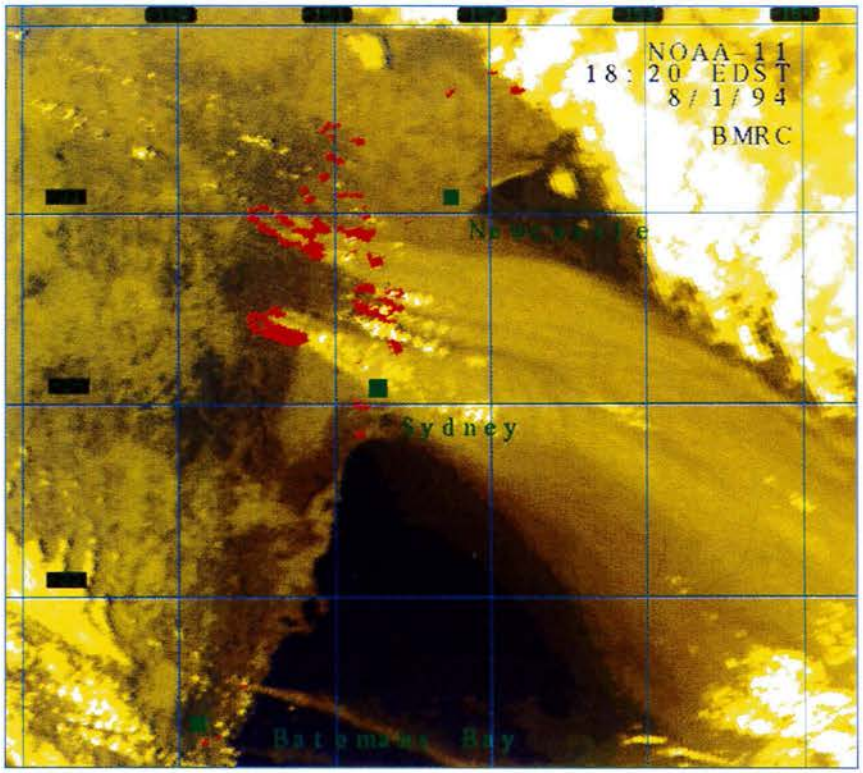

9.5

CLIMATE AND THE CANADIAN FISHERY *

The atmospheric pressure patterns over the North Atlantic are dominated by two systems: the Icelandic Low and the Bermuda-Azores High. The difference in winter atmospheric pressure between the two systems is known as the North Atlantic Oscillation (NAO) Index (see Section 2.4). Since the mid-1960s, the NAO Index has shown an increasing trend, with peaks in the early 1970s, mid-1980s and the 1990s. Cold temperatures and heavy ice conditions in the Labrador Sea are generally associated with a strong positive NAO Index. The increasing trend and the peaks in the NAO Index in the last decades have resulted in generally colder water temperatures off Newfoundland, with coldest periods in the early 1970s, mid-1980s and the 1990s (Figure 9.4). Since the mid-1980s, the northern cod stock off Labrador and eastern Newfoundland has been declining. Environmental stress linked to low water temperature appears to have contributed to the decline of cod. The establishment of a moratorium on the fishery in 1992 did not prevent the stock from falling to an all-time low abundance in 1994. Recent declines in several biological characteristics of cod (e.g. size-at-age, condition factor, recruitment) may be due to a number of factors including environmental stress. Further, the distribution patterns of cod were modified in the early 1990s, with a displacement of the fish towards deeper and more southerly warmer waters. Similar changes in abundance and distribution were also observed for other unharvested fish species off Newfoundland. The impacts of climate on fish recruitment, growth and behaviour will have to be taken into account and factored in stock rebuilding and managing strategies. Fish stocks will have to be maintained at levels of abundance high enough to absorb the effects of both fishing pressure and climatic changes.

** Adapted from a contribution by Denis D'Amours, Canada Department of Fisheries and Oceans, Biological Sciences Directorate, Ottawa, Ontario.*

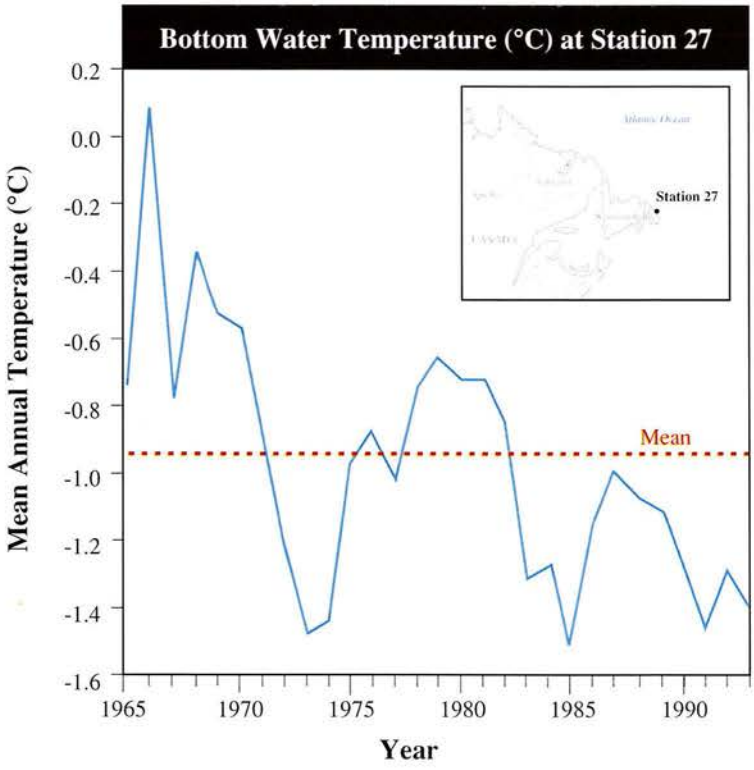

◀ *Figure 9.4* – Mean annual bottom water temperature (°C) at Station 27 near St. John's Newfoundland, 1965-1993 (Canada Department of Fisheries and Oceans, Biological Sciences Directorate, Ottawa, Ontario).

OCEAN CLIMATE, PREDATORS AND THE WEST COAST VANCOUVER ISLAND HERRING STOCK *

Survival and growth of Pacific herring are sensitive to natural fluctuations in ocean climate and ecology. It is necessary to understand this complex interplay to resolve the added effects from pollution and fishing; thereby sustaining herring stocks into the future.

One of the more important natural factors is ocean temperature, which influences herring survival and growth directly and also indirectly by altering the abundance of herring predators, principally Pacific hake. Waters off the West Coast Vancouver Island undergo alternate warm and cool periods (Figure 9.5). Warm periods since 1976 have been intensified by strong El Niño events.

During these warm periods, survival and growth of young herring are weak due to the abundance of Pacific hake and the high water temperature, frequently associated with El Niños. Strong El Niño events further reduce young herring survival because large numbers of Pacific mackerel migrate north into B.C. Waters and feed on herring, salmon and other species during the summer. The result is a decline in spawning biomass of the West Coast Vancouver Island herring stock because fewer young herring survive to join the spawning stock. Conversely, survival and growth are relatively strong when the summer biomass of hake is low and the annual water temperature is cool, in the range of 10°C.

Natural predators, rather than the fishery catch, account for most herring mortality. The eight most abundant predatory fish harvested off the West Coast Vancouver Island devour an estimated combined average of 45,000 tonnes of herring each year. This is six times greater than the average annual herring fisheries harvest of this stock (Figure 9.6).

** Adapted from State of the Environment Reporting Programme, Environmental Indicator Bulletin: Sustaining Marine Resources - Pacific Herring Fish Stocks, SOE Bulletin No. 94-5, Environment Canada, Ottawa, Ontario. September 1994, pp. 6.*

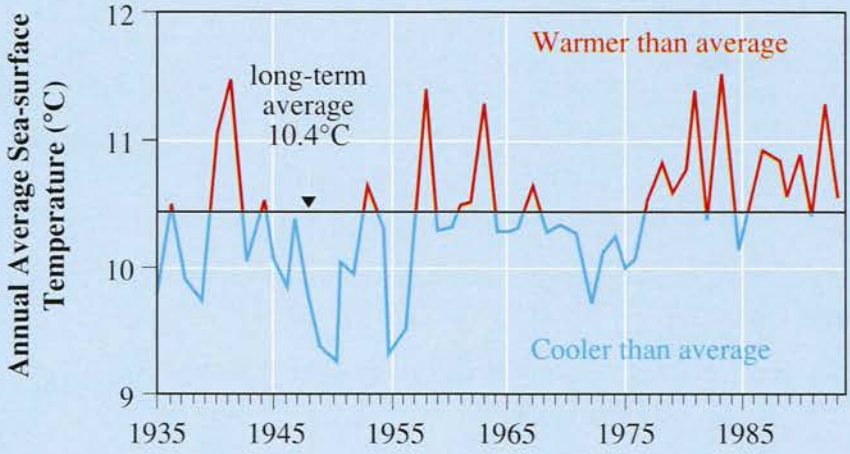

Figure 9.5 – Sea surface temperature off the west coast of Vancouver Island, 1935-1993 (from Canada Department of Fisheries and Oceans, Sidney, B.C.).

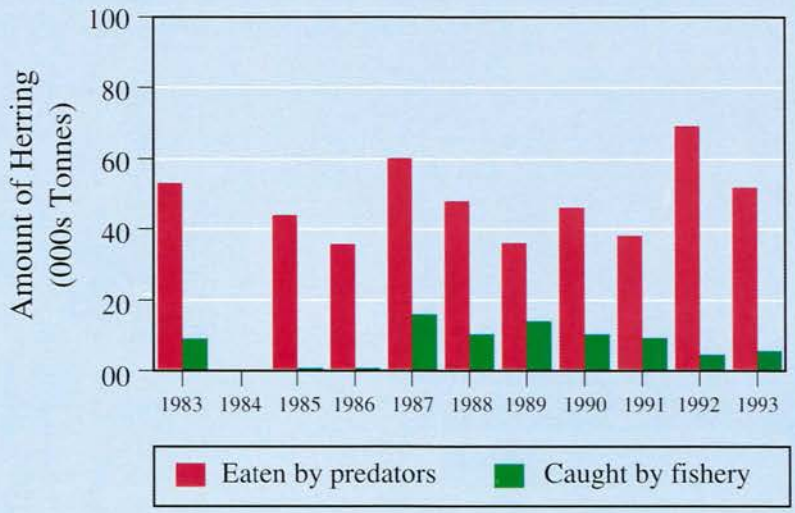

Note: Commercial fishery closed 1985-1986, and other catch < 1,000 t. No data for 1984.

Figure 9.6 – Predation and fishery harvest of West Coast Vancouver Island herring stock, 1983-1993 (from Canada Department of Fisheries and Oceans, Nanaimo, B.C.).

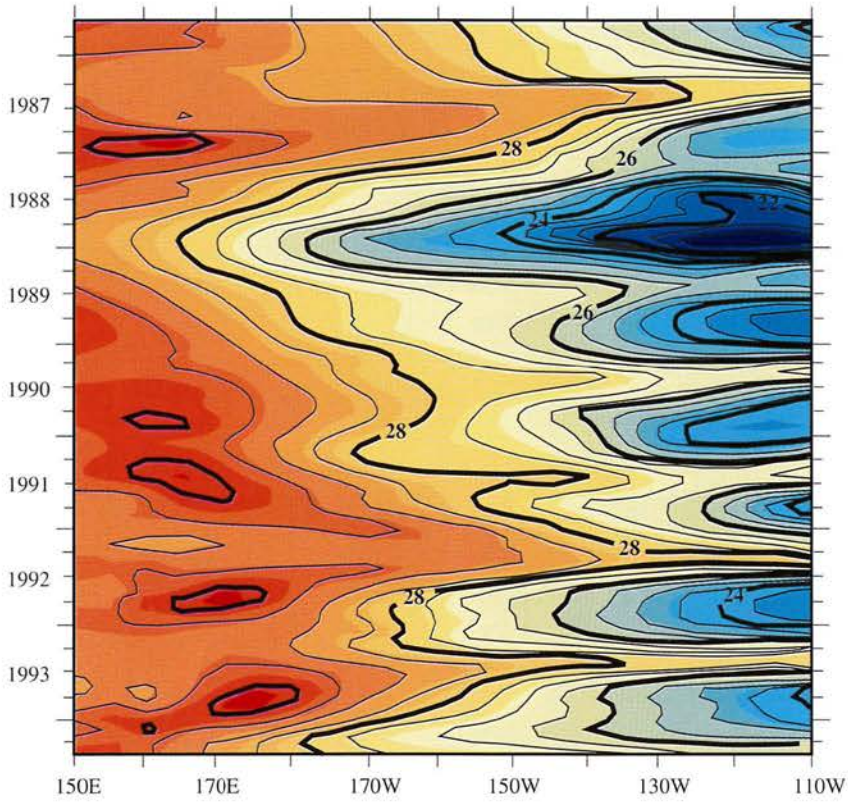

▲ *Figure 10.1* – Monthly mean SST (°C) averaged between 2°N and 2°S as a function of time and longitude based on TAO buoy data. Contour interval is 0.5°C (from Pacific Marine Environmental Laboratory, National Oceanic and Atmospheric Administration, Seattle, WA).

With their large heat capacity and mobility, oceans are the world's great heat reservoirs and heat exchangers and the source of much of the moisture that falls as rain and snow. Sea-surface temperatures (SST) and their associated heat and moisture fluxes generate atmospheric convection and winds and affect weather events such as storms and hurricanes. Oceans are also a source of and a sink for carbon dioxide, containing 50 times as much carbon as does the atmosphere. The vastness of the oceans alone, covering almost three quarters of the Earth's surface, ensures them a vital role in the dynamics of the atmosphere.

In order to understand and model quantitatively the global circulation of the ocean and to make the best long-range predictions of weather and climate on time-scales of up to decades, we need a full description of the state of the ocean and its variability.

In recent years, several operational ocean monitoring and data management systems have been established by many scientific organizations around the world. This chapter features a selection of analyses of key oceanographic variables during the review period.

Figure 10.2 – Monthly mean SST anomalies averaged between 2°N and 2°S as a function of time and longitude based on TAO buoy data. Contour interval is 0.5°C (from Pacific Marine Environmental Laboratory, National Oceanic and Atmospheric Administration, Seattle, WA).

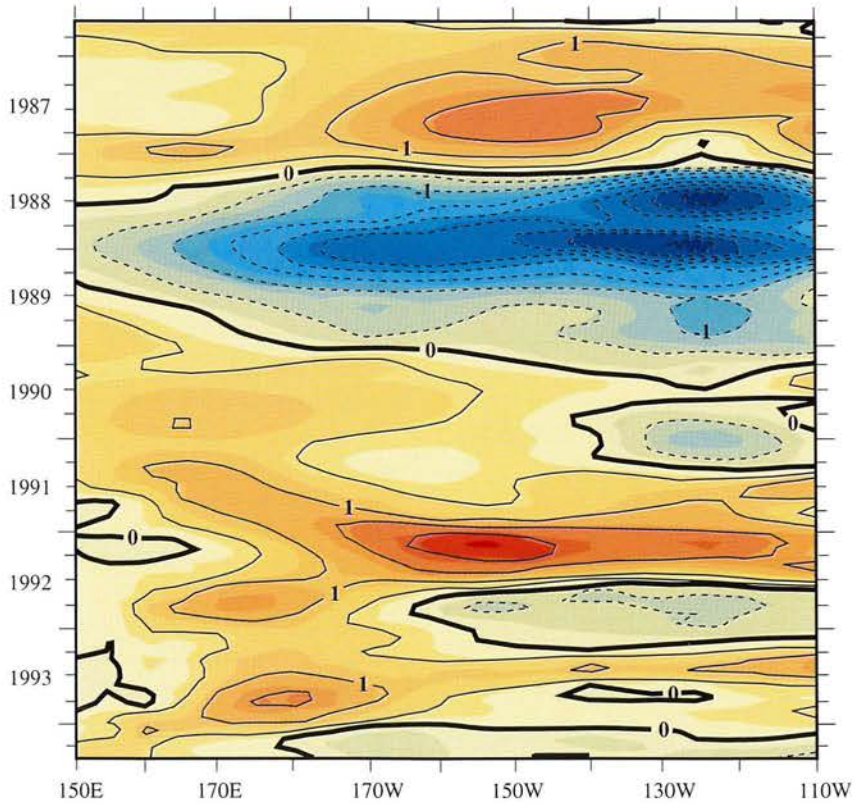

10.1 OCEANOGRAPHIC VARIABLES DURING THE 1991-93 ENSO

The TOGA-TAO array (see box on p. 96) provides an unprecedented *in situ* data network for routine monitoring of tropical Pacific surface wind, sea-surface temperature, thermocline depth and upper ocean current variations. The data are of sufficient accuracy and resolution to allow, for the first time, the preparation of operational analyses that describe important processes and the basin-scale thermal and dynamic structure of the upper ocean.

The tropical oceans can be divided into an upper mixed layer, in which temperatures are similar to those at the surface, and a deep colder layer below. The temperature decreases rapidly with depth in the transition zone that separates the two layers. This thin layer, in which the vertical temperature gradient is a maximum,

is called the thermocline. The 20°C isotherm is found within the thermocline and is used as an index of its depth. A deep thermocline is associated with high SSTs and a shallow thermocline with low SSTs.

Throughout much of 1990 and early 1991, conditions in the equatorial Pacific pointed to a weak ENSO. A ENSO really began to take shape in September 1991 with a sharp rise in SST associated with a westerly wind burst of several weeks duration west of the dateline. Figures 10.1 to 10.6 illustrate the evolution of key oceanographic variables during the 1991 to 1993 ENSO event, as monitored by the TAO buoy array along the equator of the tropical Pacific, and as described by McPhaden (1993).

- By March 1991, 28°C SST values, usually confined to the west of 170°W along the equator, appeared as far east as 110°W (Figure 10.1). Conversely, under the influence of intense local westerly wind forcing, SSTs decreased to near-normal temperatures in the western Pacific (Figure 10.2).
- Early in 1992, the eastward expansion of the western Pacific warm pool was associated with a reversal of the westward-flowing South Equatorial Current across the basin (Figure 10.3). At 165°E, the maximum eastward flow in the surface layer was over 100 cm s^{-1} in January 1992. Current fluctuations on monthly time-scales at 140°W led those at 110°W by about 2 to 3 weeks.
- Figure 10.4 shows the changes in the depth thermocline, as tracked by the 20°C isotherm, across the equatorial Pacific from June 1991 through 1993. The departures from the mean depth clearly show the interannual changes associated with the ENSO cycle, e.g. flattening of the thermocline during the warm episode. In August 1991, the 20°C isotherm was 100 m deeper at 165°E than at 110°W. By February 1992, the 20°C isotherm was only about 35 m deeper at 165°E than at 110°W; moreover, the slope of the 20°C isotherm had reversed between 140 and 170°W. By May 1992, the thermocline was anomalously shallow throughout much of the equatorial Pacific, so that temperature anomalies near 100 m depths were negative from the western Pacific eastward to near 110°W (Figure 10.5). The thermocline again deepened in the central and eastern equatorial Pacific between October and December 1992, as subsurface temperature anomalies increased.
- These thermocline fluctuations are also reflected in the analyzed upper ocean heat storage anomalies (Figure 10.6).
- Tide gauge records (Figure 10.7) have long been used as an index of changes in thermocline depth. The association between a deeper (shallower) thermocline and lower (higher) sea level can be clearly identified in the record since June 1991. From late 1991 to early 1992,

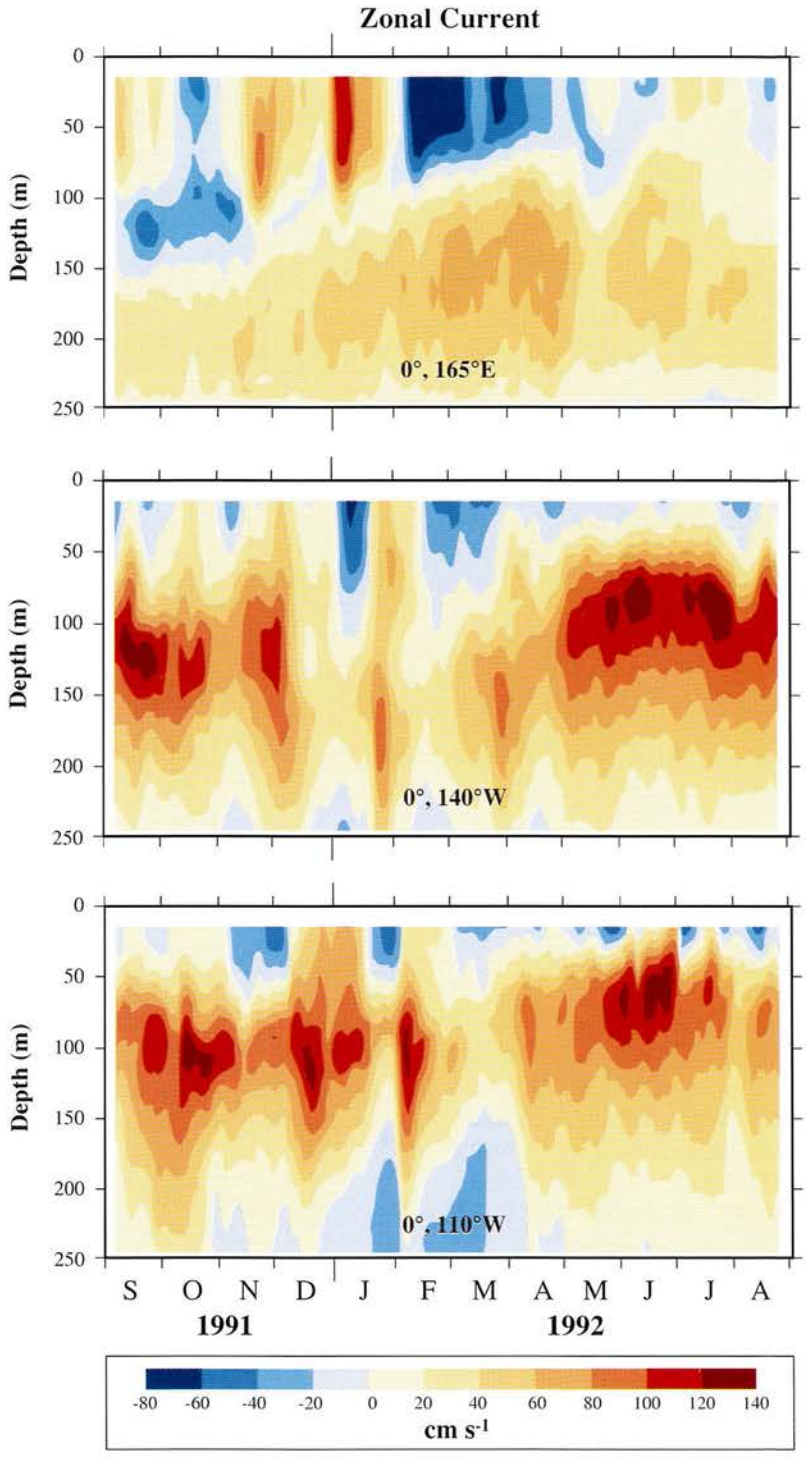

▲ *Figure 10.3* – Contour plots of zonal velocity (cm s-1) in the top 250 m on the equator at 165°E, 140°W and 110°W for September 1991 to August 1992. Westward (negative) flow is shaded blue; eastward (positive) flow is shaded yellow to red (from Pacific Marine Environmental Laboratory, National Oceanic and Atmospheric Administration, Seattle, WA).

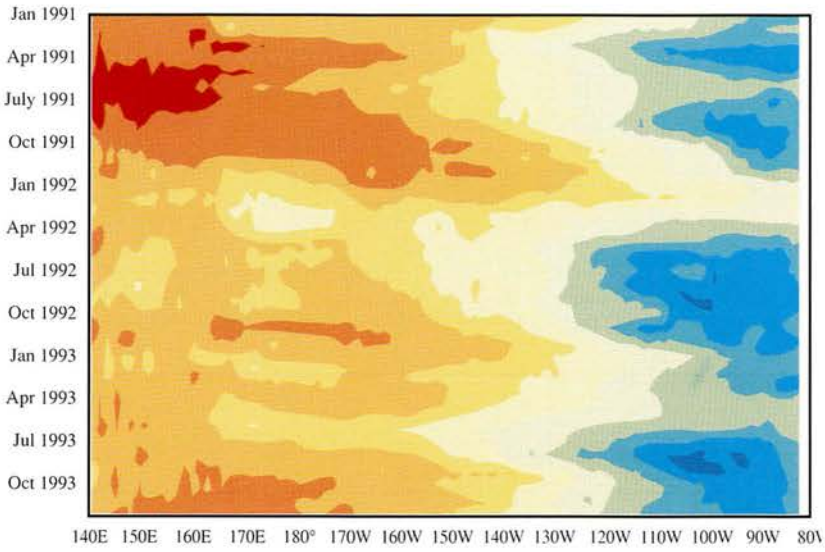

Figure 10.4 – Depth (metres) of the 20°C isotherm across the equatorial Pacific (from NOAA/NWS/NMC/CAC, Washington, DC).

when the thermocline was relatively shallow in the western equatorial Pacific, and deeper than normal in the eastern Pacific, the tide gauge stations showed the opposite changes in sea level. Also evident in both records is the well-known eastward progression of anomalies associated with the major features of the ENSO cycle.

10.2

WARMER THAN NORMAL SEA-SURFACE TEMPERATURES IN THE NORTH ATLANTIC AND PACIFIC OCEANS

Time series of sea-surface temperatures, based on an analysis of data in a 5° x 5° grid, confirms significant positive monthly anomalies for northern regions of both the Atlantic and Pacific oceans during the review period (Figure 10.8). North Atlantic temperature departures were positive but less than they had been during most of the past six years.

Time-latitude analyses (not shown) reveal negative anomalies

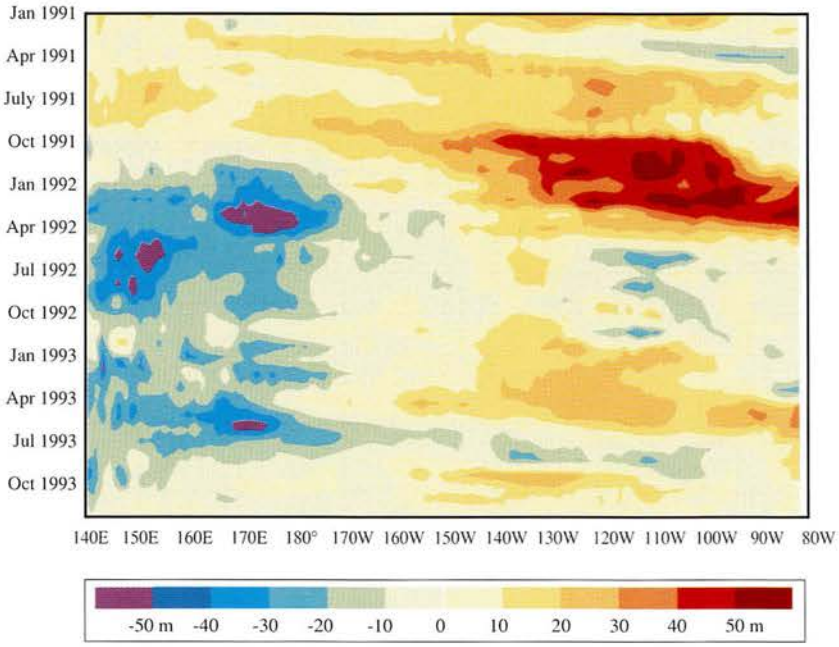

Figure 10.5 – Anomalies in the depth of the 20°C isotherm. The broad scale changes in the thermocline associated with the ENSO cycle that are discussed in Chapter 2 are evident in the multi-month time-scale pattern of anomalies. The figure also shows the signature of eastward propagating Kelvin waves that are excited by synoptic and intra-seasonal variations in surface winds. They result in eastward propagating changes in the depth of the thermocline (from NOAA/NWS/NMC/CAC, Washington, DC).

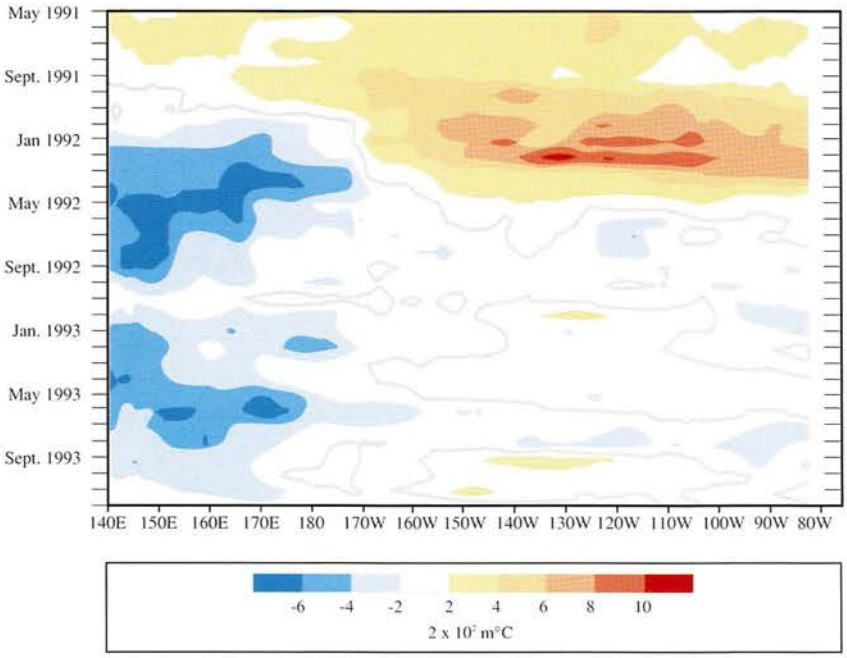

Figure 10.6 – Anomalies of heat storage (integrated temperature) along the equator in the upper 408 m of the Pacific Ocean. The contour interval is 2x102 m°C, with red (blue) shading for anomalies greater than 2x102 m°C (less than -2x102 m°C). Anomalies are computed with respect to the 1983-1992 base period (from NOAA/NWS/NMC/CAC, Washington, DC).

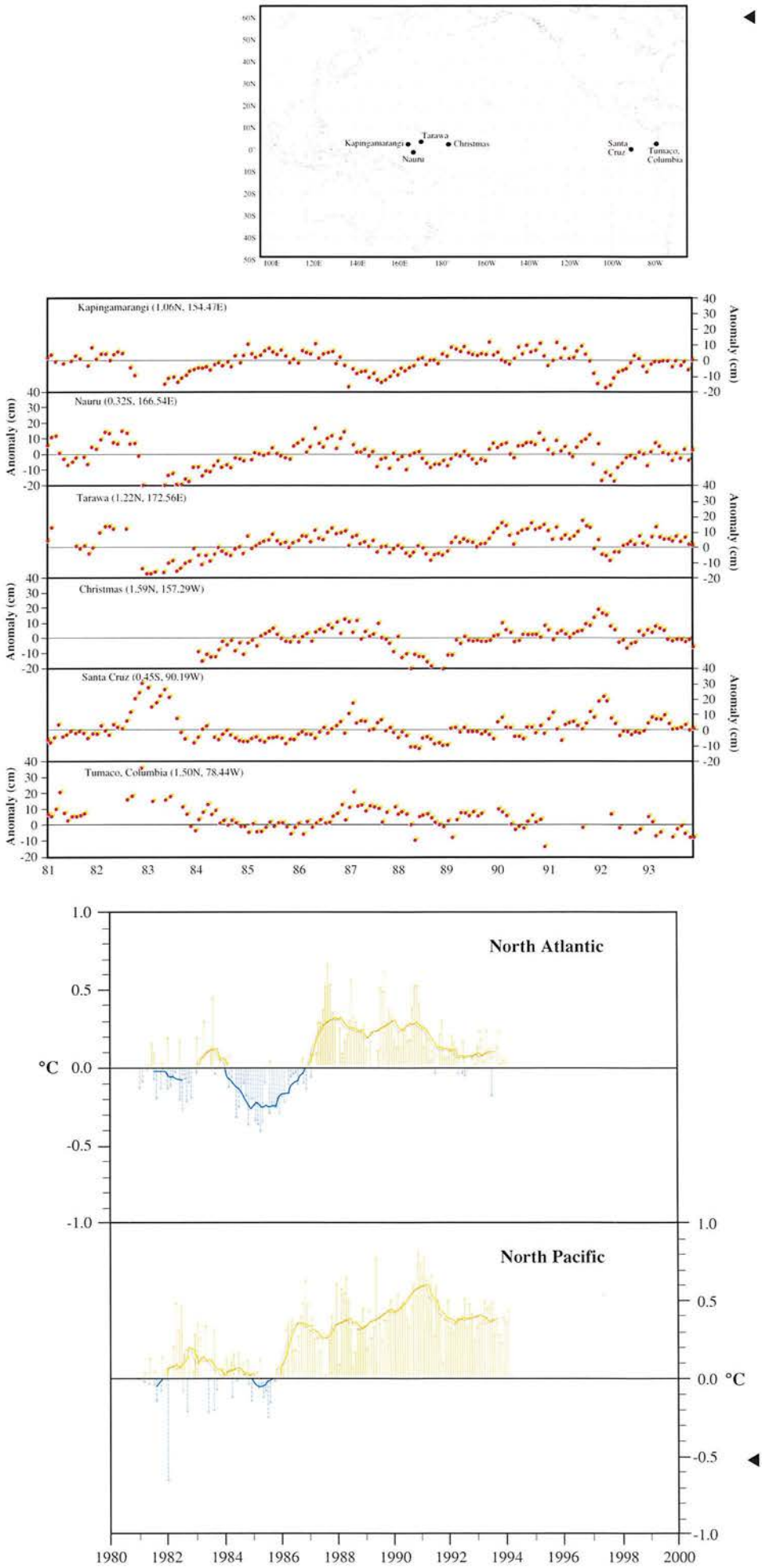

Figure 10.7 – Sea-level anomalies (1991 to 1993) at several tide gauges across the low-latitude Pacific (from Specialized Oceanographic Center (SOC) for Mean Sea Level in the Pacific, Department of Oceanography, University of Hawaii at Manoa).

over the high latitudes of the North Atlantic and positive anomalies in middle latitudes from 1991 to 1993, especially in fall/winter 1992-93. Positive sea-surface temperature anomalies prevailed over the Pacific during the review period, although from April 1993 on colder-than-normal temperatures were observed in the middle latitudes of the basin.

10.3 BALTIC INFLOW IN JANUARY 1993

In January 1993, strong westerly gales, following southerly and southeasterly winds, led to an intensive inflow that interrupted the 16-year stagnation of the central Baltic deep water. The high frequency of strong westerly winds had a positive effect on the ecology of the Baltic Sea. An intensive inflow of highly oxygenated water occurred that interrupted the most significant and serious stagnation period ever observed over the Baltic Sea.

The most important changes in the water exchange between the North Sea and the Baltic take place through the narrow and shallow Danish Straits. Inflow processes to the Baltic Sea, culminating in strong inflows of highly saline and oxygenated water, are rare events. Since the mid-seventies, the frequency and intensity of major inflows have changed. Only a few events have occurred since then and no major inflows have occurred between February 1983 and the end of 1992 (Figure 10.9).

As to the causes, both meteorological and oceanographic

Figure 10.8 – Monthly and 12-month running means of sea-surface temperature anomalies for the North Atlantic and North Pacific Oceans; based on the reference period 1957 to 1986 (from Institute for Global Climate and Ecology, Moscow).

factors are responsible for the occurrence of major inflow events. Strong westerly winds cause both: the destruction of haline stratification as upper layers mix with saline-rich deeper layers in the southern Kattegat and Belt area; and substantial sea-level differences between the Kattegat and the Baltic. The latter is strongly correlated with zonal winds. A minimum duration of westerly winds and positive sea-level differences are necessary prerequisites for major inflows.

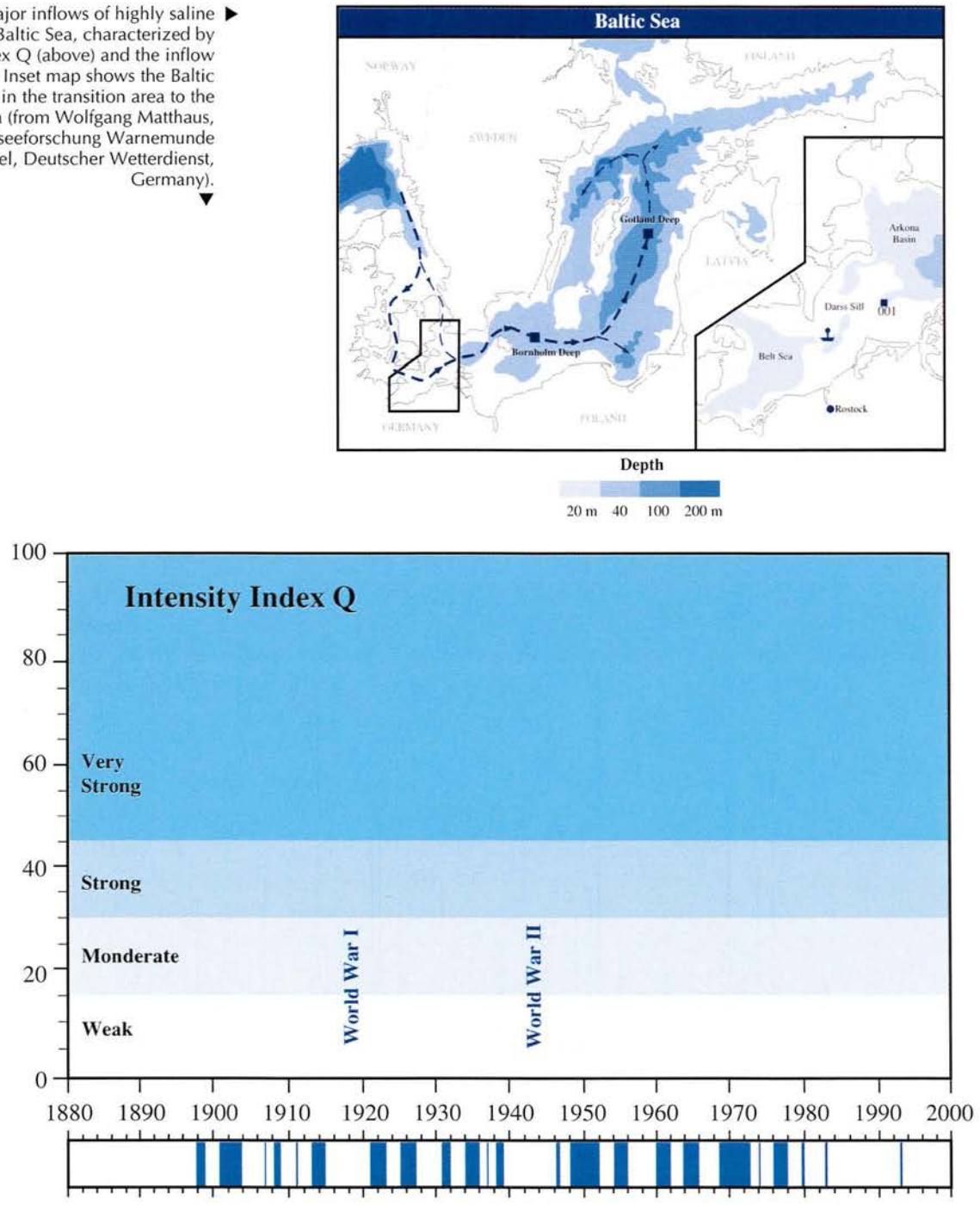

Figure 10.9 – Major inflows of highly saline water into the Baltic Sea, characterized by an intensity index Q (above) and the inflow groups (below). Inset map shows the Baltic Sea and the sills in the transition area to the North Sea (from Wolfgang Matthaus, Institut für Ostseeforschung Warnemunde and Reiner Tiesel, Deutscher Wetterdienst, Germany).

TOGA TROPICAL ATMOSPHERE OCEAN (TAO)*

A major effort of international ocean observing programmes is directed towards obtaining fields of variability in order that significant climate parameters can be compared with each other and with model simulations and so that the evolution of the fields can be monitored in a coherent fashion. An example of such an ocean observing system is the TOGA Tropical Atmosphere Ocean (TAO) Array in the tropical Pacific. TOGA-TAO proposes to maintain an array of approximately 70 wind and thermistor chain moorings and current meter moorings that span the basin from 95°W in the eastern Pacific to 135°E in the west (Figure 10.10). TOGA-TAO has a multi-national base of support, that presently involves cooperation among a number of countries including the USA, France, Japan and the Republic of Korea.

Plans for TOGA in the early 1980s called for the development of a "thin monitoring" array of *in situ* measurements based on an enhancement of existing capabilities. Prototype Autonomous Temperature Line Acquisition System (ATLAS) moorings providing measurements of air temperature, SST and subsurface temperature to 500 m were first deployed in 1984. All data were transmitted to shore in real-time, utilizing NOAA's polar orbiting weather satellites for data relay. These initial deployments were followed in 1985 by the installation of regional scale meridional arrays that spanned the equator along 110°W and along 165°E. Recognition of the importance of the surface wind field in driving the tropical ocean circulation led to the addition of real-time wind measurements to ATLAS moorings in 1986. Three years later, relative humidity sensors were added to studies of atmospheric boundary layer dynamics and air-sea exchange processes. The early technical successes of the ATLAS mooring programme and the recognized value of the data for short-term climate studies led to multi-national plans for a basin-scale expansion of the array during the second half of TOGA (1990 to 1994).

TOGA-TAO, as it is now constituted, also includes a small number of Profile Telemetry of Upper Ocean Currents (PROTEUS) and conventional current-meter moorings along the equator. Sensors have been added to several moorings in the western Pacific to measure salinity, rainfall and incoming shortwave radiation for specialized research purposes.

TAO data are widely available to the research community. A subset of the real-time TAO data stream is retransmitted on the Global Telecommunication System (GTS), so that the meteorological measurements are available for assimilation into atmospheric numerical weather prediction models at, for example, the European Centre for Medium Range Weather Forecasts (ECMWF), the Fleet Numerical Oceanography Center (FNOC) and the USA National Meteorological Center (NMC). Real-time TAO SST measurements are included in weekly blended analyses of *in situ* and satellite data at NMC, subsurface thermal data are assimilated directly into NMC operational ocean model and wind data are incorporated into the Florida State University (FSU) monthly ship wind analyses. Data from the TAO Array have also been used to validate satellite-derived estimates of SST, wind speed, sea level, surface geostrophic currents, rainfall and most recently estimates of surface wind velocity from the ERS-1 scatterometer.

An interactive system has been developed for displaying the real-time data from these buoys in a modern workstation environment. The real-time TAO display software, data sets, animations and other graphics products are provided to remote users on the Internet network and are available to oceanographic and meteorological institutions, nationally and internationally. Research scientists have easy access to the data sets from the TOGA-TAO array and convenient procedures for display, comparison and analysis.

The TAO Display Software provides easy access to the most recent twelve months of real-time data from the ATLAS and Current Meter buoys in the array. This prototype allows a quick assessment of the current state of the tropical Pacific. Other data are animations available from the TAO buoys, the NMC Operational Analyses model, climatological averages and selected related data sets.

** Adapted largely from McPhaden, 1993 and Soreide et al., 1994 and from material available from NOAA's Pacific Marine Environmental Laboratory, Seattle, WA.*

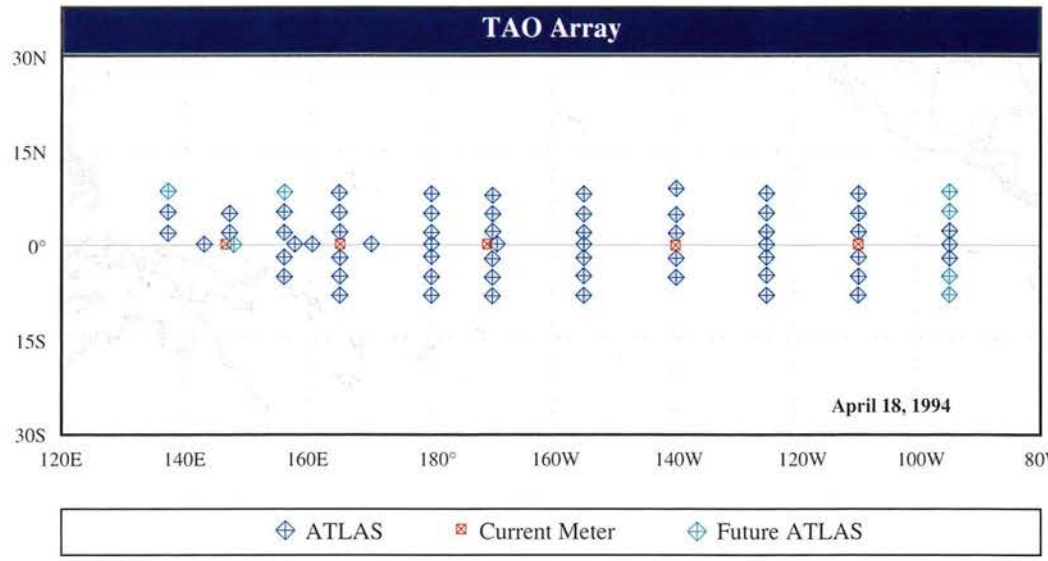

Figure 10.10 – The TOGA-TAO Array in April 1994 and its final configuration December 1994 (from Pacific Marine Environmental Laboratory, National Oceanic and Atmospheric Administration, Seattle, WA).

10.4

OBSERVED CHANGES IN DEEP OCEAN TEMPERATURES

The oceans, with a mean depth of in excess of 3,000 m, and with 3 m of water having the same thermal capacity as the atmosphere, have by far the largest heat capacity in the climate system. As a result, absorption of heat by the ocean could substantially delay increases in surface warming resulting from changing greenhouse gas concentrations.
Coupled ocean-atmosphere models of transient climate change (e.g. Stouffer et al., 1989) indicate significant delays in surface warming over the Southern Ocean and the North Atlantic Ocean, as a result of the oceans uptake of heat. This uptake of heat and the resultant thermal expansion is one of the main contributions to global sea level rise (Church et al., 1991; Wigley and Raper, 1987).

The ocean has a much sparser data base from which to examine climate variations than is available for the atmosphere. However, over the last few years, there has been greater activity focused on measuring decadal-scale changes in ocean properties, primarily using new data sets becoming available from the World Ocean Circulation Experiment.

Repeated oceanographic observations such as those reported here will play an important role in understanding the nature and cause of climate change and in testing coupled ocean-atmosphere models of climate change.

The North Atlantic

The most conclusive evidence for changes in ocean climate comes from repeated occupations of North Atlantic trans-ocean sections. A section at 24°N has now been occupied three times during the International Geophysical Year in 1957, during 1981 and most recently in 1992. Roemmich and Wunsch (1984) showed that over the 24-year period between 1957 and 1981 there was a basin-wide warming between 800 m and 2500 m with a maximum temperature difference of about 0.15°C (Figure 10.11). The most recent results (Parilla et al., 1994) show a similar warming over the

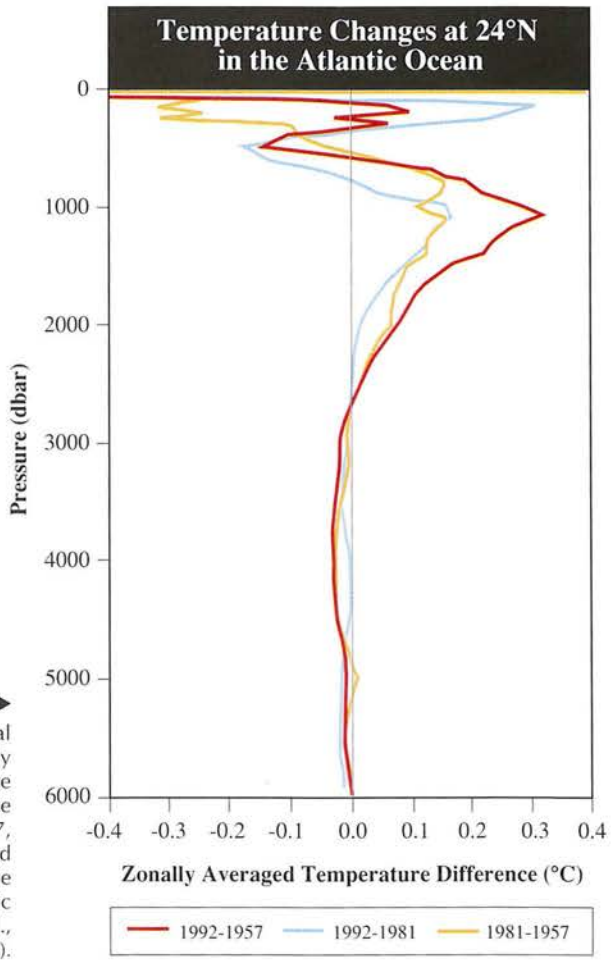

Figure 10.11 – Vertical profiles of the zonally averaged temperature difference (°C) over the time periods 1981-1957, 1992-1981 and 1992-1957 at 24°N in the subtropical North Atlantic Ocean (Parilla et al., 1994).

Figure 10.12 – Changes in decadal-scale ocean temperature (°C) across 24°N in the subtropical North Atlantic between cruises in 1957 and 1992. The data show considerable warming across the midwater (500-3000 m) layer and cooling within the surface layers and below 3000 m (Parilla et al., 1994).

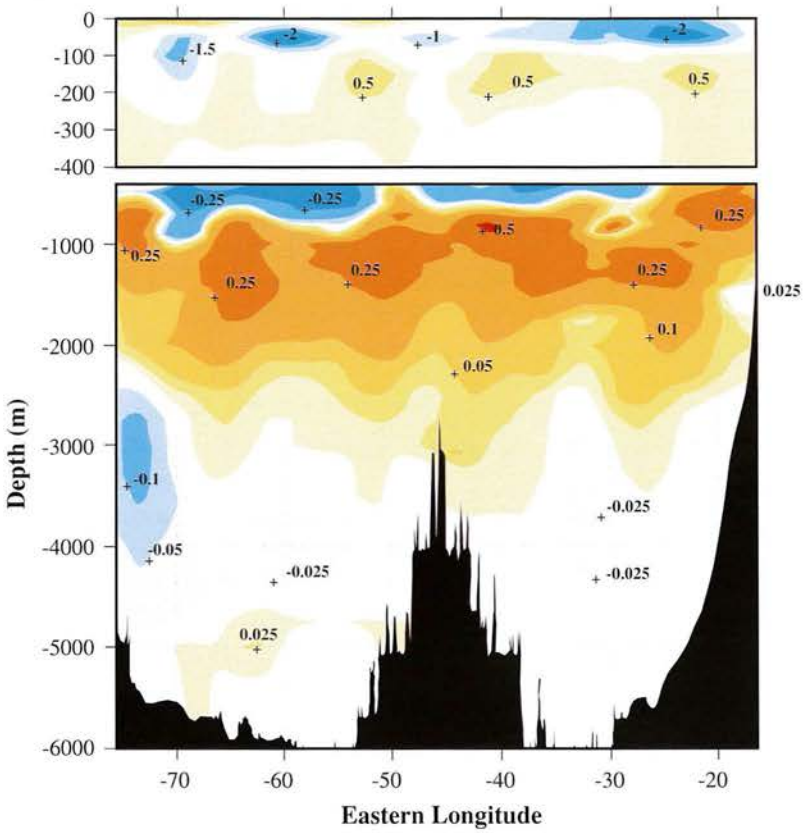

11–year period between 1981 and 1992 (Figure 10.11). Over the 35-year period between 1957 and 1992, the warming is remarkably uniform right across the zonal extent of the Atlantic Ocean (Figure 10.12). The maximum basin-wide warming of just over 0.3°C, equivalent to 1°C per century, occurs at a depth of 1100 m (Figure 10.11). This warming is equivalent to a sequestering of heat at an average rate of 1 W m-2 and is equivalent to a local sea level rise from thermal expansion of about 3 cm. The only area where there is a coherent cooling is in the region of the deep western boundary current (75°W at 3000 m depth). In the surface layer, unresolved seasonal variations dominate. Analysis of salinity variations along the 24°N section is currently underway.

Recent analysis of the long (since 1954) time-series hydrographic station near Bermuda (32°N, 65°W) indicates a low-frequency (decadal) variability of amplitude of about 0.5°C in the upper 500 m falling to about 0.05°C in the 1500 to 2500 m depth range. Consistent with the 24°N results, these variations are superimposed on a longer term warming trend (0.5°C per century) in the 1500 to 2500 m depth range (Joyce, unpublished manuscript).

An interesting feature of this analysis is that the observed warming is occurring in the ocean interior in contrast the surface intensified warming in the current generation of climate models (Manabe et al., 1992).

The only high latitude region where there are enough data available to examine variations in subsurface conditions is the North Atlantic. Recently, Read and Gould (1992) have reported that waters between Greenland and the UK were on average 0.08°C and 0.15°C colder in 1991 than in 1962 and 1981 respectively. The cause appeared to be renewed formation of intermediate water in the Labrador Sea from cooler and fresher source waters. Dickson et al. (1988) documented the advection of cold fresh water, the "Great Salinity Anomaly", around the North Atlantic subpolar gyre from its origins north of Iceland in the mid-to-late 1960s until its return to the Greenland Sea in the early 1980s. Model simulations show that changes in subpolar Atlantic salinities exert a profound influence of winter convection and can trigger glacial/interglacial transitions. Ice core data (e.g. GRIP Project Members, 1993) and climate model results (Mikolajewicz and Maier-Reimer, 1990; Weaver and Hughes, 1994; and others) indicate that the subpolar Atlantic is subject to rapid climate variations.

The Pacific Ocean

The first evidence of similar variations in the southern hemisphere to those reported in the North Atlantic come from repeat sections occupied in 1967 and 1989/1990 at 43°S and 28°S in the western South Pacific (Bindoff and Church, 1992). At 43°S, the maximum warming occurs at depths of 500 m and 3000 m, with a depth averaged warming of 0.04°C (Figure 10.13). At 28°S, the warming is relatively uniform throughout the water column, with a depth averaged increase of 0.03°C. As in the North Atlantic, a heat flux approaching 1 Wm-2 is required for these depth averaged warmings and they are equivalent to a local sea level rise from thermal expansion of 2-3 cm. Perhaps of more significance was the decrease in salinity at constant density (and temperature, Figure 10.13) in the 200 to 700 m depth range. Although model results suggest that climate change should be largest in the main thermocline, observation of this warming will in general be masked by eddy and seasonal variability. However, Bindoff and Church (1992) argue that climate change and variability may be more easily detected from changes in water mass properties on density surfaces. Bindoff and McDougall (1994) used an inverse technique to infer that the changes observed between 300 and 700 m at 43°S were a result of warming at the surface where the water masses were formed during contact with the atmosphere. Similar analysis currently underway (Bindoff, personal communication,

1994) for the upper 2000 m of the high southern latitude Indian Ocean is finding similar results to those found for the 43°S section in the Tasman Sea.

In the North Pacific off California, hydrographic time-series of the upper 500 m over the past 42 years indicate that temperatures have increased uniformly in the upper 100 m by 0.8°C and that temperatures have risen significantly to depths of about 300 m. This is equivalent to a local sea level rise of 0.9 ±0.2 mm/year compared to the coastal sea level rises in the region of between 1 and 3 mm/year. Further north at Ocean Station PAPA (50°N, 145°W), Thomson and Tabata (1989) used a thirty-year time series of hydrographic data to estimate the secular trend in surface steric height relative to 1000 m. They find a rate of rise of 1.1 mm/year.

Approximately 67% of the increase in steric level is due to thermal expansion between 100 m and 1000 m and the remaining 33% is due to the halosteric component confined to the upper 100 m.

THE WORLD OCEAN CIRCULATION EXPERIMENT

The main goal of the World Ocean Circulation Experiment (WOCE) is to develop reliable ocean models that are essential for modelling and predicting climate variability and change, particularly the regional impacts of climate change, and to collect the data necessary to test these models.

The WOCE observational programme (1990-1997) has brought about a dramatic change in the number of oceanographic data sets available for climate research. For the first time, researchers have a quasi-synoptic *in situ* global data set available. As well as the traditional data sets from hydrographic programmes measuring ocean temperatures, salinities and nutrients and moored current observations, WOCE data include many new types of global observations: global tracer data sets for CFCs, tritium/helium, 14C; global near surface velocities from current-following drifters; global velocities at depths of about 1000 m from deep floats and repeat observations from a near global set of XBT lines. In addition, process studies will provide improved model parameterizations of interior mixing and the process of subduction.

WOCE has insisted on the highest quality of data to ensure that it they can be used effectively for the developing, testing and improving of the global ocean models needed for reliably modelling the climate system and climate change. The transient tracer data set is one of the valuable new tools that is already being used for assessing the accuracy of models and particularly for assessing the ability of the oceans to absorb heat as atmospheric concentrations of greenhouse gases increase.

These *in situ* data sets will be complemented by satellite data of unprecedented accuracy and utility. The TOPEX/POSEIDON satellite (launched August 1992) data set has resulted in a considerable improvement in ocean tide models and allowed, for the first time, observations of global ocean variability on time scales as short as 10 days. This data stream is complemented by the non-WOCE satellites ERS1 and 2 with their wind scatterometers and altimeter systems.

After the end of the observational programme, WOCE will have an energetic analysis and synthesis phase. Activities that will be undertaken include compilation of global data sets in a form useful for global synthesis and modelling, production of gridded data sets and atlases of properties, estimates of water mass inventories and renewal rates and new estimates of ocean variability at both the mesoscale and for the first time the global scale. Combination of the several different types of data sets will allow the ocean heat and freshwater and other property fluxes and their exchange with the atmosphere to be estimated with unprecedented accuracy.

WOCE results will provide a baseline view of the world ocean against which future (and past) change may be assessed. Comparison of the WOCE data set with the historical archive is already providing new information on the rates of change in the ocean (see Section 10.4).

All of the above activities are analyses which can be confidently performed. Many of the analysis tools for these products are already available. The ultimate success of WOCE will be achieved when all the WOCE data sets are combined with the best numerical models to give a more reliable description of the ocean circulation. This is currently an area of very active research - the possibility of this type of combination of global quasi synoptic data with high resolution global models has never before been possible. This theoretical development will not end with the end of WOCE, but must continue, presumably under the banner of new international programmes such as the Climate Variability and Prediction Research Programme (CLIVAR), if reliable predictions of future climate are to be realized.

** Adapted from a contribution submitted by John Church, Climate Programme, CSIRO Division of Oceanography, Canberra, Australia.*

GLOBAL SEA-LEVEL OBSERVING SYSTEM: THE BEGINNINGS OF AN OPERATIONAL ACTIVITY OF GOOS *

The Global Sea-Level Observing System is an international system initiated in 1985 and coordinated by IOC, to provide high-quality standardized sea-level data from a global network of over 300 sea-level stations. The measuring system is known as GLOSS because it provides data for deriving the Global Level of the Sea Surface by averaging out waves, tides and short-period meteorological events. The GLOSS network has been designed to observe large-scale sea-level variations of global implications.

This network monitors sea-level changes that should be indicative of global warming, ocean circulation patterns and climate variability. It contributes data to international research programmes such as TOGA and WOCE. It also provides high quality data for practical applications of national importance. The measurements of the GLOSS gauges are complemented by satellite altimetry measurements.

The following elements define GLOSS (IOC Technical Series No. 35, 1990):

- A global network of permanent sea-level stations to obtain standardized sea-level observations; this forms the primary network to which regional and national sea-level networks can be related;

The GLOSS network consists of 308 sea-level stations operated and maintained by 87 countries. As of October 1993, 210 stations were considered operational and provided data to PSMSL and specialized sea-level centres established within IGOSS, TOGA and WOCE.

- Data collection for international exchange with unified formats and standard procedures including both near real-time as well as delay-mode data collection;

The Permanent Service for Mean Sea-Level (PSMSL) at the Proudman Oceanographic Laboratory in the UK collects and archives data from all GLOSS stations in the form of monthly mean values and acts as a Global GLOSS data centre. It is expected that hourly and daily values will be made available from all stations by the originators. Sea-level data from selected GLOSS stations are also submitted in near-real time to four specialized sea-level centres.

- Data analysis and product preparation for scientific and/or practical applications;

At present PSMSL regularly provides information on PSMSL data holdings as well as available sea-level data to all interested scientists and institutions upon request. The PSMSL also provides information on sea level trends and statistics.

- Assistance and training for establishing and maintaining sea-level stations as part of GLOSS while improving national sea-level networks;
- A selected set of GLOSS tide-gauge bench marks will be connected to a global geodetic reference system (i.e., the conventional terrestrial frame established by the International Earth Rotation Service).

In order to predict as possible sea-level rise and its effects on human activities, one can monitor mean sea-level variations using a tide gauge whose height is also being monitored, at least periodically, by referencing it to a geocentric coordinate system. Otherwise, it is impossible to remove and be aware of any fictitious sea-level changes appearing in a record of a tide-gauge. Such unreal sea-level variations can be caused by a crustal movement of the region. Recent progress of space geodetic technologies has made it possible to measure an absolute position of a tide gauge accurately.

** Adapted from an article in the GOOS News, March 1994, No. 1, pp. 6-7.*

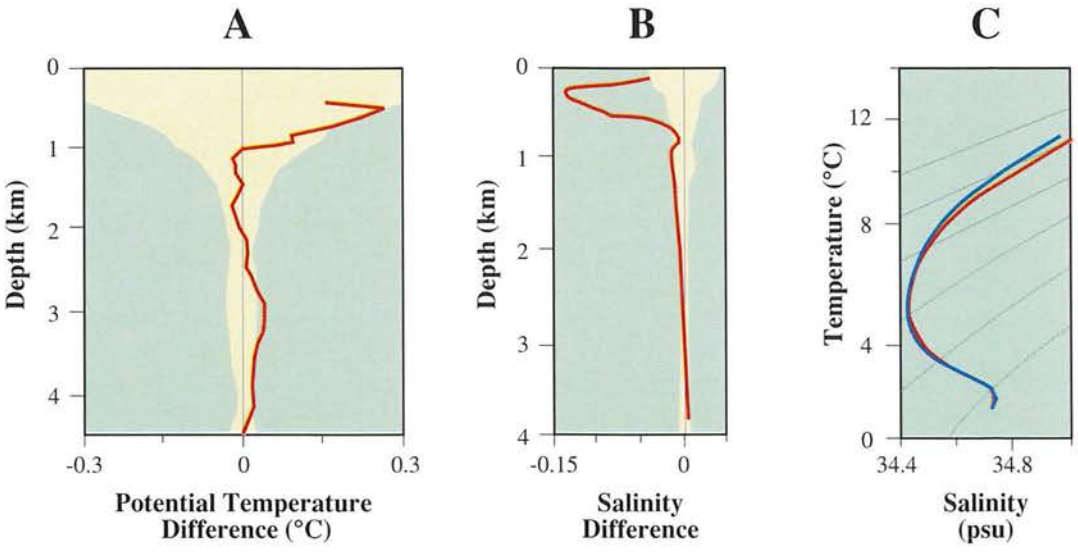

Figure 10.13 – Mean temperature changes and sectional averages of the change in salinity and potential temperature on constant density surfaces (plotted as a function of depth) for the 43°S section in the Tasman Sea. The light shaded region is the 90% confidence interval. In "C", the mean potential temperature-salinity relationship for the 43°S section in 1967 (lower, red line) and 1990 (upper, blue line) is shown; the six curved lines are potential density surfaces (after Bindoff and Church, 1992).

MORE SEVERE OZONE DEPLETION POSSIBLE BEFORE IT STARTS TO SLOW DOWN EARLY NEXT CENTURY

CHAPTER 11

During 1992 and 1993, the Antarctic ozone hole (see accompanying box on page 102) and mid-latitude, winter-spring, northern hemisphere ozone amounts were both measured at record low values. The record low ozone is considered a combined result of: very cold lower stratospheric temperatures (facilitating chemical ozone destruction by human-made halogenated product); of specifics of the atmospheric circulation related to the westerly phase of the equatorial stratospheric quasi biennial oscillation (QBO); and partly of increased concentrations of sulphate aerosols emanating from the eruption of Mount Pinatubo in the Philippines in June 1991.

Another volume in the series of WMO Ozone Assessments was prepared and reviewed during 1994 by teams of over 300 international experts. Readers are referred to the WMO Scientific Assessment of Ozone Depletion: 1994, for a thorough discussion of the scientific issues surrounding stratospheric ozone depletion. Some of the findings, especially those related to ozone trends, are summarized here.

11.1 MID-LATITUDES OF NORTHERN AND SOUTHERN HEMISPHERES

Anomalously low ozone was measured over mid-latitudes of the northern hemisphere during 1992 and 1993 (Bojkov et al., 1993). An example of this is seen in Figure 11.1, which shows ozone monthly anomalies smoothed by 12-month running means for North America and Europe (Bojkov and Fioletov, 1995). Below-normal amounts occurred throughout 1992 with the largest negative anomalies during winter-spring of 1992-93 when the northern hemisphere had the lowest ever recorded ozone values. Over North America, in Europe, from the Atlantic to the Ural Mountains, and over Siberia, in an area extending from middle latitudes to the Arctic Circle, the monthly mean values of total ozone were 10-25% lower than the long-term mean. The decline over middle latitudes in the southern hemisphere was much smaller.

Over the globe during the last 15 years, mid-latitude downward trends during winter-spring have averaged about twice those of summer and autumn. The annual ozone decrease since 1979 has been 4 to 5% per decade at mid-latitudes in both hemispheres which is 1 to 2% greater than the rate calculated since 1970. No statistically significant trends exist over the tropics (20°S-20°N).

11.2 ANTARCTIC OZONE HOLE DEEPENS AND WIDENS

During the austral springs of 1992 and 1993, the Antarctic ozone hole was larger in areal extent and lower in ozone amount than at any previously recorded time. The minimum total ozone of less than 100 Dobson units (DU), early October 1993, was the lowest ever measured anywhere on earth. Ozonesonde vertical profile measurements at the Antarctic stations showed a region totally devoid of ozone from 14 to 19 km for a few consecutive weeks. According to the 1994 Ozone Assessment, chemical perturbations of the well recognized chlorine and bromine reactions on polar stratospheric clouds complemented with reactions on sulphate aerosol are the most likely causes.

As reported in the bi-weekly WMO Antarctic ozone bulletins, the ozone hole in 1993 started to form in early August, the earliest ever recorded. The period of maximum depletion lasted from mid September to the end of October. For one or two days in late September, the ozone hole imbedded in the rotating polar vortex extended over inhabited regions of the extreme south of South America. The long-term average values were depleted by about 40%. At the start of the second half of October 1993, there was still an extended area with total ozone less than 125 DU. The polar vortex with lower-stratospheric temperatures of less than -75°C remained stable. The South Pole station reported values of 86 and 81 DU on October 4 and 5, 1993, respectively, and the Halley Bay station measured 98, 97, 98 and 99 DU on October 15, 16, 17 and 21, respectively. The preliminary monthly mean value for Halley Bay in October 1993 was 114 DU, nearly as low as the record low daily value of 108 DU measured in spring 1992.

The spatial evolution of the Antarctic ozone hole since 1979 as

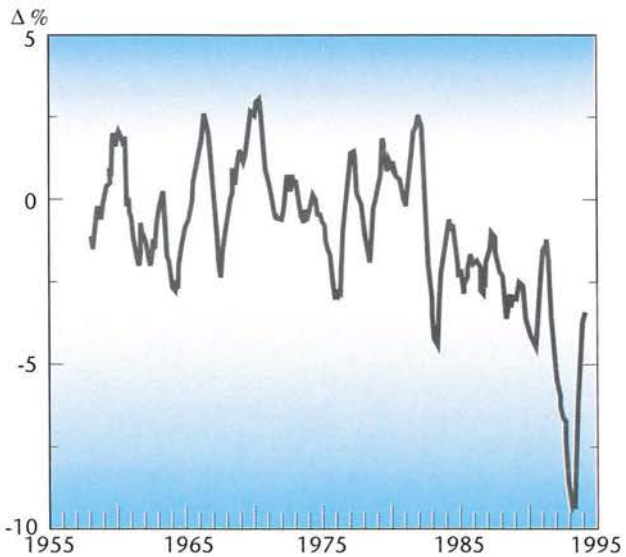

Figure 11.1 – Total ozone deviations (%) from the 1964-1980 average of all North American and European stations smoothed by 12-month running mean indicate ozone decline starting in the 1970's with extreme values in 1992/1993 (source: Bojkov and Fioletov, 1995).

AN OZONE FACT SHEET *

Ozone is a triatomic form of oxygen, which exists mainly in the stratosphere (90% of all ozone is between 12 and 45 km) forming a thin blanket (~0.300 cm at normal pressure) which shields the Earth's surface from the biologically harmful ultraviolet radiation and is an important radiative contributor to the temperature structure of the atmosphere.

CFCs are human-produced unreactive chemicals which, once released, can stay in the atmosphere for 50 to 150 years. When transported upwards in the stratosphere, they are broken up by ultraviolet light to produce active chlorine compounds, able through a series of catalytic reactions to destroy many ozone molecules.

Halons (bromine-containing chemicals used mostly in fire retardants) have a similar but stronger ozone-destroying effect than CFCs in the stratosphere since the bromine is many times (>30) more efficient in destroying the ozone molecules.

WHAT HAS HAPPENED TO THE TOTAL OZONE?

In the Antarctic spring of 1991, rapid ozone destruction to below 200 m DU, dubbed the ozone hole, was first reported. It has now confirmed that 30-40% losses in the total ozone have occurred during October every year since the early 1980s. The ozone recovers only after the circumpolar stratospheric vortex breaks down and extensive air exchange with mid-latitudes is re-established, usually in late November.

NASA aircraft measurements made in the Antarctic spring of 1987 showed high levels of ClO, coinciding with low ozone. Considered together with other surface data, these measurements proved that the Antarctic spring ozone hole was caused by active chlorine and bromine involved in a series of heterogeneous reactions.

Measurements made in the Arctic stratosphere in January and February 1989 showed ClO concentrations as high as in the Antarctic, while in the period December 1991-March 1992, the measured ClO concentrations exceeded three times those over the Antarctic. It was concluded that the air was primed for serious ozone depletion given certain conditions.

In 1988, the WMO/NASA Ozone Trends Panel published (as WMO Ozone Report No. 18) analysed measurements taken from 1957 to 1986 by the Global Ozone Observing System stations and concluded that, in the northern hemisphere, there had been a statistically significant drop of over 5% in ozone levels in the winter-spring season polewards of 40°N between 1969 and 1986. Satellite measurements show similar ozone losses everywhere outside the tropics. The Ozone Assessment 1991 (WMO Ozone Report No. 25) demonstrated that these losses became stronger and significant also during the summer thus extending well into the growing seasons over both hemispheres.

WHEN DID THE ANTARCTIC OZONE HOLE FIRST APPEAR?

The Antarctic ozone hole is a new phenomenon. Figure 11.3 shows that observed ozone over the Antarctic first revealed obvious decreases in the early 1980s compared to data obtained since 1957. The ozone hole is formed each year when there is a sharp decline (currently up to 60%) in the total ozone over most of Antarctica for a period of about two months during southern hemisphere spring (September and October). Observations from three other stations in Antarctica, also covering several decades, reveal similar progressive, recent decreases in springtime ozone. The ozone hole has been shown to result from destruction of stratospheric ozone by gases containing chlorine and bromine, whose sources are mainly human-made halocarbon gases.

Before the stratosphere was affected by human-made chlorine and bromine, the naturally occurring springtime ozone levels over Antarctica were about 30-40% lower than springtime ozone levels over the Arctic. This natural difference between Antarctic and Arctic conditions was first observed in the late 1950s by Dobson. It stems from the exceptionally cold temperatures and different winter wind patterns within the Antarctic stratosphere as compared to the Arctic. This is not all the same phenomenon as the marked downward trend in total zone in recent years referred to as the ozone hole and shown in Figure 11.2.

Changes in stratospheric meteorology cannot explain the ozone hole. Measurements show that wintertime Antarctic stratospheric temperatures of past decades have not changed prior to the development of the hole each September. Ground, aircraft and satellite measurements have provided, in contrast, clear evidence of the importance of the chemistry of chlorine and bromine originating from human-made compounds in depleting Antarctic ozone in recent years.

A single report extremely low Antarctic winter ozone in one location in 1958 by an unproven technique has been shown to be completely inconsistent with the measurements depicted here and with all credible measurements of total zone.

CAUSE OF THE OZONE LOSS IN POLAR LATITUDES

The extremely cold temperatures (-80°C and lower) that occur in the polar stratosphere in winter allow polar stratospheric clouds to form. Chemical reactions taking place on the cloud droplets and other aerosol surfaces convert inactive forms of chlorine to active forms and tie up some nitrogen compounds that normally serve as a buffer. The active chlorine released in a denitrified and dehydrated stratosphere rapidly depletes the ozone in the presence of sunlight.

There are basic differences between both temperature and circulation patterns over the Arctic and Antarctic, which are reflected in different ozone losses. Even though the picture in the Antarctic is relatively clear, many aspects of what happens in the Arctic are less certain, although a further, stronger ozone decline can be expected in northern subpolar latitudes as a result of increased concentrations of chlorine and bromine compounds especially at extremely cold stratospheric temperatures during the winter-spring season.

** Adapted from a contribution by Rumen D. Bojkov, 1992: Changes in Polar Ozone,* WMO Bulletin, *41(2):171-180.*

observed by satellite instrument is shown in Figure 11.2. The mean October data show a progression toward lower values over Antarctica. The mean austral spring (September-October-November) total ozone values for the four long-term observing stations in Antarctica showed a decline of over 40%, while in the summer season (January-February-March) the decline was only 6-7%, (see Figure 11.3).

11.3 REDUCING THE RATE OF INCREASE OF OZONE DAMAGING HALOCARBONS

A major implication of the research findings of the Ozone Assessment is that the application of Montreal Protocol and its amendments and adjustments is clearly reducing the rate of increase of anthropogenic halocarbons which are considered the main reason for the ozone decrease. If all nations comply with the Protocol, around the turn of the century stratospheric chlorine and bromine abundances should peak with associated ozone depletion. At this time, the maximum ozone loss over northern mid-latitudes in winter/spring, for example, is expected to be on the average about 12-13%. The rate of decline of stratospheric chlorine and bromine, however, will be very gradual through the twenty-first century because of the long residence times of CFC species, but eventually the ozone layer is expected to recover after the middle of the next century.

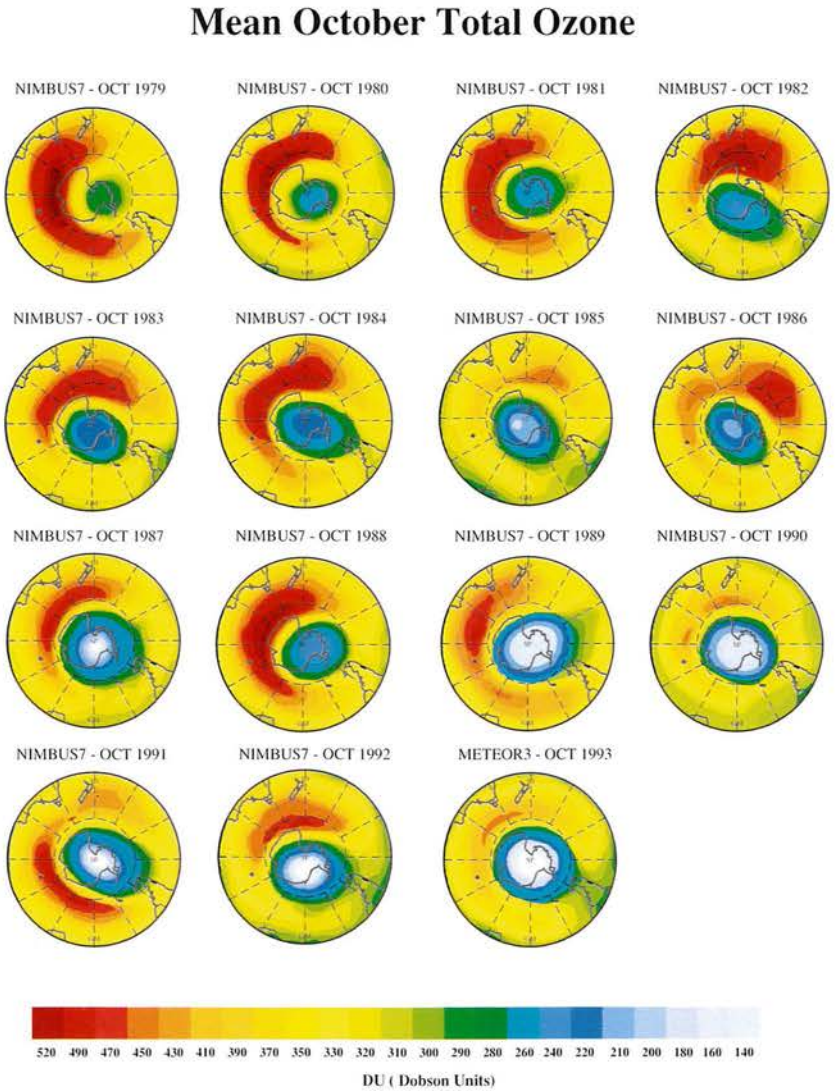

▲ *Figure 11.2* – Monthly mean October total ozone (colour-coded in Dobson units) over the southern hemisphere, 1979 to 1993, from TOMS instruments on NIMBUS 7 and METEOR 7 satellites (from analysis prepared by P. Lehmann, Bureau of Meteorology Ozone Unit, Australia with data obtained by NASA/Goddard Space Flight Center, USA).

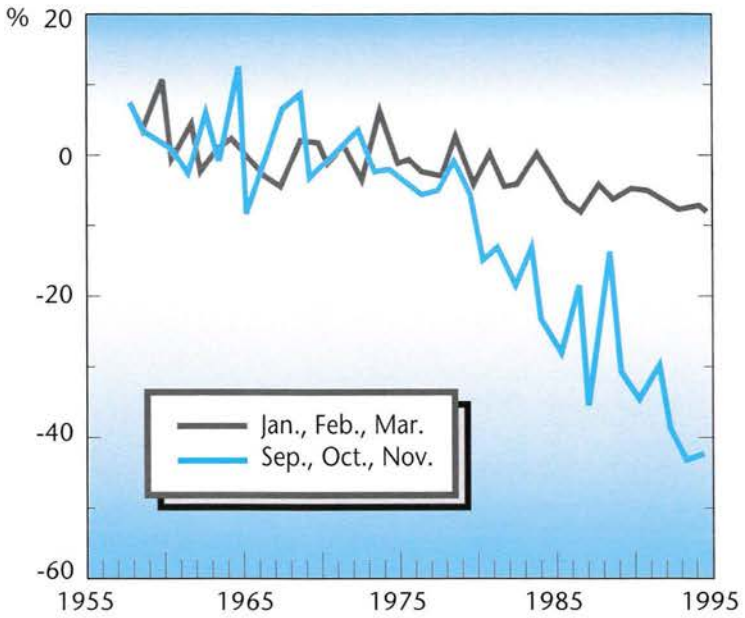

Figure 11.3 – Total ozone deviations for two seasons in the Antarctic from pre-ozone hole (1957-1978) averages (source Bojkov WMO Bulletin 43(2) 1994). Summary of data from stations Faraday, Syowa, Halley Bay, South Pole. ▶

RECORD LOW OZONE VALUES ALSO OVER NORTH AMERICA IN EARLY 1993

Measurements of ozone made over Canada and a large part of the USA during the first four months of 1993 indicated that total ozone has been about 11 to 17% below normal. (Figure 11.4 shows the total ozone departure for March 1993 over northern middle and high latitudes.) Low values were recorded at all nine of the Canadian mid-latitude ground-based monitoring sites and in most USA sites. Record low averages for the period from December 1992 to April 1993 are indicated by the negative deviations in Figure 11.5 which is based on measurements that have been made since the 1960s at three mid-latitude stations in northeastern North America.

Comparing January to April 1993 ozonesonde profile measurements with those from earlier years indicates that the ozone deficit is in the lower stratosphere between pressure levels of 40 and 200 hPa (the same altitudes where aerosols from the Mount Pinatubo volcanic eruption have been observed), the peak loss being 30% at 100 hPa (16 km). (Adapted from a contribution by Kerr et al., 1993).

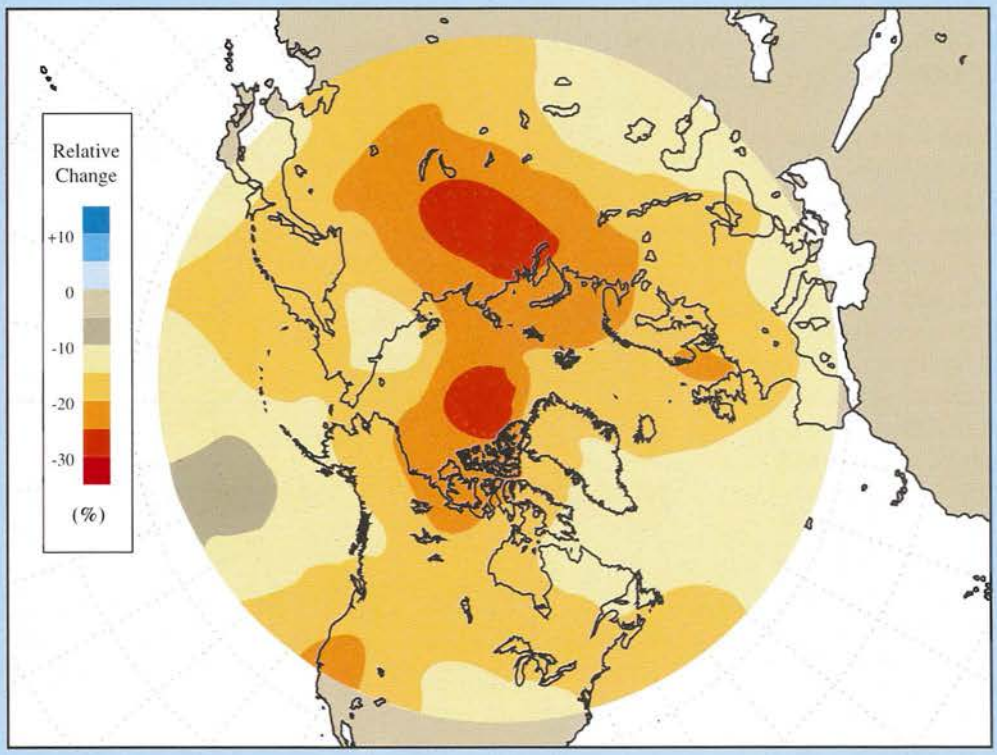

▲ *Figure 11.4* – Total ozone departure (%) for March 1993 from the mean (1979-1982) showing large ozone deficiencies over northern middle and high latitudes (from analysis by J.B. Kerr and E.W. Hare, Atmospheric Environment Service, Downsview, Ontario, using data supplied by NASA/Goddard Space Flight Center, Greenbelt, MD).

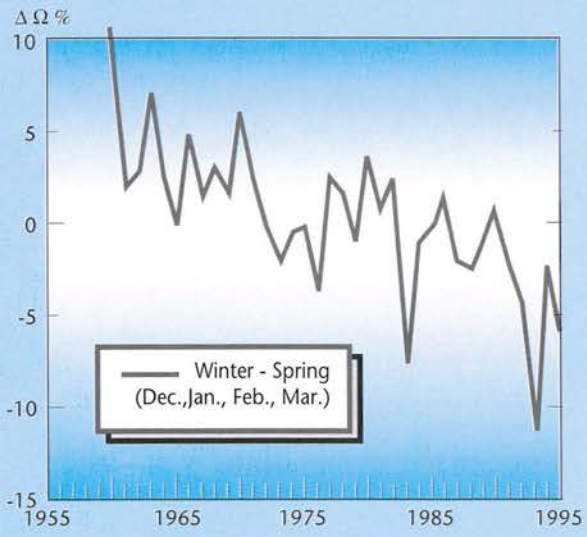

◀ *Figure 11.5* – Percentage differences of total ozone values in the December 1992 to April 1993 winter-spring season from the 1964-1980 average total ozone values at Toronto, Caribou and Goose stations in the northeast part of North America (source: Bojkov and Fioletov, 1995).

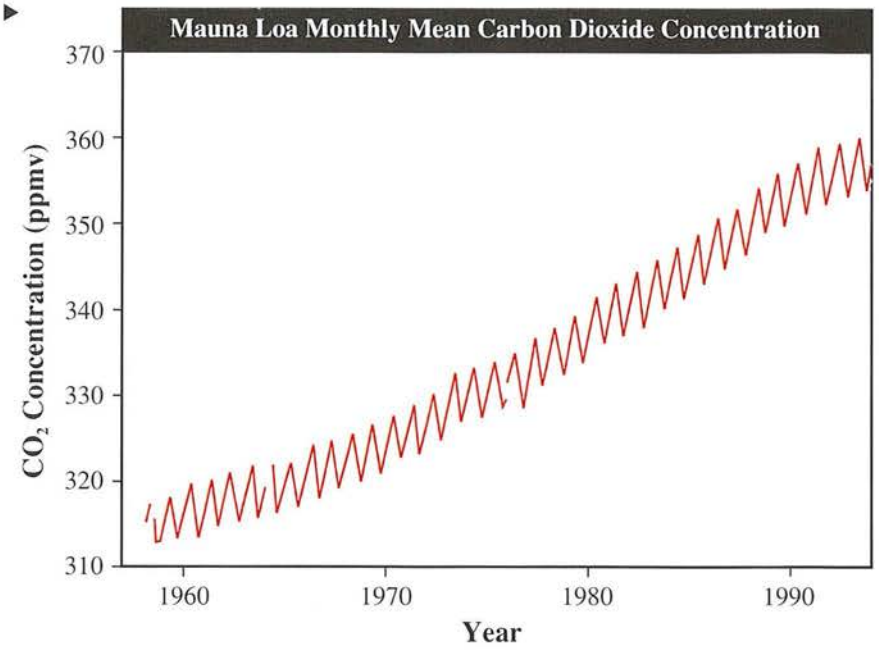

Figure 12.1 – Monthly mean carbon dioxide concentration (parts per million) measured at Mauna Loa Observatory, Hawaii, 1958 to 1993. Data have been updated and combined from the programmes of Keeling et al. (1989) of the Scripps Institution of Oceanography and Thoning and Tans (1989) of NOAA.

Atmospheric gaseous components other than nitrogen, oxygen, argon and water vapour are called trace gases. The trace gases affect climate through their role as infrared radiative absorbers (greenhouse gases) and some also provide a source of chlorine to the upper atmosphere that leads to depletion of stratospheric ozone.

During the 1980s, the long-term growth rates for many trace gases was steadily upward. During 1991-93, however, the growth rates for several important trace gases decreased, notably for carbon dioxide, methane and several chlorofluorocarbons (CFCs). There was no uniform cause for the growth rate changes because each species' sources and sinks are governed by quite different processes.

Recently, two comprehensive assessments of atmospheric trace gases prepared by international groups of experts were published. Readers are referred to those reports for further detail. One report focuses on stratospheric ozone depletion (Sanhueza et al., 1994) and the other on climate change and greenhouse gases (Prather et al., 1994).

12.1 CARBON DIOXIDE

Carbon dioxide is the most significant radiatively important trace gas. Today, it alone accounts for about 60% of the radiative forcing due to all trace greenhouse gases. Systematic monitoring of carbon dioxide began in 1957, when its global average concentration was about 315 ppm. The WMO now coordinates an expanding global network supported by some 20 nations.

Figure 12.1 illustrates the long-term record of monthly mean carbon dioxide concentration at Mauna Loa Observatory, Hawaii. The annual mean there for 1993 was almost 357 ppm, which approximates the global mean. Significantly, one can also clearly see that during 1992 and 1993 the rate of increase of carbon dioxide slowed.

During the 1980s, the global growth rate of carbon dioxide was about 1.5 ppm per year whereas for 1992 and 1993 it averaged only about one-half of that. The reasons for the slow down are unclear. Since the release of carbon dioxide due to fossil fuel usage did not decrease significantly, an increase in the natural uptake by the terrestrial biosphere (plants or soils) particularly (Conway et al., 1994) and oceans is the likely cause. Why these natural processes may have been more effective during this time is also unclear, but there could be a relation to the cooler global temperatures due to the Pinatubo eruption. Looking ahead, indications from early 1994 are that the carbon dioxide growth rates are increasing

Figure 12.2 – A slow down in the growth rate of carbon dioxide levels (from analyses prepared by Pieter Tans and Thomas Conway, NOAA/CMDL Carbon Cycle Group, Boulder, CO).

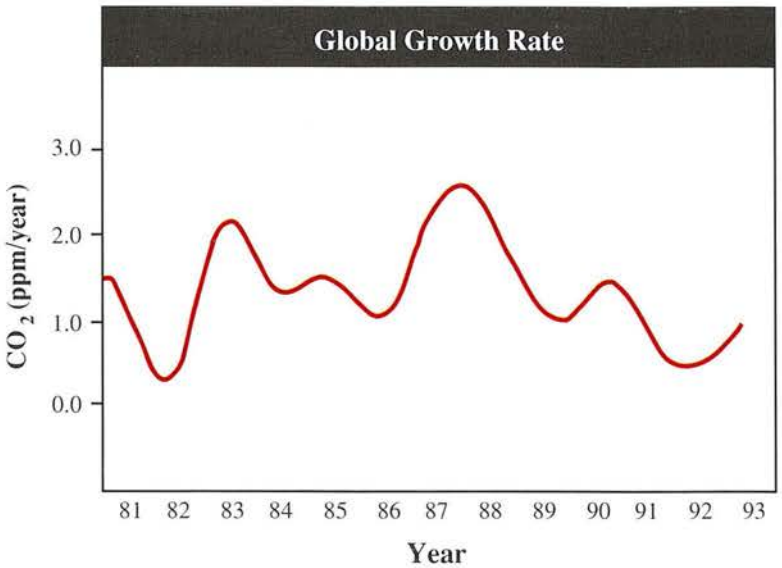

toward the levels of the previous decade (Figure 12.2).

12.2 METHANE

Following carbon dioxide, methane is the next most important greenhouse gas, accounting for about 15% of the trace gas radiative forcing. The sources of most methane in the atmosphere are biological anaerobic processes (both anthropogenic, such as rice growing, and natural, such as permafrost melting), but fossil fuel use accounts for about 20% of the annual methane emissions. Removal of methane from the atmosphere is mainly due to its reaction with the hydroxyl radical. The pre-industrial global mean concentration was about 720-740 ppb, less than half of current values (Etheridge et al., 1992; Nakazawa et al., 1993).

A record of methane concentrations in the atmosphere over the last 1000 years is shown in Figure 12.3 (Etheridge et al., 1992; Nakazawa et al., 1993; Blunier et al., 1993). These data, which were obtained from analyses of ancient air captured in Greenland and Antarctic ice cores, clearly show the dramatic increase of methane during the last two centuries.

The previous edition of the Review stated that the rate at which methane is increasing in the atmosphere had been decreasing. Global monitoring of methane through 1993 has shown further declines in the growth rate, although recent measurements indicate that growth rates have started to increase again. Independent measurements by Khalil et al. (1993) and by Dlugokencky et al. (1994) show that the 1992 global methane increase was only about 5 ppb per year compared to values of about 20 ppb per year in 1980. The cause is unclear (Prather et al., 1994).

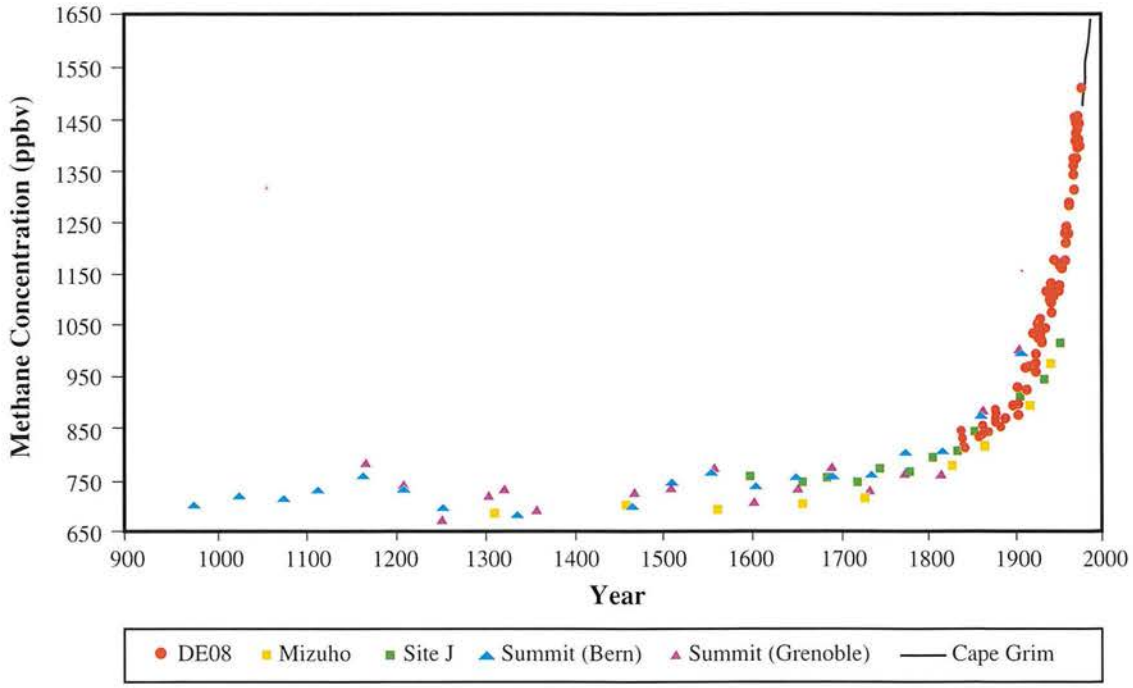

▲ *Figure 12.3* – Methane concentration derived from ice cores from Greenland (Summit) and Antarctica over the past 1000 years along with recent direct measurements from Cape Grim Australia (adapted from Prather et al.,1994).

12.3 CARBON MONOXIDE

Carbon monoxide is not a greenhouse gas itself, but is important in the global carbon cycle because it is formed from the oxidation of methane and its removal from the atmosphere by oxidation leads to the formation of carbon dioxide. It also has significant anthropogenic sources, including transportation and combustion.

Until the late 1980s, carbon monoxide was increasing at about 1% per year in the northern hemisphere but was not changing in the southern hemisphere. More recently, global network data (Novelli et al., 1994; Khalil and Rasmussen, 1994) have shown marked decreases throughout the globe, with the largest decreases at northern hemisphere high latitudes. The causes of these trends are not known, but possible reasons for the decline include more effective emission controls, higher concentrations of the hydroxyl radical and decreased biomass burning in the tropics.

12.4 PRECURSOR GASES FOR STRATOSPHERIC OZONE DEPLETION

The most significant anthropogenically produced species for stratospheric ozone depletion are CFC-11, CFC-12, HCFC-22, CFC–113, the halons, carbon tetrachloride and methyl chloroform.

TABLE 12.1. Recent halocarbon trends reported in the 1994 Ozone Depletion Assessment compared to those reported in the 1991. Assessment (adapted from Sanhueza et al., 1994).

Compound	Chemical Formula	1994 Assessment			1991 Assessment	
		Period	pptv/yr	%yr	pptv/yr	%yr
CFC–11	$CFCl_3$	1990–92	2.5	0.9	9.3–10.1	3.7–3.8
CFC–12	CF_2Cl_2	1990–92	13	2.6	16.9–18.2	3.7–4.0
CFC–113	$C_2F_3Cl_3$	1990–92	2.5	3.1	5.4– 6.2	9.1
Carbon Tetrachloride	CCl_4	1990–92	-1	-0.8	1.0–1.5	1.2
Methyl Chloroform	CH_3CCl_3	1990–92	3.5	2.2	4.8–5.1	3.7
HCFC-22	CF_2ClH	1992	7.0	6.9	5–6	6–7
HCFC-142b	$C_2F_2ClH_3$	1992	~1	~30	No data	
HCFC-141b	$C_2FCl_2H_3$	1993	~0.75	~200	No data	
H-1211	CF_2ClBr	< 1990–92	0.075	3	0.2–0.4	15.
H–1301	CF_3Br	< 1990–92	0.16	8	0.4–0.7	20.

In the last two issues of *The Global Climate System* tables were presented showing the concentrations and growth rates of these and other trace gases important for either greenhouse climate warming or stratospheric ozone depletion. An updated version of those tables is presented here as Table 12.1.

There is now clear evidence that the growth rates of several of these gases decreased noticeably during the last three years in direct response to provisions of the Montreal Protocol and its Amendments (Sanheuza et al., 1994; Prather et al., 1994). Figure 12.4 shows the measurement record since 1977 for CFC-12 (Elkins et al., 1993). The slower growth rates of recent years are evident. Atmospheric mixing ratios of CFC-11 and methyl chloroform are now increasing at only a few ppt per year while carbon tetrachloride appears to be decreasing. In contrast, HCFC-22, which is not regulated by the protocols, continues its steady increase and CFC-113, an important cleaning agent in the microelectronics industry, has only recently begun to show a decreased growth rate.

The data from several independent global monitoring programmes all document the success of the Montreal Protocol and its Amendments in reducing chlorine emissions. Unfortunately, many of these human-produced chlorine- and bromine-containing species have atmospheric lifetimes of decades and, therefore, will be present well into the next century at levels significant for ozone depletion.

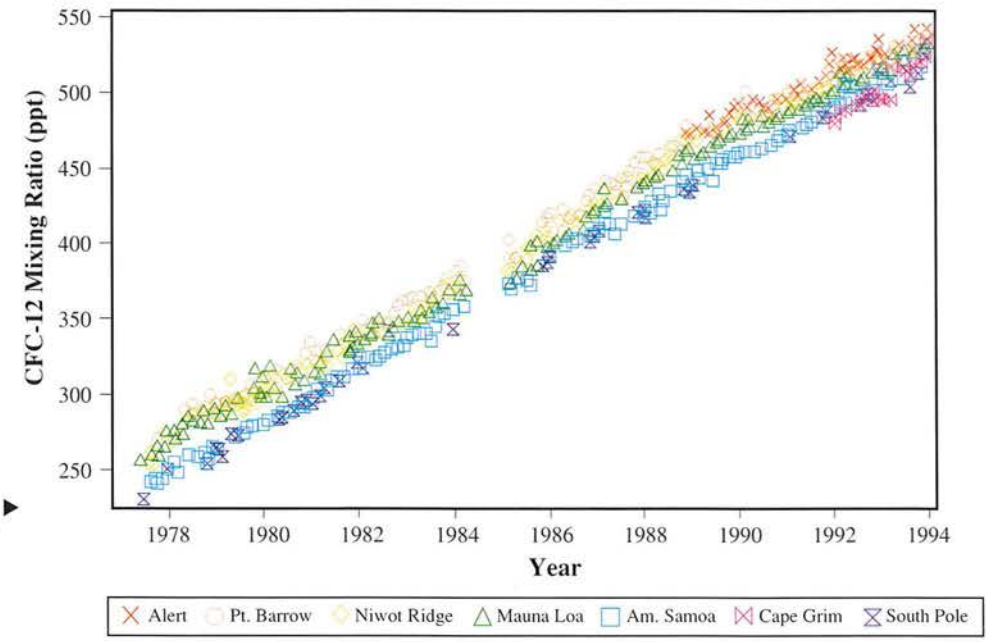

Figure 12.4 – Monthly mean ▶ CFC-12 mixing ratios in parts per trillion measured at ground level from several different observation sites from 1977 through 1993 (from Elkins et al. 1993).

The varying responses of snow cover, ice extent and other cryospheric variables to fluctuations in climate make them useful indicators for monitoring changes in the global climate system and for revealing long-term climate trends. In linking climate forcing and cryospheric response, however, it is important to consider differences in lag time between those quantities that respond rapidly to change, such as lake ice and snow cover, and those that respond more slowly over decades or centuries, such as continental ice-sheets and permafrost. Regional effects such as latitude, elevation and climatic regime are also important when considering climate forcing and cryospheric response.

13.1 SNOW COVER

Snow cover is the most transient and variable cryospheric form, which can change the surface characteristics of large land areas in just a few days. Monitoring the extent and albedo of snow cover and, more recently, its water equivalent on a continental or hemispheric scale has greatly improved with the advent of satellite observing systems. Figure 13.1 is a satellite-derived, 21-year time series of snow cover area, spanning the winters (December through February) 1973 to 1993, for the northern hemisphere. The data show considerable variability from year to year, with a range of 10-15 percent.

The areal extent of northern hemisphere snow cover in autumn (not shown) steadily increased since 1990. Snow-cover area during 1993 was the largest since 1976, some 20.7 million km^2, and the third highest in the 21-year record. Colder conditions in western Russia and northern Europe during autumn of 1993 were reflected in large areas with increased duration of snow cover. Snowfall was large enough over these regions to maintain an excess of snow cover even though overall precipitation was generally at or below normal. Canada was characterized by below-normal snow cover in the west and above-normal snow cover in the east during that season.

Two of three winters during the review period had above-normal snow cover. During December 1992 through February 1993, the northern hemisphere experienced its largest extent of snow cover since 1986. Snow cover was especially heavy and persistent over western North America, Asia Minor and western Siberia (Figure 13.2). In contrast, less than normal snow cover was experienced in the eastern USA, northern Europe and Scandinavia, and the southern flanks of the Great Siberian Plain.

13.2 SEA ICE

Records of sea-ice amount and concentration have long been used as climatic indicators. Reasonably consistent sea-ice data for polar regions are available from satellites back to 1973.

Arctic sea-ice extent is generally at a maximum in February and a minimum in August. Time series of sea-ice area for February (Figure 13.3) show increases since

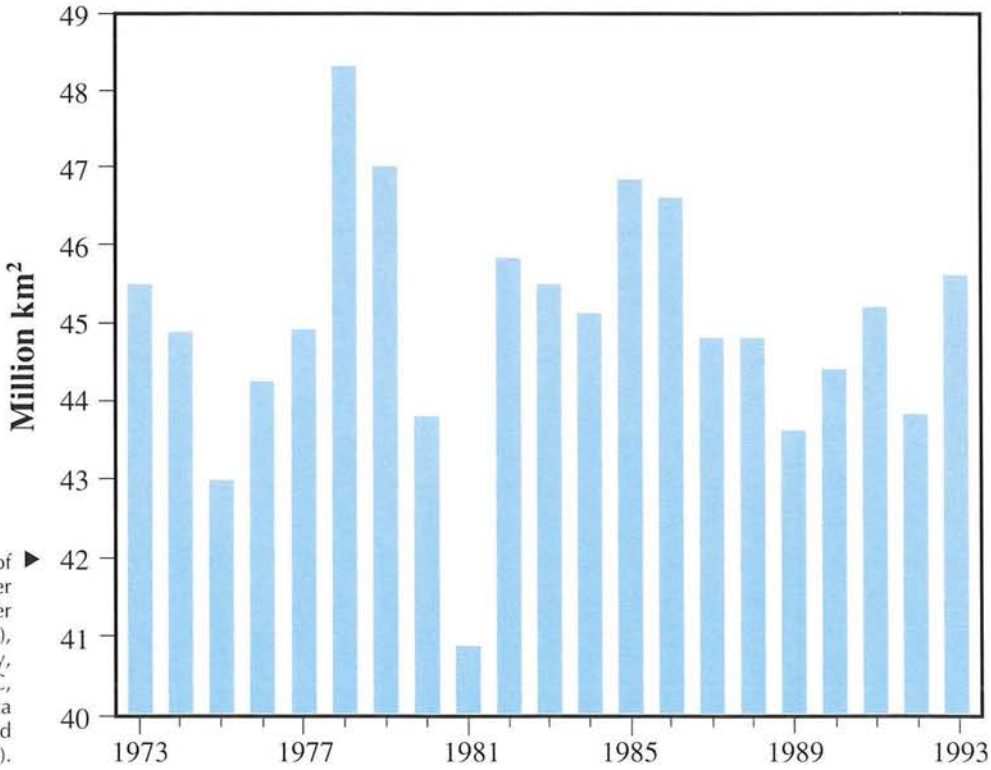

Figure 13.1 – Time series of northern hemisphere snow-cover area (106 km2) for winter (December through February), estimated from satellite imagery, (from NOAA/NWS/NMC/CAC, Washington, DC, using data provided by NOAA/NESDIS and D. Robinson, Rutgers University).

1991. However, the August values (not shown) have remained below the 21-year average since 1989. The February 1993 values were above average for the first time since 1988, but the entire time series shows no systematic trends.

After exhibiting a period of extreme variability early in the record, the fluctuations in Antarctic sea-ice area have been extremely small over the past several years. Antarctic sea-ice area was above the 21-year mean in both February 1993 (not shown) and August 1993 (Figure 13.4), the time of minimum and maximum areal coverage, respectively. The August 1993 Antarctic sea-ice extent is the largest since 1985. There appears to be no relationship between sea-ice area and global trends in surface temperature over the limited period of satellite records.

The Gulf of Riga was ice-free for the fourth year in succession in 1992. The last long ice-free period was 1973 to 1975.

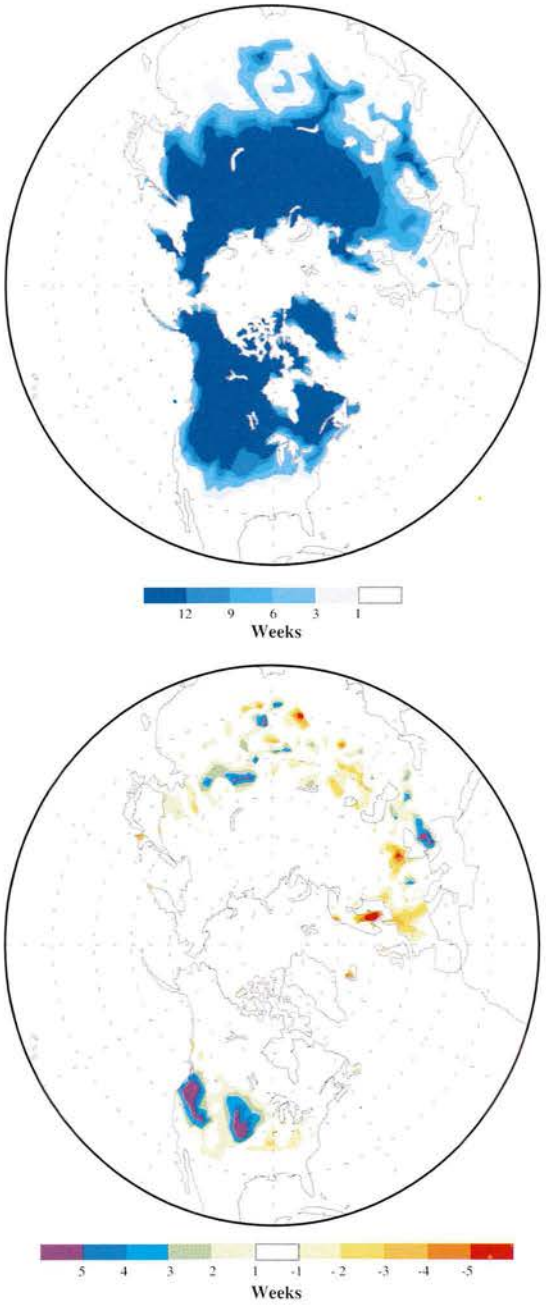

Figure 13.2 – Winter 1992-93 snow-cover duration in weeks of snow cover (top) and anomaly (bottom). Anomalies are departures from the 1973-1993 base period (from NOAA/NWS/NMC/CAC, Washington, DC). ▶

▼ *Figure 13.3* – Time series of Arctic sea ice (105 km²) for February. Mean based on period 1973 to 1993 (from NOAA/NWS/NMC/CAC, Washington, DC)..

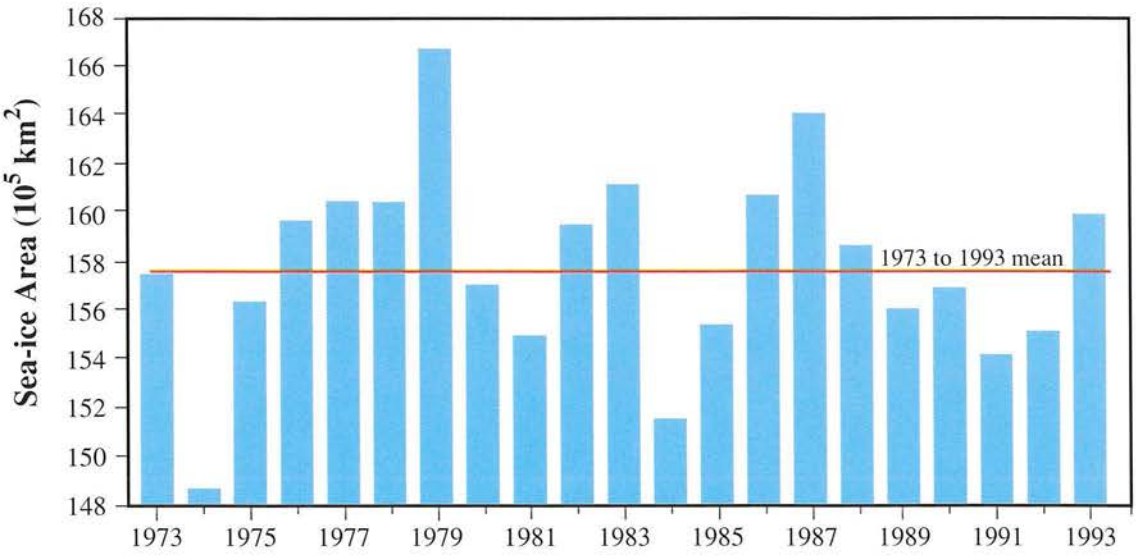

13.3

SEA-ICE HIGHLIGHTS IN CANADA

At the beginning of the review period, ice conditions along the eastern coast of Newfoundland-Labrador and in the Gulf of St. Lawrence were the worst in 25 years, as Arctic ice continued to drift southwards along the Labrador coast. Only towards the end of July did the ice start decaying and break up into patches. The pack ice, some 3-5 m thick, was unusually hard and accompanied by large ice flows up to 3 km in diameter. Icebergs were mixed in with the pack ice along the coast. Ice entered many small harbours. Damage to commercial vessels was extensive, inshore fishing was delayed more than eight weeks and coastal ferry services were severely affected.

A very stable position of the Arctic vortex, over northern Baffin Island during winter 1991 and spring 1992 was responsible for more than 22 consecutive weeks of below-normal temperatures. In 1992, ice breakup in the eastern Arctic was delayed by two to three weeks and ice thickness was generally greater than average. Fast ice was especially prominent along Baffin Island and the Labrador coast, delaying the resupply of many isolated coastal communities. Hudson Bay, which is normally

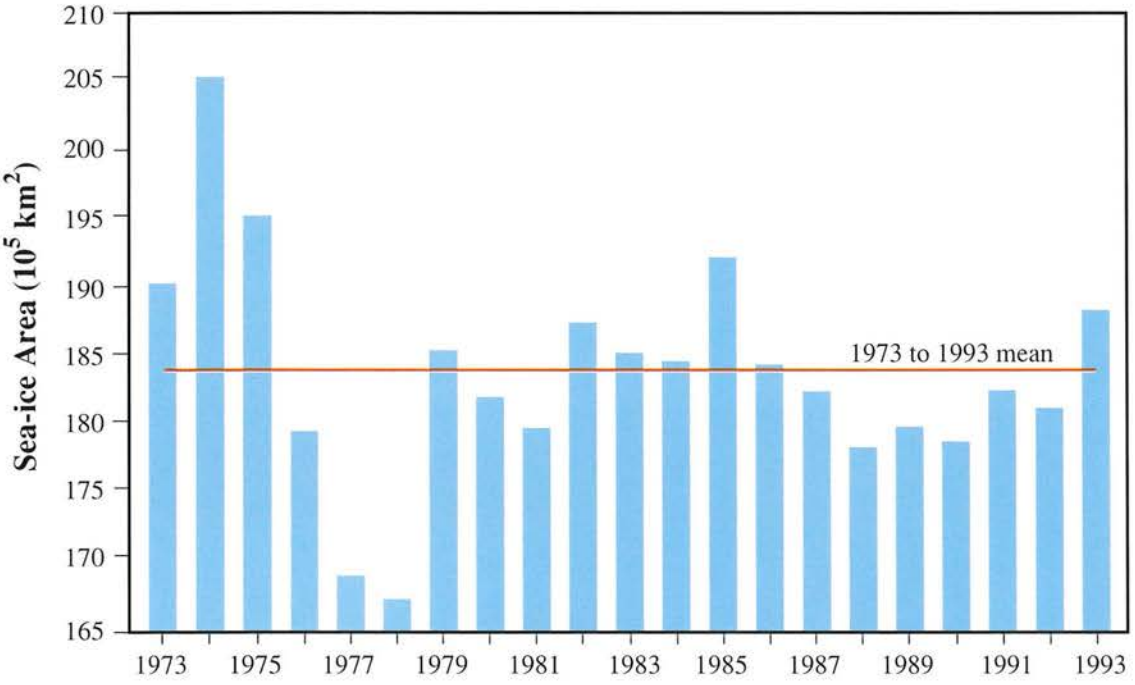

▲ *Figure 13.4* – Time series of Antarctic sea ice (105 km²) for August. Mean based on period 1973 to 1993 (from NOAA/NWS/NMC/CAC, Washington, DC).

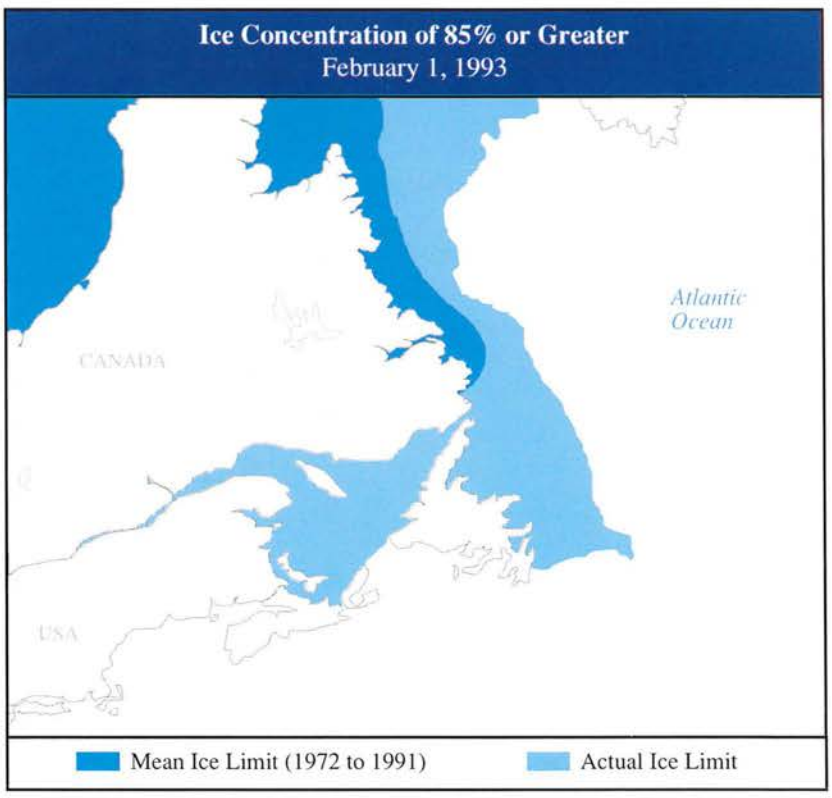

Figure 13.5 – Ice cover anomalies along the east coast of Canada, February 1, 1993 (from Arvids Silis, Climate Processes and Earth Observation Division, Atmospheric Environment Service, Canada Department of the Environment, Downsview, Ontario). ▶

ice-free by early August, was still covered by ice. On the other hand, in the western Arctic and the Beaufort Sea, ice conditions were normal.

For the third consecutive winter, colder than normal temperatures in the winter 1992-93 again disrupted marine traffic in Atlantic Canada. Since the beginning of November 1992, air temperatures were consistently 2 to 5°C colder than normal not only off the east coast of Newfoundland but also in the Gulf of St. Lawrence. The sea ice extended considerably farther down the east coast into Newfoundland waters compared with the mean limits of ice (Figure 13.5). The Canadian Coast Guard reported that ice conditions were between four to five weeks ahead of normal (worse) in January 1993. Abnormally cold weather in January and February promoted rapid ice growth in the Gulf of St. Lawrence and produced some of the most difficult ice conditions in recent memory. Every day seven or eight ships became stuck in the ice and had to wait several days to be cleared. Only the heaviest ice-breakers could make headway in the Gulf.

The year 1993 started off with more than the normal amount of solid ice on the eastern coast of Canada and in the Bering Sea. By June 1993, breakup was normal in northern Baffin Bay and ahead in the Beaufort Sea owing to a milder spring. In September 1993, usually the month with the minimum extent of sea ice in Canadian waters, there were normal amounts of solid ice cover throughout the Arctic Archipelago.
During the autumn, temperatures were colder than normal in northern Quebec and the eastern Arctic. As a result, the ice extent was greater than normal in Baffin Bay and Hudson Bay. Ice conditions at the end of November were looking more like those prevailing in January.

At the end of November 1993, ice cover was normal in most areas of the Arctic. The major exceptions were Baffin Bay and Hudson Bay where solid ice cover was farther south than normal by 300 and 900 km, respectively. Expressed as an areal extent, normally the Hudson Bay-Hudson Strait area has a 20% solid ice cover. By the end of November, 75% of the area was covered by solid ice, primarily as a result of persistently cooler than normal temperatures in the eastern Canadian Arctic (Figure 13.6).

13.4

LAKE ICE

Freeze-up and break-up records from lakes in middle to high

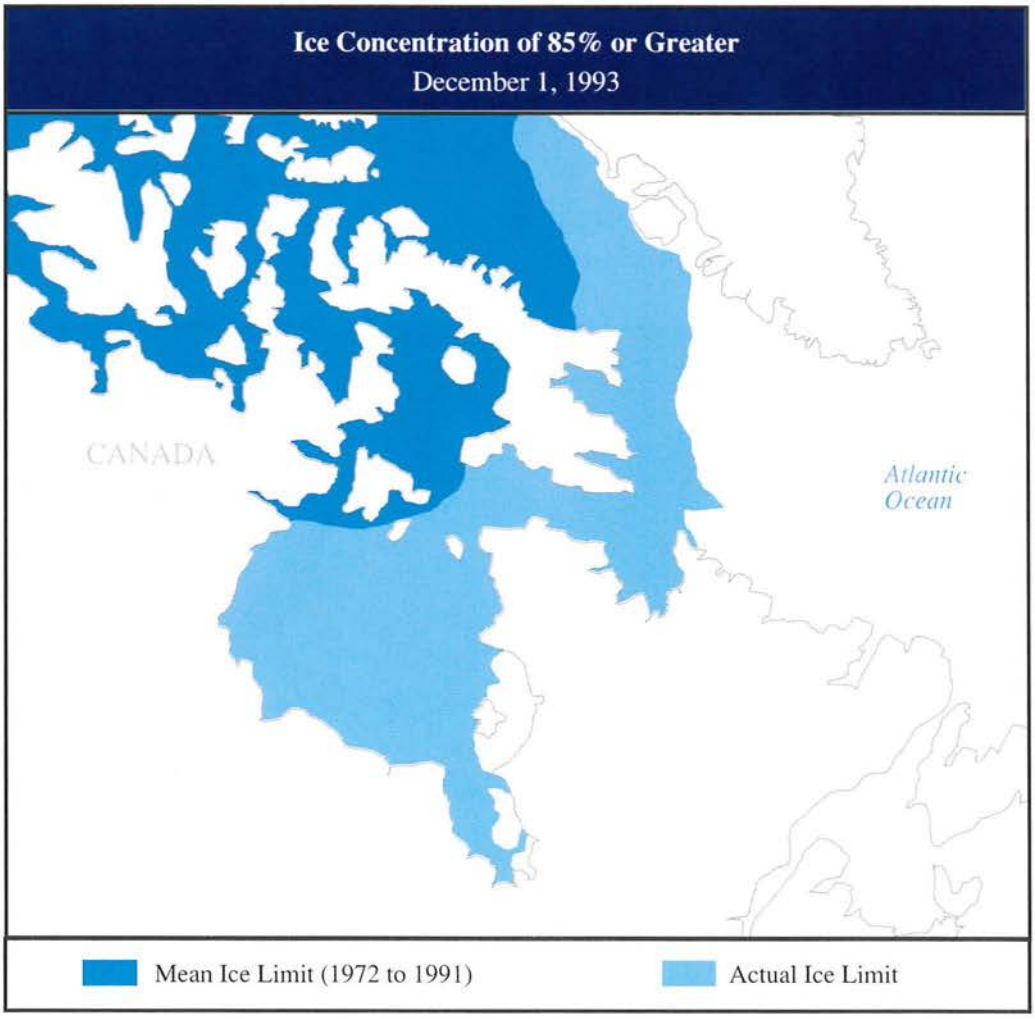

▲ *Figure 13.6* – Ice cover anomalies in the Canadian Arctic, December 1, 1993 (from Arvids Silis, Climate Processes and Earth Observation Division, Atmospheric Environment Service, Canada Department of the Environment, Downsview, Ontario).

LONG-TERM VARIABILITY IN CANADIAN SNOW COVER DURATION*

Research on long-term variability in Canadian snow cover is being carried out as part of the CRYSYS programme (Use of the Cryospheric System to Monitor Global Change in Canada). CRYSYS is a Canadian interdisciplinary research programme within NASA's Earth Observing System (EOS) Programme to monitor Earth systems from space. Two basic scientific goals of CRYSYS are (1) to improve understanding of the role of the cryosphere in the climate system and in global change; and (2) to develop capabilities for monitoring and understanding regional and hemispheric variations in cryospheric variables.

Figure 13.7 shows the interannual variability in reconstructed annual snow cover duration over the western Prairies for the last 100 years. The reconstructed data were developed using daily snowfall and maximum temperature in a calibrated melting degree-day model. The method was able to account for about 70% of the observed interannual variability in snow cover for the Prairies region in the calibration period (1955-91). Similar results were obtained in an independent calibration and verification using historical daily snow depth data from several sites in North Dakota obtained from David Robinson at Rutgers University.

Reconstruction of snow cover is necessary because observed daily snow depth data are only available in digital format from 1955 on. Figure 13.7 exhibits a trend toward *increasing* snow cover duration over much of this century, followed by a rapid decline in snow cover during the 1970s and 1980s (the period of available satellite coverage, see Figure 13.8). The recent decrease is mainly due to significant reductions in spring snow cover. It can be seen in Figure 13.7 that the duration of snow cover in the Prairies is characterized by large interannual variability and there is some evidence of cyclical variations in the 15-25 year interval. Seen in this longer-term context, it is apparent that recent changes in snow cover duration resulting from earlier snow disappearance in the spring are still well within the range of natural variability observed this century.

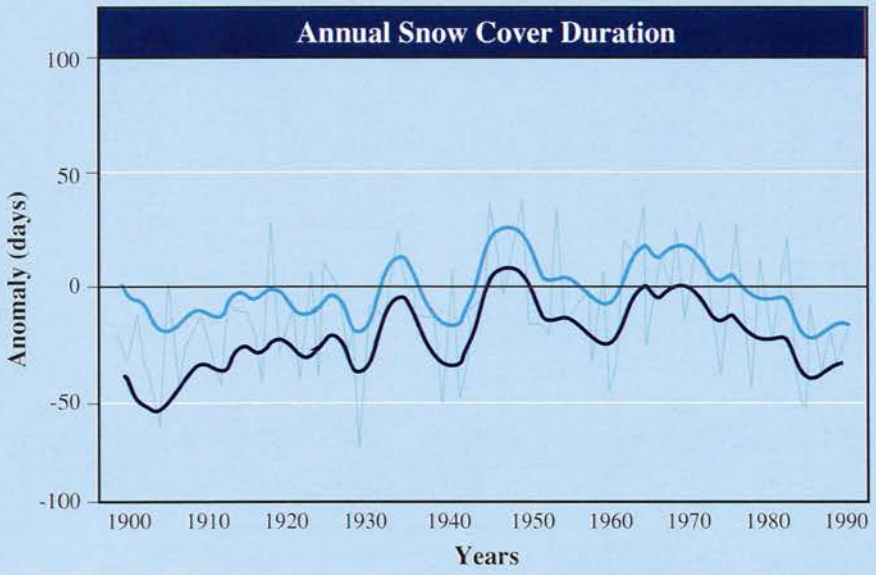

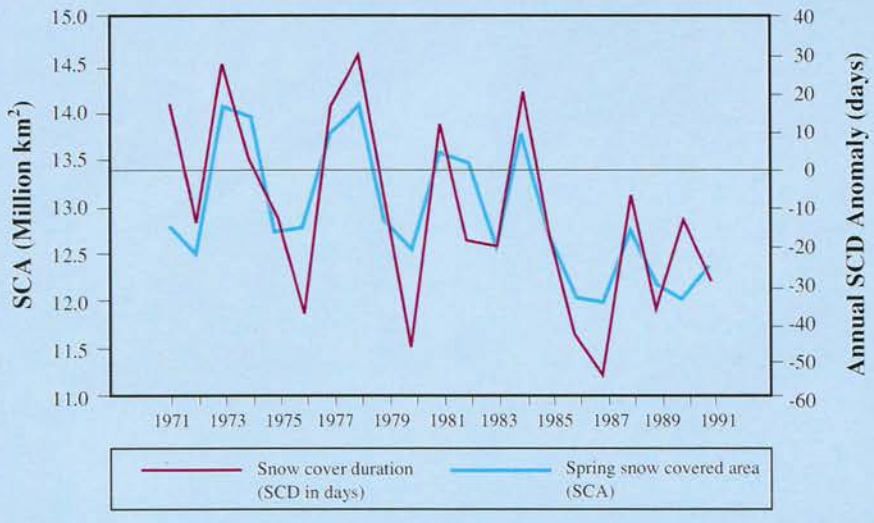

** Adapted from a contribution by Ross Brown, Climate Processes and Earth Observation Division, Atmospheric Environment Service, Environment Canada, Downsview, Ontario.*

◀ *Figure 13.7* – Annual variability in reconstructed snow-cover duration (snow cover ≥ 2 cm) over the western Prairies. Heavy lines are 9-term binomial filtered 95% confidence limits for the regional average. Wider limits in the early period of record reflect the lower number of stations used to derive the regional average (from Ross Brown, Climate Processes and Earth Observation Division, Atmospheric Environment Service, Canada Department of the Environment, Downsview, Ontario).

◀ *Figure 13.8* – Annual variability in snow cover duration over the western Prairies and spring (March-May) snow covered area for North America (from Ross Brown, Climate Processes and Earth Observation Division, Atmospheric Environment Service, Canada Department of the Environment, Downsview, Ontario and data supplied by D. Robinson, Rutgers, University).

latitudes provide a useful index of temperature trends in the transition seasons. Lake-ice time series from the late 1960s to the late 1980s across western and central Canada illustrate a tendency toward earlier break-up of the ice cover (Figure 13.9). The duration of the ice-free season has increased by upwards of 20 days over 30 years, mainly because of earlier break-up dates in the spring - a consequence of warmer spring temperatures and reduced snow cover. Recently, however, beginning in 1989-1990, the ice season has averaged about two to three weeks longer than it was during the early 1980s, as a result of cooler spring temperatures.

Since the spring of 1992, Canada has used passive microwave satellite data to monitor break-up on large lakes. Special Sensor Microwave Imager (SSM/I) satellite data from a USA Defense Meteorological Satellite (DMSP) are presently used. Figure 13.10 illustrates the break-up on Great Slave Lake, in the Northwest Territories for 1993. May 28 was the first indication of open water near Fort Resolution. This area of open water remained approximately uniform until June 8, when a major break-up occurred. In the course of two days, the open water area increased from about 10% to about 85% and, by June 21, the break-up was almost complete. The break-up on Great Slave Lake was about 12 days earlier than in 1992, not surprising given the above-normal temperatures in spring 1993.

AVALANCHE DISASTER IN SOUTHEASTERN TURKEY IN THE WINTER OF 1992*

Although they do not cause as much damage as earthquakes and floods, many avalanches occur during the winter months in the mountainous parts of eastern Anatolia, Turkey. Each year an average of 40 people are victims of avalanches in Turkey. In February 1992, an avalanche disaster in southeast Turkey killed seven times the usual number of people and was the greatest loss on record - 284 lives.

On January 1, 1992, heavy snowfall accompanied by low temperatures (-12°C) and strong winds induced a snow avalanche in the eastern and southern parts of Turkey. Snow depths were close to 100 cm. On January 30, a major cyclone located over northern Crimea tracked back towards the middle of the Black Sea bringing huge snowfalls to the eastern and southeastern region of Turkey. In a similar situation on February 8, a short wave trough settled over northern Turkey when more fresh snow fell on top of the old snow over southeastern Anatolia. The sudden accumulation of light snow with a density varying from 130 kg/m^3 at 1970 m to 200 kg/m^3 at 2240 m produced a thick, unstable surface snow layer. This caused the loose snow to advance across a great distance over mostly bare slopes that could not impede the onslaught. The combination of deep snows and alternating day and night temperatures that lubricated the avalanche-prone steep slopes triggered the avalanche.

** Adapted from a contribution by Ibrahim Gurer and Ayhan Sayin, Avalanche Disaster in Southeastern Turkey in the Winter of 1992, WMO Bulletin, 42(1):44-48, January 1993.*

Scenes of the aftermath of two avalanches whith struck the Van-Hakkari-Cukurca road in south-eastern Anatolia, Turkey, in February 1992 (from WMO Bulletin)

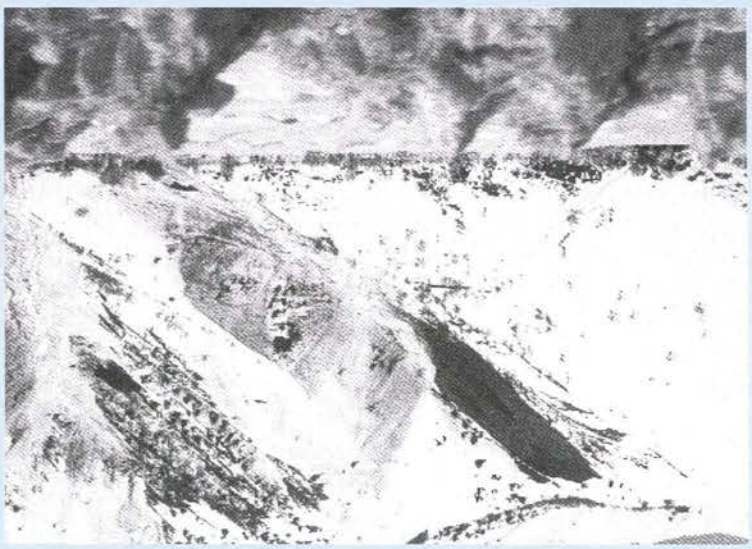

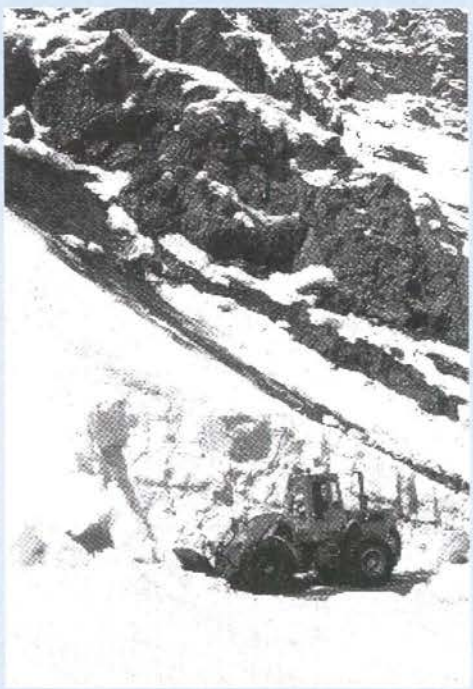

The beginning of the 1991-92 winter ice season was slightly delayed over Lake Ontario and Lake Erie but was near normal over Lake Huron and Lake Superior. In general, the ice cover throughout the winter months remained significantly lighter than normal over the entire area and, more particularly, over Lake Erie. The accumulated freezing degree-days over the Great Lakes were below normal from December 1991 through February 1992 as a result of warmer than normal temperatures. Although a reversal to above-normal freezing degree-days occurred in March 1992, overall winter accumulations of freezing degree-days meant thinner and less extensive ice conditions than normal.

Ice conditions in lakes Erie and Ontario were about three to four weeks behind normal at the end of January 1993. By early April, ice melt was about 1 to 2 weeks behind normal. Some thick and medium

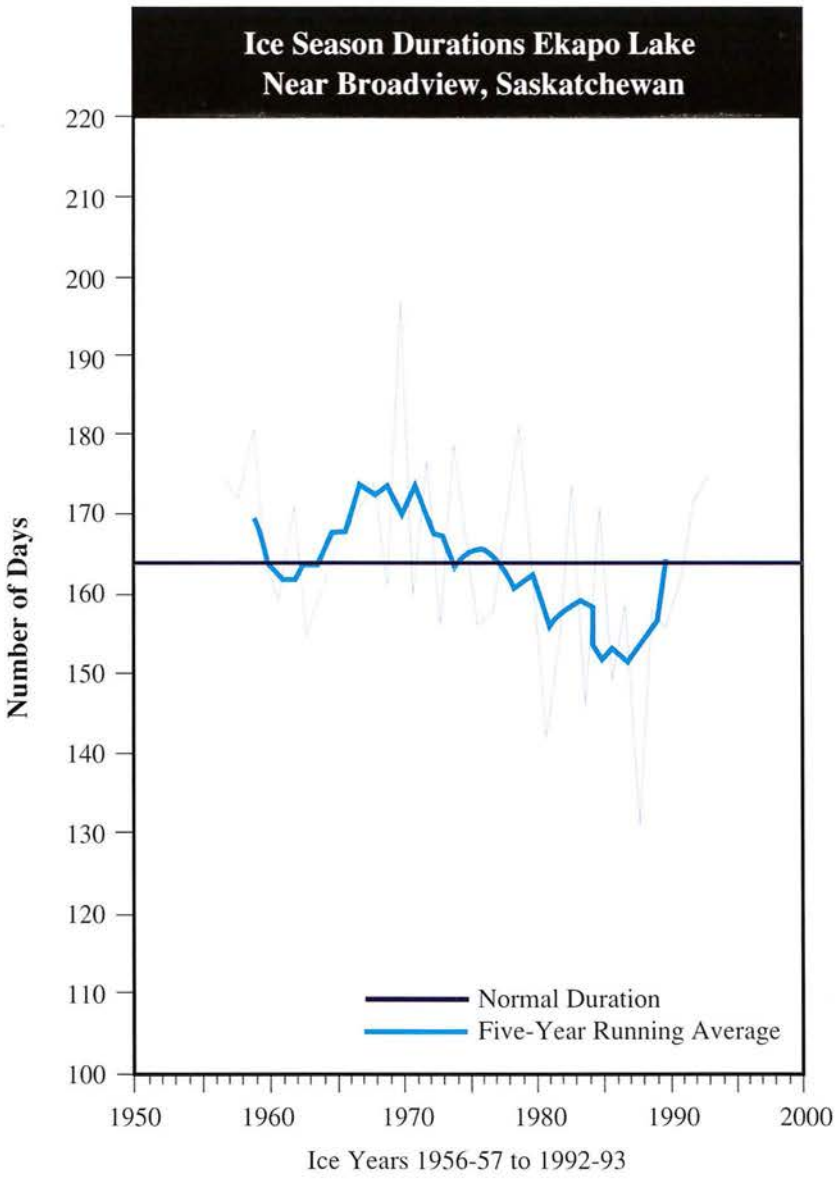

Figure 13.9 – Mean ice-season duration (days) for Ekapo Lake near Broadview, Saskatchewan, Canada, ice years 1956-57 to 1992-93 (from Walter Skinner, Climate Processes and Earth Observation Division, Atmospheric Environment Service, Canada Department of the Environment, Downsview, Ontario).

Figure 13.10 – Pair of images illustrating brightness temperatures (K) for two stages of ice break-up on Great Slave Lake June 8 and 10, 1993 from passive microwave sensors (from Michael Davey and Anne Walker, Climate Processes and Earth Observation Division, Atmospheric Environment Service, Canada Department of the Environment, Downsview, Ontario).

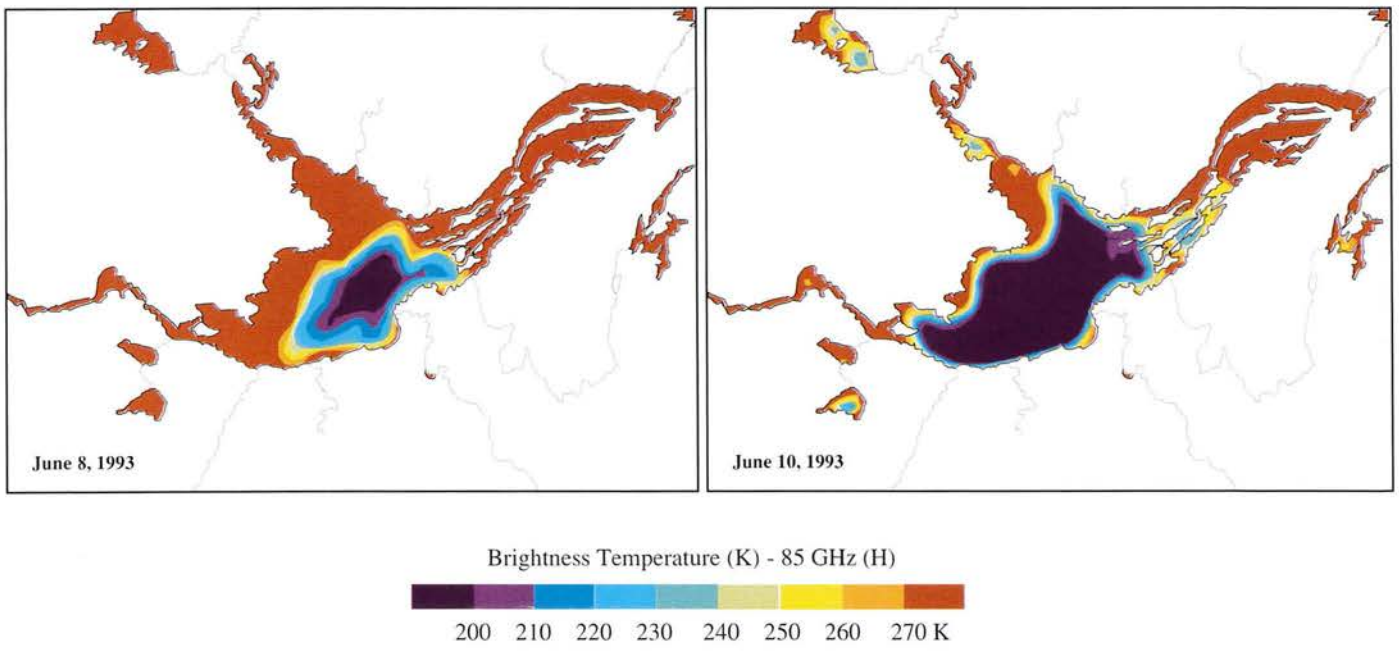

lake ice existed in the northeastern part of lake Ontario and in the St. Lawrence River during the second week. The last remains of ice in Long Point Bay and the southwestern part of Lake Erie melted during the first half of April as well. By the end of January 1993, ice conditions were about three to four weeks behind normal for both Lake Huron and Georgian Bay and Lake Superior. By the end of the second week of April, only the extreme southern part of Lake Huron and the northeast and southwestern shores of Georgian Bay had open-drift to close-pack thick and medium lake ice. In Lake Superior, the ice extent was about 5 to 6 weeks behind normal in mid-February but quickly became near normal by the end of the month and remained so until the end of the 1992-93 season. Figure 13.11 is an analysis of Great Lakes ice concentration during the time of maximum ice coverage about March 21, 1992 and 1993.

The percentage of ice on Lake Ladoga in Russia is shown in Figure 13.12 for the winters of 1991-92 and 1992-93. Of significance, the ice-covered area was above or close to the long-term average only in November 1992. Ice conditions were lighter than normal in both winters owing to the warmer than normal temperatures in December through March by about 4 to 5°C. Maximal ice cover in the winter of 1991-92 was the second lowest during the observation period of record dating back to 1951. The maximal ice cover in these two winters was close to values observed in the previous three winters, making five consecutive very mild winters - something that has never been observed on Lake Ladoga before.

13.5

LAND ICE

No conclusive evidence is available on whether the massive Greenland and Antarctic ice-sheets are growing or shrinking. Although the Antarctic ice-sheet appears to be growing, the Greenland sheet appears to be in equilibrium. Speculation exists that

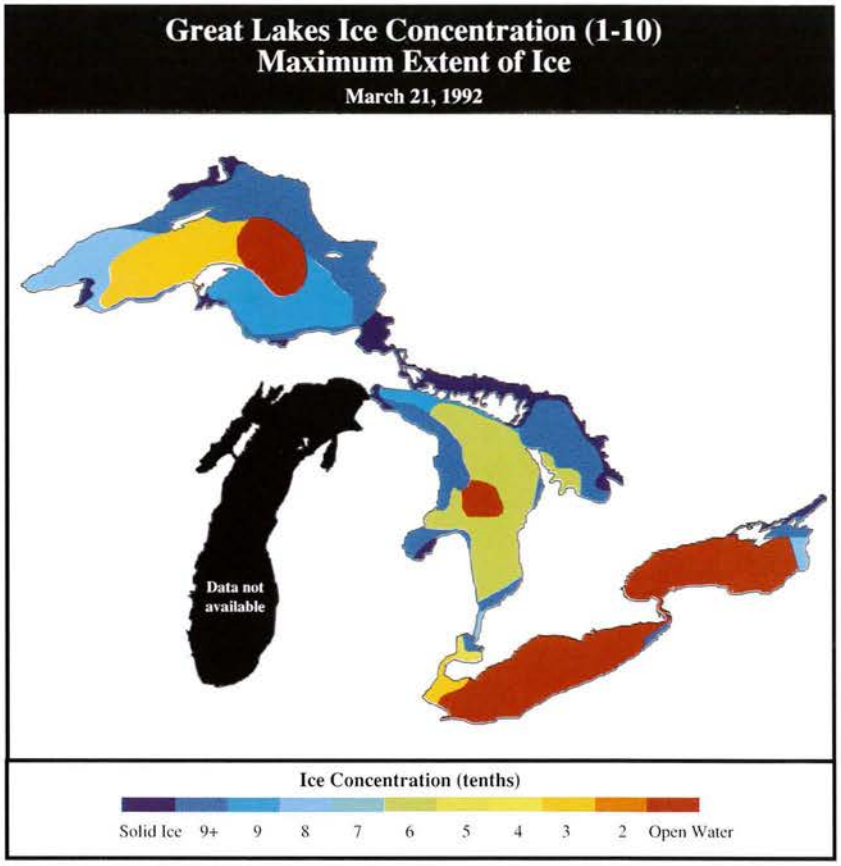

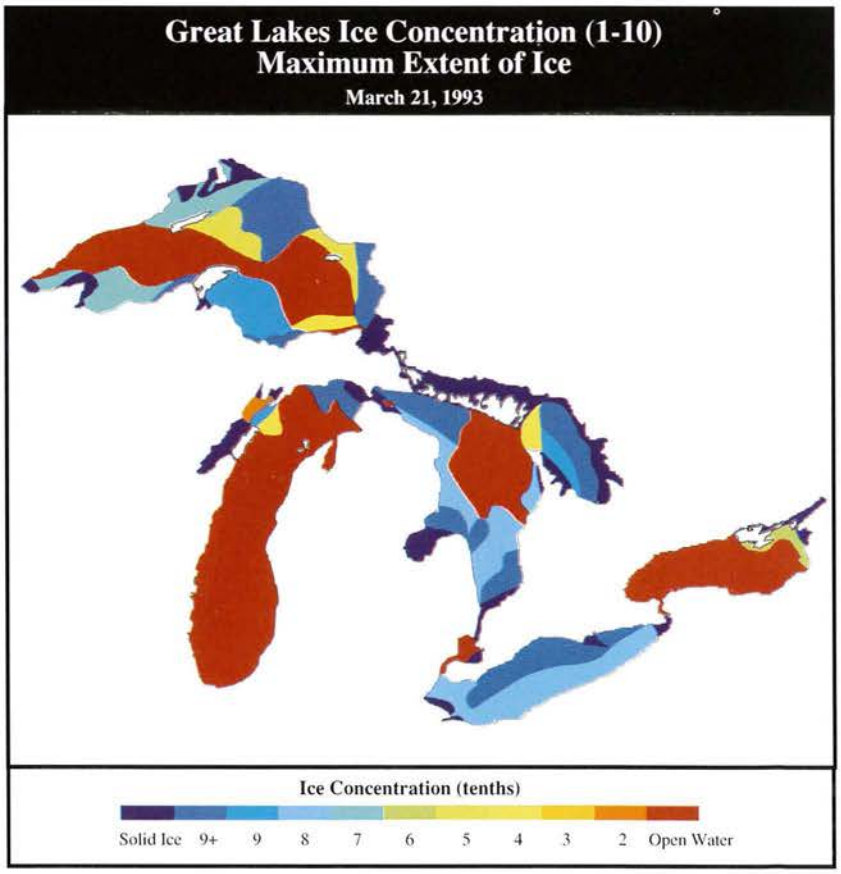

▲ Figure 13.11 – Analysis of Great Lakes ice concentration during maximum coverage March 21, 1992 and 1993 (from Fred Richardson, Ice Central Ottawa, Canada Department of the Environment).

climate warming has increased the amount of calving from the Greenland and Ellesmere Island glaciers, thus increasing the number of icebergs along the northwest Atlantic Coast.

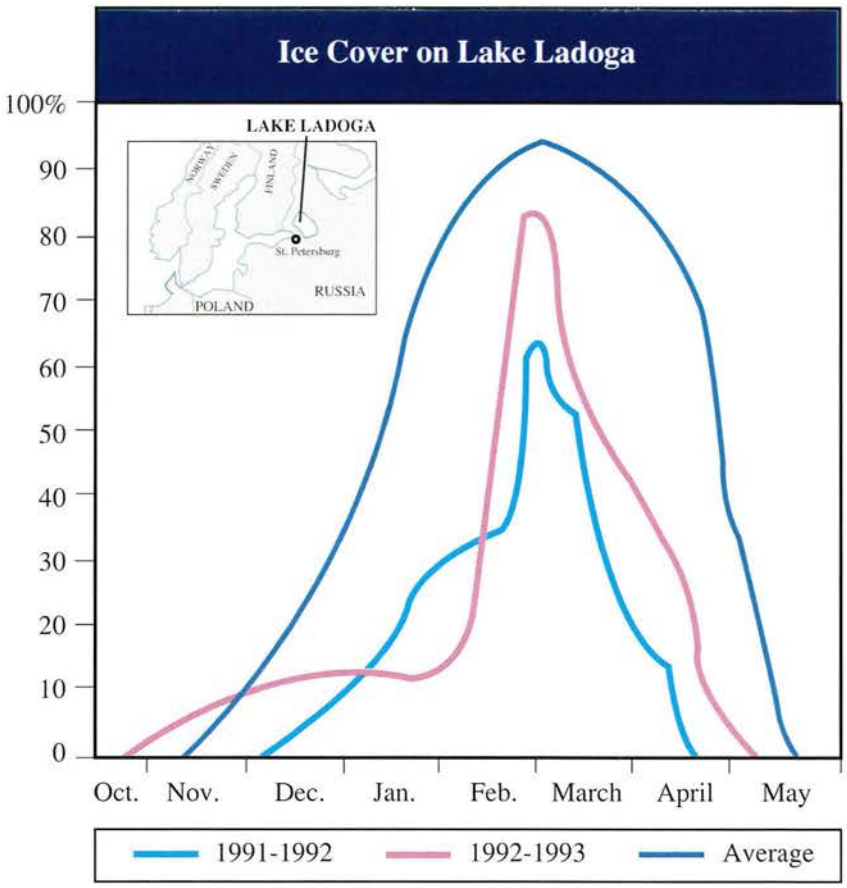

Figure 13.12 – Total ice coverage (including drift ice) on Lake Ladoga for two recent winters and for an average period based on the period 1951-1990 (from Hydrometeorological Centre of Russia, Moscow).

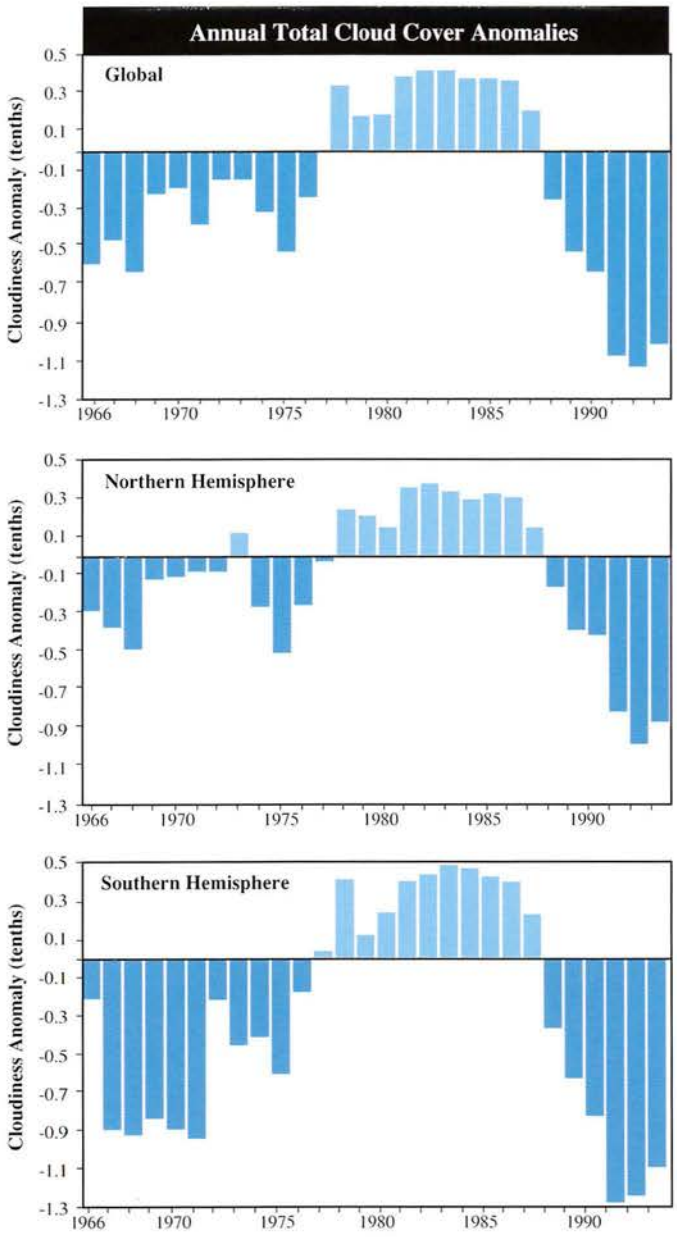

Figure 14.1 – Time-latitude section of the anomalies (departures from the 1966-1985 normals) of the monthly mean total cloudiness, averaged for specific latitudinal circles expressed in tenths, for January 1989 to November 1993 (from Institute for Global Climate and Ecology, Moscow).

Figure 14.2 – Zonal average cloudiness anomalies for the period 1989-1993 (from Institute for Global Climate and Ecology, Moscow).

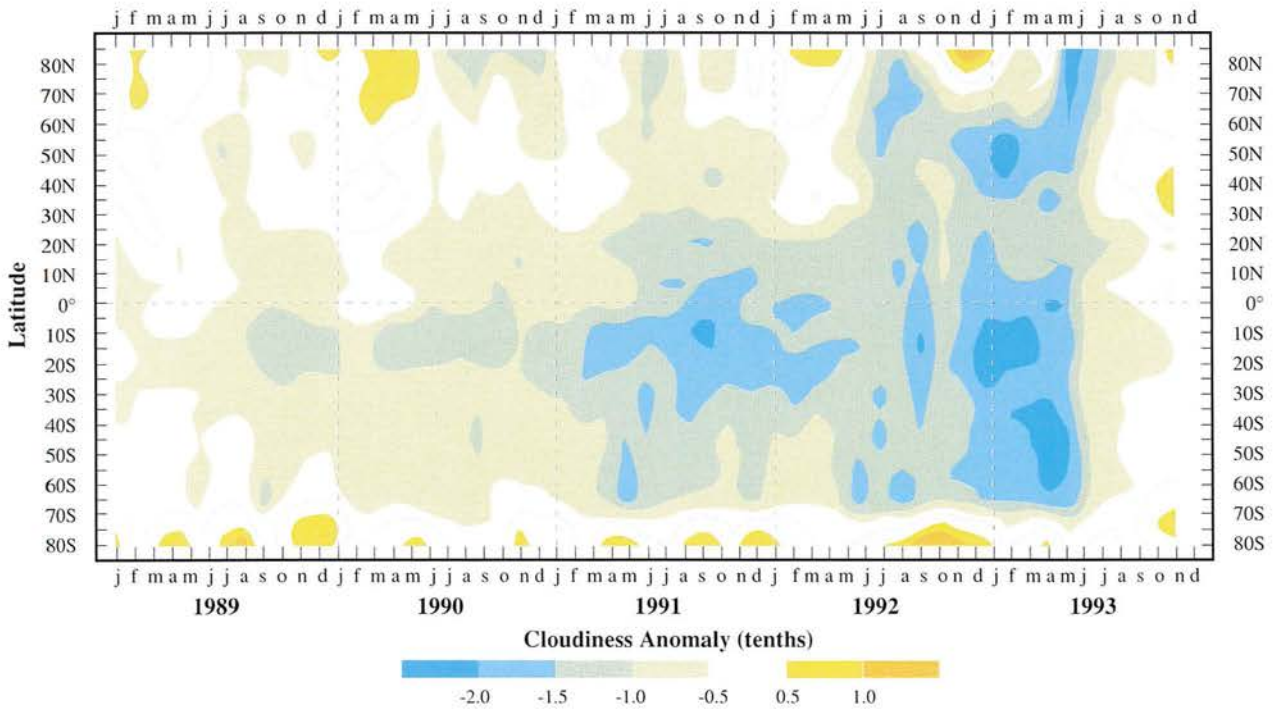

Changes in global cloud cover are another indicator of feedback in the global climate system. In this chapter, results of subjective interpretation of visual and infrared images are given as received from the Institute for Global Climate and Ecology in Moscow. These analyses were based on information obtained from "METEOR" polar orbiting satellites. It should be noted that these results in some aspects differ from other estimations, e.g. those obtained through the International Satellite Cloud Climatology Project (ISCCP). Nevertheless these results may be worth consideration since they complement the analyses previously made using other satellite systems.

The original METEOR imagery (January 1966 to December 1993) was analyzed onto a 5° latitude by 10° longitude global grid. Annual values were calculated from monthly

cloudiness values that were computed by averaging daily data. Interannual variability in these data is three to four times larger than the analysis from the International Satellite Cloud Climatology Project (ISCCP) (Rossow et al., 1993). Part of this difference may have resulted from changes in the orbital characteristics of various satellites in the METEOR series.

According to these results, (Figure 14.1) cloudiness in 1992 was at its record lowest total of any year in the past 26 years of satellite observations. During 1993, global cloud cover increased slightly compared to the 1992 values, with the most pronounced increases occurring in the second half of the year. By November 1993, global monthly mean values equalled the normal for the period 1966 to 1985. Both the northern and southern hemispheres showed this relative increase in cloud cover in 1993.

Similar monthly analyses for the Northern Atlantic and Pacific Oceans (not shown) point out a decreasing trend in average cloudiness during the last half of the 1980s to 1992. On the other hand, cloudiness increased in 1993 to near normal values. ISCCP results do not, however, reveal these types of trends.

Figure 14.2 shows the time versus latitude variation in zonal average cloudiness anomalies for the northern and southern hemispheres from 1989 to 1993. Pronounced regional negative anomalies occurred in both hemispheres. Only Antarctica had persistent positive anomalies during the five years; however, even these were not large.

A map of the annual mean cloudiness anomaly (Figure 14.3) for the 12-month period December 1992 to November 1993 shows negative values across most of the globe except over Antarctica.

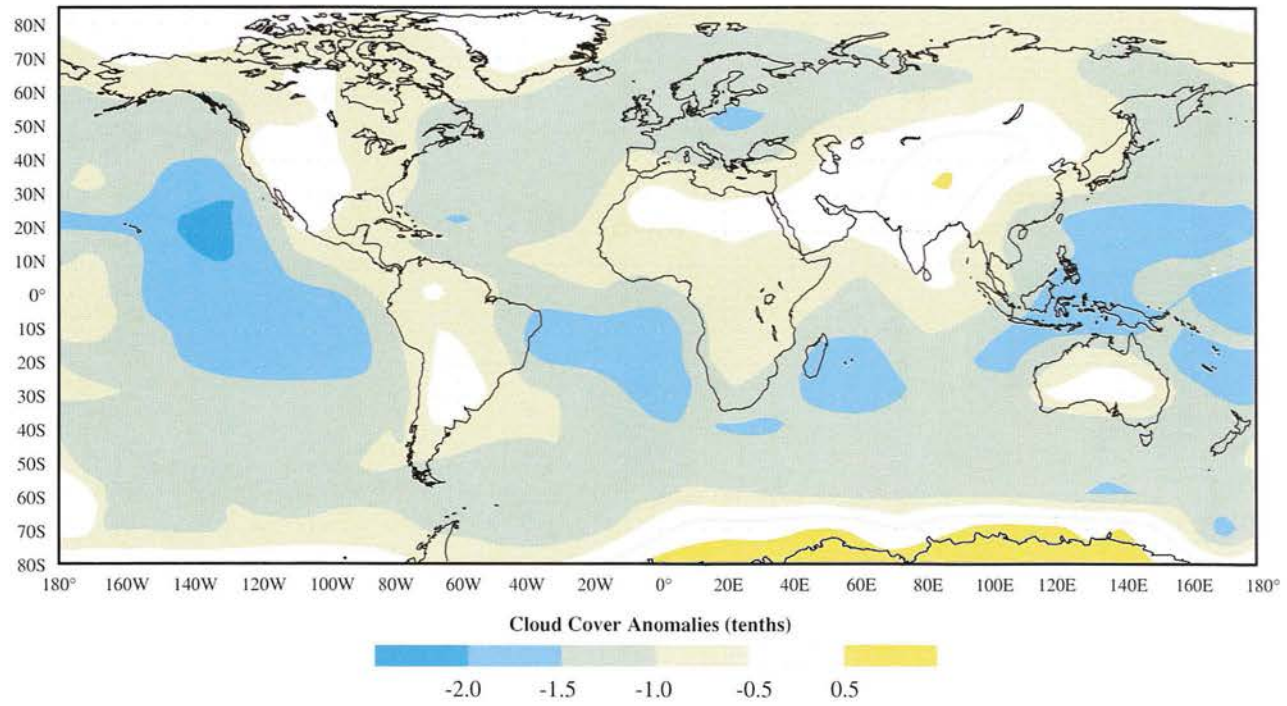

▲ *Figure 14.3* – Annual cloudiness anomalies for the period December 1992 to November 1993 based on the reference period 1966-1985, expressed in tenths (from Institute for Global Climate and Ecology, Moscow).

TROPICAL-EXTRATROPICAL INTERACTIONS IN THE SOUTHERN HEMISPHERE

Satellite imagery frequently shows extensive cloudbands extending from tropical to mid-latitudes over the southern hemisphere. Such bands are important channels of latent heat and moisture into higher latitudes and, significantly, form a major rain source for many subtropical and mid-latitude regions. In particular, tropical moisture is frequently transported to higher latitudes when tropical cloud systems link with mid-latitude fronts or depressions, often triggering widespread, heavy rain. Such "tropical-extratropical interactions" often take the form of long, continuous bands of cloud extending southeast from tropical convective areas; typically a north-south oriented band forms when a developing trough links a tropical cloud mass (associated with, e.g. thermally-induced convection, or an easterly wave) with a mid-latitude system.

Tropical-extratropical cloudbands and interactions occur in preferred locations and seasons. A very persistent band extends from near the Solomon Islands southeast to the mid-latitude South Pacific and is referred to as the South Pacific Convergence Zone (Vincent, 1994). This band is highly sensitive to ENSO, being displaced east of normal during Warm Pacific episodes and westward in the cold phase. Significant rainfall anomalies result over the South Pacific islands. Another important band extends in the Austral summer from the Amazon Basin region southeast to the central Atlantic (the South Atlantic Convergence Zone). This is a major rain-producer for southeastern South America and variations in its position and intensity can produce significant rainfall anomalies there. Over southern Africa, so-called "tropical-temperate troughs" link tropical cloud systems with mid-latitude disturbances. Such systems contribute the bulk of summer rain in inland areas - about 60% (Harrison, 1984) -and may generate major floods (Lindesay and Jury, 1991).

▲ Goes 7 Satellite image for July 28, 1993 at 1800Z showing frontal system and the occurrence of cyclogenesis during the episode (from CPTEC/Instituto Nacional de Pesquisas Espaciais, Brazil).

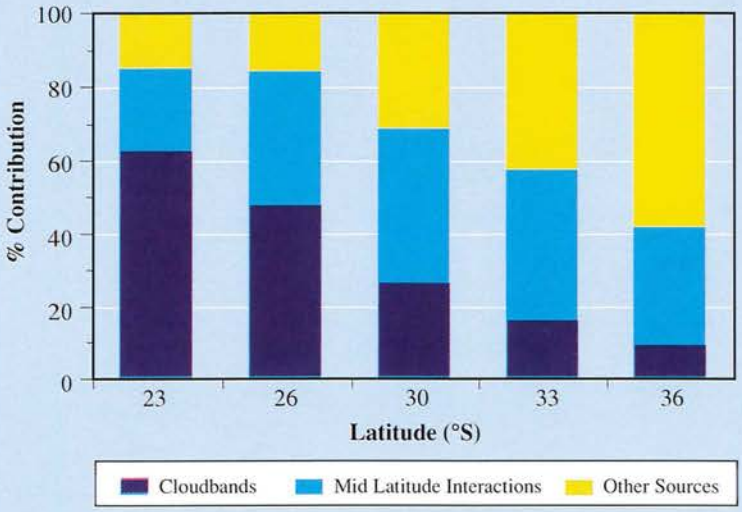

▲ *Figure 14.4* – Mean (1978–92) percentage contribution of tropical-extratropical cloudbands and midlatitude interactions to rainfall over eastern Australia, April through October, as a function of latitude (from National Climate Centre, Bureau of Meteorology, Melbourne, Australia).

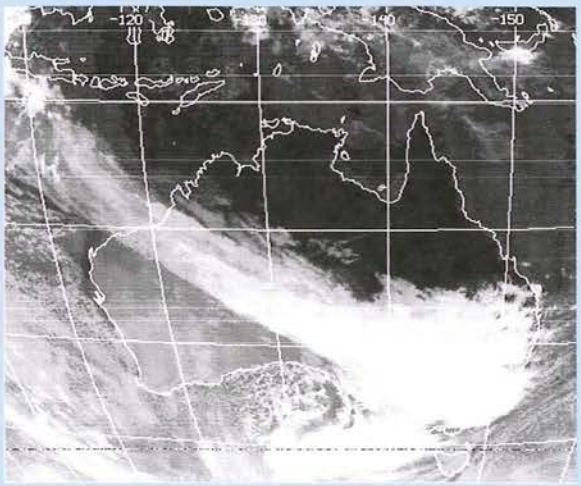

▲ A tropical-extratropical cloudband extends across central Australia and interacts with a midlatitude depression, August 29, 1992. Such systems produce valuable rains over inland Australia. Similar systems occur in many other parts of the Southern Hemisphere (from Bureau of Meteorology, Melbourne, Australia).

Similar systems produce heavy rain episodes over Australia and the Tasman Sea-New Zealand region (e.g. Hill, 1969). In Australia, they exert most influence in the agriculturally crucial period fall through spring. In late fall/winter, cloudbands extending from the adjacent tropical oceans occasionally produce rains of 50-100 mm over otherwise dry parts of western and cental Australia (see photograph). These account for over 80% of cool-season rain over northwestern Australia and about 50-60% over the northeast (Figure 14.4). Interactions involving either of these cloudbands, or (especially in spring) convective cloud systems over northern Australia, contribute much of inland eastern Australia's winter-spring rainfall. Rainfall from these interactions is greatly reduced during ENSO (Wright, 1993).

ABOVE-NORMAL WATER LEVELS IN LARGE LAKES AND INLAND SEAS

CHAPTER 15

Large lakes and inland seas serve as excellent indicators of climatic variability and change. With large surface areas and limited outflow capacity, large lakes filter out short-term variability and respond to longer term variations in the hydrologic cycle of precipitation, runoff and lake evaporation occurring over large regional basins.

15.1 NORTH AMERICAN GREAT LAKES

The Laurentian Great Lakes system comprises an area of 766,000 km^2 of which 246,000 km^2 are lake surface. It encompasses Lakes Superior, Michigan, Huron, St. Clair, Erie and Ontario. Because of their large size and storage capacities, and constricted outlet channels, the system is naturally well regulated and thus responds slowly to changes in water supply. Short-term variations in supplies usually have relatively minor effects on water levels. However, periods of six months or longer of consistently high or low supplies can cause noticeable changes in lake levels. As a result, the lakes historically fluctuate through a very small range in water levels, approximately 1.8 m from record lows to record highs.

In the period of this review water levels remained significantly above their long-term (1900 to 1991) average for lakes Michigan, Huron, Erie and Ontario and were near or slightly below long-term mean levels for Lake Superior. Figure 15.1 shows the long history of levels for lakes Erie and Superior.

The accumulated effects of the heavy precipitation from the 1992 summer and the subsequent winter, the severe ice and snow conditions in the St. Lawrence River and the record high water supplies in April 1993 combined to push Lake Ontario's level to the highest it had been since 1973. The early May 1993 level was within 10 cm of the record for the twentieth century that was set in 1952.

Great Slave Lake is located in the Northwest Territories of Canada. It has a basin area of 28,568 km^2, an elevation of 156 m and a mean depth of 614 m. As shown in Figure 15.1, the water level fluctuates through the same range as Lake Superior.

It has also continued to be at above average levels for the past several years.

The Great Salt Lake in Utah has a surface area of 4,360 km^2, an elevation of 1,280 m and a depth of 15 m. Water level anomalies are somewhat similar to those occurring in the Great Lakes. The lake has also continued at above average levels since its historic peak in 1986-87.

15.2 CASPIAN SEA LEVELS

The Caspian Sea is also considered to be a good indicator of climatic variability and change. During the last 60 years, there have been two periods of abrupt change in the levels of the Sea. The first was a dramatic drop in the 1930s (the lowest value was reached in 1934-39 when the sea level dropped 1.5 m in six years, i.e. by 20 to 30 cm per year) and the second was a rise after 1977 up to the present (in six years from 1978 the sea level rose by nearly 1 m and it has continued to a height of 2.05 m, with only an insignificant temporary decrease in 1989).

The main cause of the abrupt decline in the 1930s was a decrease in runoff, due to natural climatic variability. The contemporary increase in the Caspian Sea level is accounted for by the decrease in the difference between evaporation and precipitation, by a runoff increase and, to a certain degree, by the damming of the Kara Bogaz Gol (Bay).

In 1992-93, the rise in sea level continued, although at a somewhat slower pace as compared with 1991. Figure 15.2 illustrates the observed variations in the Caspian Sea level due to both natural factors (such as natural variations of runoff, precipitation, evaporation) and anthropogenic ones (such as the artificial regulation of runoff and the damming of Kara Bogaz Gol) since 1880. The same figure also depicts a model-computed sea level, using a detailed water balance equation, in an attempt to remove anthropogenically caused variations.

15.3 MURRAY-DARLING RIVER (AUSTRALIA) DISCHARGE

Figure 15.3 depicts the annual total and five-year running mean of discharge from Australia's

▼ *Figure 15.1* – Water level anomalies for lakes Erie and Superior, Great Slave Lake and Great Salt Lake (from NOAA, National Climatic Data Center, Asheville, NC).

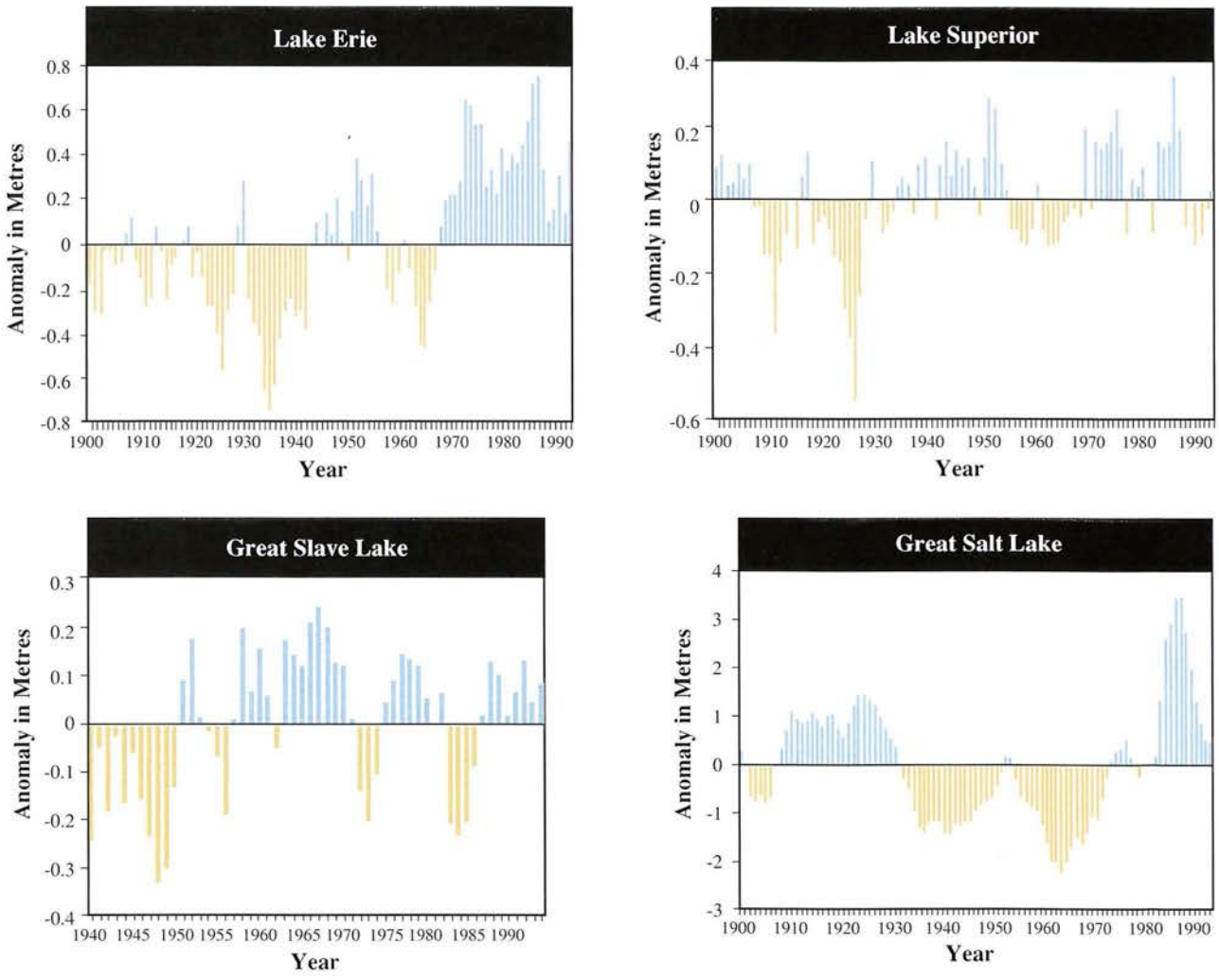

Murray-Darling river system at the Hume Reservoir for the period 1891-92 to 1992-93. The figure strikingly depicts the extreme interannual variability of the flows. Compare, for example, the difference in discharge between the 1914 and 1917 observations. For the period of this review, the values have been above the long-term mean, continuing a general upward trend in the past five or six years.

▼ *Figure 15.2* – Annual mean elevations (m) of the Caspian Sea for the period 1880 to 1993 (from All-Union Research Institute of Marine Fisheries and Oceanography and the Institute for Global Climate and Ecology, Moscow).

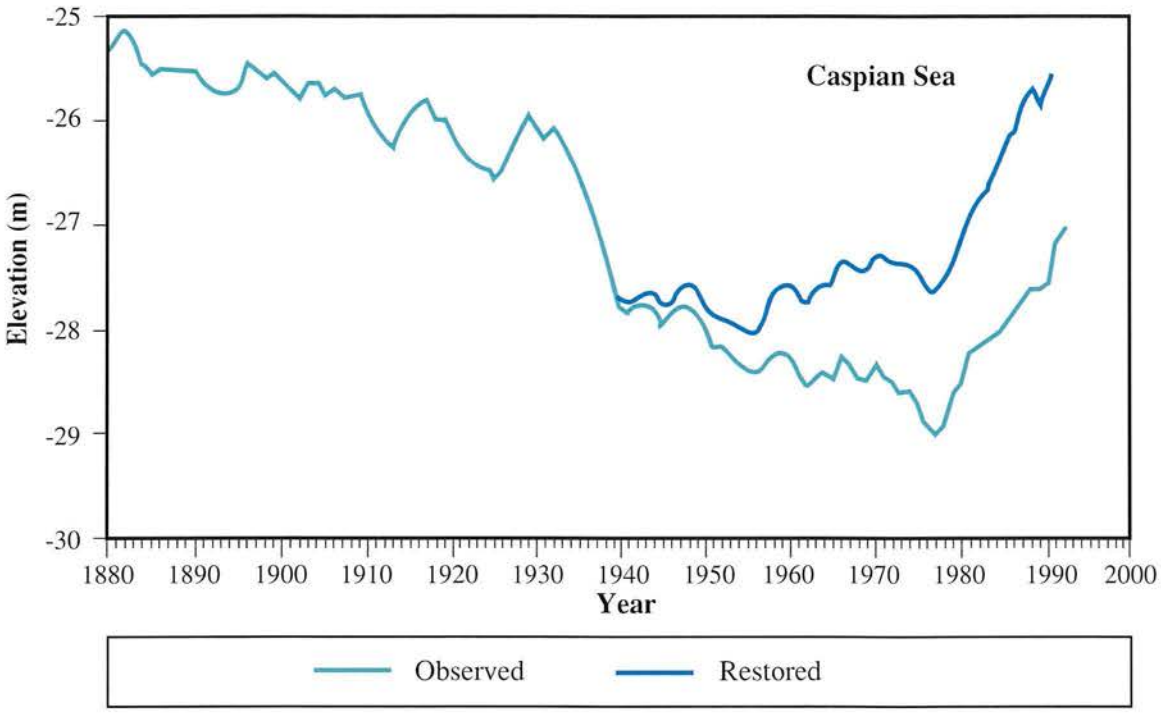

Figure 15.3 – Annual discharge (May-April) and five-year running mean discharge of the Murray-Darling river system at the Hume Reservoir 1891/92 to 1992/93. Values are in gigalitres (GL). A feature is the extreme interannual variability of the flows (compare, for example, 1914 and 1917) (from A. Close, Murray-Darling Basin Commission, Canberra and the National Climate Centre, Bureau of Meteorology, Melbourne, Australia).

▼

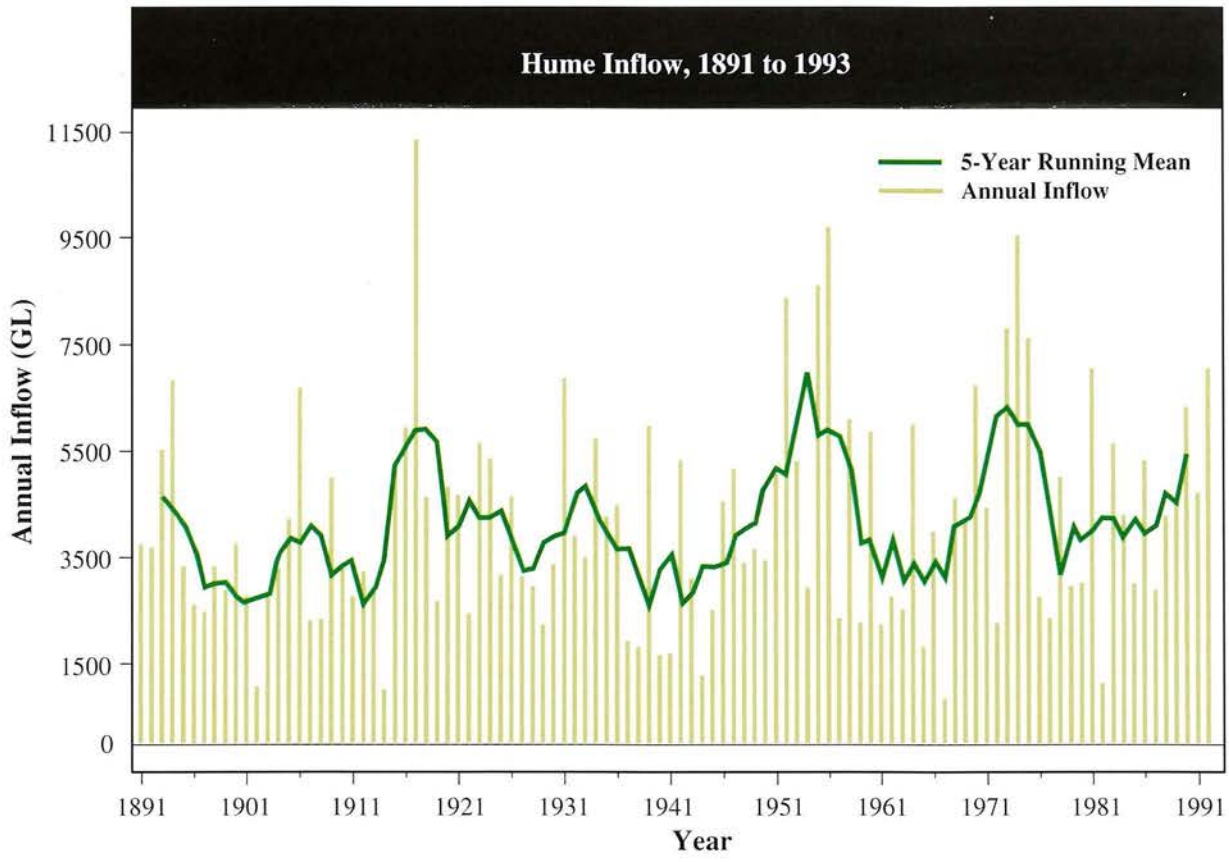

June - August 1991

1. Torrential monsoon rains inundated the southwest coast of India during early June including a two-day, 750 mm deluge at Bombay.
2. Unprecedented severe local storms in early June destroyed or damaged 3,300 dwellings and 250 public buildings in the Maldives.
3. Torrential rains in central Europe during the last two weeks of July caused the worst flooding in Austria in 30 years.
4. Abnormally dry weather in western Europe during August forced river barges to reduce their loads on the Rhine River in Germany.
5. Rainfall totals up to 700 mm from Typhoon Gladys in mid August left at least 11,000 people homeless in the southwest of the Republic of Korea.

September - November 1991

6. Typhoon Mireille, Japan's deadliest storm since 1971, smashed into western Japan in September taking over 50 lives.
7. Typhoons Orchid, Pat and Ruth affected the northwest Pacific during October with at least 44 deaths when Ruth struck Luzon.
8. Dozens of October and November low temperature records were shattered by an Arctic outbreak in western North America.
9. Ten weeks of dry weather across the North China Plain hampered autumn and winter planting in Shanxi and Shandong provinces.
10. Six tropical cyclones, of which 2 were super typhoons and 3 were typhoons, occurred over the northwest Pacific in November. This was twice the 31-year average.

December 1991 - February 1992

11. Wet weather persisted throughout the season in the southern USA. Days of heavy rains in Texas in December caused extensive flooding and US $75 million in damage.
12. Lack of adequate rain since early October and high temperatures in Zimbabwe killed thousands of cattle and scorched crops.
13. The 1991-92 eastern Australia rainy season started slowly with extensive dryness through mid January then, in February, some locations in Queensland received 250 to 325 mm of rain causing the worst flooding this century.
14. It was a brutal, cold winter in the Middle East and northern Africa with several winter storms, including one which dumped a 30 cm snowfall on Jerusalem in February.

March - May 1992

15. At the end of March, severe drought conditions plagued Sri Lanka as most regions had received less than 10 mm of rain since early January.
16. Severely dry weather persisted into March over much of western Europe and northwestern Africa. In Portugal, the dry spell was one of the worst this century, leaving reservoirs half empty and damaging fodder crops.
17. The 7-month (October - April) 1991-92 rainy season was exceptionally dry over much of southern Africa, damaging crops and forcing some nations to seek humanitarian aid.
18. Above normal temperatures that affected much of western North America since December continued into May causing an early snow melt.

June - August 1992

19. A tropical depression dumped up to 592 mm of rain on west central Florida in June producing some of the worst flooding this century.
20. Dry weather from May though July in north central Europe engendered numerous wildfires and damaged crops, particularly in Poland.
21. Unusually cold winter weather affected southern and western Brazil and southwestward through the rest of South America.
22. Warm summer weather in central and eastern Europe persisted to the end of August with temperatures rising to 39°C in Ukraine.
23. At least US $20 billion damage was caused by Hurricane Andrew which tracked through the northern Bahamas and Florida in late August.

CHRONOLOGICAL SUMMARY OF A CLIMATE ANOMALIES

CHAPTER 16

September - November 1992

24. In early Septemer, torrential monsoonal downpours in northern India and Pakistan produced landslides and catastrophic flooding.

25. The earliest snow in 16 years whitened Moscow and the heaviest snow for so early in the season since 1925 blanketed Stockholm as a blast of Arctic air swept through Scandinavia, the Baltics and northwestern Russia in mid October.

26. A few weeks of light to moderate precipitation in November brought an end to 33 weeks of dry weather over Greece and Turkey.

27. Extensive areas of the central interior of China received less than 25% of normal precipitation from mid September to mid November.

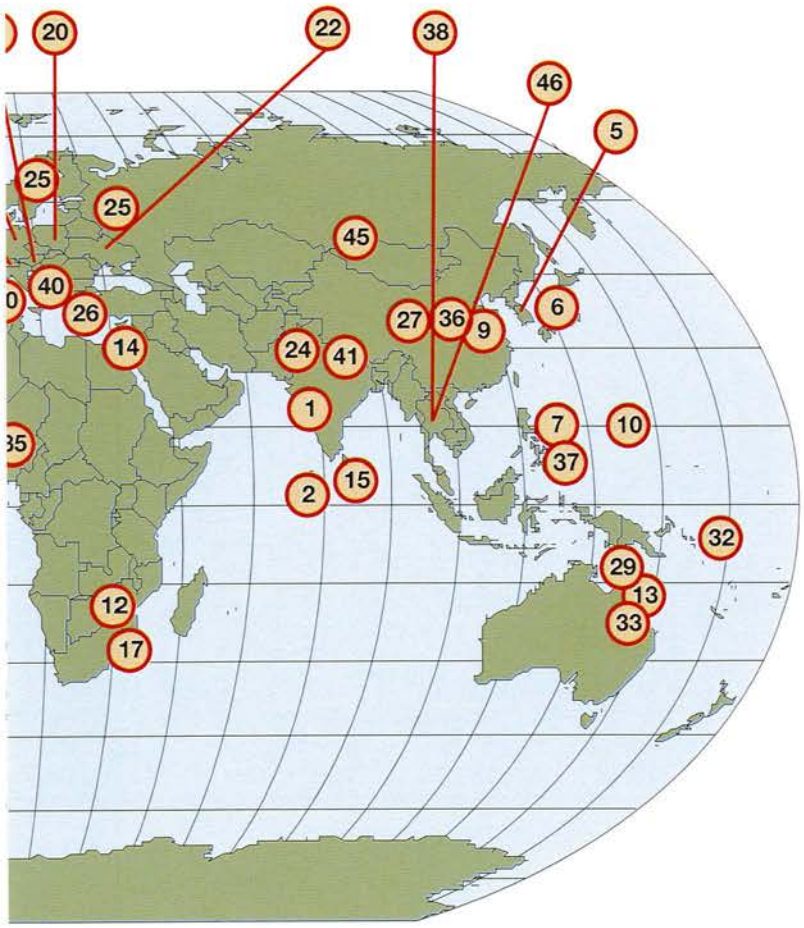

December 1992 - February 1993

28. December brought inundating rains to Bolivia and Argentina. A rain-triggered landslide took hundreds of lives in a Bolivian mining camp in mid December.

29. During the two weeks covering mid December, 500-700 mm of rain deluged parts of Cape York Peninsula in northeastern Australia.

30. After a stormy, rainy autumn,three months of dry weather afflicted central and western parts of the Mediterranean basin.

31. The drought in the far western USA was broken by copious amounts of winter season precipitation, exceeding 600% of normal in places.

32. February rainfall over east-central French Polynesia was three times the average.

March - May 1993

33. A dry March exacerbated rainfall deficiencies in eastern Queensland, Australia extending deficiencies to two years in some localities.

34. Wet weather afflicted the east coast of North America in March and April which included the "storm of the century" in mid March.

35. Exceptionally cold air during the last week of March dropped the temperature to 8°C in some areas near the Niger/Nigeria border.

36. Heavy rains at the end of April brought relief from an extended dry spell in east-central China with one hailstorm claiming more than 30 lives.

37. The end of May marked nearly three consecutive dry months across the Philippines.

June - August 1993

38. Well below normal precipitation in Thailand in June affected the nation's corn crop.

39. While record flooding affected the midwestern USA, abnormally hot and dry weather caused drought conditions in the southeast.

40. Hot and dry summer weather affected Italy, Greece and Bulgaria. The combinations of pollution and heat in June in Greece caused thousands to seek medical treatment.

41. Up to 535 mm of rain during the last week of July aggravated earlier severe flooding in Nepal which was the worst in 70 years and took as many as 12,000 lives.

42. Highs near 39°C at the end of August exacerbated dry conditions in northeast Argentina.

September - November 1993

43. Excessive amounts of rain fell in most of western Europe during September and October. More than 1000 mm of rain fell on parts of south central Switzerland, causing flooding.

44. Strong Santa Ana winds in southern California engendered more than a dozen wildfires at the end of October, destroying hundreds of homes and displacing more than 30,000 people.

45. Beginning in early November, exceptionally cold weather afflicted central Asia and eastern Europe with temperatures plummeting to -50°C in parts of northern Russian Federation and central Mongolia.

46. At the end of November, Typhoon Kyle dumped up to 350 mm of rain which caused severe flooding in Vietnam and northern Thailand.

WMO'S ROLE IN THE INTERNATIONAL DECADE FOR NATURAL DISASTER REDUCTION [1]

Professor G.O.P. Obasi,
Secretary-General
World Meteorological Organization
Geneva, Switzerland

Introduction

Natural disasters have menaced humankind since the start of history. Millions of lives have been lost in the countless cyclones, recurring earthquakes, frequent floods, droughts, volcanic eruptions and other extreme events that hit the globe repeatedly. Suffering, hardship, damage to property and loss of livelihood feature all too frequently in the aftermath of such natural disasters.

Probably more than three million people have been killed over the last 25 years by natural disasters, while a further one billion people have been adversely affected in some way. The analysis of disaster statistics compiled for the period 1967 to 1991 (Figure 17.1) indicates a rising trend in the number of people affected by natural disasters. Extreme meteorological and hydrological events account for 62% of all events recorded as natural disasters. If those associated with weather events, such as landslides and bush fires, are included, the percentage rises to 85%. Over the same period, about 3.5 million people were killed by meteorological and hydrological events, while about 2.8 billion were affected by them (Table 1). The cost of these disasters is enormous. There are social costs in terms of the affected population. There are economic losses too which rose globally from US$ 44 billion in 1991 to US$ 62 billion in 1992, an increase of 40%.

Developing countries are hit the hardest by natural disasters. Ninety percent of the deaths occurring from natural disasters are in developing countries. Vulnerable economies can be set back years and even by decades. When Hurricane David struck Dominica in 1979, the damage was so severe that its gross domestic product dropped by 20%. By 1983, it had not returned to the 1978 level. With a global average of 80 such tropical storms every year and about 100 potentially disastrous earthquakes, floods, tsunamis and volcanic eruptions, natural disasters threaten much needed sustainable development.

Sustainable development requires that we plan so that the needs of future generations can be met, while we satisfy those of the present generation. This challenge was addressed by the United Nations Conference on Environment and Development (UNCED) through the Rio Declaration and Agenda 21. It is a challenge of increasing importance, considering that the world population is growing rapidly and will probably reach 10 billion before the middle of the next century.

TABLE 1

TOTAL NUMBER OF EVENTS AND DEATHS FOR EACH TYPE OF NATURAL DISASTER 1967–1991.

TYPE	NUMBER OF EVENTS	NUMBER KILLED
a) Weather events		
Hurricanes, typhoons	894	896,063
Flood	1358	304,870
Storm	819	54,500
Cold and heat wave	133	4926
Drought	430	1,333,728
b) Associated with weather events		
Avalanche	29	1237
Landslide	238	41,992
Fire	729	81,970
Insect infestation	68	0
Famine	15	605,832
Food shortage	22	252
Epidemic	291	124,338
C) Geological		
Earthquake	758	646,307
Volcano	102	27,64
Tsunami	20	6390

[1] Adapted from presentations made by Professor Obasi at the Symposium on the International Decade for Natural Disaster Reduction, January 24, 1994 in Nashville, Tennessee and at the World Conference on Natural Disaster Reduction, May 23, 1994 at Yokohama, Japan.

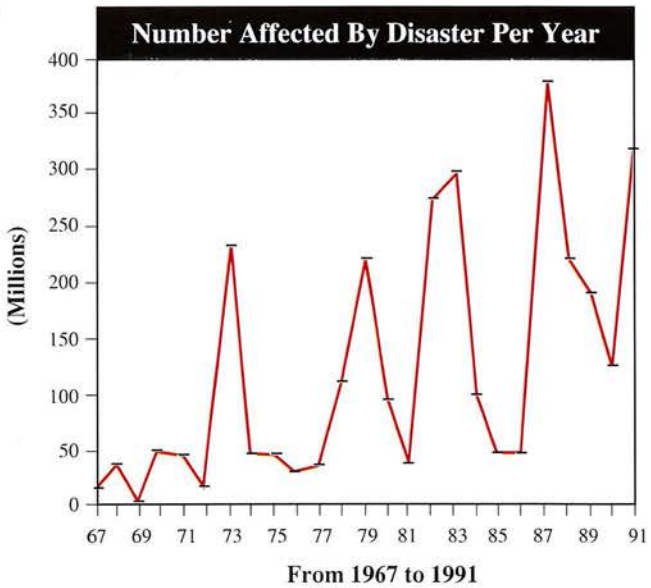

▲ *Figure 17.1* – Numbers affected by natural disasters per year, 1967-1991.

In other words, its objectives have been similar to those of the IDNDR. Consequently, WMO welcomed and has supported the Decade. Several of the Organization's ongoing programmes, such as the Tropical Cyclone Programme and the Operational Hydrology Programme, contribute directly to the Decade, but one responsibility places this Organization in a unique position for natural disaster reduction. It is our responsibility for the global weather system that operates in real-time. Through the World Weather Watch (WWW), the WMO collects, processes and exchanges meteorological and related environmental data, analyses and forecasts. It also makes available, in real and non-real time, analyses, forecasts and other products to meet the needs of its members, of other WMO programmes and of relevant programmes of other international organizations.

WWW includes the Global Observing System (GOS), Global Telecommunications System (GTS) and the Global Data Processing System (GDPS). It is probably the only truly global system, functioning continuously, day and night to reduce the impact of natural disasters on humankind. The WWW collects thousands of observations every hour from land, sea and air and from satellites in space to make forecasts. These forecasts come from a network of three world, 26 regional and 175 national centres.

The success of the WWW is vividly illustrated by the recent cyclone in Bangladesh. Only about 200 people were killed in May 1994 compared with 138,000 due to a similar cyclone in 1991. A government of Bangladesh spokesperson attributed this achievement principally to improvements in warning systems and evacuation, acknowledging the assistance of WMO to the former. Similar systems for countering other types of natural disasters are lacking. Clearly, the World Weather Watch has much to offer in concept and in practice to the remaining areas of geophysics and the different natural disasters they deal with.

WMO Programme for the IDNDR

Naturally, WMO has its own specific contribution to the Decade. This aims to improve risk assessment, to provide timely warnings, to reduce the impact of disasters on the population and to assess the degree of success of disaster reduction methods. This contribution includes three special projects and a fourth shared with the International Council of Scientific Unions. These projects are:

***1.** The tropical cyclone warning system for the southwest Indian Ocean region;*

***2.** Comprehensive Risk Assessment (CRASH) to promote a comprehensive approach risk management in order to enhance the effectiveness of efforts to reduce the loss of life and damage caused by natural disasters through the application of geographic information systems, remote sensing and results of seismic hazard studies;*

***3.** System for Technology Exchange for Natural Disasters (STEND) to identify and facilitate the transfer of available technology for use in reducing the adverse effects of natural disasters;*

***4.** The tropical cyclone disasters projects, in collaboration with ICSU, in order to improve prediction of tropical cyclones so that populations under threat may learn to rely on these predictions and consequently to follow measures recommended for their protection.*

These are practical projects designed to help save lives and reduce property damage, relying on the long-established sense of common purpose and cooperation between the Meteorological and Hydrological Services of the world and their dedication to the task of protecting the communities they serve. These projects also build on the fact that for many types of natural disasters we already know enough on how to mitigate them: the problem is to disseminate and apply what we know.

◀ Tornado 10 km northwest of Plainview, Texas (NOAA).

The Future

WMO intends to continue to provide its strong contribution to the IDNDR for the remainder of the Decade. At the end of the Decade, WMO would be very willing to shoulder such responsibilities that might be foreseen for the 21st Century. For example, a small secretariat might be needed to maintain the momentum of the Decade, which WMO would be willing to host. Another possibility is that the World Weather Watch might be expanded into a comprehensive disaster prevention system to combat all types of natural disasters. More lives could be saved and more damage avoided by an integrated approach to preparedness.

During the first half of the IDNDR, we have become better aware of the nature, impacts and implications of natural disasters, as well as the challenges that face humankind in the areas of natural disaster reduction and possible courses of action to mitigate their adverse effects. With this better awareness comes a greater responsibility to take the necessary steps to address the relevant areas of concern.

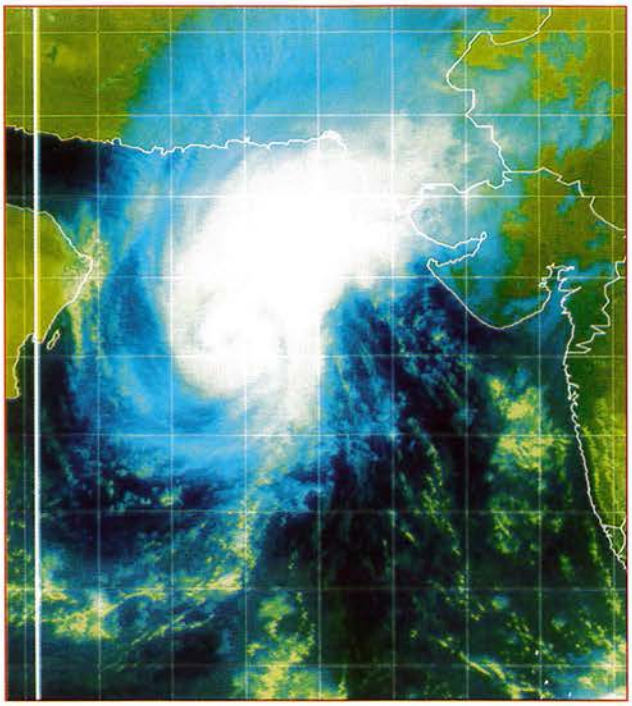

▲ INSAT2A cloud image on November 14, 1993 at 0600 UTC showing severe cyclone over Arabian Sea (from India Meteorological Department).

YOKOHAMA STRATEGY FOR A SAFER WORLD PRINCIPLES

1 - Risk assessment is a required step for the adoption of adequate and successful disaster reduction policies and measures.

2 - Disaster prevention and preparedness are of primary importance in reducing the need for disaster relief.

3 - Disaster prevention and preparedness should be considered integral aspects of development policy and planning at national, regional, bilateral, multilateral and international levels.

4 - The development and strengthening of capacities to prevent, reduce and mitigate disasters is a top priority area to be addressed during the Decade so as to provide a strong basis for follow-up activities to the Decade.

5 - Early warnings of impending disasters and their effective dissemination using telecommunications, including broadcast services, are key factors to successful disaster prevention and preparedness.

6 - Preventive measures are most effective when they involve participation at all levels, from the local community through the national government to the regional and international level.

7 - Vulnerability can be reduced by the application of proper design and patterns of development focused on target groups, by appropriate education and training of the whole community.

8 - The international community accepts the need to share the necessary technology to prevent, reduce and mitigate disaster; this should be made freely available and in a timely manner as an integral part of technical cooperation.

9 - Environmental protection as a component of sustainable development consistent with poverty alleviation is imperative in the prevention and mitigation of natural disasters.

10 - Each country bears the primary responsibility for protecting its people, infrastructure and other national assets from the impact of natural disasters. The international community should demonstrate strong political determination required to mobilize adequate and make efficient use of existing resources, including financial, scientific and technological means, in the field of natural disaster reduction, bearing in mind the needs of the developing countries, particularly the least developed countries.

HOW THE INTERNATIONAL CLIMATE ORGANIZATIONS AND PROGRAMMES FIT TOGETHER

Dr J.W. Zillman
President of World Meteorological Organization, Director of Meteorology Bureau of Meteorology Melbourne, Australia

As is the case for operational weather forecasting, international cooperation has always been essential for the study of climate and the provision of climatological services. Much of the early history of international cooperation in meteorology was based on the need for coordination and standardization in climatological measurement and monitoring. When the World Meteorological Organization (WMO) was established in 1950, it inherited from its non-governmental predecessor, the International Meteorological Organization (IMO), an active Commission for Climatology (CCl) which, with various name changes, provided the principal mechanism for intergovernmental coordination of climate matters until the late 1970's.

With the increasing recognition of the pervasive influence of climate on virtually all aspects of human activity that led to, and was further enhanced by, the (First) World Climate Conference and the establishment of the World Climate Programme (WCP) in 1979, the number of players on the international climate scene began to increase rapidly with special foci, in line with the four major thrusts of the WCP, on climate data, research, impacts and applications to water resources, energy, agriculture and a range of other socio-economic sectors. Within the United Nations (UN) system, the Food and Agriculture Organization (FAO), the United Nations Educational Scientific and Cultural Organization (UNESCO) and the United Nations Environment Programme (UNEP), in particular, took up key aspects of the climate issue, the non-governmental International Council of Scientific Unions (ICSU) joined WMO in co-sponsorship of the research component of the World Climate Programme and a number of countries instituted national climate programmes involving agencies with links into other international organizations, which, in turn, soon took up aspects of the climate issue relevant to their respective fields of responsibility.

The international institutional climate arrangements became still more complex and more interlinked, following the rise of the greenhouse issue during the 1980's, with ICSU's 1986 establishment of the International Geosphere-Biosphere Programme (IGBP), the 1988 establishment of the joint WMO- UNEP Intergovernmental Panel on Climate Change (IPCC) and the UN General Assembly's response to the 1987 Brundtland Commission report including its decision to convene the 1992 United Nations Conference on Environment and Development (UNCED) for which a Framework Convention on Climate Change (FCCC) soon emerged as a potential centrepiece. The developments of the early 1990's, including the 1990 Second World Climate Conference, the restructuring of the World Climate Programme and the establishment of the Global Climate Observing System (GCOS) by the Eleventh World Meteorological Congress in 1991, the convening of the April 1993 Intergovernmental Meeting on the World Climate Programme and the entry into force of the FCCC in March 1994, added further major players to the web of international organizations dealing with the various aspects of climate.

Although many dozens of international organizations are now significantly involved in climate matters in one way or another, it is appropriate, for present purposes, to single out the following:

- *The World Meteorological Organization (WMO), an independent intergovernmental organization which is responsible, under its Convention, for a wide range of activities related to weather and climate and which, by agreement with the United Nations, also serves as the UN Specialized Agency for meteorology and operational hydrology. WMO is responsible for international coordination of climate monitoring, research and applications and for providing an authoritative international scientific voice on matters related to climate change. Its principal subsidiary body for dealing with climate matters is its Commission for Climatology on which all Member countries are entitled to be represented by national climate experts;*
- *The United Nations Environment Programme (UNEP) which is the main UN programme dealing with climate issues with particular responsibility for climate impact and response issues and associated activities in relation to ozone layer depletion and desertification;*
- *The joint WMO-UNEP Intergovernmental Panel on Climate Change (IPCC) which was established in 1988 to provide a broadly based assessment of knowledge of the science, impacts and response strategy options for dealing with climate change and which continues in existence as the principal international assessment mechanism in respect of human-induced climate change;*
- *The United Nations Educational Scientific and Cultural Organization (UNESCO) and especially its Intergovernmental Oceanographic Commission (IOC) which shares with WMO the intergovernmental responsibility for oceanographic aspects of climate science;*
- *The Conference of the Parties (COP) to the Framework Convention on Climate Change (FCCC) which held its First Session in Berlin in March-April 1995 and especially its Subsidiary Bodies for Scientific and Technological Advice (SBSTA) and for Implementation (SBI).*

Similarly, although many different international programmes have been formulated to deal with climate and climate related activities, the following are of special significance:

- *The World Climate Programme (WCP) which provides the international framework to assist countries to apply climate information and knowledge for economic and social benefit and for the achievement of sustainable development and the implementation of the UNCED Agenda 21. Following its restructuring by the 1991 World Meteorological Congress, it has four separate components as follows:*
  - *World Climate Data and Monitoring Programme (WCDMP),*
  - *World Climate Applications and Services Programme (WCASP),*
  - *World Climate Impact Assessment and Response Strategies Programme (WCIRP),*
  - *World Climate Research Programme (WCRP),*

  and, in response to the 1993 Intergovernmental Meeting on the WCP, is being developed along four main thrusts associated with: dedicated observations of the climate system; climate services for sustainable development; studies of climate impact assessments and response strategies to reduce vulnerability; and new frontiers in climate science and prediction. It is under the leadership of WMO with co-sponsorship by several other international organizations. Overall coordination is provided by the Executive Heads of the sponsoring agencies and the Coordinating Committee for the WCP (CCWCP) with each of the component programmes having its own planning and coordinating body and consisting of a number of major projects, activities and experiments;
- *The International Geosphere-Biosphere Programme (IGBP) which complements the primarily physical science-based WCRP in dealing with chemical and biological aspects of climate change. It is an interdisciplinary research effort designed to describe and understand the interactive physical, chemical and biological processes that regulate the earth, the unique environment that it provides for life, the changes that are occurring and the manner in which they are influenced by human activities. The IGBP, which is a non-governmental ICSU programme under the leadership of the Scientific Committee for the IGBP (SC-IGBP) is built around a number of core projects;*
- *The Human Dimensions of Global Environmental Change Programme (HDP) which, though not yet well established internationally, is intended to provide a social science complement to the WCRP and IGBP by serving as a framework for describing and understanding the human role in causing global change and the consequence of such change for society;*
- *The Global Climate Observing System (GCOS) including the climate-related elements of the Global Ocean Observing System (GOOS) and the Global Terrestrial Observing System (GTOS), which is built upon existing global climate observing systems such as the WMO World Weather Watch (WWW), the joint WMO-IOC IGOSS (Integrated Global Ocean Services System), the IOC Global Sea Level Observing System (GLOSS), the WMO Global Atmosphere Watch (GAW) and other existing and proposed programmes. GAW is closely associated with and underpins, but is not formally a part of, the WCP.*

The present situation thus involves a host of international organizations and programmes, both governmental and non-governmental, dealing with many different, but interacting, aspects of climate. While it is clearly not possible to describe or depict the separate roles of all the relevant international organizations and programmes and their interlinkages in a short article, it may, nevertheless, be useful to attempt to present the "big picture" to assist in setting the various individual organizations and activities in their broader context.

As the framework for a simplified view of the big picture, it is instructive to view the essential elements of the climate issue from three different perspectives as follows:

- *the main components of the climate system:*
  - *atmosphere,*
  - *ocean,*
  - *land;*
- *climate variability (in the sense of natural variability) and change (in the restricted sense of human-induced change in which it is used in FCCC circles) as a component of the larger set of issues associated with global environmental change (in its broadest sense);*
- *the various aspects of the climate issue now receiving attention through international organizations and programmes which may usefully be grouped as follows:*
  - *observation (i.e. data collection) which underpins virtually everything else;*
  - *monitoring (i.e. description of the current state of the climate system or its component parts or regions);*
  - *applications (to problems of food, water, energy, etc.) and services (data, information, advice, etc.);*
  - *understanding (i.e. research) projections (decadal and longer time scales) and prediction (on a range of timescales from seasonal and interannual);*
  - *impact assessment and development of response strategies; and*
  - *implementation of strategies for protection of the global environment.*

Figure 1 shows the domain of responsibility of several of the key climate organizations and programmes on the matrices represented by the intersection of the first and second of these groupings with the third. The various acronyms are as described above.

Figure 2 provides a simplified depiction of some of the main interrelationships in organizational terms including especially the formal lines of reporting for the main planning/coordinating bodies which have been assigned responsibility for the various programmes and subsidiary bodies. Many other organizations and programmes are, of course, involved and each of the

components of the World Climate Programme has itself a detailed substructure. The Global Climate Observing System (GCOS) is shown as underpinning the activities of the World Climate Programme (WCP) and is itself built upon a number of existing global observational programmes.

▼ *Figure 1* – The general domain of responsibility of a number of international climate and global change programmes and organizations.

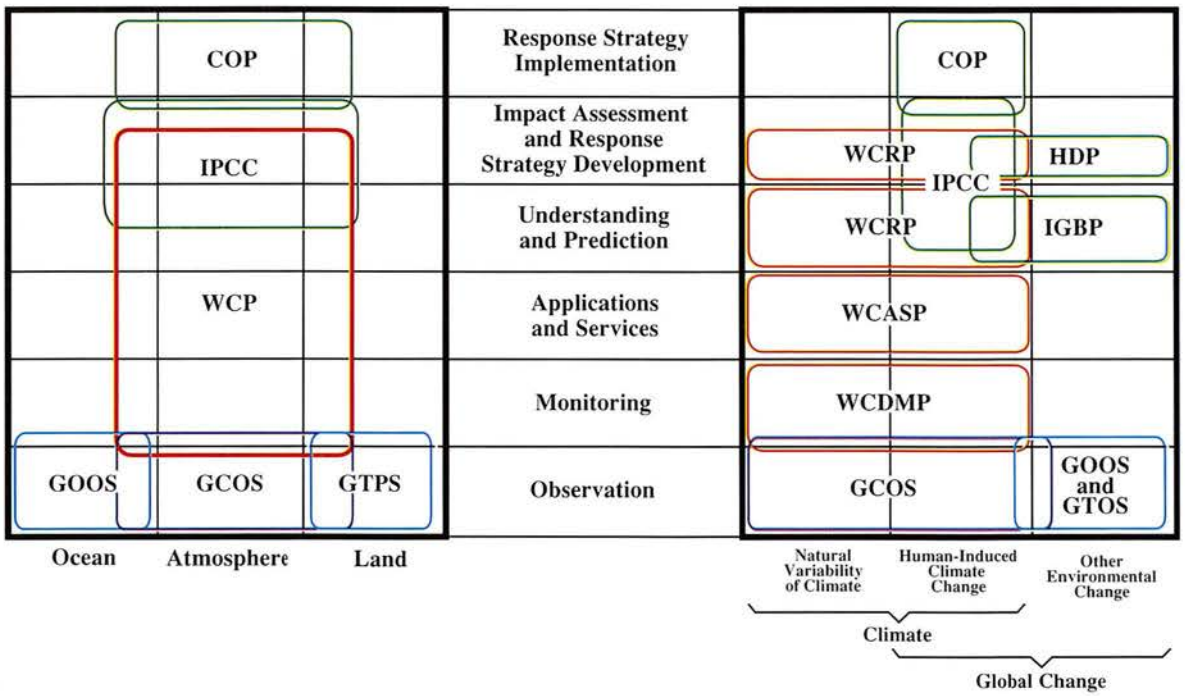

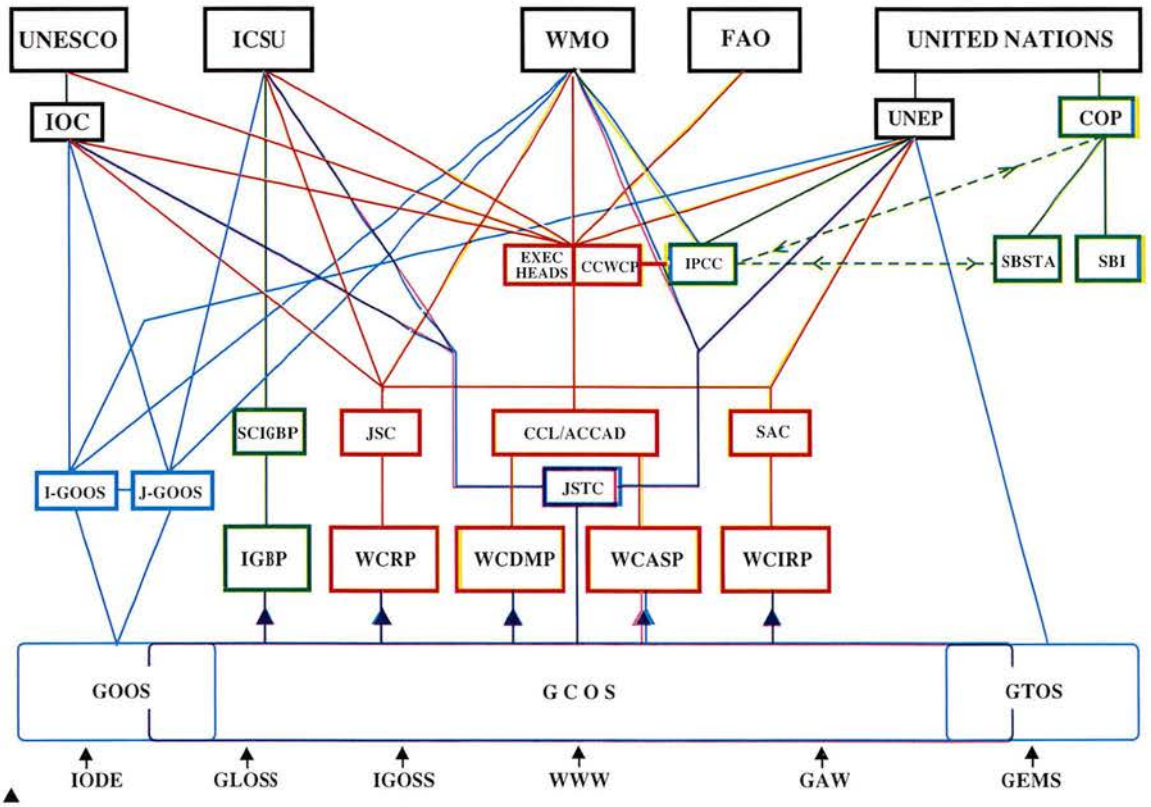

Figure 2 – The main international organizations and programmes involved with climate issues and their respective lines of formal reporting (solid) and communication (broken). The World Climate Programme (WCP) and its components are shown in red, the various bodies dealing with climate change and global change in green and the underpinning global observing systems are shown in blue.

The individual organizations and programmes are as follows:

ACCAD	Advisory Committee on Climate Applications and Data
CCl	WMO Commission for Climatology
CCWCP	Coordinating Committee for the World Climate Programme
COP	Conference of the Parties to the Framework Convention on Climate Change
FAO	Food and Agriculture Organization of the UN
GAW	WMO Global Atmosphere Watch
GCOS	Global Climate Observing System
GEMS	UNEP Global Environmental Monitoring System
GLOSS	IOC Global Sea-Level Observing System
GOOS	Global Ocean Observing System
GTOS	Global Terrestrial Observing System
IGBP	International Geosphere-Biosphere Programme
IGOSS	WMO-IOC Integrated Global Ocean Services System
I-GOOS	Intergovernmental Committee for the Global Ocean Observing System
IOC	Intergovernmental Oceanographic Commission of UNESCO
IODE	International Oceanographic Data and Information Exchange
IPCC	Intergovernmental Panel on Climate Change
ICSU	International Council of Scientific Unions
J-GOOS	Joint Scientific and Technical Committee for the Global Ocean Observing System
JSC	Joint Scientific Committee for the World Climate Research Programme
JSTC	Joint Scientific and Technical Committee for the Global Climate Observing System
SAC	Scientific Advisory Committee for the World Climate Impact Assessment and Response Strategies Programme
SBI	Subsidiary Body for Implementation
SBSTA	Subsidiary Body for Scientific and Technological Advice
SCIGBP	Scientific Committee for the IGBP
UN	United Nations
UNEP	United Nations Environment Programme
UNESCO	United Nations Educational, Scientific and Cultural Organization
WCASP	World Climate Applications and Services Programme
WCDMP	World Climate Data and Monitoring Programme
WCIRP	World Climate Impact Assessment and Response Strategies Programme
WCRP	World Climate Research Programme
WMO	World Meteorological Organization
WWW	World Weather Watch

THE GLOBAL CLIMATE OBSERVING SYSTEM, GCOS[2]

Dr Douglas M. Whelpdale
Atmospheric Environment Service
Environment Canada
Downsview, Ontario, Canada

Background

The Global Climate Observing System was established after the Second World Climate Conference in 1990 to ensure the acquisition of global observations required to meet needs for:

- *Climate system monitoring, climate change detection and response monitoring, especially in terrestrial ecosystems;*
- *Data and information for application to national economic development;*
- *Research toward improved understanding, modelling and prediction of the climate system.*

Observations are to be made for the atmosphere, the oceans, the land surface, the cryosphere and the biosphere, using both surface-based and space-based observing methods. GCOS will also include a comprehensive data acquisition and management system. The first priorities for GCOS are to coordinate and facilitate the critical observational tasks necessary to address the principal climate science and application issues, such as seasonal and interannual climate prediction, early detection of climate trends and change due to human activities and the reduction of the major uncertainties in climate prediction.

Scientific Planning

GCOS is sponsored by the World Meteorological Organization (WMO), the Intergovernmental Oceanographic Commission (IOC) of UNESCO, the United Nations Environment Programme (UNEP) and the International Council of Scientific Unions (ICSU). The overall concept and scope of the GCOS is being formulated under the guidance of the Joint Scientific and Technical Committee (JSTC), which is responsible for identifying requirements, defining design objectives and recommending coordinated actions. The Committee is supported by the Joint Planning Office (JPO) in Geneva, Switzerland at the Headquarters of the WMO.

GCOS is a phased programme, building upon existing observational activities of operational and research programmes of participating countries, such as those coordinated by the WMO for the atmosphere. Many of the observations being made for numerical weather prediction also meet requirements for climate. Close cooperation with ongoing WMO programmes such as the World Weather Watch, the World Climate Programme and the Global Atmosphere Watch will continue to ensure international coordination. Based on requirements and current capability, and in concert with existing programmes, recommendations are being developed for enhancements and new observations to ensure that climate needs are met.

In a similar fashion for the world oceans, the JPO is cooperating with the IOC in efforts to establish a Global Ocean Observing System (GOOS). For the GCOS programme, the key issue will be to ensure that long-term, routine, globally-relevant, scientifically-based and systematic measurements from the ocean are obtained. Requirements for climate monitoring and for climate modelling are being developed in concert with the Ocean Observation System Development Panel (OOSDP). The JSTC will review these requirements and transmit them to appropriate organizations for implementation.

For the land surface, the JPO is participating actively in the planning and development of the Global Terrestrial Observing System (GTOS) now being established by several international organizations, including the four who sponsor GCOS and FAO. GTOS is being designed to meet the needs for comprehensive information from both natural and managed ecosystems. For the GCOS programme, the key issue will be to ensure that the components of the terrestrial system which are required for climate monitoring and for input into climate models for validation and prediction are obtained. However, GCOS also has the objective to address impacts of climate change, particularly on terrestrial ecosystems, and will cooperate with GTOS to develop plans to obtain appropriate data.

Building Upon An Operational System

The GCOS Plan outlines a comprehensive development strategy. It proposes an Initial Operational Observing System, which is to consist of currently operational elements, necessary enhancements, which may be identified at this time, and a comprehensive data management system. The first step in the strategy focuses on the essential ingredients of the initial system and, for this, inputs have been solicited from the community at large. Secondly, an assessment of current capabilities is being made to indicate resources already committed and observational products already available. Comparisons between the requirements and available data will indicate where priority is to be placed. The result will be a suite of specific recommendations to be presented to appropriate bodies for implementation. In the GCOS Plan, a number of enhancements to existing systems were identified and specific actions have been proposed to implement them.

[2] Adapted largely from Whelpdale, 1994 and from published materials available from the IPCC and GCOS.

The following are examples of some of the currently operational components of GCOS:

- *The World Weather Watch (WWW)*
- *The Global Atmosphere Watch (GAW)*
- *The Integrated Global Ocean Services System (IGOSS)*
- *The Global Sea Level Observing System (GLOSS)*
- *The Global Environmental Monitoring System (GEMS)*
- *Hydrosphere measurements*
- *Cryosphere measurements*
- *Research programmes*

To satisfy climate system requirements, the current operational components will need substantial enhancement and in many cases, new components will have to be added. Many of the recommended enhancements aim to ensure the long-term continuity of satellite observations from instruments now planned, or developed as research instruments on one-time missions, but which will provide data of demonstrated value for operational climate work. Other enhancements include increasing numbers of sites, stations and buoys as expansions to existing networks, increasing ranges of measurements at existing stations, extending the geographical coverage where essential and improving the accuracy of measurements. Examples of such enhancements include:

- *Closing gaps in the coverage of polar orbiting satellites*
- *Increasing the number of WWW stations in remote areas*
- *Making permanent the TOGA moored array network and upper air stations*
- *Enhancing the network of drifting buoys in data-sparse areas*
- *Vertical water vapour distribution from multi-spectral microwave instruments*
- *Satellite measurements of stratospheric aerosols*
- *Enhanced observations of column ozone, particularly in tropical areas*
- *Measurements from VOS, drifting buoys and moored arrays in regions with inadequate satellite coverage*
- *Routine fields of the fraction of photosynthetically-active radiation (FPAR)*
- *Continuation of experimental 1-km AVHRR data on land-cover condition*
- *Improvements in precipitation and runoff networks; use of modern data collection, transmission and dissemination systems*
- *Monitoring iceberg discharge with high-resolution visible and infrared imagers and SAR.*

Examples of new operational components are:

- *Microwave scatterometers for ocean-surface wind velocities*
- *Wind stress derived from microwave scatterometers*
- *Use of space-based observations to develop operational techniques for soil moisture and roughness*
- *Occasional altimeter missions (in near-90 degree orbit) to measure crucial circumpolar regions of the Antarctic ice sheet.*

Data Management System

One of the key elements of GCOS will be a comprehensive global data management system to address the full range of data issues, such as: data collection, metadata, quality control, assimilation, distribution, archiving, final disposition and utilization of all data relevant to GCOS. The data management strategy calls for a reliance upon existing programmes and institutions, the use of international standards, and constant monitoring and evaluation of the system. Such a system will eventually be an international system of distributed databases which provide for effective end-to-end management of all data pertinent to GCOS. The system will ensure that:

- *All required data are collected in a consistent manner;*
- *Data are subject to rigorous quality control procedures;*
- *Products needed to meet GCOS requirements are developed and routinely produced;*
- *All GCOS-relevant data and products are stored in suitable archives;*
- *All data and products are easily accessible at the lowest possible cost.*

The Task Ahead

The development of the detailed observational requirements has been guided by the priorities determined by the JSTC. Specific technical details, (sampling, coverage, resolution, spatial and temporal issues, accuracy and precision) are being compiled and measurement options being evaluated. Action proposals will be presented to appropriate organizations, national agencies and consortia. WMO programmes will be expected to help meet GCOS requirements for meteorological and hydrological observations, communication networks, modelling activities and data management. For oceanographic requirements, the primary providers will be appropriate bodies of the IOC. In particular, GCOS oceanic observational needs will be developed in cooperation with the International Committee for GOOS (I-GOOS). Since there will be a strong emphasis on the use of space-based observations for GCOS, requirements will be presented to space agencies for action, through the Committee on Earth Observations Satellites (CEOS).

Sharing Observations for All to Benefit

To meet its objectives, GCOS must rely on national contributions from a wide range of disciplines. The system should eventually operate as a coordinated entity so that data stored at many different sites are accessible as if stored in a single location.

Developed and developing countries will be involved

equally and both will derive benefits. For developing countries, GCOS will actively support capacity building and training activities.

The development of GCOS both internationally and nationally should lead to a number of opportunities for cooperating countries and agencies.

Examples are:

- *To make data more accessible and data management systems more responsive, for both national and international users;*
- *To evaluate the merit of a more integrated approach to climate data management, i.e. to include, for example, data from agriculture, forestry, the insurance industry, in addition to those from atmosphere, ocean and terrestrial ecosystem networks;*
- *For industry to provide instruments, communications equipment and expertise for GCOS observing systems.*

AN INITIAL OPERATIONAL SYSTEM

The first step in the development of GCOS is to define and develop an initial operational system which will include:

- The currently operational components
- The enhancements to the current operational components for which the technology is proven,
- A comprehensive global data management system.

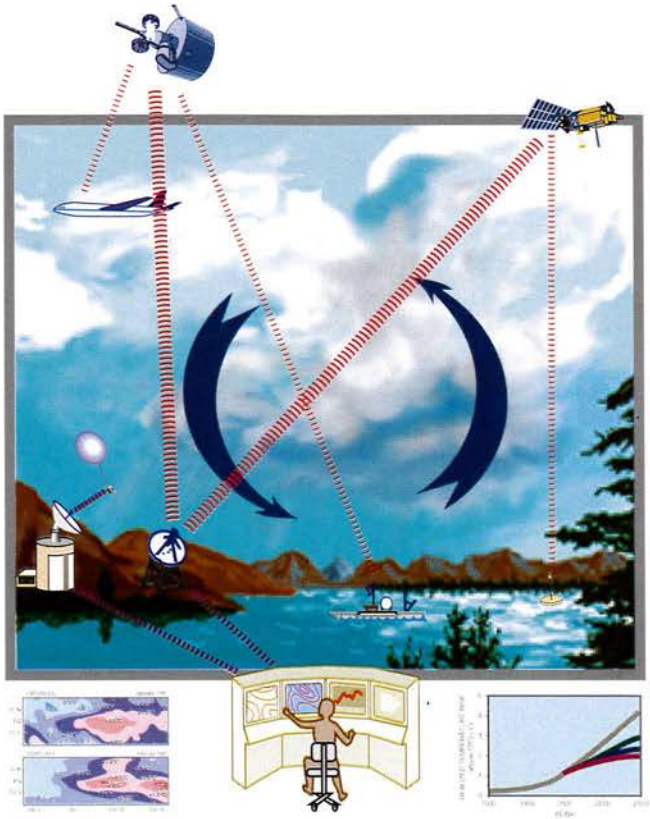

To meet its objectives, GCOS must rely on national contributions. Developed and developing countries should be involved equally; both should derive benefits. For developing countries GCOS will actively support capacity building and training activities.

METADATA AND ITS IMPORTANCE TO CLIMATE MONITORING

Michael Crowe[3]
Climate Perspectives Branch
National Climatic Data Center
Asheville, NC

All communication among people is performed within a certain context of understanding. The more aware that the communicating parties are of this context, the more efficient and valuable the communication process becomes. Much of the time the context is understood, but sometimes this understanding can be erroneous and lead to mistakes and confusion. For example, a European, if hearing that the temperature in Paris in November was 60° would assume the scale used was Celsius and quickly understand that someone was in error. However, to a resident of the USA, who is used to the Fahrenheit scale, that report would be well within acceptable limits. Each assumed a certain context of this report and one was mistaken.

Metadata, which may be loosely defined as data, or information, describing other data, is often critical in defining the context of information and thus in avoiding mistakes such as the one described above. Within the scientific context of monitoring the climate system, we can narrow the scope of metadata by considering our data as that which were observed or sensed by an observer or instrument, or derived from such observations, and our metadata as information directly relating to the observations and explaining how the data have been subsequently processed. Therefore, for in situ

[3] The author wishes to acknowledge the assistance of Dr Raino Heino, CCl Rapporteur on Metadata and Archival Survey for Climate History, and Chief Climatologist with the Finnish Meteorological Institute.

Metadata and Global Baseline Data Sets

The development of research quality global baseline climatological data sets is an important part of the World Climate Data and Monitoring Programme (WCDMP) of the WMO. The National Climatic Data Center in the USA is contributing to the development of the Comprehensive Aerological Reference Data Set (CARDS) to this effort. In the production of this high quality data set of long-term, daily, upper air observations, CARDS is both using and generating metadata, and these functions are essential to ensure the integrity of the final product. Metadata is inextricably woven into each of the six major components of the CARDS project:

1) The production of the long-term daily upper air data set. The final data set will be comprised of contributions from many countries which were received in varying formats. CARDS developed a standard format which it uses. The format itself and its description are invaluable pieces of metadata.
2) The development of algorithms to correct and flag errors. These algorithms and the associated flags are metadata.
3) The assessment of the homogeneity of the data and corrections for biases. The assessment and correction techniques are described in the peer-reviewed literature and are made available as metadata to researchers.
4) Analysis of data to help ensure against errors and biases. The analysis techniques will be described as part of the rich collection of metadata for CARDS.
5) Development of software for the operational ingest of future data into the CARDS database. Metadata will be generated which will describe the volume and source of the data received and processed.
6) Distribution of data to the research user community. The CARDS data set must be carefully inventoried so that users will know the spatial and temporal extent of the data. This inventory is a crucial piece of metadata.

Finally, one of the most important sets of metadata for CARDS will be the station history information (Figure 1). Information concerning the location, identification, observational practices and instruments used at each of the observing sites throughout history is being compiled.

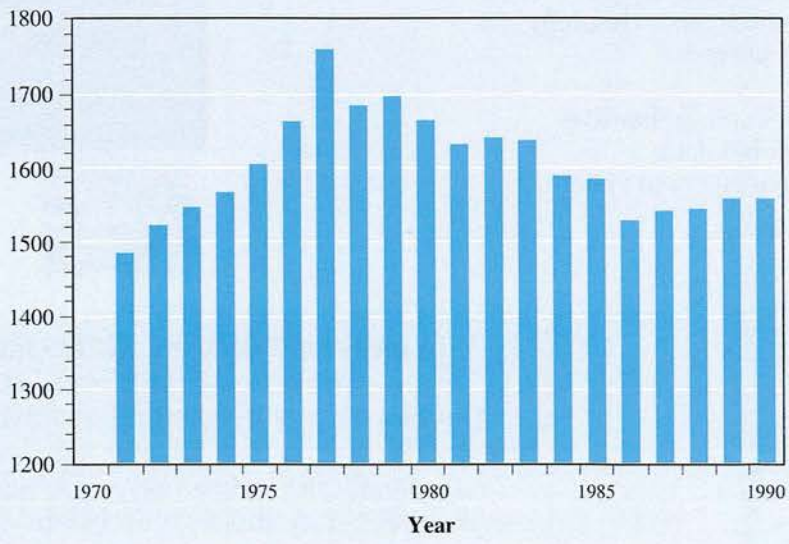

Figure 1 – The number of stations taking upper air observations according to the CARDS station history, Version 2.0. ▶

data, metadata may be the latitude, longitude and elevation of an observing site, the type and specifications of instruments used to observe the different variables or the technique used to calculate the average daily temperature. As data are collected and synthesized for climate purposes, the metadata would include how a data set is formatted and what geographical area and time period it represents.

With remotely sensed data, such as satellite retrievals, the data in its rawest form is an electrical voltage, which is then converted to a meteorological parameter using pre-calculated calibration coefficients. In this case, the observed value is the voltage and the calibration coefficients are metadata. Most users of the data would only have the calibrated observed parameter to use. But if there was an error in the coefficients, either they or the raw data or both must be saved in order to recreate the original sensor value.

To perform scientific analysis and research, metadata is invaluable and should be easily and routinely available. For scientists studying climate variability and change, metadata must be available for entire data sets containing long-term retrospective data. Long-term changes due to real causative, and factors have been (and probably will be) small and slow and are hidden under large year-to-year variability. Climatic records are normally mixtures of both apparent and real variations. Various factors, such as changes in instruments and their exposures, observation times and averaging methods, and observation sites and their environments introduce biases, or inhomogeneities into the data. There are some statistical methods available which are useful in detecting the presence but not the cause of these biases. The historical metadata is thus essential for a successful study of data homogeneity and only homogeneous data are useful for monitoring climate variability and change.

Despite the importance of metadata, the majority of existing environmental data sets are inadequately described. For many, there is no metadata and for others it exists in non-digital and non-standardized form and is unavailable to the majority of potential users. Such complete and accurate documentation is needed now to aid researchers in analysing the potential impacts of climate variability and change. Scientific papers, which are the fruits of these analyses, may then be added to the set of metadata for each data set. It is vital, then, that metadata be rescued from single-copy paper media and then made available in a user-friendly system to allow full access by the scientific community.

1 INTRODUCTION AND HIGHLIGHTS

AUSTRALIAN BUREAU OF METEOROLOGY, *1991 to 1992: Climate Monitoring Bulletin, Southern Hemisphere.* National Climate Centre, Melbourne (monthly issue).

AUSTRALIAN BUREAU OF METEOROLOGY, *1993: Climate Monitoring Bulletin, Australia.* National Climate Centre, Melbourne (monthly issue).

CAC, *1991 to 1993: Climate Diagnostics Bulletin.* NOAA/NWS/NMC, Washington, DC (monthly issue).

CAC, *1991 to 1993: Weekly Climate Bulletin.* NOAA/NWS/NMC, Washington, DC.

HALPERT, M.S. and C.F. ROPELEWSKI (EDITORS), *1991: Climate assessment:* A decadal review 1981-1990. Department of Commerce, NOAA/NWS/NMC/CAC, Washington, DC, 109 pp.

HALPERT, M.S. and C.F. ROPELEWSKI (EDITORS), *1992: Third annual climate assessment 1991.* NOAA/NWS/NMC/CAC, Washington, DC, 74 pp.

HALPERT, M.S. and C.F. ROPELEWSKI (EDITORS), *1993: Fourth annual climate assessment 1992.* NOAA/NWS/NMC/CAC, Washington, DC, 90 pp.

HALPERT, M.S., G.D. BELL, V.E. KOUSKY AND C.F. ROPELEWSKI (EDITORS), *1994: Fifth annual climate assessment 1993.* NOAA/NWS/NMC/CAC, Washington, DC, 111 pp.

LE COMTE, D., *1992: Highlights around the world.* Weatherwise, 45 (1): 13-22.

LE COMTE, D., *1993: Highlights around the world.* Weatherwise, 46 (1): 14-17.

LE COMTE, D., *1994: Highlights around the world.* Weatherwise, 47 (1): 23-27.

LIMBERT, D.W.S., *1992: Weather events in 1991 and their consequences.* WMO Bulletin, 41(4): 420-431.

LIMBERT, D.W.S., *1993: The human and economic impacts of weather events in 1992.* WMO Bulletin, 42(4): 333-341.

NATIONAL INSTITUTE OF WATER AND ATMOSPHERIC RESEARCH INC., *1992 to 1993: South Pacific Climate Monitor.* (Monthly issue, Reid Basher, editor).

WMO, *1992: The global climate system in 1991.* WMO Bulletin, 41(3): 319-322.

WMO, *1993: The global climate system in 1992.* WMO Bulletin, 42(3): 230-233.

WMO, *1994: WMO statement on the status of the global climate in 1993.* WMO-No. 809, 20 pp.

WMO and UNEP, *1985: The Global Climate System - A critical review of the climate system during 1982-1984.* World Climate Data Programme, 52 pp.

WMO and UNEP, *1987: The Global Climate System - Autumn 1984-Spring 1986.* World Climate Data Programme, 87 pp.

WMO and UNEP, *1990: The Global Climate System - Climate System Monitoring June 1986-November 1988.* World Climate Data Programme, 70 pp.

WMO and UNEP, *1992: The Global Climate System - Climate System Monitoring December 1988-May 1991.* World Climate Data and Monitoring Programme, 110 pp.

WMO and UNEP, *1991 to 1993: Climate System Monitoring (CSM) Monthly Bulletin.* World Climate Data and Monitoring Programme (monthly issue).

2 GLOBAL ATMOSPHERIC AND OCEANIC CIRCULATION

BARNSTON, A.G. and R.E. LIVEZEY, *1987: Classification, seasonality and persistence of low-frequency atmospheric circulation patterns.* Monthly Weather Review, 115: 1083-1126.

DINIES, E., *1968: Monatliche und jährliche Breitenkreismittel des Luftdrucks auf der Nordhalbkugel für die Jahre 1899 bis 1967.* Berichte des Deutschen Wetterdienstes, Nr. 109.

EMMRICH, P., *1991: 92 Jahre nordhemisphärischer Zonalindex.* Meteorologische Rundschau, 43: 161-169.

GRUZA, G.V. and L.V. KOROVKINA, *1991: Climatic monitoring of blocking processes of the middle of westerlies in northern hemisphere.* Meteorology and Hydrology, 8: 11-17.

GRUZA, G.V. and L.V. KOROVKINA, *1991: A seasonal feature of space distribution of blocking indices in northern hemisphere.* Meteorology and Hydrology, 3: 108-110.

HALPERT, M.S. and C.F. ROPELEWSKI, *1992: Surface temperature patterns associated with the Southern Oscillation.* Journal of Climate, 5(6): 577-593.

HARRISON, M.S.J., *1984: A generalized classification of South African rain-bearing synoptic systems.* Journal of Climatology, 4(5): 547-560.

HENDERSON, K.G. and P.J. ROBINSON, *1994: Relationships between the Pacific/North American teleconnection patterns and precipitation events in the southeastern USA.* International Journal of Climatology, 14(3): 307-324.

HILL, H.W., *1969: A synoptic study of a large-scale meridional trough in the Tasman Sea-New Zealand area.* New Zealand Journal of Science, 12: 576-593.

KOROVKINA, L.V., *1989: Synoptic-climatological characteristics of the blocking processes in the atmosphere.* Reviews, All Union Scientific Research Institute of Hydrometeorological Information - World Data Centre, Obninsk, Russia, 52 pp.

LEIGHTON, R.M., *1993: Monthly anticyclonicity and cyclonicity in the southern hemisphere: 15 year (1973-1987) averages.* Technical Report 67, Bureau of Meteorology, Melbourne.

LEIGHTON, R.M., *1994: Monthly anticyclonicity and cyclonicity in the southern hemisphere; averages for January, April, July and October.* International Journal of Climatology, 14(1): 33-46.

NICHOLLS, *N.* and *A. KARIKO, 1993: East Australian rainfall events: Interannual variations, trends, and relationships with the Southern Oscillation.* Journal of Climate, 6(6): 1141-1152.

RASMUSSON, *E.M.* and *T.H. CARPENTER, 1982: Variations in tropical sea surface temperature and surface wind fields associated with the Southern Oscillation/El Niño.* Monthly Weather Review, 111: 517-528.

ROGERS, J.C., *1984: The association between the North Atlantic Oscillation and the Southern Oscillation in the northern hemisphere.* Monthly Weather Review, 112: 1999-2015.

ROPELEWSKI, C.F. and M.S. HALPERT, *1986: North American precipitation and temperature patterns associated with the El Niño/Southern Oscillation (ENSO).* Monthly Weather Review, 114: 2352-2362.

ROPELEWSKI, C.F. and M.S. HALPERT, *1987: Global and regional scale precipitation patterns associated with the El Niño/ Southern Oscillation.* Monthly Weather Review, 115: 1606-1626.

ROPELEWSKI, C.F. and M.S. HALPERT, *1989: Precipitation patterns associated with the high index phase of the Southern Oscillation.* Journal of Climate, 2(2): 268-284.

SHILING PENG and L.A. MYSAK, *1993: A teleconnection study of interannual sea surface temperature fluctuations in the northern North Atlantic and precipitation and runoff over Western Siberia.* Journal of Climate, 6(5): 876-885.

SMITH, I., *1994: Indian Ocean sea-surface temperature patterns and Australian winter rainfall.* International Journal of Climatology, 14(3): 287-306.

TIBALDI, S., E. TOSI, A. NAVARRA AND L. PEDULLI, *1994: Northern and southern hemisphere seasonal variability of blocking frequency and predictability.* Monthly Weather Review, 122(9): 1971-2003

VAN LOON, H. and J.C. ROGERS, *1978: The seesaw in winter temperatures between Greenland and northern Europe (Part I: General description).* Monthly Weather Review, 106: 296-310.

VINCENT, D., *1994: The South Pacific Convergence Zone (SPCZ): A review.* Monthly Weather Review, 22(9): 1949-1970.

WALKER, G.T., *1924: Correlations in seasonal variations of weather, IX.* Memoirs of the Royal Meteorological Society, 24: 275-332.

WALKER, G.T. and E.W. BLISS, *1932: World Weather, V. Memoirs* of the Royal Meteorological Society, 4: 53-84.

WALLACE, J.M. and D.S. GUTZLER, *1981: Teleconnections in the geopotential height field during the northern hemisphere winter.* Monthly Weather Review, 109: 784-812.

WAYLEN, P.R., M.E. QUESADA and C.N. CAVIEDES, *1994: The effects of El Niño/Southern Oscillation on Precipitation in San Jose, Costa Rica.* International Journal of Climatology, 14(5): 559-568.

WRIGHT, W.J., *1993: Tropical-extratropical cloudbands and Australian rainfall.* Preprints for the Fourth International Conference on Southern Hemisphere Meteorology and Oceanography (Hobart, Australia, March 29 to April 2, 1993), American Meteorological Society, Boston, MA, 283-284.

3 TEMPERATURE

ANGELL, J.K., *1988: Variations and trends in tropospheric and stratospheric global temperatures, 1958-1987.* Journal of Climate, 1(12): 1296-1313.

BLUTH, G.J.S., S.D. DOIRON, C.C. SCHNETZLER, A.J. KRUGER and L.S. WALTER, *1992: Global tracking of the SO_2 clouds from the June 1991 Mount Pinatubo eruptions.* Geophysical Research Letters, 19: 151-154.

CAO, H.X., J.F.B. MITCHELL and J.R. LAVERY, *1992: Simulated diurnal range and variability of surface temperature in global climate model for present and doubled CO_2 climates.* Journal of Climate, 5(9): 920-943.

DUTTON, E.G. and J.R. CHRISTY, *1992: Solar radiative forcing at selected locations and evidence for global lower tropospheric cooling following the eruptions of El Chichón and Pinatubo.* Geophysical Research Letters, 19: 2313-2316.

ELLIS, H.T. and R. PUESCHEL, *1971: Solar radiation: Absence of trends at Mauna Loa.* Science, 172: 845.

FOLLAND, C.K. and D.E. PARKER, *1991: Worldwide surface temperature trends since the mid-19th century.* Greenhouse-Gas-Induced Climatic Change: A critical appraisal of simulations and observations, (M.E. Schlesinger, editor), Elsevier Scientific Publishers, 173-194.

GRAF, H.-F., I. KIRCHNER, A. ROBOCK and I. SCHULT, *1993: Pinatubo eruption winter climate effects: Model versus observations.* Climate Dynamics, 9: 81-93.

HANSEN, J., A. LACIS, R. RUEDY and M. SATO, *1992: Potential climate impact of Mount Pinatubo eruption.* Geophysical Research Letters, 19: 215-218.

IPCC, *1992: Climate Change 1992: The supplementary Report to the IPCC Scientific Assessment.* WMO/UNEP, Cambridge University Press, 200 pp.

JONES, P.D., *1994: Recent warming in global temperature series.* Geophysical Research

Letters, 21(12): 1149-1152.
JONES, P.D. and K.R. BRIFFA, *1992: Global surface air temperature variations during the twentieth century: Part 1, spatial, temporal and seasonal details.* The Holocene, 2: 165-179.
JONES, P.D. and P.M. KELLY, *1988: Cause of interannual global temperature variations over the period since 1861.* Long and Short Term Variability of Climate (H. Wanner and U. Siegenthaler, editors), Earth Sciences, Springer-Verlag, Berlin, 16: 18-34.
JONES, P.D., P.YA. GROISMAN, M. COUGHLAN, N. PLUMMER, W.-C. WANG and T.R. KARL, *1990: Assessment of urbanization effects in time series of surface air temperature over land.* Nature, 347: 169-172.
KARL, T.R., H.F. DIAZ and G. KUKLA, *1988: Urbanization: Its detection and effect in the U.S.A. climatic record.* Journal of Climate, 1(11): 1099-1123.
KARL, T.R., G. KUKLA and J. GAVIN, *1984: Decreasing diurnal temperature range in the U.S.A. and Canada from 1941 through 1980.* Journal of Climate and Applied Meteorology, 23: 1489-1504.
KARL, T.R., G. KUKLA, V.N. RAZUVAYEV, M.J. CHANGERY, R.G. QUAYLE, R.R. HEIM, JR, D.R. EASTERLING and C. B. FU, *1991: Global warming: Evidence of asymmetric diurnal temperature change.* Geophysical Research Letters, 18: 2253-2256.
KARL, T.R., P.D. JONES, R.W. KNIGHT, G. KUKLA, N. PLUMMER, V. RAZUVAYEV, K.P. GALLO, J. LINDESAY, R.J. CHARLSON and T.C. PETERSON, *1993: A new perspective on recent global warming: Asymmetric trends of daily maximum and minimum temperature.* Bulletin of the American Meteorological Society, 74: 1007-1023.
KODERA, K. and K. YAMAZAKI, *1994: A possible influence of recent polar stratospheric coolings on the troposphere in the northern hemisphere winter.* Geophysical Research Letters, 21(9): 809-812.
LONG, C.S. and L.L. STOWE, *1994: Using the NOAA/AVHRR to study stratospheric aerosol optical thicknesses following the Mount Pinatubo eruption.* Geophysical Research Letters, 21(20): 2215-2218.
MANNEY, G.L., R.W. ZUREK, A. O'NEILL, R. SWINBANK, J.B. KUMER, J.L. MERGENTHALER and A.E. ROCHE, *1994: Stratospheric warmings during February and March 1993.* Geophysical Research Letters, 21(9): 813-816.
PARKER, D.E., P.D. JONES, C.K. FOLLAND and A. BEVAN, *1994: Interdecadal changes of surface temperature since the late nineteenth century.* Journal of Geophysical Research, 99(D7): 14373-14400.
REYNOLDS, R.W., *1993: Impact of Mount Pinatubo aerosols on satellite-derived sea surface temperatures.* Journal of Climate, 6(4): 768-774.
REYNOLDS, R.W. and D.C. MARSICO, *1993: An improved real-time global sea-surface temperature analysis.* Journal of Climate, 6(1): 114-119.
ROBOCK, A. and J. MAO, *1992: Winter warming from large volcanic eruptions.* Geophysical Research Letters, 19: 2405-2408.
SATO, M., J.E. HANSEN, M.P. MCCORMICK and J.B. Pollack, *1993: Stratospheric aerosol optical depths, 1850-1990.* Journal of Geophysical Research, 98: 22987-22994.
SEAR, C.B., P.M. KELLY, P.D. JONES and C.M. GOODESS, *1987: Global surface-temperature responses to major volcanic eruptions.* Nature, 330: 365-367.
SHERIDAN, P.J., R.C. SCHNELL, D.J. HOFMANN and T. DESHIER, *1992: Electron microscope studies of Mt. Pinatubo aerosol layers over Laramie, Wyoming during summer 1991.* Geophysical Research Letters, 19: 203-206.
SPENCER, R.W. and J.R. CHRISTY, *1992: Precision and radiosonde validation of satellite grid point temperature anomalies, Part II: A tropospheric retrieval and trends during 1979-90.* Journal of Climate, 5(8): 858-866.
SPENCER, R.W. AND J.R. CHRISTY, *1993: Precision lower stratospheric temperature monitoring with the MSU: Technique, validation and results 1979-91.* Journal of Climate, 6(6): 1194-1204.
SRIVASTAVA, H.N. ET AL., *1992: Decadal trends in climate over India.* MAUSAM, 43: 7-20.
STOWE, L.L., R.M. CAREY and P.P. PELLEGRINO, *1992: Monitoring the Mt. Pinatubo aerosol layer with NOAA-11 AVHRR data.* Geophysical Research Letters, 19(2): 159-162.
THAPLIYAL, V. ET AL., *1991: Climate changes and trends over India.* MAUSAM, 42: 333-338.
TREPTE, C.R., R.E. VEIGA and M.P. MCCORMICK, *1993: The poleward dispersal of Mount Pinatubo volcanic aerosol.* Journal of Geophysical Research, 98: 18563-18573.
WOODWARD, W.A. and H.L. GRAY, *1993: Global warming and the problem of testing for trend in time series data.* Journal of Climate, 6(5): 953-962.
XU QUN, *1983: Solar constant, volcanic dusts and long-range forecasting.* Meteorological Monthly, Beijing, 6: 7-10.
XU QUN, *1994: The distribution of large scale climate anomalies in 1992 and their relationship with the eruption of Pinatubo.* Quarterly Journal of Applied Meteorology, Beijing (in press).

4 PRECIPITATION

ALLAN, R.J. and M.R. HAYLOCK, *1993: Circulation features associated with the winter rainfall decrease in southwestern Australia.* Journal of Climate, 6(7): 1356-1367.
ARKIN, P.A. and P.P. XIE, *1994: The Global Precipitation Climatology Project: First Algorithm Intercomparison Project.* Bulletin of the American Meteorological Society, 75(3): 401-420.
CAC, 1991-94: *Climatic Diagnostics Bulletin (June 1991-November 1993).* NOAA/NWS/NMC, Washington, DC.
CAC, 1991-94: *Weekly Climate Bulletin (June 1991-November 1993).* NOAA/NWS/NMC, Washington, DC.
FERNANDO, T.K. and L. CHANDRAPALA, *1992: Global warming and rainfall variability - the Sri Lankan situation.* Proceedings of the 5th International Meeting on Statistical Climatology (Toronto, Canada, June 22-26, 1992).
GPCC, *1992: Monthly precipitation estimates based on gauge measurements on the continents for the year 1987.* WCRP and Deutscher Wetterdienst, Report No. DWD/K7/WZN-1992/08-1, 24 pp.
GPCC, *1993: Global area-mean monthly precipitation totals on a 2.5° grid for the year 1988.* Deutscher Wetterdienst, Report No. DWD/WZN-1993/07-1, 20 pp.
GROISMAN, P.YA., *1991: Data on present-day precipitation changes in the extratropical part of the northern hemisphere. Greenhouse-Gas-Induced Climate Change:* A Critical Appraisal of Simulation and Observation, (M.E. Schlesinger, editor), Elsevier, 297-310.
GRUZA, G.V. and Y.G. APASOVA, *1981: Climatic variability of monthly precipitation totals of the northern hemisphere.* Meteorology and Hydrology, 5: 5-6.
INTERNATIONAL DROUGHT INFORMATION CENTER, *1989-91: Drought Network News. 1991-1994,* University of Nebraska.
RASMUSSON, E.M. and P.A. ARKIN, *1993: A global view of large-scale precipitation variability.* Journal of Climate, 6(8): 1495-1522.
RUDOLF, B., *1993: Management and analysis of precipitation data on a routine basis.* Proceedings of the WMO International Symposium on Precipitation and Evaporation (Bratislava, September 20, 1993, M. Lapin and B. Sevruk, editors), 1: 69-76.
WMO, *1994: Assessing a precious resource... water.* WMO-No. 801, 12 pp.
WMO, *1993: World Climate News.* 3: 10 pp.

5 DROUGHTS

CAC, *1982-present: Climate Diagnostics Bulletin.* NOAA/NWS/NMC, Washington, DC.
COAKLEY, J.A. JR and R.D. CESS, *1985: Response of the NCAR community climate model to the radiative forcing by the naturally occurring tropospheric aerosols.* Journal of Atmospheric Sciences, 42(16): 1677-1692.
DAS, P.K., *1986: Monsoon.* Fifth International Meteorological Organization (IMO) Lecture, WMO-No 613, 155 pp.
DROUGHT MONITORING CENTRE, *1991-1993: Ten-Day Drought Watch for South Africa.* WMO/UNDP Project RAF/88/044, Harare, Zimbabwe.
FERNANDO, T.K., L. CHANDRAPALA and P.M. JAYATILAKA BANDA, *1992: A comparative study of the droughts of 1983, 1987 and 1992.* Proceedings of the Annual Sessions of the Sri Lanka Association for the Advancement of Science.
GARANGANGA, B.J., *1989: The onset of 1992/93 summer monsoon over southern Africa: A diagnostic study.* Unpublished M.S. thesis, Texas A & M University, 76 pp.
HARRISON, M.S.J., *1984: A generalized classification of South African rain-bearing synoptic systems.* Journal of Climate, 4(5): 547-560.
HEIM, R.R. Jr, *1993: Drought in the U.S.A.: Mid-1993 update and historical perspective. Drought Network News,* International Drought Information Center, University of Nebraska, 5(3): 14-16.
HULME, M. and P.D. JONES, *1993: Global climate change in the instrumental record.* Environmental Pollution, 83: 23-36.
LYONS, S.W., *1991: Origins of convective variability over equatorial southern Africa during austral summer.* Journal of Climate 4(1): 23-39.
MACCRACKEN, M.C. and F.M. LUTHER, *1983: Radiative and climatic effects of the El-Chichòn eruption.* Proceedings of the Fifth Conference on Atmospheric Radiation (October 31 to November 4, 1983), American Meteorological Society, 346-349.
MASIKA, R.S., *1992: Rainfall patterns in eastern Africa.* Drought Network News, International Drought Information Center, University of Nebraska, 4(3): 5-10.
NEWELL, R.E., *1979: Climate and the ocean.* American Scientist, 67: 405-416.
RAMAGE, C.S., *1979: Monsoon Meteorology.* Academic Press, New York, 296 pp.
RAO, V.B., M.C. DE LIMA and S.H. FRANCHITO, *1993: Seasonal and interannual variations of rainfall over eastern Northeast Brazil.* Journal of Climate, 6(9): 1754-1763.
ROPELEWSKI, D.F. and M.S. HALPERT, *1987: Global and regional scale patterns associated with El Niño/Southern Oscillation.* Monthly Weather Review, 115: 1606-1626.
SMITH, D.K., *1989: Natural disaster reduction: How meteorological and hydrological services can help.* WMO-No. 722, 43 pp.
THOMPSON, C.B., *1993: Drought management strategies in southern Africa: 1992/1993.* United Nations Children's Fund.
UNGANAI, L.S., *1994: Drought and southern Africa: A note from the Harare Regional*

Drought Monitoring Centre. Drought Network News, International Drought Information Center, University of Nebraska, 6(2): 7-9.

UNIVERSITY OF NEBRASKA, *1991-1993: Drought Network News,* International Drought Information Center.

VON DER HAAR, T.H., *1958-68: Variations of the earth's radiation budget in meteorological satellite instrumentation and data processing.* Final report, Contract NASW-65, 1958-68. Department of Meteorology, University of Wisconsin, 179 pp.

WANG SHAOWU, ZHAO ZONGCI ET AL., *1987: Drought/flood variation for the last 2000 years in China and comparison with global climatic change.* The Climate of China and Global Climatic Change (edited by Ye Duzhen et al.), China Ocean Press, Beijing and Springer-Verlag, Berlin Heidelberg, 20-29.

WMO, *1990: The role of the World Meteorological Organization in the International Decade for Natural Disaster Reduction.* WMO-No. 745, 32 pp.

XU QUN, *1989: Significant influence of the interannual variation of direct solar radiation on the summer monsoon climates of China and Tropical Africa.* Papers presented at the Second WMO Workshop on the Diagnosis and Analysis of Monthly and Seasonal Atmospheric Variations over the Globe, WMO-No. 261, 114-118.

Xu Qun, *1990: Significant change of winter solar radiation of China during recent 29 Years.* Scientia Sinica, Part B, 10: 1112-1120.

XU QUN, *1987: The main cause of the persistent drought in Sahel and the increasing trend of El-Niño events during recent years.* Atmospheric Radiation, Progress and Prospects (Kuo-Nan Liou and Zhou Xiuji, editors), Science Press and American Meteorological Society, 207-212.

Xu Qun, *1990: Influence of the change in direct solar radiation of clear skies on summer monsoon rainfall of Mid-east China and the Subsahara.* Extended abstracts submitted at the second week of the WMO Training Workshop on Diagnosis and Prediction of Monthly and Seasonal Atmospheric Variations (Nanjing, October 15-19, 1990), WMO-No. 363.

ZHUANG XIE and DAGANG CHEN, *1994: Drought in Beijing, 1992-93.* Drought Network News, International Drought Information Center, University of Nebraska, 6(2): 10-11.

ZINYOWERA, M.C. and L.S. UNGANAI, *1993: Drought in southern Africa. An update on the 1991-92 drought.* Drought Network News, International Drought Information Center, University of Nebraska, 4(3): 3-4.

6 FLOODS

ANONYMOUS, *1992: Hydrological and meteorological data during the rainy season of 1991.* Appendix to proceedings of the International Symposium on Torrential Rain and Flood (Huangshan, Anhui, China, October 5-9, 1992).

BENECH, B., H. BRUNET, V. JACQ, M. PAYEN, J.-C. RIVRAIN and P. SANTURETTE, *1993: La catastrophe de Vaison-La-Romaine et les violentes précipitations de septembre 1992: aspects météorologiques.* La Météorologie, 8(1): 72-90.

CAC, *1993: Special Climate Summary 93/1 - Midwestern Floods; Heat and Drought in the East.* NOAA/NWS/NMC, July 12, 1993, 8 pp.

GUTTMAN, N.B., J.R.M. HOSKING and J.R. WALLIS, *1994: The 1993 Midwest extreme precipitation in historical and probabilistic perspective.* Bulletin of the American Meteorological Society, 75(10): 1785-1792.

HALPERT, M.S., G.D. BELL, V.E. KOUSKY and C.F. ROPELEWSKI (EDITORS), *1994: Fifth annual climate assessment 1993.* NOAA/NWS/NMC/CAC, Washington, DC, 111 pp.

KIRVAR, E., *1993: Severe early July weather in northwest Turkey.* Weather, 48(3): 239-246.

LINDESAY, J.A. and M.R. JURY, *1991: Atmospheric circulation controls and characteristics of a flood event in central South Africa.* International Journal of Climatology, 11(6): 609-627.

MYERS, M.F. and G. WHITE, *1993: The challenge of the Mississippi flood.* Environment, 35: 6-9, 25-35.

USA DEPARTMENT OF COMMERCE, *1993: The Great Flood of 1993.* NOAA, Natural Disaster Survey Report.

USA GEOLOGICAL SURVEY, *1993: Precipitation in the upper Mississippi River basin, July through August 1993.* USGS Circular 1120-B, 13 pp.

USA GEOLOGICAL SURVEY, *1993: Flood discharges in the upper Mississippi River basin, July through August 1993.* USGS Circular 1120-A, 14 pp.

USA GEOLOGICAL SURVEY, *1993: Occurrence and transport of agricultural chemicals in the Mississippi river basin, July through August 1993.* USGS Circular 1120-C, 22 pp.

WILLIAMS, J., *1994: The Great Flood.* Weatherwise, 47(1): 18-22.

WMO, *1994: The American Midwest floods of summer 1993.* World Climate News, 4: 10-11.

XU QUN, *1992: Talking about long-range forecasting from the point of severe waterlogging of Yangtze-Huaihe Valley during summer 1991.* Nature Journal, 15(9): 679-684.

XU QUN, *1992: An analysis on the cause to the abnormal earliness of rainy season in central China in 1991.* Meteorological Monthly, 18(9): 17-20.

7 MONSOONS

COAKLEY, J.A. JR and R.D. CESS, *1985: Response of the NCAR community climate model to the radiative forcing by the naturally occurring tropospheric aerosols.* Journal of Atmospheric Sciences, 42(16): 1677-1692.

GOWARIKER, V. ET AL., *1991: A power regression model for long range forecast of southwest monsoon rainfall over India.* MAUSAM, 42: 125-130.

INDIA METEOROLOGICAL DEPARTMENT, *1991-1993: Reports on Monsoon Season.* MAUSAM.

INDIA METEOROLOGICAL DEPARTMENT, *1991-1993: Reports of the Asian Summer Monsoon Activity Centre, New Delhi.* Newsletters 1991, 1992, 1993.

LAING, A.G. and J. M. FRITSCH, *1993: Mesoscale convective complexes over the Indian monsoon region.* Journal of Climate, 6(5): 911-919.

MACCRACKEN, M.C. and F. M. LUTHER, *1983: Radiative and climatic effects of the El-Chichòn eruption.* Proceedings of the Fifth Conference on Atmospheric Radiation (October 31 to November 4, 1983), American Meteorological Society, 346-349.

NATIONAL ENVIRONMENTAL PROTECTION AGENCY, *1993: 1992 Report on the State of the Environment in China.* Environmental Protection, 7: 2-7.

THAPLIYAL, V. ET AL., *1992: Recent models for long range forecasting of southwest monsoon rainfall in India.* MAUSAM, 43: 239-248.

WALKER, G.T., *1923-1924: Correlation in seasonal variation of weather.* Memoirs of the India Meteorological Department, 24.

WANG JIANMING, *1993: Researches of the development of township's factories, environmental problems and their countermeasures.* Environment Science (Beijing), 14(4): 24 pp.

WANG SHAOWU, ZHAO ZONGCI ET AL., *1987: Drought/flood variation for the last 2000 years in China and comparison with global climatic change.* The Climate of China and Global Climatic Change (edited by Ye Duzhen et al.), China Ocean Press, Beijing and Springer-Verlag Berlin Heidelberg, 20-29.

WENG DUMING, *1984: A preliminary study of climatic characteristics of atmospheric transparency over Nanjing.* Scientia Meteorologica Sinica, 2: 81 pp.

WMO, *1994: The 1993 Indian monsoon - a very good year.* World Climate News, 4: 10.

WMO, *1994: Heavy winter monsoon in Malaysia.* World Climate News, 5: 9.

XU QUN, *1990: Notable change of solar radiation of clear skies in China for recent 29 winters.* Scientia Sinica (Part B), 10: 1112-1120.

XU QUN and YAN YIWEN, *1992: Significant increasing greenhouse effect on the winter temperature of northern China.* Proceedings of the Fifth International Meeting on Statistical Climatology (Toronto, Canada, June 22-26, 1992), 57-59.

XU QUN, *1965: The plum rains (Meiyu) of the Middle and Lower Yangtze Valley for 80 recent years.* Acta Meteorologica Sinica, 34(4): 507-518.

XU QUN, *1989: The influence of ENSO and volcanic eruptions on summer monsoon rain belts in eastern China.* Journal of the Academy of Meteorological Sciences, 4(3): 283-290.

XU QUN, *1992: Talking about long-range forecasting from the point of severe waterlogging of the Yangtze-Huaihe Valley during summer 1991.* Nature Journal (Shanghai), 15(9): 679-684.

8 SEVERE STORMS

ANGEL, W., *1992: National Summary of Tornadoes, 1992.* Storm Data with Annual Summaries, 34(12): 76-93.

AVILA, L.A. and M. MAYFIELD, *1994: Eastern Pacific hurricanes.* Weatherwise, 47(1): 44-47.

AVILA, L.A. and R.J. PASCH, *1992: North Atlantic hurricanes -1991.* Mariner's Weather Log, 37(3): 14-20.

AVILA, L.A. and R.J. PASCH, *1992: Atlantic hurricanes: Bob hogs the headlines.* Weatherwise, 45(1): 34-41.

BURT, S., *1993: Another new North Atlantic low pressure record.* Weather, 48(4): 98-103.

CAC, *1991 to 1993: Weekly Climate Bulletin.* NOAA/NWS/NMC, Washington, DC.

CHINA METEOROLOGICAL ADMINISTRATION, *1993: China Climate Bulletin.* 10 pp.

CROWTHER, H.G., *1993: Tornadoes hit new heights.* Weatherwise, 46(1): 29-37.

CROWTHER, H.G., *1994: Tornadoes strike far and wide.* Weatherwise, 47(1): 28-37.

EMMRICH, P., *1991: 92 Jahre nordhemisphärischer Zonalindex.* Meteorologische Rundschau, 43: 161-169.

GRAZULIZ, T.P., *1991: Significant tornadoes, 1880-1989. Volume I: Discussion and analysis.* Environmental Films, St. Johnsbury, VT, 526 pp.

INDIA METEOROLOGICAL DEPARTMENT, *1991, 1992, 1993: Reports on cyclonic disturbances over North Indian Ocean.* Regional Specialized Meteorological Centre Tropical Cyclones - New Delhi.

INDIA METEOROLOGICAL DEPARTMENT, *1991, 1992, 1993: Weather reports.* MAUSAM.

JOINT TYPHOON WARNING CENTRE STAFF, *1994: Western North Pacific typhoons, 1992.*

Mariner's Weather Log, 38(1): 34-40.
LE COMTE, D. and D. SECORA, *1993: Cyclones slam into the Philippines and Viet Nam.* U.S. Weekly Weather and Crop Bulletin, December 14, 1993, 19.
LEFTWICH, P.W., L.F. WILSON and H.G. CROWTHER, *1992: Tornadoes: Record pace continues.* Weatherwise, 45(1): 23-33.
MAYFIELD, M. and L. AVILA, *1993: Atlantic hurricanes.* Weatherwise, 46(1): 18-24.
MAYFIELD, M. and L. AVILA, *1993: North Atlantic hurricanes -1992.* Mariner's Weather Log, 37(3): 17-25.
MAYFIELD, M. and L. AVILA, *1994: North Atlantic hurricanes -1993.* Mariner's Weather Log, 38(2): 10-16.
MAYFIELD, M. and E.N. RAPPAPORT, *1992: Eastern Pacific hurricanes: Long season, but normal numbers.* Weatherwise, 45(1): 42-46.
MCCALLUM, E. and N.S. GRAHAME, *1993: The Braer storm - 10 January 1993.* Weather, 48(4): 103-107.
NESDIS, *1992: Storm Data with Annual Summaries.* USA Department of Commerce, NCDC, Asheville, NC, 34(12).
RAPPAPORT, E.N. and M. MAYFIELD, *1992: Eastern North Pacific Hurricane Season-1991.* Mariner's Weather Log, 36(2): 21-22.
RAPPAPORT, E.N. and M.B. LAWRENCE, *1993: Eastern North Pacific Hurricanes-1992.* Mariner's Weather Log, 37(3): 10-17.
RAPPAPORT, E.N. and M.B. LAWRENCE, *1993: Eastern Pacific hurricanes.* Weatherwise, 46(1): 25-28.
RAPPAPORT, E.N. and R.J. PASCH, *1994: Atlantic hurricanes.* Weatherwise, 47(1): 38-43.
RAPPAPORT, E.N. and R.J. PASCH, *1994: Eastern North Pacific Hurricanes-1993.* Mariner's Weather Log 38(2): 17-25.
ROSENHAGEN, G., *1993: Erheblich vermehrte Sturmhäufigkeit über dem Nordatlantik auch im Winter 1992/93.* Die Witterung in Bersee, Nr. 3.
WILLIAMS, J., *1992: Tracking Andrew from ground zero.* Weatherwise, 45(6): 8-13.
WMO and UNEP, *1992: The Global Climate System - Climate System Monitoring December 1988 to May 1991.* World Climate Data Programme, 110 pp.
XU QUN, *1989: The influence of ENSO and volcanic eruptions on summer monsoon rain belts in eastern China.* Journal of the Academy of Meteorological Sciences, 4(3): 283-290.
XU QUN, *1990: Influence of the change in direct solar radiation of clear skies on summer monsoon rainfall of mid-east China and Subsahara.* Extended abstracts submitted at the second week of the WMO Training Workshop on Diagnosis and Prediction of Monthly and Seasonal Atmospheric Variations (Nanjing, October 15-19, 1990), WMO-No. 363: 212-219.

9
BIOLOGICAL SYSTEM

CHU, P.-S. ET AL., *1994: Detecting climate change concurrent with deforestation in the Amazon basin: Which way has it gone?* Bulletin of the American Meteorological Society, 75(4): 579-584.
FAO, *1992: Special feature - Drought devastation of crops threatens food supplies in southern Africa.* Food Outlook, (FAO/GIEWS), May 1992, 18-20.
FAO, *1990: Forest Resources Assessment 1990 Project.* Rome, Italy.
LIMBERT, D.W.S., *1992: Weather events in 1991 and their consequences.* WMO Bulletin, 41(4): 420-431.
LIMBERT, D.W.S., *1993: The human and economic impacts of weather events in 1992.* WMO Bulletin, 42(4): 333-341.
ZAMBIAN DEPARTMENT OF METEOROLOGY, *1994: Zambia National Early Warning System, Season 1993/94.* Crop Weather Bulletin, 17: 16 pp.

10
OCEANS

ATLAS, R., S.C. BLOOM, R.N. HOFFMAN, J.V. ARDIZZONE and G. BRIN, *1991: Space-based surface wind vectors to aid understanding of air-sea interactions.* EOS, Transactions of the American Geophysical Union, 72: 201-208.
BATES, J., *1991: High-frequency variability of special sensor microwave/imager derived wind speed and moisture during an intra-seasonal oscillation.* Journal of Geophysical Research, 96: 3411-3423.
BINDOFF, N.L. and J.A. CHURCH, *1992: Warming of the water column in the southwest Pacific Ocean.* Nature, 357: 59-62.
BINDOFF, N.L. and T.J. MCDOUGALL, *1994: Diagnosing climate change and ocean ventilation using hydrographic data.* Journal of Physical Oceanography, 24: 1137-1152.
BORNGEN, M., P. HUPFER and M. OLBERG, *1990: Occurrences of absence of strong salt influxes into the Baltic Sea.* Beiträge zur Meereskunde, Berlin, 61: 11-19.
BOTTOMLEY, M., C.K. FOLLAND, J. HSIUNG, R.E. NEWELL and D.E. PARKER, *1990: Global Ocean Surface Temperature Atlas (GOSTA).* Joint Meteorological Office/Massachusetts Institute of Technology Project, HMSO, London, 20+iv pp. and 313 plates.
CHENEY, R.E., B.C. DOUGLAS and L. MILLER, *1989: Evaluation of GEOSAT altimeter data with application to tropical Pacific sea level variability.* Journal of Geophysical Research, 94: 4737-4748.
CHURCH, J.A., J.S. GODFREY, D.R. JACKETT and T.J. MCDOUGALL, *1991: A model of sea-level rise caused by ocean thermal expansion.* Journal of Climate, 4(4): 438-456.
DICKSON, R.F., J. MEINCKE, S.-A. MALMBERG and A.J. LEE, *1988: The "Great Salinity Anomaly" in the northern North Atlantic 1968-1982.* Progress in Oceanography, 20(2): 103-151.
GREENLAND ICE-CORE PROJECT (GRIP) MEMBERS, *1993: Climate instability during the last interglacial period recorded in the GRIP ice core.* Nature, 364: 203-207.
HALPERN, D., M.H. FRIELICH and R.S. DUNBAR, *1993: Evaluation of two January-June 1992 ERS-1 AMI wind vector data sets.* Proceedings of First ERS-1 Symposium (Cannes, November 4-6, 1992), European Space Agency.
JOYCE, T.M., *1993: The long-term hydrographic record at Bermuda.* Unpublished manuscript.
LEETMAA, A. and M. JI, *1989: Operational hindcasting of the tropical Pacific.* Dynamics of Atmospheres and Oceans, 13: 465-490.
LEGLER, D.M., *1991: Producing surface wind products for oceanographers.* Proceedings of the IGOSS/IOC Ocean Products Workshop (Tokyo, Japan, April 1991), 59-76.
LIU, T., *1988: Moisture and latent heat flux variabilities in the tropical Pacific derived from satellite data.* Journal of Geophysical Research, 93: 6749-6760.
MANABE, S., R.J. STOUFFER, M.J. SPELMAN and K. BRYAN, *1991: Transient responses of a coupled ocean-atmosphere model to gradual changes of atmospheric CO2. Part I: Annual mean response.* Journal of Climate, 4(8): 785-818.
MATTHAUS, W. and H. FRANCK, *1992: Characteristics of major Baltic inflow - A statistical analysis.* Continental Shelf Research, 12: 1375-1400.
MATTHAUS, W., H.U. LASS and R. TIESEL, *1993: The major Baltic inflow in January 1993.* ICES Statutory Meeting, Dublin, Paper ICES CM.1993/c: 51.
MCPHADEN, M.J., *1993: TOGA-TAO and the 1991-93 El Niño/Southern Oscillation event.* Oceanography, 6(2): 36-44.
MCPHADEN, M.J., H.B. MILBURN, P.A. ARKIN, O.W. THIELE, J. WILKERSON and W.F. KRAJEWSKI, *1993: Moored optical rain-gauge measurements from the equatorial Pacific Ocean.* Proceedings of the Fourth International Conference on Precipitation (Iowa City, April 26-28, 1993), 32-33.
MIKOLAJEWICZ, U. and E. MAIER-REIMER, *1990: Internal secular variability in an ocean general circulation model.* Climate Dynamics, 4: 145-156.
PARRILLA, G., A. LAVIN, H. BRYDEN, M. GARCIA and R. MILLARD, *1994: Rising temperatures in the subtropical North Atlantic Ocean over the past 35 years.* Nature, 369: 48-51.
PICAUT, J., A.J. BUSALACCHI, T. DELCROIX and M.J. MCPHADEN, *1992: Rigorous open-ocean validation of TOPEX/POSEIDON sea level in the western equatorial Pacific.* TOPEX/POSEIDON Joint Verification Plan, NASA, Jet Propulsion Laboratory, 92-2, V14-V16.
PICAUT, J., A.J. BUSALACCHI, M.J. MCPHADEN and B. CANUSAT, *1990: Validation of the geostrophic method for estimating zonal currents at the equator from GEOSAT altimeter data.* Journal of Geophysical Research, 95: 3015-3024.
READ, J.F. and W.J. GOULD, *1992: Cooling and freshening of the subpolar North Atlantic Ocean since the 1960s.* Nature, 360: 55-57.
REYNOLDS, R.W., *1988: A real-time global sea surface temperature analysis.* Journal of Climate, 1(1): 75-86.
REYNOLDS, R.W., *1991: Sea surface temperature analyses from in situ data.* TOGA Notes, 5: 8-12.
ROEMMICH, D., *1992: Ocean warming and sea-level rise along the southwest USA Coast.* Science, 257: 373-375.
ROEMMICH, D. and C. WUNSCH, *1984: Apparent changes in the climatic state of the deep North Atlantic Ocean.* Nature, 307: 447-450.
SOREIDE, N.N., D.C. MCCLURG, W.H. ZHU, D.W. DENBO and M.J. MCPHADEN, *1994: TAO software for real-time and historical TOGA-TAO data display and analysis.* Tenth International Conference on Interactive Information and Processing Systems for Meteorology, Oceanography and Hydrology (Nashville, TN, January 23-28, 1994), American Meteorological Society, 285-290.
STOUFFER, R.J., S. MANABE AND K. BRYAN, *1989: Interhemispheric asymmetry in climate response to a gradual increase of atmospheric CO2.* Nature, 342: 660-662.
THOMSON, R.E. and S. TABATA, *1989: Steric sea-level trends in the northeast Pacific Ocean: Possible evidence of global sea-level rise.* Journal of Climate, 2(6): 542-553.
WEAVER, A.J. and T.M.C. HUGHES, *1994: Rapid interglacial climate fluctuations driven by North Atlantic Ocean circulation.* Nature, 367: 447-450.
WIGLEY, T.M.L. and S.C.B. RAPER, *1987: Thermal expansion of sea water associated with global warming.* Nature, 330: 127-131.

11
STRATOSPHERIC OZONE

BOJKOV, R.D., *1992: Changes in polar ozone.* WMO Bulletin, 41(2): 171-180.
BOJKOV, R.D., C.S. ZEREFOS, D.S. BALIS, I.C. ZIOMAS and A.F. BAIS, *1993: Record low total ozone during northern winters of 1992 and 1993.* Geophysical Research Letters, 20: 1351-1354.
BOJKOV, R.D. and V.E. FIOLETOV, *1995:*

Estimating the global ozone characteristics during the last 30 years. Journal of Geophysical Research, 100 (in press).
BOJKOV, R.D., *1994: The ozone layer - recent developments.* WMO Bulletin, 43(2): 113-116.
CHANDRA, S. and R.D. MCPETERS, *1994: The solar cycle variation of ozone in the stratosphere inferred from Nimbus 7 and NOAA 11.* Journal of Geophysical Research, 99(D10): 20665-20672.
HERMAN, J.R. and D. LARKO, *1994: Low ozone amounts during 1992-1993 from Nimbus 7 and Meteor 3 total ozone mapping.* Journal of Geophysical Research, 99(D2): 3483-3496.
HOFMANN, D.J. ET AL., *1994a: Recovery of stratospheric ozone over the U.S.A. in the winter of 1993-1994.* Geophysical Research Letters, 21: 1779-1782.
HOFMANN, D.J., S.J. OLTMANS, J.A. LATHROP, J.M. HARRIS and H. VOMEL, *1994b: Record low ozone at the South Pole in the spring of 1993.* Geophysical Research Letters, 21(6): 421-424.
JAPAN METEOROLOGICAL AGENCY, *1993: Monitoring of global warming and ozone depletion: 1992 Summary.* 36 pp.
JOHNSON, B.J., T. DESHLER and W.R. ROZIER, *1994: Ozone profiles at McMurdo Station, Antarctica during the austral spring of 1992.* Geophysical Research Letters, 21(4): 269-272.
KERR, J.P., D.I. WARDLE and D.W. TARASICK, *1993: Record low ozone values over Canada in early 1993.* Geophysical Research Letters, 20: 1979-1982.
KOMHYR, W.D., R.D. GRASS, R.D. EVANS, R.K. LEONARD, D.M. QUINCY, D.J. HOFMANN and G.L. KOENIG, *1994: Unprecedented 1993 ozone decrease over the U.S.A. from Dobson spectrophotometer observations.* Geophysical Research Letters, 21(3): 201-204.
KRZYSCIN, J.W., *1994: On the interannual oscillations in the northern temperate total ozone.* Journal of Geophysical Research 99(D7): 14527-14534.
LARSEN, N., B. KNUDSEN, I.S. MIKKELSEN, T.S. JORGENSEN and P. ERIKSEN, *1994: Ozone depletion in the Arctic stratosphere in early 1993.* Geophysical Research Letters, 21(15): 1611-1614.
WMO, *1991: Scientific assessment of ozone depletion: 1991.* Global Ozone Research and Monitoring Project - Report No. 25.
WMO, *1995: Scientific assessment of ozone depletion: 1994.* Global Ozone Research and Monitoring Project - Report No. 37, 581 pp.
WMO, *1993: Global Atmosphere Watch - Ozone hole bigger and deeper.* World Climate News, 2: 8-9.
WMO, *1994: Ozone destruction breaks new records.* World Climate News, 5: 4-5.
WMO, *1993: Ozone layer deficit in northern hemisphere.* World Climate News, 3: 12-13.
XUE XI TIE, G.P. BRASSEUR, B. BRIEGLEB and C. GRANIER, *1994: Two-dimensional simulation of Pinatubo aerosol and its effect on stratospheric ozone.* Journal of Geophysical Research, 99(D10): 20545-20562.

12
TRACE GASES

BLUNIER, T., J. CHAPPELLAZ, J. SCHWANDER, J. BARNOLA, T. DESPERTS, B. STAUFFER and D. RAYNAUD, *1993: Atmospheric methane record from a Greenland ice core over the past 1000 years.* Geophysical Research Letters, 20: 2219-2222.
CONWAY, T.J., P.P. TANS, L.S. WATERMAN, K.W. THONING, D.R. KITZIS, K.A. MASARIE and N. ZHANG, *1994: Evidence for interannual variability of the carbon cycle from the National Oceanic and Atmospheric Administration/Climate Monitoring and Diagnostics Laboratory Global Air Sampling Network.* Journal of Geophysical Research, 99(D11): 22831-22856.
DLUGOKENCKY, E J., K.A. MASARIE, P.M. LANG, P.P. TANS, L.P. STEELE and E.G. NISBET, *1994: A dramatic decrease in the growth rate of atmospheric methane in the northern hemisphere during 1992.* Geophysical Research Letters, 21(1): 45-48.
ELKINS, J.W., T.M. THOMPSON, T.H. SWANSON, J.H. BUTLER, B.D. HALL, S.O. CUMMINGS, D.A. FISHER and A.G. RAFFO, *1993: Decrease in the growth rates of atmospheric chlorofluorocarbons 11 and 12.* Nature, 364: 780-783.
ETHERIDGE, D.M., G.I. PEARMAN and P.J. FRASER, *1992: Changes in tropospheric methane between 1841 and 1978 from a high accumulation rate Antarctic ice core.* Tellus, 44B: 282-294.
FRASER, P.J., S. PENKETT, R. HARRIS, Y. MAKIDE and E. SANHUEZA, *1991: Source gases: concentrations, emissions, and trends.* Scientific Assessment of Ozone Depletion: 1991, WMO Global Ozone Research and Monitoring Project - Report No. 25.
KANE, R.P., *1994: Interannual variability of some trace elements and surface aerosol. International* Journal of Climatology, 14(6): 691-704.
KEELING, C.D., R. BACASTOW, A. CARTER, S. PIPER, T. WHORF, M. HEIMANN, W. MOOK and H. ROELOFFZEN, *1989: A three-dimensional model of atmospheric CO2 transport based on observed winds 1. Analysis of observational data.* Aspects of Climate Variability in the Pacific and the Western Americas, D.H. Peterson (editor), Geophysical Monograph, 55: 165-236.
KHALIL, M.A.K. and R.A. RASMUSSEN, *1994: The global decrease of carbon monoxide and its causes.* Report of the WMO Sponsored Meeting of Carbon Monoxide (CO) Experts, P. Novelli and R. Rossen (editors), Boulder, CO (in press).
NAKAZAWA, T., T. MACHIDA, M. TANAKA, Y. FUJII, S. AOKI and O. WATANABE, *1993: Differences of the atmospheric CH4 concentration between the Arctic and Antarctic regions in preindustrial agricultural era.* Geophysical Research Letters, 20: 943-946.
NOVELLI, P.C., K.A. MASARIE, P.P. TANS and P.M. LANG, *1994: Recent changes in atmospheric carbon monoxide.* Science, 263: 1587-1590.
PRATHER, M., R. DERWENT, D. EHHALT, P. FRASER, E. SANHUEZA and X. ZHOU, *1994: Other trace gases and atmospheric chemistry.* Chapter 2 of the IPCC Scientific Assessment 1994, WMO (in press).
SANHUEZA, E., P. FRASER and R. ZANDER, *1994: Source gases: Trends and budgets.* Part 1, Chapter 2 in Scientific Assessment of Ozone Depletion: 1994, WMO Global Ozone Research and Monitoring Project - Report No. 37, 581 pp.
STEELE, L.P., E.J. DLUGOKENCHY, P.M. LANG, P.P. TANS, R.C. MARTIN and K.A. MASARIE, *1992: Slowing down of the global accumulation of atmospheric methane during the 1980s.* Nature, 358: 313-316.
THONING, K.W. and P.P.TANS, *1989: Atmospheric carbon dioxide at Mauna Loa Observatory, 2. Analysis of NOAA/GMCC data, 1974-1985.* Journal of Geophysical Research, 94: 8549-8565.
WATSON, R.T., L.G. MEIRA FILHO, E. SANHUEZA and A. JANETOS, *1992: Greenhouse gases: Sources and sinks.* Chapter A1 in Houghton, J.T., B.A. Callander and S.K. Varney, Climate Change, the Supplementary Report to the IPCC Scientific Assessment, Cambridge University Press, Cambridge, UK.
WATSON, R.T., H. RODHE, H. OESCHGER and U. SIEGENTHALER, *1990: Greenhouse gases and aerosols.* Chapter 1 in Houghton, J.T., G.J. Jenkins and J.J. Ephraums, Climate Change, the IPCC Assessment, Cambridge University Press, Cambridge, UK.
WMO, *1994: Carbon dioxide growth slows down.* World Climate News, 5: 6.

13
CRYOSPHERE

BARRY, R.G., F.M. FALLOT and R.L. ARMSTRONG, *1994: Assessing decadal changes in the cryosphere: Eurasian snow cover.* Proceedings of the Fifth Symposium on Global Change Studies, American Meteorological Society, Boston, MA, 148-155.
BROWN, R.D. and B.E. GOODISON, *1993: Recent observed trends and modelled interannual variability in Canadian snow cover.* Proceedings of 50th Eastern Snow Conference (Quebec City, Quebec, June 9-10, 1993), 389-397.
DAVEY, M. and A. WALKER, *1993: Great Slave Lake ice break-up, spring 1993.* Climatic Perspectives, Environment Canada, 15: 8-9.
ENVIRONMENT CANADA, *1992-1994: Canadian Great Lakes summary of ice conditions for the winter 1991-1992 (1992-1993 and 1993-1994).* Ice Central, Ottawa.
GROISMAN, P.YA. and D.R. EASTERLING, *1994: Variability and trends of total precipitation and snowfall over the U.S.A. and Canada.* Journal of Climate, 7(1): 183-205.
GROISMAN, P.YA., R.W. KNIGHT, R.R. KARL and R.R. HEIM JR, *1993: Inferences of the North American snowfall and snow cover with recent global temperature changes.* Proceedings of Snow Watch '92 Conference (Niagara-on-the-Lake, Canada, March 30-April 1, 1992), 44-51.
GROISMAN, P.YA., T.R. KARL and R.W. KNIGHT, *1994a: Changes of snow cover, temperature, and radiative heat balance over the northern hemisphere.* Journal of Climate, 7(11): 1633-1656.
GROISMAN, P.YA., T.R. KARL and R.W. KNIGHT, *1994b: Observed impact of snow cover on the heat balance and rise of continental spring temperatures.* Science, 263: 198-200.
GURER, I. and A. SAYIN, *1993: Avalanche disaster in southeastern Turkey in the winter of 1992.* WMO Bulletin, 42(1): 44-48.
HUGHES, M.G. and D.A. ROBINSON, *1993: Snow cover variability in the Great Plains of the U.S.A.: 1910-1988.* Proceedings of 50th Eastern Snow Conference, (Quebec City, Quebec, June 8-10, 1993), 35-42.
KARL, T.R., P.YA. GROISMAN, R.W. KNIGHT and R.R. HEIM JR, *1993: Recent variations of snow cover and snowfall in North America and their relation to precipitation and temperature variations.* Journal of Climate, 6(7): 1327-1344.
LEATHERS, D.J. and D.A. ROBINSON, *1993: The association between extremes in North American snow cover extent and U.S.A. temperatures.* Journal of Climate, 6(7): 1345-1355.
MARKO, J.R., D.B. FISSEL, P. WADHAMS, P.M. KELLY and R.D. BROWN, *1994: Iceberg severity off eastern North America: its relationship to sea ice variability and climate change.* Journal of Climate, 7(9): 1335-1351.
MEDRES, P.L., *1957: Ice regime of Lake Ladoga based on airborne observations data.* USSR State Hydrological Institute, Proceedings, Volume 66.
REYCRAFT, J. and W. SKINNER, *1993: Canadian lake ice conditions: An indicator of climate variability.* Climatic Perspectives, Environment Canada, 15: 9-15.
ROBINSON, D.A. ET AL., *1993: Global snow cover monitoring: An update.* Bulletin of the American Meteorological Society, 74(9): 1689-1696.
ROBINSON, D.A., F.T. KEIMIG and K.F. DEWEY,

1991: Recent variations in northern hemisphere snow cover. Proceedings of the 15th Annual Climate Diagnostics Workshop (Asheville, NC, October 29 to November 2, 1990), 219-224.
SILIS, A., *1993: East coast sea ice extent.* Climatic Perspectives, Environment Canada, 15: 12-13.
SILIS, A., *1993: 1993 - The ice year in review.* Climatic Perspectives, Environment Canada. 15: 4-5.
SKINNER, W. R., *1991: Lake ice conditions as a cryospheric indicator of climate variability in Canada.* Atmospheric Environment Service, Internal Report, July.
YANG, S. and L. XU, *1994: Linkage between Eurasian winter snow cover and regional Chinese summer rainfall.* International Journal of Climatology, 14(7): 739-750.

14 GLOBAL CLOUDINESS

HARRISON, M.S.J., *1984: A generalized classification of South African rain-bearing synoptic systems.* Journal of Climatology, 4(5): 547-560.
HILL, H.W., *1969: A synoptic study of a large-scale meridional trough in the Tasman Sea-New Zealand area.* New Zealand Journal of Science, 12: 576-593.
LINDESAY, J.A. and M.R. JURY, *1991: Atmospheric circulation controls and characteristics of a flood event in central South Africa.* International Journal of Climatology, 11(6): 609-627.
MATVEEV, L.T., *1986: Global field of cloudiness.* Hydrometeoizdat, Leningrad, 179 pp (in Russian).
MOKHOV, I. and M.E. SCHLESINGER, *1993: Analysis of global cloudiness: 1. Comparison of Meteor, Nimbus-7, and ISCCP satellite data.* Journal of Geophysical Research, 98: 12849-12868.
ROSSOW, W.B. and A.A. LACIS, *1990: Global, seasonal cloud variations from satellite radiance measurements. Part II: Cloud properties and radiative effects.* Journal of Climate, 3(11): 1204-1253.
ROSSOW, W.B. and L.C. GARDER, *1993: Validation of ISCCP cloud detections.* Journal of Climate, 6(12): 2370-2393.
ROSSOW, W.B., A.W. WALKER and L.C. GARDER, *1993: Comparison of ISCCP and other cloud amounts.* Journal of Climate, 6(12): 2394-2418.
TSELIOUDIS, G. and W.B. ROSSOW, *1994: Global, multiyear variations of optical thickness with temperature in low and cirrus clouds.* Geophysical Research Letters, 21(20): 2211-2215.
VINCENT, D., *1994: The South Pacific Convergence Zone (SPCZ): A review.* Monthly Weather Review, 22(9): 1949-1970.
WRIGHT, W.J., *1993: Tropical-extratropical cloudbands and Australian rainfall.* Preprint for the Fourth International Conference on Southern Hemisphere Meteorology and Oceanography (Hobart, Australia, March 29-April 2, 1993), American Meteorological Society, Boston, MA, 283-284.

15 WATER LEVELS

GOLITSYN, G.S. and G.N. PANIN, *1989: Contemporary changes of the Caspian Sea level.* Meteorologija i Gidrologija, 1: 57-64.
GOLITSYN, G.S., A.V. DZUBA, A.G. OSIPOV and G.N. PANIN, *1990: Regional climate changes and their impacts on the Caspian Sea level rise.* Doklady, USSR Academy of Sciences, 313(5): 1224-1227.
GOVERNMENT OF CANADA, *1993: Monthly Water Level Bulletin -Great Lakes and Montreal Harbour.* Canadian Hydrographic Service and Inland Waters Directorate, 6 pp.
RODIONOV, S.N., *1988: Recent climate change in the Caspian Sea basin.* Hydrometeoizdat, 124 pp (in Russian).

16 CHRONOLOGICAL SUMMARY

JAYATILAKA BANDA, P.M., *1994: Weather synopses from June 1991-November 1993.* Department of Meteorology, Sri Lanka.
ROPELEWSKI, C.F. and M.S. HALPERT, *1987: Global and regional precipitation patterns associated with the El Niño/Southern Oscillation.* Monthly Weather Review, 115: 1606-1626.

17 FEATURE ARTICLES

BRUCE, J.P., *1994: Natural disaster reduction and global change.* Bulletin of the American Meteorological Society, 75(10): 1831-1835.
OBASI, G.O.P., *1994: Statement on the Occasion of the World Conference on Natural Disaster Reduction.* (Yokohama, Japan, May 23, 1994), WMO, 6 pp.
OBASI, G.O.P., *1994: WMO's role in the International Decade for Natural Disaster Reduction.* Bulletin of the American Meteorological Society, 75(9): 1655-1661.
WHELPDALE, D.M., *1994: The climate system and GCOS.* Proceedings of the Workshop on Canadian Climate System Data (Quebec City, Quebec, May 16-18, 1994), Government of Canada. 3-11.
WMO, *1994: Observing the world's environment: Weather, climate and water.* WMO-No. 796., 42 pp.
WMO, *1990: The role of the World Meteorological Organization in the International Decade for Natural Disaster Reduction.* WMO-No. 745, 32 pp.

LIST OF ABBREVIATIONS USED IN THE REVIEW

AOT	Aerosol Optical Thickness
ATLAS	autonomous temperature line acquisition system
AVHRR	Advanced Very High Resolution Radiometer
CAC	Climate Analysis Center (Washington, DC)
CFCs	chlorofluorocarbons
CMDL	Climate Monitoring and Diagnostics Laboratory
COP	Conference of the Parties (to the UN FCCC)
CPTEC	Centro de Previsao do Tempo e Estudos Climaticos
CRYSYS	Cryospheric System to Monitor Global Change in Canada
CSIRO	Commonwealth Scientific and Industrial Research Organization (Australia)
CSM	Climate System Monitoring
DMSP	Defence Meteorological Satellite Programme
DU	Dobson units
ECMWF	European Centre for Medium Range Weather Forecasts
ENSO	El Niño/Southern Oscillation
EOS	Earth Observing System
ERS-1	European Remote Sensing Satellite - 1
EU	Eurasian index
FAO	Food and Agriculture Organization of the UN
FCCC	UN Framework Convention on Climate Change
FPAR	fraction of photosynthetically active radiation
FNOC	Fleet Numerical Oceanography Center
FSU	Florida State University
GAW	WMO Global Atmosphere Watch
GCOS	Global Climate Observing System (WMO/IOC/ICSU/UNEP)
GEMS	Global Environmental Monitoring System
GEOSAT	Geodesic Satellite (USA)
GIEWS	Global Information and Early Warning System on food and agriculture
GLOSS	Global Sea-level Observing System
GOOS	Global Ocean Observing System (IOC/WMO/ICSU/UNEP)
GPCC	Global Precipitation Climatology Centre
GPCP	Global Precipitation Climatology Project
GTS	WWW Global Telecommunication System (WMO)
HMSO	Her Majesty's Stationery Office
ICSU	International Council of Scientific Unions
IGOSS	Integrated Global Ocean Services System (IOC/WMO)
INMET	Instituto Nacional de Meteorologia
INPE	Instituto Nacional de Pesquisas Espaciais
IPCC	Intergovernmental Panel on Climate Change (WMO/UNEP)
IOC	Intergovernmental Oceanographic Commission (UNESCO)
ISCCP	International Satellite Cloud Climatology Project
ITCZ	Intertropical Convergence Zone
MSU	Microwave Sounding Unit
NAO	North Atlantic Oscillation
NASA	National Aeronautics and Space Administration (USA)
NCAR	National Center for Atmospheric Research (USA)
NCDC	National Climatic Data Center (Asheville, NC)
NESDIS	National Environmental Satellite Data and Information Service (Washington, DC)
NMC	National Meteorological Centre (WWW)
NOAA	National Oceanic and Atmospheric Administration (USA)
NWS	National Weather Service
OLR	outgoing long-wave radiation
PNA	Pacific/North American index
ppb(v)	parts per billion (109) (by volume)
ppm(v)	parts per million (106) (by volume)
ppt(v)	parts per trillion (1012) (by volume)
PROTEUS	profile telemetry of upper ocean currents
PSC	polar stratospheric cloud
PSMSL	Permanent Service for Mean Sea-Level (UK)
QBO	Quasi-Biennial Oscillation
SACZ	South Atlantic Convergence Zone
SADC	Southern Africa Development Community
SAR	Synthetic Aperture Radar
SLP	sea-level pressure
SO(I)	Southern Oscillation (Index)
SST	sea surface temperature
TAO	tropical atmosphere ocean
TD	total duration (blocking index)
TI	total intensity (blocking index)
TOGA	Tropical Ocean-Global Atmosphere Programme (WCRP)
TOMS	total ozone mapping spectrometer
TOPEX	Typhoon Operational Experiment
UN	United Nations
UNDP	United Nations Development Programme
UNEP	United Nations Environment Programme
UNESCO	United Nations Educational, Scientific and Cultural Organization
UTC	Universal Time Coordinated
VOS	Voluntary Observing Ship
WCDMP	World Climate Data and Monitoring Programme

WCDP	World Climate Data Programme
WCP	World Climate Programme (WMO)
WCRP	World Climate Research Programme (WMO/ICSU)
WMO	World Meteorological Organization
WOCE	World Ocean Circulation Experiment (WCRP)
WPO	West Pacific Oscillation
WWW	World Weather Watch (WMO)

CONTRIBUTORS

Lead Authors

IRACEMA CAVALCANTI, Instituto Nacional de Pesquisas Espaciais, São Paulo, Brazil;
JOHN CHURCH, Climate Programme, CSIRO Division of Oceanography, Hobart, Tasmania, Australia;
MICHAEL CROWE, National Climatic Data Center (NOAA), Asheville, NC, USA;
B.N. DEWAN, India Meteorological Department, Shivaji Nagar, India;
CHRIS FOLLAND, Hadley Centre for Climate Prediction and Research, Meteorological Office, Bracknell, UK;
BRAD GARANGANGA, Drought Monitoring Centre, Harare,, Zimbabwe;
G.V. GRUZA, Institute for Global Climate and Ecology, Moscow, Russian Federation;
MICHAEL HALPERT, Climate Analysis Center (NOAA), Washington, DC, USA;
RAINO HEINO, Finnish Meteorological Institute, Helsinki, Finland;
PHILIP JONES, Climatic Research Unit, University of East Anglia, Norwich, UK;
G.O.P. OBASI, Secretary-General, WMO, Geneva, Switzerland;
JIM PETERSON, Environmental Research Laboratories (NOAA), Boulder, CO, USA;
DAVID PHILLIPS, Atmospheric Environment Service, Downsview, Ontario, Canada;
EUGENE RASMUSSON, Department of Meteorology, University of Maryland, College Park, MD, USA;
PAUL REILLY, National Ocean Service, Ocean Products Branch (NOAA), Camp Springs, MD, USA;
GUDRUN ROSENHAGEN, Deutscher Wetterdienst, Seewetteramt, Hamburg, Germany;
PETER SCHOLEFIELD, World Climate Programme Department, WMO, Geneva, Switzerland;
MARY VOICE, National Climate Centre, Bureau of Meteorology, Melbourne, Australia;
DOUGLAS WHELPDALE, Atmospheric Environment Service, Downsview, Ontario, Canada;
WILL WRIGHT, National Climate Centre, Bureau of Meteorology, Melbourne, Australia;
XU QUN, Jiangsu Meteorological Institute, Nanjing, China;
JOHN ZILLMAN, President of World Meteorological Organization, Director of Meteorology Bureau of Meteorology, Melbourne, Australia.

Other Contributors

Rumen Bojkov, WMO, Geneva, Switzerland.
Ross Brown, Department of the Environment, Downsview, Canada;
T. Casey, P. Lehmann, P. Leigh, R. Leighton, J. Lindesay, D. Vincent, Bureau of Meteorology, Melbourne, Australia;
A. Close, Murray-Darling Basin Commission, Canberra, Australia;
Denis D'Amours, Department of Fisheries and Oceans, Ottawa, Canada;
T.T. Gibson, Antarctic CRC, University of Tasmania, Hobart, Australia;
Pavel Ya. Groisman, State Hydrological Institute, Leningrad, Russian Federation;
Ibrahim Gurer, Department of Geological Engineering, Ankara, Turkey;
Tom Karl, National Climatic Data Center, Asheville, NC, USA;
Wolfgang Matthaus, Institut für Ostseeforschung Warnemunde, Germany;
Michael J. McPhaden and Nancy Soreide, Pacific Marine Environmental Laboratory, Seattle, WA, USA;
Raymond P. Motha, Joint Agricultural Weather Facility, USA Department of Agriculture, Washington, DC, USA;
Jeffrey C. Rogers, Department of Geography, The Ohio State University, Columbus, OH, USA;
Bruno Rudolf, R. Franke and R. Tiesel, Deutscher Wetterdienst, Germany;
Ayhan Sayin, Turkish State Meteorological Service, Ankara, Turkey.

Principal editor: David Philips

Graphics: Image One Productions, Ontario, Canada

Design: Bernard Chazine, Siena

Phototypesetting and photolythography: Bernard & Co., Siena

Printed in Italy by: Centrooffset, Siena

September 1995